



A University of Sussex PhD thesis

Available online via Sussex Research Online:

<http://sro.sussex.ac.uk/>

This thesis is protected by copyright which belongs to the author.

This thesis cannot be reproduced or quoted extensively from without first obtaining permission in writing from the Author

The content must not be changed in any way or sold commercially in any format or medium without the formal permission of the Author

When referring to this work, full bibliographic details including the author, title, awarding institution and date of the thesis must be given

Please visit Sussex Research Online for more information and further details



Insights into Apolipoprotein E: Understanding the Major Genetic Risk Factor for Alzheimer's Disease

Ana-Caroline Raulin

A thesis submitted in fulfilment
of
the requirements for the degree of Doctor of Philosophy
at
The University of Sussex
Department of Life Sciences
Sussex Neuroscience

September 2019

Declaration

I hereby declare that this thesis has not been and will not be, submitted in whole or in part to another University for the award of any other degree.

Signature :

Acknowledgements

And here we are, two hundred and fifty or so pages later... Completing this PhD has been quite the adventure, and it would not have been possible without the unending support of my supervisor, Prof. Louise Serpell. Louise, thank you so much for the opportunity you have given me. You have guided me throughout this project and allowed me to grow as a scientist. You always believed in my abilities, especially at times when I didn't. Most importantly, we celebrated the highs (with wine and karaoke), and you supported me through the lows (with biscuits and coffee). I would also like to thank Sussex Neuroscience for funding my research, conference and courses attendance. I would like to give special thanks to Dr. Ruth Staras for her encouragements. Thank you to my thesis committee members, Prof. John Atack, Dr. Erika Mancini and Prof. Jenny Rusted for their helpful suggestions and guidance. Thanks to Dr. Pascale Schellenberger, to Dr. Yan Gu and to the Ancillary Unit staff, in particular to Danielle, and Alex Stuart for their help and support.

To the Serpell lab members, past and present: Dr. Youssra Al-hilaly, Dr. Mahmoud Maina, Dr. Lucas Kraft, Dr. Karen Marshall, Dr. Kate Fennell, Dr. Devkee Vadukul, Kurtis Mengham, Kamillia Kasbi, Dr. Saskia Pollack and Luca Biasetti, thank you! I could not have hoped for a better team to work with. Youssra, you guided me through my first experiments, and I will be forever grateful to you for caring about me in and out of the lab. Lucas, you've taught me so much and it was a pleasure to work and collaborate with you. Thanks for getting me started on the project. Mahmoud, I have learned so much through our stimulating discussions, thank you! Karen, thank you for your support and for helping me out when I needed it – I really appreciate it! Also, karaoke. Need I say more? Kate, my dissection teacher! Thank you so much for having taken the time to teach me. Devkee, even now that you've moved abroad, you've remained available and helpful and thanks for that (thanks FaceTime!). To my office pals, Kurtis and Kamillia, thanks for putting up with my chit-chat! I wish you guys all the best in completing your respective PhDs. Saskia, you were always there to cheer me up and encourage me when times were hard, and I will forever be grateful, thank you. Luca, my PhD bro, I don't think I have ever met such a patient and helpful person – really. I know I can be a handful at times, but I could always count on you, from you helping me in the lab to listening to my continual complaining (I am French after all), so thanks!

To my programme pals, Leonie, Richard, Sofia, and Devin: what an adventure! For the support throughout, from Brighton, to Amsterdam, to Lisbon...Thanks! I would like to thank Devin in particular for bearing with me. You have been a great source of support these past three years – best flat-mate ever! I don't think I could have finished this whole ordeal without X-Files, and It's Always Sunny, and karaoke (again). To the amazing friends I have made along the way, Léa, Steph, Matina, Caroline (my lab kid) – you've made this adventure sweeter. Thank you.

Finally, I would like to thank my friends and family. Vikki, thanks for letting me practice my presentations on you! Colette, my sister from another mother: gracias por siempre estar ahí y aunque no estés aquí físicamente, nunca me has fallado. Tu apoyo estos últimos meses ha sido esencial. Gracias por California.

Mathilde (la chapi), François (mon binôme de labo), Seb (le best), Papa : j'espère vous avoir rendu fiers. Je vous aime très fort. Jamás en la vida hubiera podido hacer esto sin tu apoyo, Mamita. Gracias por todas esas velas que me prendiste, por escucharme hablar de mis células y de las proteínas, ¡y por darme consejos, aunque no supieras mucho de eso! Je t'aime Maman.

"The truth is out there".

Abstract

Sporadic, late-onset Alzheimer's disease (LOAD) is the leading cause of dementia. Advanced age is the main culprit for LOAD, but the $\epsilon 4$ variant of *APOE* has been identified as a major genetic risk factor. *APOE* encodes Apolipoprotein E (ApoE), which exists as three isoforms. ApoE3, the most common one, confers a neutral chance for LOAD onset whereas ApoE4 presents a risk and ApoE2 is protective.

This thesis explores different avenues taken to understand the differences between the three ApoE isoforms, with the ultimate goal being to answer why and how only ApoE4 increases an individual's susceptibility for LOAD.

In Chapter 3, the structure, stability, and propensity for aggregation for the isoforms were compared using a recombinant model of human ApoE.

In Chapter 4, I conducted a thorough exploration of both the impact of the *APOE* genotype on vulnerability to oxidative stress and ApoE's differential response to oxidative stress itself, using recombinant protein and cultures from human ApoE targeted-replacement mice.

Finally, in Chapter 5, the interaction between ApoE and ageing was explored by quantifying longitudinal changes in ApoE expression in human ApoE3 and ApoE4-targeted replacement mice. Additionally, differences in markers of ageing between mice were examined.

The results presented in this thesis highlight the fact that ApoE2 and ApoE3 outperform ApoE4. Out of the three isoforms, ApoE4 was the more prone to self-assembly, which is a pathogenic feature of LOAD. While no major differences could be spotted at the tissue level, significant dissimilarities appeared in how the structure of ApoE isoforms is affected by oxidative and reducing conditions, with results suggesting that ApoE2 and to a lesser extent ApoE3 could function as scavengers of oxidative agents. Finally, overall ApoE levels were found to be reduced in ApoE4 targeted-replacement mice compared to ApoE3-mice, especially at old age; and ApoE4 mice appeared to have increased markers of ageing compared to ApoE3 mice. Taken together, these results attest to the complexity of LOAD and show the great number of ways ApoE could be differentially implicated in its onset.

Table of Contents

Declaration.....	1
Acknowledgements	2
Abstract.....	4
Table of Contents.....	5
List of figures	10
List of tables	12
Abbreviations	13
Amino acid code	16
Chapter 1 - Introduction	17
1.1. Outline of this thesis.....	17
1.2. Alzheimer's disease: overview, potential causes and associated risk factors	18
1.2.1. Overview	18
1.2.2. Potential causes for AD onset.....	19
1.2.3. Genetic risk factors for AD	22
1.2.4. Environmental risk modifiers for AD.....	27
1.3. ApoE: discovery, structure and function.....	31
1.3.1. Discovery of ApoE	31
1.3.2. Structure of ApoE.....	32
1.3.3. Physiological function of ApoE.....	35
1.4. ApoE is the major risk factor for AD	41
1.4.1. ApoE and A β	41
1.4.2. ApoE and tau pathology.....	45
1.4.3. ApoE in additional AD pathologies.....	46
1.5. ApoE in the context of protein misfolding and aggregation.....	48
1.5.1. Protein misfolding and aggregation	48
1.5.2. Evidence for differential, isoform-dependent propensity for ApoE to aggregate.....	50
1.6. ApoE and oxidative stress.....	52
1.6.1. Oxidative stress in AD.....	52

1.6.2. Multiple and differential roles for ApoE in the antioxidant defence system.....	55
1.7. ApoE in the ageing brain.....	57
1.7.1. Interaction between <i>APOE</i> polymorphism and ageing	57
1.7.2. Low prevalence of ϵ 4 homozygotes and an animal model to overcome this	58
1.7.3. ApoE and accelerated cognitive ageing.....	59
1.8. Aims and objectives of this thesis	60
1.8.1. Aim 1: Self-assembly properties of ApoE	60
1.8.2. Aim 2: ApoE and oxidative stress	60
1.8.3. Aim 3: ApoE throughout lifespan	61
Chapter 2 – Materials and methods.....	62
2.1. Materials.....	62
2.1.1. Plastics.....	62
2.1.2. Buffers, chemicals and materials for protein sample preparation	62
2.1.3. Buffers, chemicals and materials for cell and molecular biology	65
2.1.4. Buffers and chemicals for brain tissue protein extraction	68
2.1.5. Gel electrophoresis, western blot and agarose gel.....	69
2.1.6. Antibodies	71
2.1.7. Protein assay kits.....	72
2.1.8. Equipment and microscopes.....	72
2.1.9. Animals	74
2.2. Routine techniques and sample preparation relative to protein-based experiments.....	75
2.2.1. Recombinant protein production and purification of human ApoE in <i>E. coli</i>	75
2.2.2. Recombinant protein sample preparation for structural characterisation	78
2.2.3. Recombinant protein sample preparation for self-assembly assays.....	79
2.2.4. Recombinant protein sample preparation under oxidative and reducing conditions.....	79
2.3. Routine techniques and sample preparation relative to cell-based experiments	80
2.3.1. Cell culture and dissections	80
2.3.2. Cell treatment.....	81
2.3.3. RNA and protein extraction from cells	81

2.4. Routine techniques and sample preparation relative to brain tissue-based experiments.....	84
2.4.1. Brain tissue collection and homogenisation.....	84
2.4.2. Protein extraction and fractionation	85
2.5. Biophysical techniques.....	86
2.5.1. Mass spectrometry.....	86
2.5.2. Analytical ultracentrifugation	86
2.5.3. Circular dichroism spectroscopy	87
2.5.4. Tryptophan fluorescence spectroscopy	89
2.5.5. Thioflavin-T fluorescence assay for detection of protein self-assembly.....	91
2.5.6. Transmission Electron microscopy	93
2.5.7. X-Ray Fibre diffraction	94
2.5.8. Waltz algorithm	94
2.6. Cell and molecular biology	95
2.6.1. Live/dead assay using fluorescence microscopy.....	95
2.6.2. Reverse transcription and quantitative polymerase chain reaction.....	95
2.7. Biochemistry.....	98
2.7.1. Total protein quantification.....	98
2.7.2. One-dimension sodium dodecyl sulphate polyacrylamide gel electrophoresis.....	98
2.7.3. Native gel electrophoresis.....	99
2.7.4. Western (immuno) blotting and dot blot.....	99
2.7.5. Enzymatic assays	100
2.8. Statistical analyses.....	102

Chapter 3 - Self-assembly properties of recombinant human

Apolipoprotein E	103
3.1. Introduction	103
3.2. Summary of methods.....	106
3.3. Results	107
<i>Structural characterisation of recombinant human ApoE produced in E. coli...</i>	<i>107</i>
3.3.1. Production and purification of rApoE2	107
3.3.2. Structure of rApoE in phosphate buffer.....	111
<i>Differential self-assembly properties of rApoE isoforms.....</i>	<i>119</i>
3.3.3. rApoE4, but not E2 and E3, self-assembles under physiological conditions.....	119
3.3.4. Kinetics of rApoE self-assembly	121

3.3.5. Inhibition of rApoE4 fibril formation by rApoE3 and rApoE3	125
<i>Characterisation of rApoE4 fibrils</i>	128
3.3.6. Morphology of rApoE4 fibrils	128
3.3.7. Nature of rApoE4 fibrils	130
3.4. Discussion	133
3.5. Conclusion	142
Chapter 4 - Apolipoprotein E and oxidative stress	143
4.1. Introduction	143
4.2. Summary of methods	147
4.3. Results	149
<i>Increased susceptibility associated with APOE ϵ4/ϵ4</i>	149
4.3.1. Impact of the APOE genotype on antioxidant balance in ApoE-TR mice	149
4.3.2. ApoE expression as a response to cytotoxic insults in SH-SY5Y and in primary neuronal culture	151
<i>Effect of oxidative and reducing conditions on rApoE</i>	157
4.3.3. Secondary and tertiary structure of rApoE under redox conditions	157
4.3.4. Both oxidative and reducing conditions affect rApoE self-assembly...	164
4.4. Discussion	173
4.5. Conclusion	181
Chapter 5 - Apolipoprotein E and ageing	182
5.1. Introduction	182
5.2. Summary of methods	185
5.3. Results	186
5.3.1. ApoE phenotype-dependent changes in ApoE protein levels across lifespan	186
5.3.2. Nuclear localisation of ApoE	190
5.3.3. Levels of age markers in E3/E3 and E4/E4 mice are phenotype- dependent	191
5.4. Discussion	195
5.5. Conclusion	201
Chapter 6 - Discussion and future directions	202
6.1. Self-assembly of ApoE	203
6.1.1. Self-assembly of ApoE <i>in vitro</i> is restricted to rApoE4	203
6.1.2. Self-assembly of ApoE <i>in vivo</i>	204

6.2. ApoE and the antioxidant system.....	207
6.2.1. ApoE as an antioxidant protein.....	207
6.2.2. ApoE and the antioxidant balance across lifespan	208
6.3. ApoE, a direct and indirect transcription factor?	211
6.3.1. Nuclear localisation of ApoE and implications	211
6.3.2. Disulphide bridge formation – a signalling moiety.....	211
6.4. ApoE as a therapeutic target.....	212
6.5. Concluding remarks	214
Bibliography	216
Appendix 1.....	242
Appendix 2.....	249
Appendix 3.....	252
Appendix 4.....	254

List of figures

Figure 1.1 Potential causes for AD: an overview	23
Figure 1.2 Genetic and environmental disease modifiers	30
Figure 1.3 Representation of <i>APOE</i> polymorphism	32
Figure 1.4 Structure of ApoE.....	35
Figure 1.5 The structure of ApoE influences its function.....	39
Figure 1.6 Binding of ApoE to A β and consequences on A β pathology.....	44
Figure 1.7 Gain of toxic function/ loss of function associated with ApoE4	47
Figure 1.8 Amyloid fibrils	50
Figure 1.9 Oxidative stress and oxidative damage	53
Figure 2.1 Production of rApoE isoforms.	75
Figure 2.2 Isolation of RNA and protein from treated cells.....	82
Figure 2.3 Mouse brain tissue collection and processing.....	84
Figure 2.4 Reference CD spectra of α -helical, α -sheet and intrinsically disordered proteins.....	88
Figure 3.1 Structure of ApoE isoforms	104
Figure 3.2 Comparison of <i>APOE</i> ϵ 2 and <i>APOE</i> ϵ 4 plasmid sequence.....	108
Figure 3.3 Purification of rApoE2 as followed by gel electrophoresis	109
Figure 3.4 Primary sequence of rApoE isoforms.....	110
Figure 3.5 Size-distribution of rApoE in PB	112
Figure 3.6 Secondary structure of rApoE isoforms characterised by CD.....	115
Figure 3.7 Tertiary structure of rApoE by Trp fluorescence spectroscopy	117
Figure 3.8 Detection of fibril formation by ThT fluorescence spectroscopy.....	120
Figure 3.9 Micrographs of rApoE before and after a 24 h and a 3 d incubation period	121
Figure 3.10 Kinetics of rApoE fibril formation as followed by ThT fluorescence spectroscopy	123
Figure 3.11 Following filament formation by gel electrophoresis	125
Figure 3.12 Effect of co-incubation of rApoE4 with either E2 or E3 on self-assembly	126
Figure 3.13 rApoE4 fibril formation followed by TEM over 24 h.....	129
Figure 3.14 Growth of rApoE4 filaments over time	130
Figure 3.15 Nature of rApoE4 filaments	131
Figure 3.16 Small round species in rApoE3 and rApoE4	138
Figure 4.1 Met residues in ApoE.....	145
Figure 4.2 CAT and SOD activity in ApoE-TR mice across lifespan	150

Figure 4.3 ApoE expression in SH-SY5Y following excitotoxicity	152
Figure 4.4 Primary cortical neurons' viability following exposure to toxins.....	154
Figure 4.5 ApoE expression in primary cortical neurons following toxic exposure.....	155
Figure 4.6 Secondary structure of rApoE isoforms in the presence of H ₂ O ₂ and DTT	158
Figure 4.7 Changes in the shape of rApoE α -helices with increasing amounts of H ₂ O ₂	161
Figure 4.8 Tertiary structure of rApoE isoforms in the presence of H ₂ O ₂ and DTT	163
Figure 4.9 Self-assembly of rApoE under harsh oxidative and reducing conditions ...	164
Figure 4.10 Micrographs of rApoE assembled under harsh oxidative and reducing conditions	165
Figure 4.11 Zoomed-in micrographs of rApoE assembled under harsh oxidative conditions	166
Figure 4.12 Self-assembly of rApoE under milder oxidative conditions	169
Figure 4.13 Self-assembly of rApoE under milder reducing conditions.....	172
Figure 4.14 Non-reducing gel electrophoresis of rApoE before and after harsh oxidation	179
Figure 5.1 Detection of changes in ApoE levels across lifespan by WB.....	187
Figure 5.2 Comparison of ApoE levels in ApoE3-TR and ApoE4-TR mice.....	189
Figure 5.3 ApoE in the nucleus	190
Figure 5.4 Protein carbonyl content in old ApoE3- and ApoE4- TR mice	192
Figure 5.5 Changes in α -Tubulin levels in old ApoE-TR mice	194
Figure 5.6 Normalised ApoE levels by age groups	197
Figure 6.1 Hypotheses behind sporadic AD.....	202
Figure 6.2 ApoE and A β in acidic compartments	206
Figure 6.3 Associations between antioxidant enzyme activities and oxidative damage with soluble ApoE levels across lifespan in ApoE-TR mice	209
Figure 6.4 Summary	215

List of tables

Table 1.1 Additional susceptibility genes	26
Table 2.1 Chemicals used in protein sample preparation	63
Table 2.2 Chemicals used in buffers and media for tissue culture and cell treatment ..	66
Table 2.3 Primers sequences.....	68
Table 2.4 Chemicals used in protein extraction buffers	68
Table 2.5 Chemicals used in gel electrophoresis and western blot	69
Table 2.6 Antibodies for immunoblotting	71
Table 2.7 Cycling parameters for site-directed mutagenesis	76
Table 2.8 ReadyProbes specifications	95
Table 2.9 Optimised primers concentrations.....	96
Table 3.1 Sedimentation analysis of recombinant rApoE isoforms in PB	113
Table 3.2 Secondary structure analysis of rApoE isoforms.....	114
Table 3.3 Thermal denaturation parameters	114
Table 3.4 Chemical denaturation parameters	118
Table 3.5 Secondary structure analysis of rApoE4 before and after self-assembly....	132
Table 3.6 Summary of the structural characterisation of rApoE isoform	136
Table 4.1 Detailed secondary structure of rApoE isoform under physiological, oxidative and reducing conditions	159
Table 4.2 Effect of oxidative conditions on α -helical content	160
Table 4.3 Statistical comparison of $[\theta]_{222/208 \text{ nm}}$ following incubation in PB vs H_2O_2	160
Table 4.4 Statistical comparison of $[\theta]_{222/208 \text{ nm}}$ between isoforms at higher rApoE: H_2O_2	162
Table 6.1 Segmental linear regression best-fit slopes	210
Table 6.2 ApoE-targeted therapies	212

Abbreviations

		<i>Defined in:</i>
1D-SDS-PAGE	One-dimension SDS polyacrylamide gel electrophoresis	Chapter 2
3C	3C protease cleavage	Chapter 2
A β	β -amyloid peptide	Chapter 1
AD	Alzheimer's disease	Chapter 1
ANOVA	Analysis of variance	Chapter 2
ApoE	Apolipoprotein E	Chapter 1
ApoE-TR	Human ApoE targeted replacement	Chapter 1
APP	Amyloid precursor protein	Chapter 1
AraC	Cytosine arabinoside	Chapter 2
AUC	Analytical ultracentrifugation	Chapter 1
BCA	Bicinchoninic acid	Chapter 2
BSA	Bovine serum albumin	Chapter 2
CAT	Catalase	Chapter 2
CD	Circular Dichroism	Chapter 1
cDNA	Complementary DNA	Chapter 2
CJD	Creutzfeldt-Jacob disease	Chapter 1
CNBr	Cyanogen bromide	Chapter 4
CNS	Central nervous system	Chapter 1
Cq	Amplification cycle	Chapter 2
CSF	Cerebrospinal fluid	Chapter 1
ddH ₂ O	Double distilled water	Chapter 2
dH ₂ O	Distilled water	Chapter 2
DMEM/F-12	Dulbecco's Modified Eagle Medium/Nutrient Mixture F-12	Chapter 2
DMSO	Dimethyl sulfoxide	Chapter 2
DTT	Dithiothreitol	Chapter 2
<i>E. coli</i>	<i>Escherichia Coli</i>	Chapter 2
EDTA	Ethylenediaminetetraacetic acid	Chapter 2
EtOH	Ethanol	Chapter 2
FCS	Foetal Calf Serum	Chapter 2

GPx	Glutathione peroxidase	Chapter 1
GSH	Glutathione	Chapter 1
GuHCl	Guanidine hydrochloride	Chapter 1
HBSS	Hank's Balanced Salt Solution	Chapter 2
HDL	High density lipoproteins	Chapter 1
HEPES	4-(2-hydroxyethyl)-1-piperazineethanesulfonic acid	Chapter 2
His-tag	Histidine-tag	Chapter 2
HNE	4-hydroxynonenal	Chapter 1
HRP	Horseradish Peroxidase	Chapter 2
HSPGs	Heparan sulfate proteoglycans	Chapter 1
IMAC	Immobilised metal affinity chromatography	Chapter 2
IPTG	Isopropyl β -D-1-thiogalactopyranoside	Chapter 2
LDL	Low-density lipoproteins	Chapter 1
LDLR	ApoB,E-LDL receptor	Chapter 1
LOAD	Late-onset Alzheimer's disease	Chapter 1
LRP1	LDL-receptor-related protein 1	Chapter 1
MCI	Mild cognitive impairment	Chapter 1
MEM	Modified Eagle Medium	Chapter 2
MeOH	Methanol	Chapter 2
MPO	Myeloperoxidase enzymatic	Chapter 4
MW	Molecular weight	Chapter 3
MWCO	Molecular weight cut-off	Chapter 2
NB	Neurobasal medium	Chapter 2
NFT	Neurofibrillary tangles	Chapter 1
NMR	Nuclear magnetic resonance	Chapter 2
NMRSD	Normalised root mean square deviation	Chapter 3
OCI	Organochloride	Chapter 1
OP	Organophosphate	Chapter 1
P0	Post-natal day 0	Chapter 2
P1	Post-natal day 1	Chapter 2
PB	20 mM phosphate buffer, pH 7.4	Chapter 2
PBS	Phosphate buffer saline	Chapter 2
PCR	Polymerase chain reaction	Chapter 2

PD	Parkinson's disease	Chapter 1
PDL	Poly-D-Lysine	Chapter 2
Pen/strep	Penicillin/Streptomycin	Chapter 2
qPCR	Quantitative PCR	Chapter 2
rApoE	Recombinant human ApoE isoforms	Chapter 1
RM	Repeated measures	Chapter 2
RMSD	Root-mean-square deviation	Chapter 3
RNS	Reactive nitrogen species	Chapter 1
ROS	Reactive oxygen species	Chapter 1
rt	Room temperature	Chapter 2
SDS	Sodium dodecyl sulphate	Chapter 2
SEC	Size-exclusion chromatography	Chapter 2
SNP	Single nucleotide polymorphisms	Chapter 1
SOD	Superoxide dismutase	Chapter 1
TBS	Tris Buffer Saline	Chapter 2
TCEP	tris(2-carboxyethyl)phosphine	Chapter 2
TEM	Transmission electron microscopy	Chapter 2
TFA	Trifluoroacetic Acid	Chapter 2
TG	Tris-Glycine	Chapter 2
TGS	Tris-Glycine-SDS	Chapter 2
ThT	Thioflavin-T	Chapter 1
Trx	Thioredoxin	Chapter 1
Trypsin-EDTA	0.25%Trypsin- 2.21 mM EDTA	Chapter 2
VLDL	Very low-density lipoproteins	Chapter 1
WB	Western Blot	Chapter 2
XO	Xanthine 2 oxidase	Chapter 2
β -ME	β -mercaptoethanol	Chapter 2

Amino acid code

Alanine	Ala	A
Cysteine	Cys	C
Aspartic acid	Asp	D
Glutamic acid	Glu	E
Phenylalanine	Phe	F
Glycine	Gly	G
Histidine	His	H
Isoleucine	Ile	I
Lysine	Lys	K
Leucine	Leu	L
Methionine	Met	M
Asparagine	Asn	N
Proline	Pro	P
Glutamine	Gln	Q
Arginine	Arg	R
Serine	Ser	S
Threonine	Thr	T
Valine	Val	V
Tryptophan	Trp	W
Tyrosine	Tyr	Y

Chapter 1 - Introduction

1.1. Outline of this thesis

Alzheimer's disease (AD) is a very complex disorder with many hypotheses behind it, and a range of environmental risk factors modulating its onset. Adding to this complexity are also various genetic risk factors such as the $\epsilon 4$ allele of the *APOE* gene. Investigation into the role of Apolipoprotein E (ApoE) isoforms, especially in relation to AD pathological hallmarks, has boomed since 1993 (Strittmatter et al., 1993a).

This thesis explores how the role of ApoE isoforms differentially fits with some of the hypotheses behind AD, independently of the characteristic lesions and features of the disease. Methodology and experimental designs developed to this end are detailed in chapter 2.

Each result chapter deals with a specific hypothesis behind AD and a particular trait of ApoE, which is why a more focused introduction was included in all three results chapters. On the other hand, this introductory chapter gives an overview of AD as well as a broad description of the structure and function of ApoE before moving to connections between ApoE and AD pathogenesis.

The first section will focus on a brief description of AD, its potential causes and its associated pathological hallmarks. The main environmental and genetic risk factors for AD will also be outlined. The following section will cover the main known structural and functional features of ApoE. The ways in which ApoE interplays with pathological hallmarks of AD will then be briefly highlighted. The next three sections will introduce the ties between ApoE, and the selected theories of AD pathogenesis explored in this thesis: protein misfolding and aggregation, oxidative stress, and ageing. Finally, the aims of this thesis and the targeted objectives of each results chapters will be presented.

1.2. Alzheimer's disease: overview, potential causes and associated risk factors

1.2.1. Overview

According to the latest World Alzheimer Report, 50 million people worldwide are living with dementia and the number of cases is expected to triple by 2050 with the ageing population (Patterson, 2018).

AD is the most common form of dementia, representing 60% of dementia cases (Alzheimer's Association, 2017). It is a progressive and fatal neurodegenerative disorder, characterised by cognitive decline and memory loss, progressive impairment of daily living and work activities, and a plethora of neuropsychiatric symptoms and behavioural alterations.

Discovery

AD was first described in 1906 by Dr. Alois Alzheimer in A. Deter, a 51- year old patient that presented with amnesia, agnosia and aphasia. Following *post-mortem* examination of her brain, Alzheimer reported the presence of what is now known as senile plaques and neurofibrillary tangles (NFT), as well as dystrophic neurites in the neocortex (English translation of Alzheimer, 1907: Stelzmann et al., 1995).

β -amyloid

The main component of senile plaques, the β -amyloid peptide or $A\beta$, was first isolated from the twisted β -pleated sheet fibrils in cerebrovascular deposits in 1984 (Glenner & Wong, 1984). $A\beta$ is a 36 to 42 amino acid peptide widely considered essential to AD pathogenesis and diagnosis. It is a by-product of the cleavage of the amyloid precursor protein (APP), an 87 kDa transmembrane protein. APP processing follows two pathways. The "non-amyloidogenic" cleavage of APP is performed by α -secretase producing two non-pathogenic peptides (sAPP α and P3 following subsequent γ -secretase cleavage). $A\beta$ peptides are a results of APP endoproteolysis by the sequential enzymatic actions of BACE1, a β -secretase, and γ -secretase, a protein complex with presenilin 1 or 2 at its catalytic core (LaFerla et al., 2007). Senile plaques deposit extracellularly, mainly in the isocortex (Lane et al., 2018).

Tau

Microtubule-associated protein Tau was identified two years later as the principal constituent of paired helical filaments. Paired helical filaments of hyperphosphorylated Tau are abnormal intracellular inclusions that assemble to form the hallmark NFT (Kosik et al., 1986). NFT initiate in the medial temporal lobe before spreading to the isocortex (Lane et al., 2018).

Additional hallmarks

Other lesions encountered in AD *post-mortem* brain tissue include neuronal and white matter loss, overall brain shrinkage and enlargement of ventricles. Moreover, oxidative and inflammatory damage lead to energy failure and synaptic dysfunction, which are also features of the disease (Lane et al., 2018; Querfurth & LaFerla, 2010).

1.2.2. Potential causes for AD onset

Genetic mutations causing familial AD

Early-onset AD occurs in people age 30 to 60 and represent 5% of AD patients. Part of these early-onset cases are familial (1% of all AD cases), which is a very rare form of the disease that develops due to pathogenic mutations in either the gene encoding for APP (chromosome 21), for Presenilin 1 (chromosome 14) or for Presenilin 2 (chromosome 1). The most common mutations in familial AD are on chromosomes 1 and 14. Presenilin 1 mutations are responsible for the earliest and most aggressive form of AD (Selkoe, 2001; Alzheimer's Association, 2017; Joshi et al., 2012).

Late-onset AD

Late-onset, sporadic AD accounts for the great majority of the cases. It usually develops later in life after the age of 60, and its pathogenesis has yet to be fully identified.

Age is unequivocally the greatest risk factor for the development of sporadic neurodegenerative diseases like AD. The EURODEM studies conducted in the 1990s have shown that the prevalence of AD increases with age after the age of 65, doubling for every five years after that (Alzheimer's Disease International, 2008).

Ageing is an unavoidable process that results in the progressive deterioration in function and in multiple modifications at the cellular, tissue, organ and the whole-body level,

ultimately leading to death. Post-mitotic tissues, such as the brain, are at high risk to develop age-related dysfunctions (Romano et al., 2010). Ageing is closely associated with many hypotheses behind AD, such as protein misfolding and aggregation, overbearing oxidative stress, mitochondrial dysfunction, synaptic failure, reactive gliosis and neuroinflammation.

Proteinopathy

AD is in part a proteinopathy characterised by the accumulation of misfolded A β and Tau. This accumulation is precipitated and aggravated by an overwhelmed and damaged protein clearance system, and by altered protein folding by the endoplasmic reticulum, both being functional declines observed with ageing (reviewed by Querfurth & LaFerla, 2010). Proteostasis is discussed further in section 1.5.

The “amyloid cascade hypothesis” was first proposed in 1992 after the identification of causal mutations in genes involved in the generation of A β . Central to this hypothesis was that its progression was the result of an increased A β burden in affected areas of the brain, leading to the formation of senile plaques and then to NFT, neuronal cell death, and ultimately dementia (Hardy & Higgins, 1992). Evidence opposing this hypothesis include the fact that drugs targeting amyloid pathology have failed in clinical trials. In addition, the degree of dementia in life strongly correlates with the accumulation of NFT in the cerebral cortex and the hippocampus. The Tau-theory of AD was presented as an alternative explanation for the development and progression of the disease (proposed by Wischik et al., 2014).

Oxidative stress and mitochondrial dysfunction

Ageing is also associated with increased oxidative damage due to impaired antioxidant balance. Increased levels of reactive oxygen and reactive nitrogen species result in damaged proteins, lipids and DNA. Protein oxidation, oxidative damage to DNA and RNA and by-products of lipid peroxidation can all be detected both in brains and cerebrospinal fluid (CSF) of AD patients and in subjects with mild cognitive impairment (MCI). Oxidative damage in MCI suggests that oxidative stress may occur early in the pathogenesis of AD (reviewed by Zhao & Zhao, 2013). In AD, oxidative stress is closely associated with mitochondrial dysfunction. Mitochondria are one of the many A β targets in cells. A β damages mitochondria by inhibiting essential enzymes such as cytochrome c oxidase, resulting in energy failure. Mitochondrial dysfunction is primarily located at synapses where fission of mitochondria following oxidation of dynamin-like transporter protein may

be partially responsible for synaptic degeneration (reviewed by Querfurth & LaFerla, 2010).

Synaptic failure and degeneration of neural pathways

Examination of AD cortical tissue has revealed extensive synaptic loss. Quantitative morphometry estimated synapse loss to 25-35% in AD compared to control, depending on the cortical region. The number of synapses per neuron was reported to have decreased by 15 to 35% (Davies, C. A. et al., 1987). In another study, synapse density measurements pointed to a 40% synapse loss on average in the neocortex of AD patients compared to controls. Cognitive impairment correlated best with synapse loss than with amyloid and Tau pathologies (Terry et al., 1991).

Synaptic loss is preceded by synaptic dysfunction which occurs early-on in the disease pathogenesis (Selkoe, 2002). There is evidence for an influence of A β on synaptic plasticity prior to degeneration. For example, oligomeric A β *in vivo* injection inhibited long-term potentiation in the hippocampus of rats (Walsh et al., 2002). There is also mounting evidence for Tau-induced synaptic dysfunction (reviewed by Tracy and Gan, 2018).

A great number of the degenerating synapses in AD are cholinergic, marked by substantial loss of neurons in a region of the basal forebrain, the nucleus basalis of Meynert (Whitehouse et al., 1982), which most likely accounts for the measured reduction in activity of enzymes involved in acetylcholine processing (Davies, P. & Maloney, 1976). Cholinergic dysfunction as shown by decreased activity of key enzymes, namely choline acetyl transferase, correlated with cognitive decline in AD (Perry, E. K. et al., 1978).

Neuroinflammation and vascular dysfunction

Research in the AD field is increasingly moving away from a neuron-centric model of the disorder, by careful demonstration of the involvement of astrocytes, microglia and the vasculature in disease progression.

Inflammation is now viewed as crucial in AD progression. Microglia, the brain macrophages, can be both neuroprotective when preventing injury or harmful by secreting cytokines and generating reactive oxygen species. Microglia are first respondent cells following injury, and evidence shows their involvement in A β clearance. Excessive activation leads to negative microglial effects (reviewed by Fakhoury, 2018).

Extensive astrogliosis was reported by Alzheimer himself when he examined A. Deter's brain (English translation of Alzheimer, 1907: Stelzmann et al., 1995). Astrogliosis refers to an abnormal increase in astrocyte number. Astrocytes are arguably one of the most important brain cells, responsible for brain homeostasis, blood-brain barrier integrity, and synaptic maintenance among other functions. Astrocytes in AD are involved in an inflammatory response upon interaction with A β and senile plaques; and the number of astrocytes in the hippocampus correlates with the amount of NFTs present (reviewed by Fakhoury, 2018).

Last but not least, the vasculature potentially plays a crucial role in AD onset and progression. The blood-brain barrier is disrupted in AD, leading to build-up of toxins in the brain. AD tissue presents with damages to the vascular system, with decreased number of blood vessels, vascular atrophy, altered blood vessel diameter, all of it contributing to reduced cerebral blood flow, culminating in hypoxia and oxidative stress which promotes A β production and subsequent associated complications (reviewed by Rius-Pérez et al., 2018).

This section aimed to capture part of the complexity in AD, where it is hard to appreciate whether an event is either primary or secondary in the aetiology of the disease. An overview of potential causes for AD is given in Fig. 1.1.

1.2.3. Genetic risk factors for AD

Close to 5% of AD cases are inherited in a Mendelian manner with genetic mutations on genes associated with APP processing, while the rest of the cases arise from a complex interaction between genetic and environmental factors that impact both disease onset and progression. This section briefly summarises the genetic factors that influence disease aetiology. Environmental factors are outlined in section 1.2.4.

Twin studies implied that the genetic background is responsible for 60-80% of disease risk as there is a higher frequency of late-onset AD (LOAD) in monozygotic twins than in dizygotic twin siblings (Reitz & Mayeux, 2014). A number of genetic studies have been conducted to identify genes implicated in AD, such as linkage approaches and genome-wide association studies.

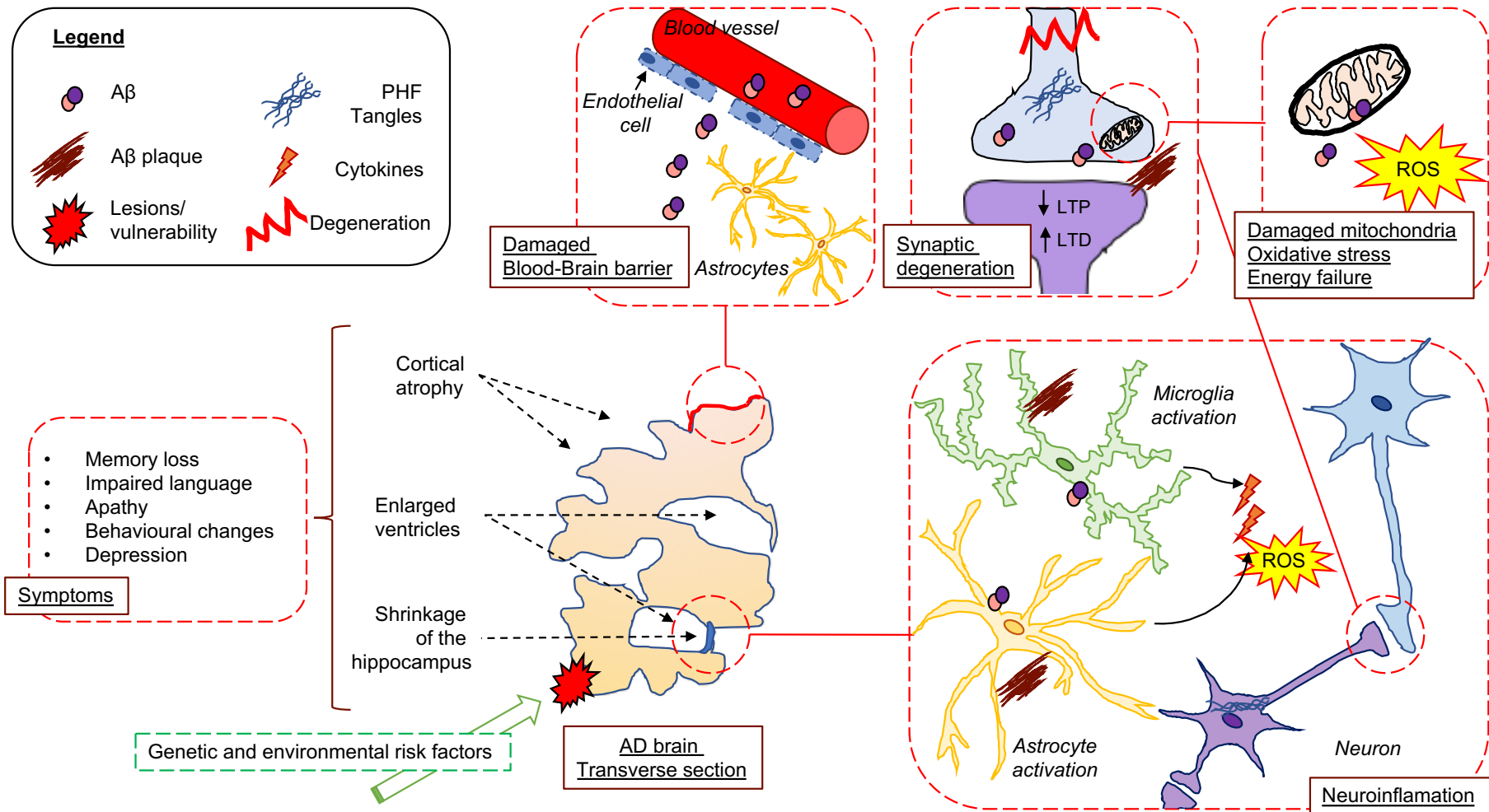


Figure 1.1 Potential causes for AD: an overview

Simplistic overview of AD, from symptoms to brain damage and lesions, and the associated pathologies: inflammation, oxidative stress, synaptic degeneration.

APOE polymorphism

Studying the genetics behind AD became prevalent after the discovery of causal mutations in familial cases. Inconsistencies in linking chromosome 21 (where the *APP* gene is located) to some AD families led scientists to posit the possible existence of either other mutations leading to early-onset AD (we now know of mutations in chromosome 1 and chromosome 14); or the absence of linkage to chromosome 21 in late-onset cases (Pericak-Vance et al., 1991). With this in mind, linkage to regions outside chromosome 21 were investigated, and Pericak-Vance et al reported in 1991 linkage to chromosome 19 in LOAD families (Pericak-Vance et al., 1991). Linkage was later narrowed down to the *APOE* gene, which is located on chromosome 19q13.2 (Strittmatter et al., 1993a). *APOE* encodes for ApoE and has three major allelic variants: $\epsilon 2$, $\epsilon 3$ and $\epsilon 4$. Their respective frequencies are 8%, 77% and 15% (Zannis et al., 1981; Utermann et al., 1982).

In 1991, ApoE was identified as one of the proteins localised to amyloid plaques (Namba et al., 1991) and in 1993, Strittmatter et al published additional evidence linking ApoE to AD: strong binding propensity to A β ; localisation to senile plaques, vascular deposits and NFT; and a disproportionately high frequency of *APOE* $\epsilon 4$ allele in families bearing LOAD (Strittmatter et al., 1993a). Corder and associates then reported the gene-dose effect of the $\epsilon 4$ allele on age and risk of onset: risk of AD onset was found to be increased by 3 with one $\epsilon 4$ allele and by 8 in homozygotes (Corder et al., 1993). Corder et al also provided evidence for reduced age of onset in $\epsilon 4$ carriers, with each allele resulting in an 8-year shift (age of onset in $\epsilon 4$ homozygotes: 68 years old, $\epsilon 4$ heterozygotes: 76 years old, $\epsilon 4$ non-carriers: 84 years old; Corder et al., 1993).

APOE $\epsilon 4$ was consistently identified as a risk gene in African Americans, Caucasians and Caribbean Hispanics in genome-wide association studies (Reitz & Mayeux, 2014). $\epsilon 4$ allele frequency in Caucasian AD cases is close to 40%, while it is a bit lower in African Americans (32%), Japanese (28%) and Hispanics (19%) (Farrer et al., 1997).

Discovery, structure and function of ApoE will be discussed in section 1.3.

Additional susceptibility genes

The fact that not all late-onset AD can be explained by carrying an *APOE* $\epsilon 4$ allele means that other factors such as additional susceptibility genes and environmental factors participate on modulating AD onset in non-Mendelian inherited cases. Genome-wide association studies have contributed in the identification of a number of other genes

associated with AD pathology. These genes can be grossly classified into three main categories: genes implicated in lipid and cholesterol metabolism; genes regulating endocytosis and vesicle-mediated transport; and genes involved in the immune response. This section offers a compilation of those genes, reviewed by Reitz & Mayeux in 2014 and Giri et al in 2016.

	Gene	Role of protein encoded / comments	Reference
Lipid and cholesterol metabolism	<i>CLU</i>	Apolipoprotein J, a lipoprotein involved in lipid transport; three SNP identified	Harold et al., 2009; Lambert et al., 2009
	<i>ACBA7</i>	Transmembrane transporter protein implicated in the formation of high-density lipoproteins and in transport of cholesterol and other lipids out of the cell; three SNP identified	Hollingworth et al., 2011
Endocytosis and vesicle-mediated transport	<i>BIN1</i>	Cytoskeleton dynamics and clathrin-mediated endocytosis, thus involved in processes affecting APP	Seshadri et al., 2010
	<i>PICALM</i>	Involved in clathrin-mediated endocytosis, indirectly affecting A β production and clearance	Harold et al., 2009
	<i>CD2AP</i>	Scaffolding protein	Hollingworth et al., 2011; Naj et al., 2011
	<i>SORL1</i>	Receptor involved in trafficking	Rogaeva et al., 2007; Lambert et al., 2013
Immune response	<i>CR1</i>	Receptor part of the complement activation family; first gene related to immunity to be identified as a risk-gene for AD; two SNPs associated with increased AD risk; one SNP linked to increased plaque deposition in the brain	Lambert et al., 2009
	<i>CD33</i>	Cell surface immune receptor	Hollingworth et al., 2011; Naj et al., 2011
	<i>MS4A</i>	Protein expressed in immune cells; exact role still unknown	
	<i>EPHA1</i>		
	<i>HLA-DRB5/DRB1</i>	Loosely linked to the immune response	Lambert et al., 2013
<i>INPP5D</i>			

Immune response	<i>MEF2C</i>	Loosely linked to the immune response	Lambert et al., 2009
	<i>TREM2</i>	TREM2 is a receptor expressed at the cell surface of microglia. It is involved in phagocytosis and in downregulating the inflammatory response. Six different variants reported in neurodegeneration. Two correspond to missense mutations leading to increased AD risk	
Additional genes	<i>CASS4</i>	Involved in cytoskeletal functions	
	<i>FERMT2</i>		
	<i>PTK2B</i>	Part of the MAP kinase signalling pathway	
	<i>NME8</i>	Involved in cell proliferation	
	<i>ZCWPWI</i>	Potentially involved in epigenetics	
	<i>CELF1</i>	Involved in mRNA processing	
<i>NCKX4</i>	Encodes a potassium-dependent sodium/calcium exchanger		

Table 1.1 Additional susceptibility genes

Information compiled from Reitz & Mayeux, 2014; Giri et al., 2016; Fenoglio et al., 2018. SNP= single nucleotide polymorphism.

Of note, trafficking, endocytosis and cytoskeletal functions are all pathways related to some extent to A β and Tau pathologies. Also noteworthy, TREM2 has received a lot of attention since it is expressed in microglia, which have been reported to play a crucial role in the progression of AD (see 1.2.2).

Most genetic studies have been conducted in Caucasians, but a number of susceptibility genes were detected in different ethnic groups. *APOE* ϵ 4 was consistently identified as a risk gene in African Americans, Caucasians and Caribbean Hispanics. *ABCA7* has been identified to confer risk at a similar level to *APOE* ϵ 4 in African Americans, and *CLU*, *PICALM* and *BIN1* were also identified in Caribbean Hispanics (reviewed in Reitz and Mayeux, 2014).

1.2.4. Environmental risk modifiers for AD

Carrying a genetic risk for AD does not equate disease onset, meaning that environmental factors must interact to modify disease risk. Environmental factors can be classified into two categories: risk factors and protective factors, which will be summed up in this section.

Risk factors

Environmental risk factors for AD fall into two groups: comorbidities and exposure to toxins.

- **Comorbidities**

Several disorders are associated with AD onset.

Cerebrovascular diseases encompass a number of events and conditions affecting blood vessels in the brain. Strokes (ischemic and haemorrhagic), vascular abnormalities and white matter disease all increase the risk for dementia through unknown mechanisms (Reitz & Mayeux, 2014).

Type 2 diabetes practically doubles the risk of AD onset, and both cerebrovascular and non-cerebrovascular mechanisms may come into play. On the one hand, type 2 diabetes is associated with increased risk for strokes; on the other hand, insulin dysregulation has an impact on A β accumulation and Tau phosphorylation, and it is associated with increased oxidative stress (formation of advanced-glycation products) and inflammation (elevated inflammatory markers) (Stožická et al., 2007).

Hypertension in mid-life has been linked to AD. High blood pressure is in part responsible for a number of brain lesions and complications: angiopathy, atherosclerosis and mini-strokes, reduced blood flow and subsequent neuronal loss and oxidative stress (Reitz & Mayeux, 2014).

Traumatic brain injury has also been linked to AD in *post-mortem* studies, particularly ϵ 4-carriers (Mayeux & Stern, 2012).

These disorders associated to AD onset may be involved in the aetiology of disease through different pathways affecting cognition, such as:

- Lesions to specific brain regions important in memory
- Increased A β deposition/ impaired clearance
- Increased Tau phosphorylation and neuronal cell death
- Inflammation

- **Exposure to toxins**

Linking AD onset to exposure to neurotoxins has proven difficult since there is no way to measure exposure accurately to date. There is nevertheless evidence linking *metal exposure* to neurodegeneration, albeit reported results are controversial. High levels of aluminium and iron as well as zinc and copper dyshomeostasis have been reported in the AD brain. Aluminium, zinc, copper and iron influence A β pathology *in vitro* and *in vivo*, on top of inducing oxidative stress and inflammation. High levels of cobalt and cadmium have also been reported in AD brains compared to controls. Cadmium has been linked to Tau pathology *in vitro*. Exposure to other metals such as lead, manganese, selenium, mercury, arsenic have been linked to AD *in vitro* and *in vivo* (Yegambaram et al., 2015).

Links between *pesticide exposure* and neurodegeneration are particularly accepted in the aetiology of Parkinson's disease (PD) since uncovering that injection of prodrug MPTP leads to development of PD. For instance, administration of the insecticide rotenone or the herbicide paraquat in animal models produces PD-like pathologies (Chin-Chan et al., 2015). Epidemiological links between pesticide exposure and AD are controversial. Nonetheless, there are reports of increased AD risk following organophosphate (OP) and organochloride (OCI) exposure (Chin-Chan et al., 2015). Richardson et al reported a potential increased susceptibility to OCI exposure in the $\epsilon 4$ carriers (Richardson et al., 2014). Pesticides like OCI and OP are known inhibitors of Acetylcholine Esterase, but they have many other, non-fully identified, non-cholinergic targets associated with oxidative stress that could help explain why acute, chronic and long-term exposure to pesticides have been associated with sporadic AD (Chin-Chan et al., 2015).

Smoking may also be linked to AD onset, although the evidence is also controversial, with positive (compensation of cholinergic loss by increasing nicotine acetylcholine receptors) and negative associations (oxidative stress and inflammation) (Mayeux & Stern, 2012).

All three groups of toxins result in increased oxidative stress, to which the brain is particularly sensitive because of low levels of antioxidants and high levels of polyunsaturated fatty acids, highly susceptible to oxidation (Chin-Chan et al., 2015).

Protective factors

Protective factors against AD most likely act through positive effects on cognition and on the cardiovascular system. These factors include social engagement, education, diet and physical activity, and can be modified to decrease the risk of AD onset.

Association of lowered AD risk onset with regular exercise may stem from positive effects on cognition through increased cerebral blood flow, oxygenation and glucose consumption (Reitz & Mayeux, 2014) and reduced vascular risk, obesity and levels of inflammation (Chen, Jen-hau et al., 2009).

A balanced diet could have positive outcomes against AD onset thanks to lowered oxidative stress damage, and lowered risk of cerebrovascular accidents (Reitz & Mayeux, 2014).

Social engagement and education have also been linked to lower AD risk through epidemiological studies. Increased cognitive reserve allows preservation of cognition in patients that otherwise have developed A β and Tau pathologies in the brain (Stožická et al., 2007).

This section has provided an overview of AD, its potential causes and risk modifiers associated, highlighting its extreme complexity (Fig. 1.2). The next section focuses on ApoE, the major determinant for AD onset.

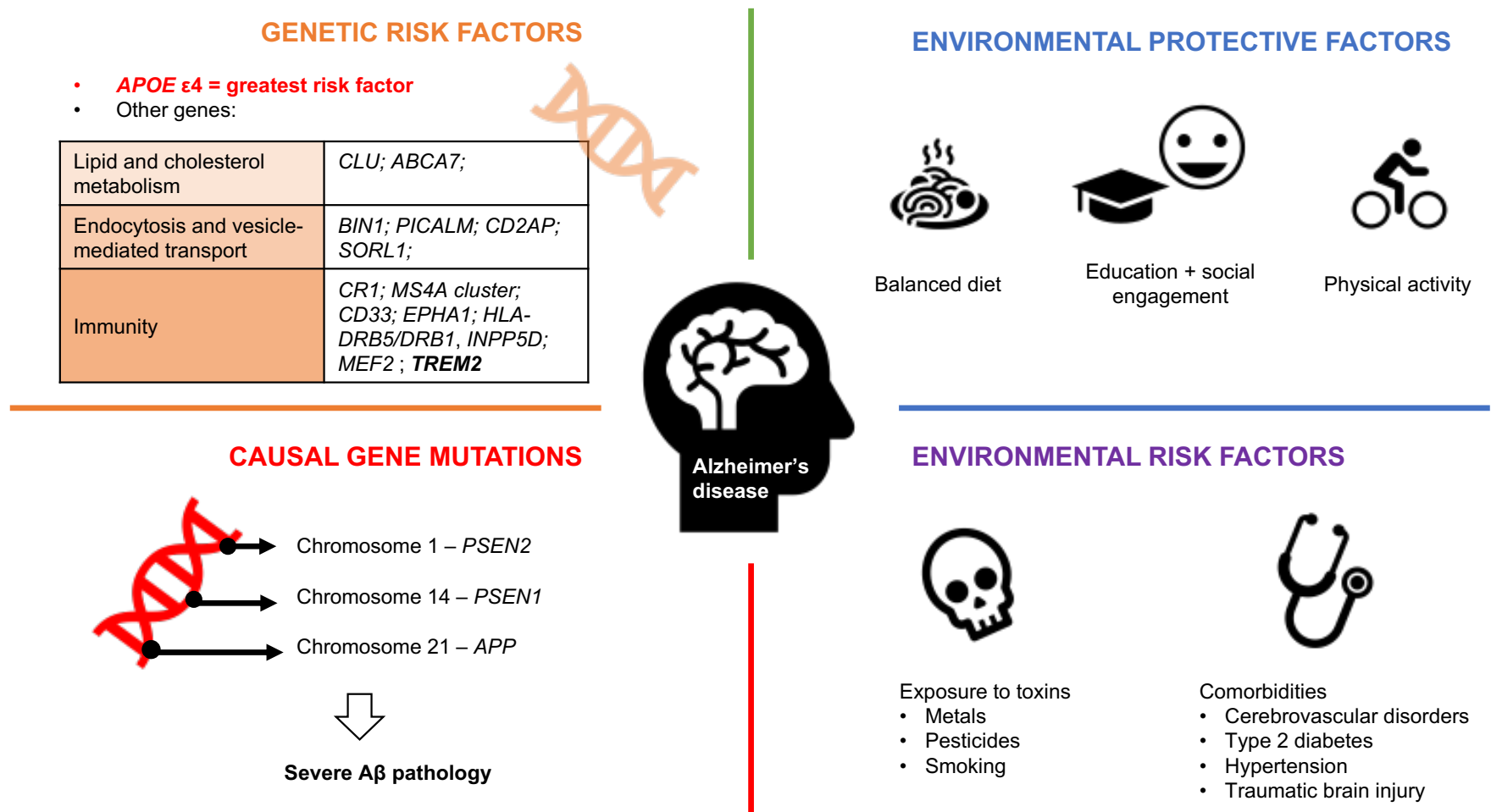


Figure 1.2 Genetic and environmental disease modifiers

Genetic and environmental factors modify the risk of AD onset. Causal genes lead to familial AD, and susceptibility genes increase the risk for LOAD. Environmental factors, both risk and protective, participate in modulating the risk of developing AD.

1.3. ApoE: discovery, structure and function

1.3.1. Discovery of ApoE

The discovery of ApoE is tied to investigation into human hyperlipidaemia, a group of diseases characterised by the build-up of very low-density lipoproteins (VLDL) abnormally rich in cholesterol in blood plasma (Havel & Kane, 1973).

Lipoproteins are macromolecules associating complex lipids such as triglycerides, cholesterol and phospholipids with one or more proteins termed apolipoproteins. There are six major classes of lipoproteins, differing in size and composition. Chylomicrons are the largest in size (diameter $d > 100$ nm); chylomicron remnants result from the action of lipoprotein lipase. They are followed by VLDL ($d = 30-90$ nm). Hydrolysis of VLDL by lipoprotein lipase at their target sites generates two other lipoproteins: intermediate low-density lipoproteins and low-density lipoproteins (LDL, $d \sim 20$ nm). Finally, high density lipoproteins (HDL) are the smallest lipoproteins ($d = 8-12$ nm) (Mahley et al., 1984).

VLDL that accumulate in patients with hyperlipidaemia have reduced electrophoretic motility and were designated as β -VLDL. Concomitant analysis proved that β -VLDL are in fact chylomicron remnants. Both were found to contain high levels of an arginine-rich protein (Havel & Kane, 1973), which had previously been described as a component of VLDL by Shore & Shore (Shore & Shore, 1973).

This arginine-rich protein was termed Apolipoprotein E by Utermann and colleagues in a study focused on the characterisation of VLDL isolated from patients with familial hyperlipoproteinemia type III, a disease co-occurring with premature atherosclerosis. Analysis of VLDL isolated from normolipidemic control patients by analytical isoelectric focusing gel electrophoresis evidenced the heterogeneity of ApoE which separated into three main components: ApoE-I, ApoE-II and ApoE-III. Comparison of VLDL from patients with familial hyperlipoproteinemia type III to controls demonstrated the absence of ApoE-III, which was thus postulated to serve as a biomarker for familial hyperlipoproteinemia. ApoE-III deficiency was postulated as responsible for the defective VLDL catabolism in familial hyperlipoproteinemia type III (Utermann et al., 1975). In a follow up study focusing on the genetics of the disease, Utermann et al described three different ApoE phenotypes based on their distribution of ApoE-II and ApoE-III: ApoE-N, ApoE-ND and ApoE-D, the latter corresponding to an ApoE-III deficiency in VLDL. ApoE patterns were mapped in three different kindreds, showing that ApoE phenotypes are inherited in a Mendelian fashion and determined by two autosomal alleles, *Apo Eⁿ* and *Apo E^d* (Utermann et al., 1977). However, the disproportionate frequency of the *Apo E^d*

allele in the absence of hyperlipoproteinemia led Utermann and colleagues to look for additional mutations responsible for the disease. They concluded that ApoE polymorphism arises from the existence of two codominant alleles previously identified at the ApoE-N/D locus, *Apo Eⁿ* and *Apo E^d*, as well as a dominant (*Apo E4⁺*) and a recessive allele (*Apo E4⁰*) at the Apo E4 locus (Utermann et al., 1980). Genetics of ApoE polymorphism was finally resolved by Zannis et al, whom explained the six identified subtypes of ApoE patterns in VLDL by the existence of three *APOE* alleles, $\epsilon 2$, $\epsilon 3$ and $\epsilon 4$ (Zannis & Breslow, 1980; Zannis et al., 1981) (Fig. 1.3) giving rise to three homozygous ($\epsilon 2/\epsilon 2$, $\epsilon 3/\epsilon 3$, $\epsilon 4/\epsilon 4$) and three heterozygous ($\epsilon 2/\epsilon 3$, $\epsilon 2/\epsilon 4$, $\epsilon 3/\epsilon 4$) genotypes. The resulting phenotypes agreed upon in the field are E2/2, E3/3 and E4/4 for homozygotes and E2/3, E2/4 and E3/4 for heterozygotes (Zannis et al., 1982).

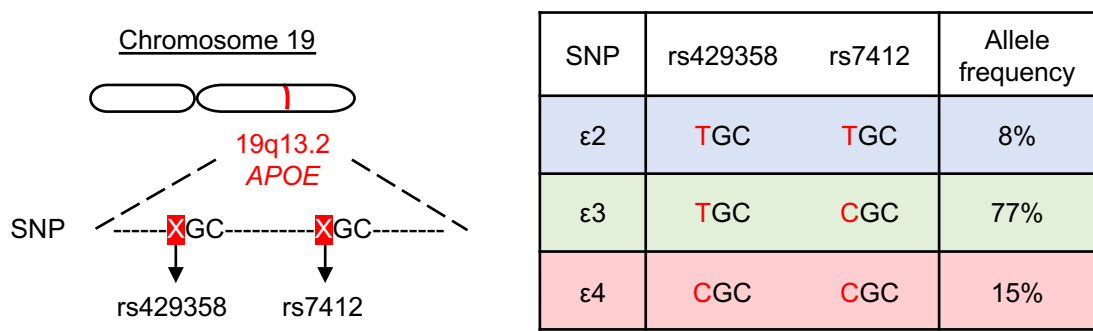


Figure 1.3 Representation of *APOE* polymorphism

Two single nucleotide polymorphisms (SNP), rs429358 and rs7412, lead to the allelic variation of *APOE*, located on chromosome 19. $\epsilon 2$ is the least frequent variant (8%), followed by $\epsilon 4$ (15%). $\epsilon 3$ is the most common allele (77%).

1.3.2. Structure of ApoE

The first identified difference between the three ApoE isoforms was their unique isoelectric focusing point: ApoE2 is the most acidic isoform, migrating to $pI \sim 5.4$, followed by ApoE3 with a pI of ~ 5.55 and finally, ApoE4 is the most basic one migrating to $pI \sim 5.75$ (Utermann et al., 1977) although these values vary: Weisgraber and colleagues have reported focusing points between pH 5.4 and 6.1 (Weisgraber et al., 1981).

Analysis of carbohydrate content in ApoE showed that ApoE from VLDL was modestly modified post-translationally, with sialic acid and galactose being the major carbohydrates present (Jain & Quarfordt, 1979). Additional bands detected in ApoE from

VLDL by isoelectric focusing gel electrophoresis corresponded to sialylated ApoE (Utermann et al., 1977). However, the vast majority of secreted ApoE (~80%) is not sialylated (Mahley et al., 1984).

Primary structure

Soon after the identification of the three *APOE* alleles and their resulting proteins, Weisgraber et al anticipated a difference between the isoforms in their respective primary sequences. Amino acid analysis revealed a Cys to Arg interchange in ApoE3 compared to ApoE2 which contains two Cys residues. They then developed a screening method to detect Cys residues in ApoE in a time-effective manner, by introducing an additional Cys per Cys residue through disulphide bridge formation using cysteamine. The additional Cys residue resulted in a shift by 2 positive charges in ApoE2 and 1 positive charge in ApoE3. Weisgraber et al used this screening technique on a E4/E4 subject. The absence of shift in charge following cysteamine treatment led them to conclude that ApoE4 lacks Cys residues but has an Arg instead, as demonstrated by amino acid analysis (Weisgraber et al., 1981).

The entire amino acid sequence of ApoE was promptly resolved by Rall et al in 1982: mature ApoE is a 299-amino acid polypeptide of approximately 34 kDa, and the three ApoE isoforms differ in their primary sequences at positions 112 and 158, whereby ApoE2 has two Cys, ApoE3 has a Cys and an Arg, and ApoE4 has two Arg (Rall, S. et al., 1982).

Secondary structure

Elucidation of ApoE's primary structure gave many indications as to what to expect in terms of secondary structure. Using the Chou-Fasman algorithm for the prediction of secondary structure, Rall and colleagues predicted ApoE to be highly α -helical (62%) with some β -turns (11%) and β -sheets (9%), and the remainder being random coil (18%). Amino acid composition also provides information relating to function. For instance, five out of eleven α -helical segments, mostly located in the C-terminal end of the protein, contain both a hydrophobic and a hydrophilic face, and amphipathic helices in apolipoproteins are involved in lipid binding (Rall, S. et al., 1982). Links between structure and function of ApoE isoforms will be discussed in more depth in the following section. Circular dichroism (CD) spectrum of ApoE in phosphate buffer supplemented with a reducing agent, confirmed its highly α -helical secondary structure, and no

significant changes in structure were detected in the presence of lipids (Yokoyama et al., 1985).

Tertiary structure

Denaturation studies allowed for a greater appreciation of the tertiary structure of ApoE. Changes in the secondary structure of ApoE3 in the presence of increasing concentration of guanidine hydrochloride (GuHCl), a chemical denaturant, were followed by CD, demonstrating the existence of two separate structural domains: a 22 kDa amino-terminal domain and a 10 kDa carboxy-terminal domain connected by a hinge region vulnerable to thrombin cleavage (Fig. 1.3B). The unfolding curve of ApoE3 also indicated the presence of a stable intermediate species (Wetterau et al., 1988). The presence of these two domains were later confirmed in ApoE2 and ApoE4 using recombinantly produced proteins (Morrow et al., 2000). The N-terminal and C-terminal fragments generated by thrombolytic cleavage have been used to model the two independent domains in ApoE.

Quaternary structure

Analytical ultracentrifugation (AUC) experiments conducted on intact ApoE suggested that it existed as a tetramer in aqueous solution (Yokoyama et al., 1985). Experiments later conducted on the two thrombolytic fragments of ApoE showed that tetramerization of ApoE was most likely mediated by the 10 kDa C-terminal fragment. The 22 kDa N-terminal domain was monomeric and globular in shape whereas the C-terminal fragment formed slightly elongated tetramers (Aggerbeck et al., 1988).

The exact structure of ApoE is far from being elucidated since there is no X-ray crystal structure of the full-length protein to date. The N-terminal domain of ApoE3 was crystallised in 1991. This domain comprises five α -helices, four of which are arranged in an anti-parallel, elongated four-helix bundle (Wilson et al., 1991). Relatively recent nuclear magnetic resonance (NMR) studies have provided information on the hinge region and the C-terminal domain. Interaction between the two terminal domains are modulated by the hinge region, which consists of two helices (Chen, J. et al., 2011).

An overview of the structure of ApoE at the primary, secondary, tertiary and quaternary levels is given in Fig. 1.4. The structure of ApoE isoforms will further be discussed in chapter 3.

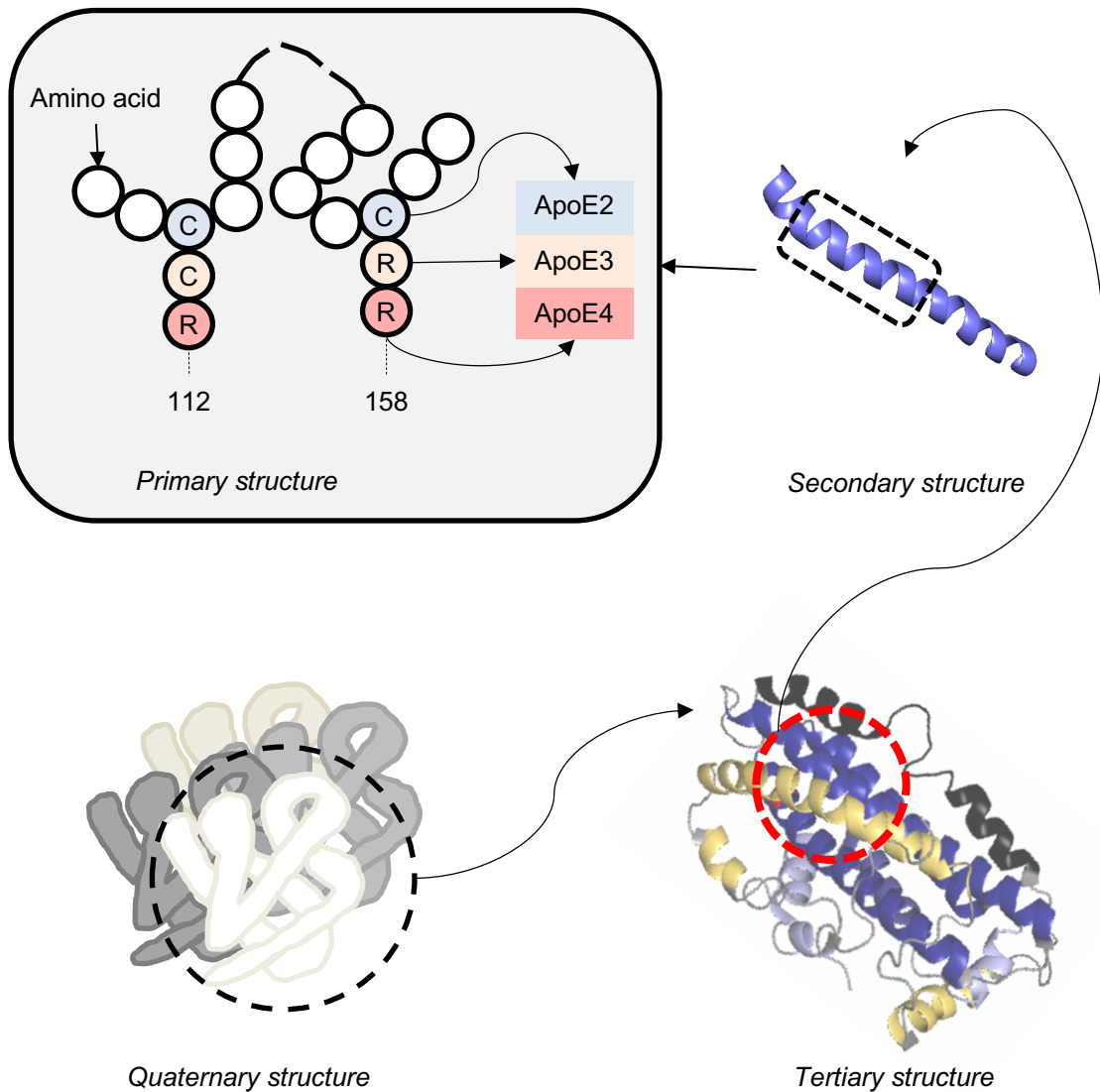


Figure 1.4 Structure of ApoE

ApoE isoforms differ in their primary amino acid sequence at position 112 and 158, where ApoE2 has two Cys (C), ApoE3 has a Cys and an Arg (R), and ApoE4 has two Arg. ApoE is a highly α -helical protein. The tertiary structure was generated from the NMR structure of ApoE3 (PDB 2L7B) – the amino-terminal domain is represented in blue, the hinge region in black, and the C-terminal domain in yellow. In solution, ApoE forms tetramers.

1.3.3. Physiological function of ApoE

Synthesis of ApoE

APOE, located on chromosome 19, is initially transcribed and subsequently translated into a 317 amino-acid precursor protein. The first 18 amino acids correspond to a signal

peptide that is cleaved to yield mature ApoE. *APOE* is for the most part transcribed in the liver in hepatic parenchymal cells; liver-produced ApoE accounts for 66-75% of total plasma ApoE (Mahley, 1988).

The second largest site of ApoE synthesis is the brain. Expression of ApoE in the brain was initially thought to be restricted to astrocytes (Boyles et al., 1985). However, ApoE was later detected in microglia and in neurons in AD tissue (Namba et al., 1991), and glia-independent neuronal ApoE synthesis was evidenced in response to injury (Aoki et al., 2003). In the periphery, ApoE was found in enteric glia and satellite cells, and in nonmyelinating Schwann cells (Boyles et al., 1985). ApoE is primarily involved physiologically in lipid metabolism both in the periphery and in the central nervous system (CNS) (Mahley, 1988; 2016).

The role of ApoE in lipid transport and metabolism is isoform-dependent

ApoE is involved in redistribution of lipid and cholesterol both within and outside their site of synthesis (Mahley, 1988). This function is a direct consequence of ApoE's structure.

- **Preferential lipid binding is mediated by domain interaction**

As was described in the previous section, ApoE C-terminal domain comprises amphipathic helices important for lipid binding (Rall, S. et al., 1982). Weisgraber demonstrated in 1990 that the N-terminal domain (1-191) of ApoE, modelled by the 22 kDa thrombolytic fragment, did not bind lipids, concluding that the carboxy-terminal domain (residues 206-299) was the region responsible for lipid binding (Weisgraber, 1990). The lipid binding domain of ApoE was later restricted to amino acids 244-272 (Dong et al., 1994) (Fig. 1.5).

ApoE is a component of chylomicrons, chylomicrons remnants, VLDL and a subclass of HDL. However, ApoE isoforms are differentially distributed among plasma lipoproteins as shown by agarose chromatography experiments. ApoE4 is particularly enriched in chylomicrons and VLDL, which are triglyceride-rich proteins. ApoE2 and ApoE3 are mostly associated with HDL, which are important in cholesterol redistribution. It is thus clear that the amino acid interchange at position 112 in the amino-terminal region has an impact on ApoE isoforms differential lipid-binding properties (Weisgraber, 1990; Mahley, 1988).

Even more so, this observation highlighted an interaction between the N-terminal and the C-terminal domains since the amino acid composition in the former impacts the lipid-

binding function of the latter. The so-called **domain interaction** was evidenced in a series of experiments (Dong et al., 1994) (Fig. 1.5):

- Identification of the exact amino acid stretch involved in modulating lipid binding preference: residues 260-272 were crucial for ApoE4 binding to VLDL rather than HDL;
- Role of Arg-112: residue 112 was not directly responsible for preferential binding modulation using rabbit and canine ApoE. Canine ApoE, which has an Arg similar to ApoE4, was distributed in a similar fashion to ApoE3 among human plasma lipoproteins;
- Examination of the crystal structure of the ApoE4 amino-terminal domain and comparison to that of ApoE3 highlighted a minor difference whereby the conformation of side chain of Arg-61 in ApoE4 is modified, promoting interaction with the C-terminal domain.

In a follow-up study, Dong and associates identified Glu-255 as the acidic residue interacting with Arg-61 in Ala mutagenesis experiments (Dong & Weisgraber, 1996).

- **Binding to lipoprotein receptors is also isoform-dependent**

Metabolism of chylomicrons, VLDL, their respective remnants and HDL by ApoE is mediated by its interaction with lipoprotein receptors from the LDL receptor family and with heparan sulfate proteoglycans (HSPGs) (Huang, Y. & Mahley, 2014). In the periphery, these ApoE-lipoprotein receptor bindings operate the uptake of lipids into hepatic and extrahepatic cells as well as the reverse cholesterol transport important in the removal of excess cholesterol from peripheral tissue (reviewed by Mahley, 1988). In the brain, ApoE synthesised mainly by astrocytes transports lipid and cholesterol to neurons through lipoprotein receptor binding (reviewed by Bu, 2009).

The receptor-binding domain of ApoE is confined to the N-terminal domain. Innerarity et al provided evidence that restricted the receptor-binding domain of ApoE to a 66 amino acid stretch starting at position 126, following a series of digestion and receptor-binding experiments (Innerarity et al., 1983). The three-dimensional structure of the LDL receptor-binding domain was later solved by X-ray crystallography. It is confined to helix 4, which is rich in basic residues available to interact with the receptor (Wilson et al., 1991).

After the ApoE isoforms were discovered, researchers could conclude that ApoE2 was the one linked to familial hyperlipoproteinemia type III where β -VLDL particles accumulate in the plasma. This accumulation was attributed to defective binding of ApoE2 to **ApoB,E-LDL receptor (LDLR)**. The source of this deficiency was targeted to

the amino acid substitution at position 158, where ApoE2 harbours a Cys instead of an Arg. Cysteine modification of Cys in ApoE2 generated a Lys analogue that resulted in increased binding of ApoE2 to LDLR in fibroblasts at levels similar to binding of ApoE3 and of ApoE4 (Weisgraber et al., 1982). Binding of ApoE to LDLR was later restricted to 6 to 8 amino acids in the 136-150 region, pointing to a role of residue 158 in modulating binding through conformational changes in this region (Mahley, 2016) (Fig. 1.5B).

LDLR is involved in VLDL and chylomicrons clearance through interaction with ApoE (Mahley & Huang, 1999). Chylomicron remnants can however be cleared through a different pathway: Kita et al reported in 1982 that chylomicron remnant clearance was unaffected in rabbits lacking LDLR, suggesting the existence of an additional lipoprotein receptor involved in lipid uptake, later identified as the **HSPG-LRP1** pathway (Kita et al., 1982). A series of crosslinking experiments in HepG2 cells allowed for the identification of the receptor responsible for remnant clearance: the LDL-receptor-related protein 1, LRP1. They did not report any isoform difference in terms of binding (Beisiegel et al., 1989). LRP1 is part of a bigger LDL-receptor-related protein family (reviewed by Bu, 2009).

In vitro studies conducted by Kowal and associates suggested that another protein must be involved to enable the interaction between ApoE and LRP1 since effective binding of chylomicron remnants to purified LRP1 required enrichment with ApoE (Kowal et al., 1989). This enrichment is mediated *in vivo* by HSPGs. Depletion of HSPGs following heparinase treatment in mice significantly decreased clearance of remnants through hepatic uptake (Ji et al., 1995).

Although the initial discovery of these receptors were made by looking at hepatic and extrahepatic transport of lipids by ApoE, they are relevant to ApoE's lipid and cholesterol transport in the brain since members of the LDLR, LRP1 and HSPGs families are expressed there as well: LRP1 is mainly expressed in neurons whereas LDLR is expressed in glia (reviewed by Bu, 2009).

- **Differential affinity for Heparin is dictated by residue-158**

Consistent with ApoE's interaction with HSPGs, ApoE binds to heparin through two heparin-binding sites, the first region spanning residues 129-160 and the second one in region 205-245 (Cardin et al., 1986). Arg to Cys substitution at position 158 impairs ApoE2 binding to heparin. Mann and associates showed that binding of ApoE2 to heparin was reduced by ~40% compared to binding of ApoE3 (Mann et al., 1995).

Fig. 1.5 gives an overview of the structure-function relationship in ApoE.

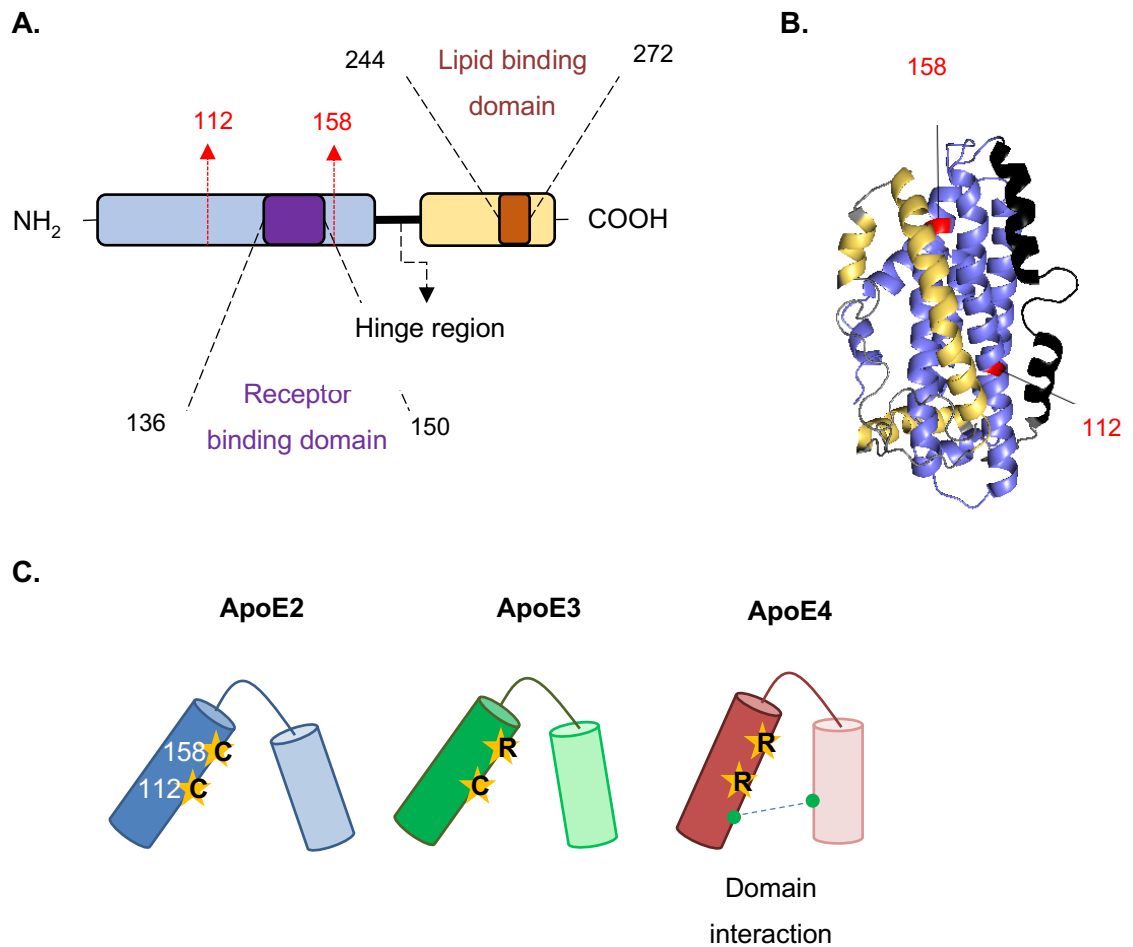


Figure 1.5 The structure of ApoE influences its function

A. ApoE is formed of two independent domains separated by a hinge region. The amino-terminal domain (blue) contains both amino acid substitution sites, residues 112 and 158 (in red), and the receptor binding domain which is contained within residues 136 and 150 (purple). The lipid binding domain of ApoE (copper) resides in its carboxy-terminal region (yellow) between residues 244 and 272.

B. NMR structure of ApoE3 (PDB 2L7B) – the amino-terminal domain is represented in blue, the hinge region in black, and the C-terminal domain in yellow. Amino acid substitution sites are indicated in red.

C. Schematic of ApoE tertiary structure highlights the amino acid substitutions at positions 112 and 158 (yellow stars), and the existence of domain interaction in ApoE4 (green dashed line linking the two domains). The tertiary structure of ApoE2 and ApoE3 is more opened than that of ApoE4. Inspired by Kanekiyo et al., 2014.

Response to injury, neurite outgrowth and cytoskeletal function

Given its role as a lipid transport protein, it is unsurprising that ApoE is also involved in repair and regeneration mechanisms.

- **In the periphery**

ApoE expression was dramatically increased following nerve injury in the rat (Ignatius et al., 1986). Boyles and colleagues provided an overview of the mechanisms involving ApoE: as axons degenerate and Schwann cells uptake myelin, resident and monocyte-derived macrophages start producing large amounts of ApoE. Cholesterol is delivered to macrophages by ApoE for storage. Initiation of the regeneration process is accompanied by increased LDLR receptors in axon tips, and Schwann cells also start to express LDLR during the remyelination phase enabling ApoE-mediated uptake of lipids and cholesterol for repair and neurite outgrowth (Boyles et al., 1989). An isoform-dependent impact of ApoE on neurite outgrowth was later reported, with ApoE3 promoting and ApoE4 inhibiting neurite extension in the dorsal root ganglion in rabbits (Nathan et al., 1994).

- **In the CNS**

Under physiological conditions, ApoE is mainly produced by astrocytes and participates in cholesterol and lipid transport, essential to synapse formation and repair (reviewed by Bu, 2009). Astrocyte-secreted ApoE, similar to macrophage-secreted ApoE, plays a role in neurite outgrowth following injury. The impact of ApoE on neurite outgrowth following entorhinal cortex lesion in a mouse model expressing either human ApoE3 or human ApoE4 by astrocytes was also proved to be isoform dependent, with astrocyte-secreted ApoE3 being an enhancer (Sun et al., 1998).

Unlike what was long believed, astrocytes are not the sole cell type to synthesise ApoE. For instance, neuronal ApoE synthesis was first identified in the hippocampus of rats in neurons that survive excitotoxic stress induced by kainic acid injection (Boschert et al., 1999). This was later supported in human, upregulation of neuronal ApoE after cerebral infarction (Aoki et al., 2003).

This will be discussed further in section 1.4 and in chapter 4.

1.4. ApoE is the major risk factor for AD

The role of ApoE in cardiovascular disorder was well established by 1993. Although ApoE is not a direct culprit, the presence of one isoform over the other can increase the risk for atherosclerosis. ApoE2 is associated with impaired lipoprotein receptor binding, facilitating the accumulation of remnants and cholesterol in the plasma and subsequently the arteries; and ApoE4 is associated with build-up of LDL as a consequence of its preferential binding to VLDL.

A role in neurobiology was also suspected. ApoE had already been linked to nerve regeneration following injury through its cholesterol transport function and more generally to neurite outgrowth, as presented in the previous section. This section focuses on a summary of the main findings that have linked ApoE, and more particularly ApoE4, to AD.

The first evidence linking ApoE to AD came from examination of brain tissue with amyloid pathologies. Immunostaining of AD and Creutzfeldt-Jacob disease (CJD) brain sections with an ApoE antibody revealed localisation of ApoE to NFT, amyloid plaques and blood vessels in AD and to prion plaques in CJD. ApoE was also localised to diffuse plaques which contain amorphous A β aggregates as opposed to well-defined amyloid fibres, suggesting a potential role of ApoE in amyloid deposition (Namba et al., 1991). Association of ApoE with NFTs provided the first evidence of localisation of ApoE in neurons; however, ApoE in neurons could well be internalised astrocyte-secreted ApoE (Namba et al., 1991).

There is also evidence for an isoform-dependent effect of ApoE on synaptic plasticity and cognition, lipid and cholesterol metabolism, oxidative stress and neuroinflammation.

1.4.1. ApoE and A β

Building on the evidence localising ApoE to A β plaques, interactions between ApoE and A β were investigated. CSF from control and AD patients was incubated with immobilized recombinant A β . Resolution of bound proteins by gel electrophoresis and immunoblotting led to the identification of ApoE and sialylated ApoE as A β binding partners. Stritmatter and associates also confirmed the localisation of ApoE to senile plaques in AD brain tissue and observed co-localisation of ApoE with A β . They also confirmed staining of ApoE in neurons and around blood vessels. Finally, by screening for *APOE* status in 30 familial AD families, they reported an increased frequency of *APOE* ϵ 4 allele in familial

AD patients (52%) compared to controls (16%). These results provided the first evidence for a link between ApoE4 and AD (Strittmatter et al., 1993a). In addition to this, the extent of amyloid pathology in sporadic AD cases was reported greater in the cerebral cortex of $\epsilon 4$ carriers, especially in the vasculature (Schmechel et al., 1993).

Binding of ApoE to A β suggests a possible role for ApoE in modulating both A β deposition and A β clearance from the brain. It may however not be the only way that ApoE influences A β pathology. For instance, the increase in levels of A β deposition associated with ApoE4 also suggests a role of ApoE in modulating A β production (Fig.1.6).

Differential binding of ApoE isoforms to A β and consequences on deposition and clearance

- **Binding of ApoE to A β**

Reports on differential binding of ApoE isoforms to A β are discrepant, with controversial results arising from the source of ApoE employed in binding studies.

In 1993, Strittmatter and colleagues reported that both delipidated ApoE3 and ApoE4 purified from plasma formed SDS-stable complexes with recombinant A β at 37°C, but that ApoE4-A β complexes were formed more readily. Abolition of complex formation and complex dissociation under reducing conditions suggested a role for methionine oxidation of ApoE in binding to A β (Strittmatter et al., 1993b). A year later, LaDu et al provided evidence to the contrary, with ApoE3-A β complexes being formed more readily than ApoE4-A β at 37°C. Recombinant ApoE used in that study was secreted by human kidney cells (LaDu et al., 1994). These results were later extended to include ApoE2, using ApoE secreted by hamster kidney cells, with the efficiency to form complexes with A β at 37°C being ApoE2>ApoE3>>ApoE4 (Aleshkov et al., 1997). Binding of ApoE to A β is thus dependent on the isoform and the lipidation status of ApoE.

These *in vitro* studies were later complemented by the isolation of ApoE-A β complexes from AD brain supernatants (Permanne et al., 1997). Moreover, targeting these complexes *in vivo* resulted in decreased A β pathology and amelioration of cognition in an APP mouse model of AD (Liu, S. et al., 2017).

- **Effect of ApoE on A β aggregation**

A role of ApoE in A β aggregation process was supported by a study conducted in an APP mouse model of AD, whereby knocking-out mouse *APOE* significantly reduced the extent of amyloid deposits (Bales et al., 1999). In an APP mouse model where mouse

APOE was replaced with human *APOE*, the $\epsilon 4/\epsilon 4$ genotype was associated with increased levels of A β and increased A β deposition compared to the mice expressing ApoE3 (Bales et al., 2009). Similarly, in healthy individuals, the $\epsilon 4$ allele was associated with higher rates of accumulation of A β (over ~4 years) and allele $\epsilon 2$ with the lowest as assessed by PET imaging (Lim & Mormino, 2017).

In vitro studies on the effect of ApoE on A β aggregation are more controversial. Delipidated ApoE accelerates *in vitro* A β fibril formation at room temperature in an isoform dependent manner, with ApoE4 enhancing A β fibrillization the most and ApoE2 the least (Ma et al., 1994). Alternatively, others have posited that all three ApoE isoforms kinetically inhibit A β fibril formation (Evans, K. C. et al., 1995; Wood, Chan, et al., 1996a), with ApoE4 potentially being less efficient at it (Kanekiyo et al., 2014). Wood and associates suggested that discrepancies may have arisen from differences in material used and different experimental conditions (Wood, Chan, et al., 1996b). Since the presence of ApoE has no effect on A β seeding properties (Evans, K. C. et al., 1995), presence of any seed contaminant in the A β preparation could mask the inhibitory effect of ApoE.

ApoE as a kinetic inhibitor of A β fibril formation was recently corroborated. Both lipidated and nonlipidated ApoE delayed A β aggregation, and ApoE4 was more efficient at it than ApoE3 (Ghosh et al., 2019).

In vivo and *in vitro* studies presented here have pointed to a paradoxical role of ApoE since it promotes A β deposition *in vivo* but inhibits A β aggregation *in vitro*.

- **ApoE isoforms and A β clearance**

The role of ApoE in diminishing A β pathology by clearance of soluble A β was first proposed in 1993, when ApoE4 was originally associated with AD. This role was imputed to ApoE being a ligand of LRP1, facilitating the endocytosis of ApoE- A β and thus reducing A β levels (Rebeck et al., 1993).

Investigation into ApoE-mediated clearance of A β across the blood-brain barrier in mice revealed that clearance of A β was particularly disrupted with ApoE4, by examining clearance of ApoE- A β complexes injected in their caudate putamen. This was attributed to a shift in clearance from the LRP1 receptor to the VLDLR receptor, which internalises ApoE4-A β slower. ApoE2- and ApoE3-A β complexes were cleared faster through LRP1 and VLDLR (Deane et al., 2008).

Alternatively, ApoE could impair clearance of A β by competitively binding to lipoprotein receptors and thus leading to A β accumulation. ApoE and A β share a number of cell

surface lipoprotein receptors as binding partners, such as LRP1 (Deane et al., 2008) and HSPGs (Fu et al., 2016). For instance, astrocyte-secreted human ApoE inhibited A β uptake into CHO cells by antagonising A β binding to HSPGs (Fu et al., 2016).

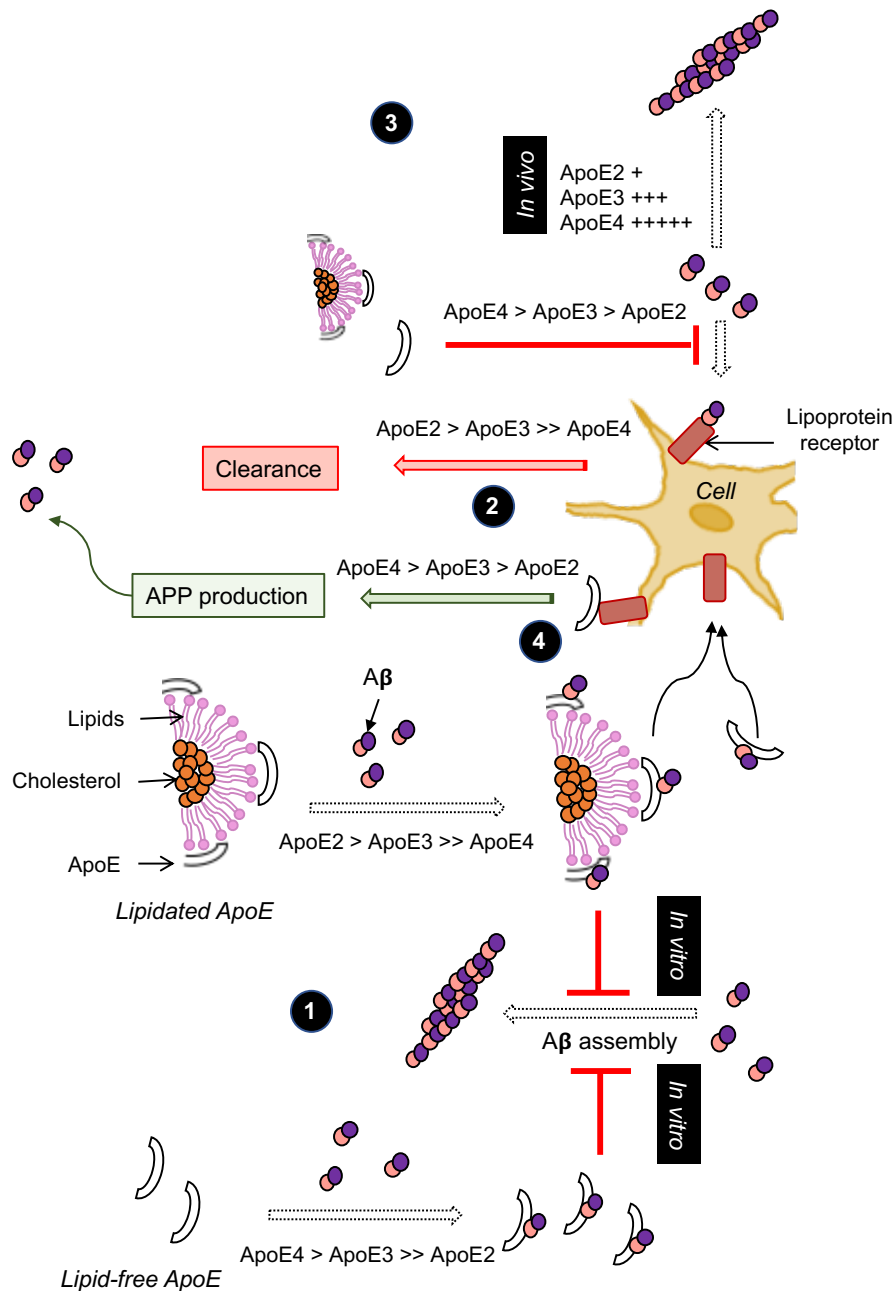


Figure 1.6 Binding of ApoE to A β and consequences on A β pathology

ApoE forms complexes with A β . A β binds more readily to lipidated ApoE2; however, it has greater affinity for nonlipidated ApoE4. *In vitro*, formation of ApoE-A β complexes inhibit A β deposition (1). ApoE can participate in A β clearance by facilitating A β endocytosis through lipoprotein receptors. Due to differential receptor binding preferences, ApoE4-A β are cleared at a slower rate (2). ApoE can also participate in A β accumulation by inhibiting A β uptake through lipoprotein receptors, enhancing A β deposition. *In vivo*, this is favoured by ApoE4 (3). Through receptor binding, ApoE can also modulate APP processing and subsequent A β production (4).

Modulation of APP processing and resulting A β production by ApoE

APP processing can be modulated by a number of lipoprotein receptors. Binding of ApoE to these receptors can either promote or inhibit APP endocytosis. Enhancement of APP endocytosis trafficking results in increased A β by promotion of APP amyloidogenic processing by BACE1 in endosomes (reviewed by Bu, 2009).

Addition of lipid-poor or lipid-free recombinant ApoE4 to rat neuroblastoma cells overexpressing human APP resulted in enhanced APP recycling and subsequent increased A β levels to a greater extent than when lipid-poor or lipid-free recombinant ApoE3 was added. Isoform-dependent effects on A β production were abolished when ApoE isoforms were lipidated. This differential effect of ApoE on APP recycling was proved to be mediated by action on LRP1 since blockage of the LRP1 pathway abolished differences between the isoforms (Ye et al., 2005). Other ApoE receptors, such as LRPB1, ApoER2 and SORL1 also modulate APP trafficking and processing (reviewed by Bu, 2009).

A recent report provided evidence for an isoform-dependent stimulation of APP transcription in human embryonic stem-cell-derived neurons by glia-secreted ApoE, with ApoE4>ApoE3>ApoE2 (Huang, Y.-W. A. et al., 2017).

A simplified overview of the ways ApoE can influence A β pathology is provided in Fig. 1.6.

1.4.2. ApoE and tau pathology

Although mostly expressed by glia in the brain, ApoE is expressed by neurons following stress or injury (see 1.3.3). Neuronal ApoE could be detrimental, depending on the isoform expressed. ApoE4 is more prone to proteolytic cleavage than ApoE3. The generated C-terminal fragments interact with phosphorylated Tau resulting in NFT-like neuronal inclusions in cell models but also in AD brains (Huang, Y. et al., 2001). In mice, these neuronal fragments of ApoE were found to be associated with increased Tau phosphorylation, particularly in neuronal ApoE4-expressing mice (Brecht et al., 2004). In human induced pluripotent stem cells, neuronal ApoE4 was also associated with increased Tau hyperphosphorylation (Wang et al., 2018).

Tau pathology seems to be exacerbated in ϵ 4 carriers. This was true in a human ApoE expressing mouse model of tauopathy, where ApoE4 increased atrophy, neuronal death

and microglial activation (Shi et al., 2017); and in AD patients, a correlation between CSF Tau levels and impairments in cortical plasticity and cognition, in addition to astrocyte survival was only observed in $\epsilon 4$ but not $\epsilon 3$ carriers (Koch et al., 2017).

1.4.3. ApoE in additional AD pathologies

Synaptic dysfunction and cognitive impairment in AD

The *APOE* status differentially participates in synaptic dysfunction, cognitive impairment and behavioural deficits in AD. For instance, an ApoE2 background prevented loss of dendritic spines in two different mouse models of AD (Lanz et al., 2003). In a different model of AD, ApoE4 background was associated with reduced locomotor activity and impaired memory function compared to human ApoE3-expressing mice (Kornecook et al., 2010). Functional brain imaging in elderly healthy $\epsilon 4$ carriers revealed functional and white matter network irregularities overall. Their right parahippocampal gyrus, a region modulating the impact of the *APOE* status on memory function, had both functional and structural white matter damage (Chen, Y. et al., 2015).

ApoE and neuroinflammation in AD

In neurodegenerative disorders, including AD, microglia lose their homeostatic function because of a switch to a chronic inflammation state. Recently, *APOE* was identified as a regulator of said switch in a subset of microglia that are common to various disorders such as amyotrophic lateral sclerosis and multiple sclerosis, in mouse models of these diseases. The switch was initiated through activation of TREM2 by apoptotic neurons, resulting in an ApoE signalling cascade starting with upregulation of ApoE expression, which in turn suppressed homeostatic microglial function and induced an inflammatory programme (Krasemann et al., 2017).

In a mouse model of AD having received bone marrow transplant (which ends in a replacement of host microglia with donor microglia) from either human ApoE3- or human ApoE4-expressing mice, inflammation was exacerbated in the ApoE4- recipient compared to ApoE3-recipients, with increased levels of the pro-inflammatory cytokine tumour necrosis factor- α and decreased levels of the anti-inflammatory cytokine interleukine-10 (Yang et al., 2013).

Extensive research has been conducted on the links between ApoE and $A\beta$, and to a lesser extent on the links between ApoE and Tau pathology. Relationships between *APOE* status and other hallmarks such as synaptic dysfunction, cognitive impairments, cholesterol levels and neuroinflammation among others have also been explored. Fig. 1.7 summarises the gain of toxic function and loss of function associated with ApoE4.

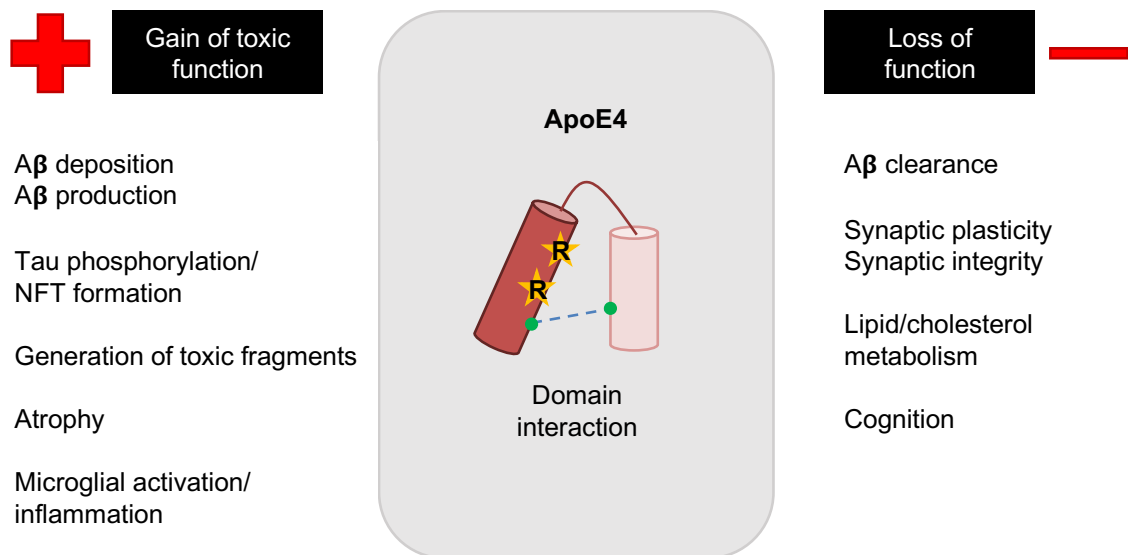


Figure 1.7 Gain of toxic function/ loss of function associated with ApoE4

ApoE4 exacerbates $A\beta$ pathology by promoting $A\beta$ production and its accumulation, and by impairing its clearance. ApoE4 is associated with increased Tau phosphorylation and tangle formation. By aggravating Tau pathology and synaptic dysfunction, ApoE4 increases brain atrophy and cognitive impairment. Through its binding to TREM2, ApoE4 is also implicated in microglial activation and subsequent inflammation. ApoE4 also generates neurotoxic fragments through proteolytic cleavage. These gain of toxic/loss of function are in addition to impaired lipid and cholesterol metabolism associated with ApoE4.

In the following three sections, differences between the ApoE isoforms will be explored in the context of protein misfolding and aggregation, oxidative stress and ageing, independently of other pathological features of AD in order to have a better appreciation of how ApoE4 sets the stage for AD onset. Differences between the ApoE isoforms in other contexts such as synaptic dysfunction or inflammation are currently explored by other research groups.

1.5. ApoE in the context of protein misfolding and aggregation

Protein misfolding and aggregation is at the centre of a number of neurodegenerative diseases in addition to AD, such as PD, Huntington's disease or amyotrophic lateral sclerosis to name a few. These disorders are distinct in the nature of the proteins implicated but share commonalities in cellular and molecular processes leading to build up of abnormal aggregates (Ross & Poirier, 2004).

This section gives a brief overview of the pathways bringing a protein in its native state to misfold and self-assemble into neurotoxic entities.

1.5.1. Protein misfolding and aggregation

Following synthesis on ribosomes, proteins adopt the most thermodynamically stable structural conformation that is innately related to their intrinsic biophysical properties (Anfinsen, 1973). Reaching a native folding state in the cell involves a number of partners such as molecular chaperones (Dobson, 2003). However, protein folding can go awry, especially with increasing age and the resulting cellular oxidative stress, despite mechanisms in place to correct errors. Incorrectly folded proteins can no longer perform their normal function and tend to accumulate, further increasing cellular stress and impairing normal cell functioning. Cells have mechanisms in place to remove these accumulating misfolded proteins; however, once these systems are overwhelmed, cells can no longer clear them out and misfolded proteins self-assemble to create filamentous structures that can themselves accumulate into bigger organised structures (Basaiawmoit & Rattan, 2010).

Protein folding and misfolding

Protein folding into their native state is not a linear mechanism. Dynamic folding and unfolding of the protein facilitate contacts between amino acids until reaching the state of lowest energy. Intermediates formed during the fluctuation process of folding can interact with their surroundings, such as the solvent, kinetically trapping the protein in this intermediate state (Kim, Y. E. et al., 2013). Attaining and maintaining proper folding in the crowded environment that constitutes cells requires the help of other proteins called molecular chaperones. A quality-control system relying on protein glycosylation and de-glycosylation allows differentiation between properly folded and misfolded

proteins. Misfolded proteins failing this quality-control test are targeted for degradation to the ubiquitin-proteasome system (Dobson, 2003; Kim, Y. E. et al., 2013). Cellular stress, by the way of changes in the microenvironment of the cell, may saturate quality-control mechanisms in place and/or overwhelm the degradation systems, leading to accumulation of misfolded proteins.

Protein aggregation

Proteins expose hydrophobic residues to the solvent in the process of misfolding, which tends to favour aggregation. Aggregates can adopt different structures. For instance, early aggregates may be amorphous or form ring-like structures (Dobson, 2003). Larger aggregates cannot be degraded by the ubiquitin-proteasome system but may be removed by autophagy (Kim, Y. E. et al., 2013). In the absence of degradation, these early aggregates can further assemble into morphologically defined species called protofilaments that are varied in size and shape. They can carry on assembling into mature fibrils (Dobson, 2003).

Many neurodegenerative diseases are characterised by the formation of degradation-resistant amyloid fibrils. Amyloid fibrils (Fig. 1.8) constitute a very specific kind of fibres formed of β -strands running perpendicular to the fibre axis, stacked into β -sheets through hydrogen bonds parallel to the fibre axis (Rambaran & Serpell, 2008). The process of amyloid fibril formation involves a switch from native conformation to β -sheet, and this can be detected by CD spectroscopy (Marshall et al., 2016). Aggregation can be detected using dyes, such as Thioflavin-T (ThT) and Congo red, which have historically been used to probe for amyloid fibres. Interaction of Congo red with amyloid fibres results in a green birefringence under cross polarised light (Rambaran & Serpell, 2008). ThT is now preferentially used to monitor assembly processes. Upon interaction with amyloid fibres, ThT undergoes a spectral change with emission at ~ 483 nm following excitation at 450 nm (LeVine, 1999; Marshall et al., 2016) (Fig. 1.8B).

Partially aligned amyloid fibrils display a characteristic cross- β pattern by X-ray fibre diffraction, with a meridional reflection of 4.7 Å along the fibril axis corresponding to the distance between β -strands and an equatorial reflection of 10 Å perpendicular to the fibril axis, which is the distance separating β -sheets (Morris & Serpell, 2012) (Fig. 1.8C).

Morphologically, amyloid fibres are straight, long and lack any branching as can be seen by transmission electron microscopy. Their length is variable, and their width is around 10 nm (Marshall & Serpell, 2009) (Fig. 1.8A).

A number of biophysical techniques mentioned here can be employed to characterise fibrils. In this thesis, CD spectroscopy, fluorescence spectroscopy, transmission electron microscopy, and X-ray fibre diffraction have been used. An overview of the basis of those techniques is given in chapter 2.

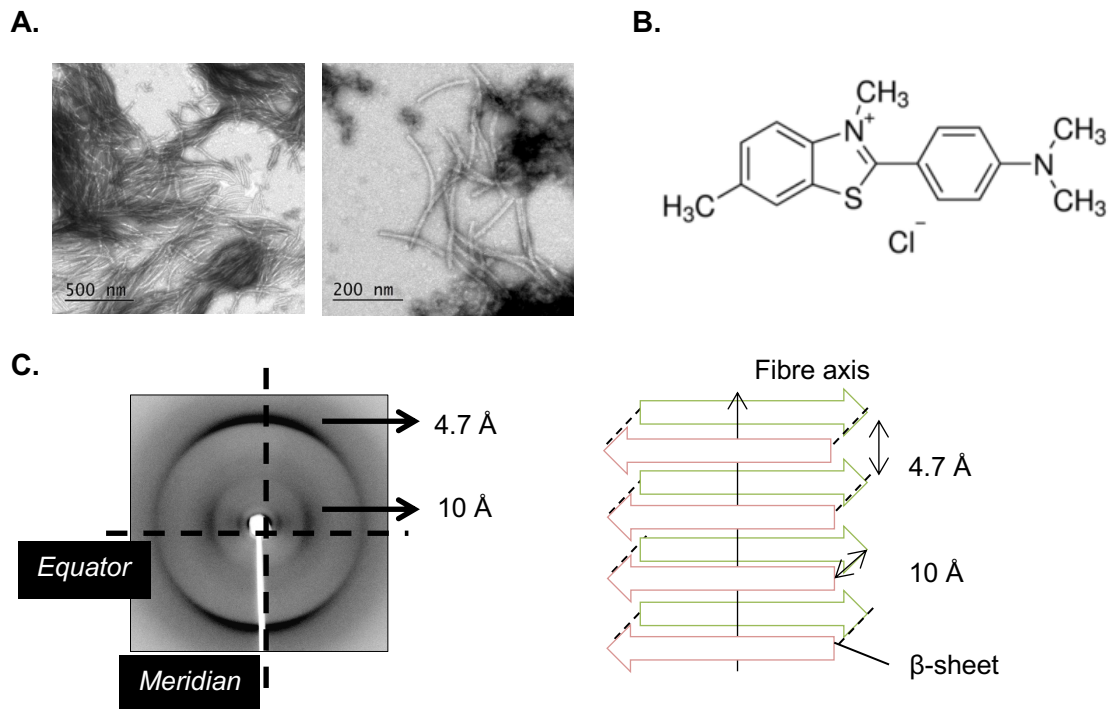


Figure 1.8 Amyloid fibrils

A. Electron micrograph of amyloid fibres – A fragment of Tau was assembled at 37°C for 24 to 48 h with shaking. Resulting fibres are of various length and straight. Scale bar: left – 500 nm; right – 200 nm.

B. Chemical structure of ThT. When interacting with fibrils, ThT emits at 483 nm following excitation at 450 nm.

C. (Left) X-ray fibre diffraction of a partially aligned amyloid fibre (provided by Prof. Louise Serpell). Amyloid fibres display a characteristic cross- β pattern, with a sharp reflection on the meridian at 4.7 Å and a reflection on the equator at 10 Å. (Right) 4.7 Å corresponds to the distance between β -strands and 10 Å to the distance separating β -sheets; adapted from Serpell, 2000.

1.5.2. Evidence for differential, isoform-dependent propensity for ApoE to aggregate

In a given environment, protein folding is determined by its primary amino acid sequence (Anfinsen, 1973). The three ApoE isoforms only differ at one to two amino acid positions,

but that substitution is enough to have an impact on their respective folding, and hence their function.

ApoE4 can form molten globules

Examination of the chemical denaturation profiles of the amino-terminal fragment of ApoE suggested the existence of thermodynamically stable intermediates particularly in ApoE4, and to a lesser extent in ApoE3 (Morrow et al., 2000; 2002). Increased susceptibility of the intermediates to pepsin digestion proved that ApoE4 intermediates had partly lost their structural integrity at the tertiary level. Conformational alterations occurred with partial retention of α -helical structure. Dynamic light scattering revealed that the ApoE4 intermediates are compact and slightly elongated. The larger hydrodynamic radius was consistent with a partial opening of the four-helix bundle that would result in exposure of the hydrophobic backbone (Morrow et al., 2002). A molten globule is a compact structure with exposed hydrophobic core that has retained most of the native secondary structure while losing the native tertiary structure. The evidence provided by Morrow and associates is thus consistent with ApoE4, and not the other two isoforms, having the propensity to form molten globules (Morrow et al., 2002).

The propensity of ApoE4 to form molten globules through its amino-terminal domain may implicate it in AD pathogenesis through multiple mechanisms such as aggregation, membrane disruption and functional alterations (reviewed by Zhong & Weisgraber, 2009).

Self-assembly of ApoE

The differential propensity of ApoE to co-aggregate with A β was presented in section 1.4.1. Evidence for self-assembly of ApoE isoforms independently of A β is limited. Hatters and colleagues provided data attesting to ApoE4's propensity to form neurotoxic amyloid-like fibrils due to its molten globule state, at 37°C and neutral pH. ApoE3 and ApoE2 were also reported to form these aggregates but at a slower rate (Hatters et al., 2006). There is also evidence for ApoE aggregates forming at acidic pH, closer to that of lysosomes (Garai et al., 2011). The possible existence of ApoE aggregates could have implication for neurotoxicity and for facilitating amyloid deposition by acting as a potential chaperone (Zhong & Weisgraber, 2009).

The exact nature of these aggregates is unclear from their report and needs further exploration. This topic will be examined more closely in chapter 3.

1.6. ApoE and oxidative stress

1.6.1. Oxidative stress in AD

Definition of oxidative stress and associated damages

Oxidative stress plays an important role in a wide range of neurodegenerative disorders, including AD, and in ageing. It occurs when the balance between oxidants and antioxidants is disrupted towards the formation of reactive oxygen species (ROS) and reactive nitrogen species (RNS). Those species include free radicals and some other molecules such as hydrogen peroxide (H_2O_2) and peroxynitrite ($ONOO^-$) (Huang, W.-J. et al., 2016).

Free radicals are atoms or molecules with a single unpaired electron in their outer orbit. Hydroxyl ($HO\bullet$), superoxide ($O_2^{\bullet-}$) and nitric monoxide ($NO\bullet$) are the most common reported cellular free radicals (Romano et al., 2010; Huang, W.-J. et al., 2016). ROS are normally generated by all eukaryotic cells as a by-product of aerobic respiration in mitochondria. Electrons leaking out of the electron transport chain can attack oxygen, producing superoxide (Romano et al., 2010).

ROS/RNS production is regulated by the antioxidant defence system. Antioxidants can be divided into two categories, enzymatic and non-enzymatic. The principal antioxidant enzymes are superoxide dismutase (SOD), catalase (CAT) and glutathione peroxidase (GPx). SOD catalyses the dismutation of superoxide radicals to H_2O_2 and oxygen; the H_2O_2 formed can further be reduced to water by the action of either CAT or GPx (Romano et al., 2010). Non-enzymatic antioxidants also participate in the maintenance of the redox state in cells. Cells are rich in glutathione (GSH), and additional antioxidants such as vitamins C and E, carotenoids and polyphenols are derived from diet (Poljsak & Milisav, 2013).

Cells are not the only source of free radicals. Indeed, environmental toxins (cigarette smoke, pesticides), heavy drinking, and other harmful substances constitute a reservoir of free radicals that can trigger oxidative stress (Poljsak & Milisav, 2013). A redox imbalance in the cell whereby the antioxidant system cannot neutralise free radicals results in an overexposure to ROS/RNS that can lead to extensive oxidation of biomolecules, including lipids, DNA and proteins. Proteins are one of the major targets of ROS, as their amino-acid residues including Cys, Met, Trp, Tyr and His among others can undergo various types of modifications.

Protein oxidation can have several consequences, such as conformational alterations affecting function. Structural changes following protein oxidation can also result in production of misfolded proteins and subsequent protein aggregation (Davies, M. J., 2005).

Fig. 1.9 illustrates oxidative stress and associated damages in cells.

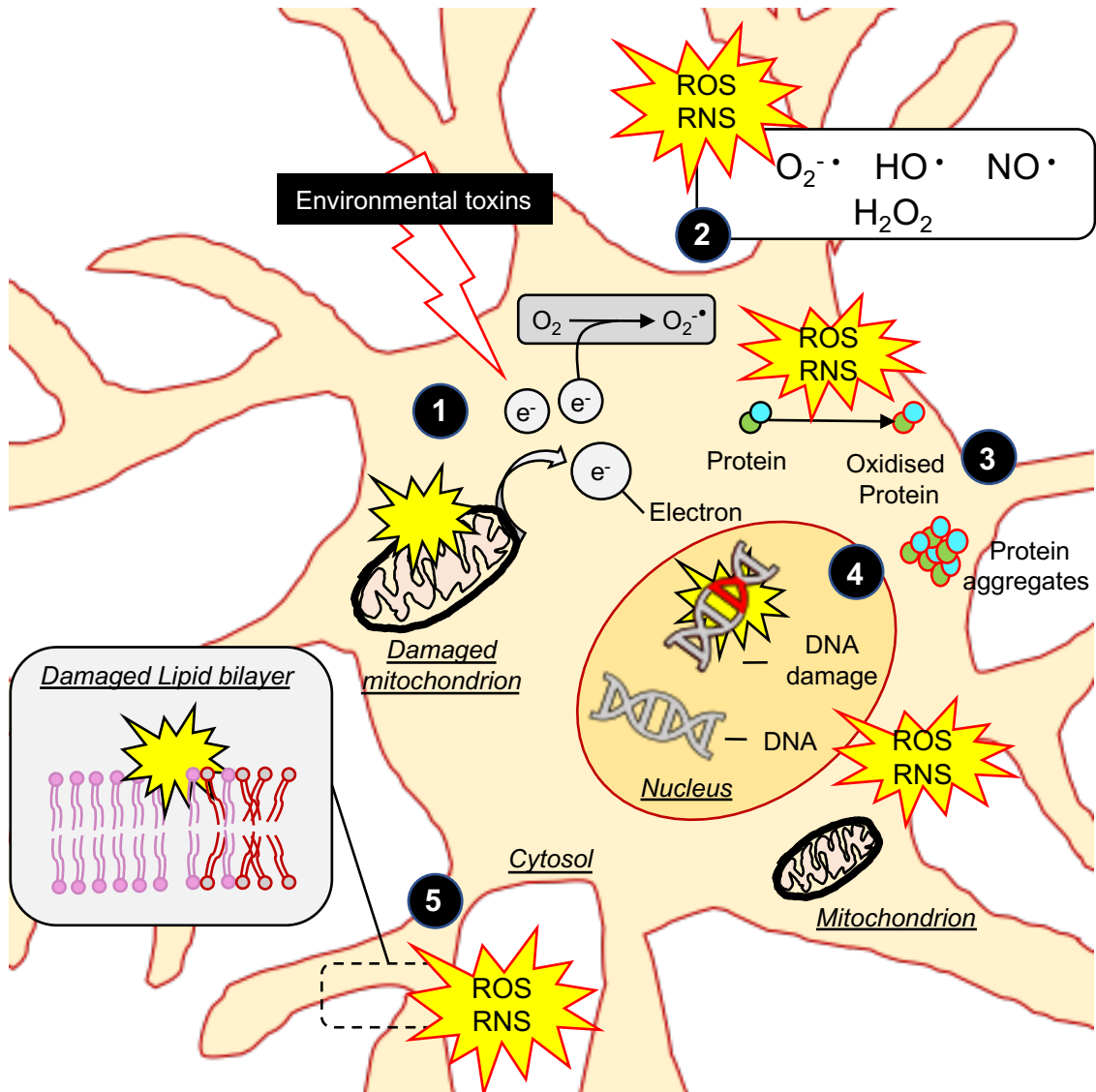


Figure 1.9 Oxidative stress and oxidative damage

Environmental toxins and other sources of stress such as protein aggregates can damage mitochondria. As a result, electrons start leaking out of the electron transport chain and can attack oxygen for example, to form highly reactive free radicals (1). ROS and RNS include free radicals and other species like H₂O₂ (2). ROS/RNS can in turn cause a series of damage in the cell. Protein oxidation leads to altered protein function and can also end in protein aggregation (3). In the nucleus, ROS/RNS can damage DNA (4). Finally, ROS/RNS can also attack lipids. Lipid peroxidation and other modifications can for instance disrupt cell membranes (5).

Evidence for altered oxidative balance in AD

The brain is an organ particularly rich in lipids composed of polyunsaturated fatty acids that are easily oxidised. Moreover, it has a very high oxygen consumption rate and relatively low levels of antioxidants compared to other organs. The brain is thus extremely vulnerable to oxidative stress (Huang, W.-J. et al., 2016; Castellani et al., 2009).

Oxidative damage to lipids, nucleic acids and proteins have been evidenced in the AD brain. One example of reported lipid peroxidation damage in AD was the detection of 4-hydroxynonenal (HNE), a highly reactive product of lipid peroxidation, in NFT in the hippocampus and cortex of AD patients, but not in control tissue (Sayre et al., 1997). With regards to nucleic acid oxidation, damage to mitochondrial and nuclear DNA, quantified by levels of 8-hydroxy-2'-deoxyguanosine, was found significant in AD cortex compared to control (Mecocci et al., 1994). Markers of protein oxidation, such as protein carbonyl content, 3-nitrotyrosine and dityrosine crosslinks, were also found to be elevated in AD brains (Smith, C. D. et al., 1991; Ansari & Scheff, 2010; Al-hilaly et al., 2013).

Alterations in the antioxidant capacity could in part be responsible for increased oxidative damage in AD. In line with this observation, levels of non-enzymatic antioxidants such as GSH in the AD frontal cortex were decreased compared to age-matched control tissue. This decrease was accompanied by diminished SOD and CAT activities, and GPx to a lesser extent (Ansari & Scheff, 2010).

Altered metal homeostasis has also been reported in AD brain tissue. For instance, redox-active iron was found to be associated with senile plaques and NFT in hippocampal sections in AD but not control tissue. Authors showed that binding of iron to AD lesions was dependent on protein conformation and pointed to ApoE as a protein both deposited in senile plaques and NFT that could interact with iron (Smith, M. a et al., 1997).

It is interesting to note that neuronal oxidative damage precedes A β pathology in Down's syndrome, which models amyloid pathology in AD. Nunomura and colleagues detected DNA and protein damage in cortical neurons previous to A β deposition (Nunomura et al., 2000). This is supported by *in vitro* data: A β accumulated in neuroblastoma cells in response to H₂O₂ exposure (Misonou et al., 2000); and Tau phosphorylation at residues implicated in hyperphosphorylation was increased following exposure to a lipid peroxidation end product, both in mouse primary neuronal cultures and in neuroblastoma cells (Gómez-Ramos et al., 2003).

1.6.2. Multiple and differential roles for ApoE in the antioxidant defence system

The possibility of oxidative stress preceding A β and Tau pathologies gives way to the exploration of which factors predispose an individual to oxidative damage. Since the *APOE* status is a major determinant of AD onset, it is relevant to explore the potential associations between ApoE and oxidative stress. These associations could be varied in nature, with ApoE playing different roles that will be explored in this section.

ApoE as a modulator of the antioxidant system

Initial links between ApoE and antioxidant balance were provided by studies in ApoE-deficient mice. In comparison to their wild type counterparts, ApoE-deficient mice exhibited higher levels of lipid peroxidation in plasma, and *in vitro* oxidation showed that lipids isolated from ApoE-deficient mice were more susceptible than lipids isolated from wild type mice (Hayek et al., 1994). ApoE-deficiency in mice also led to increased levels of antioxidants in the brain, with higher levels of GSH compared to wild types both at baseline and when challenged with an oxidative damage-inducing diet (Shea et al., 2002); and to decreased levels of SOD activity in the hippocampus of 13-month-old mice (Ramassamy et al., 2001). ApoE clearly modulates the antioxidant system in mice. In human brains, ApoE also impacts the antioxidant system in an isoform-dependent manner. AD ϵ 4 carriers displayed lower CAT and GPx activities and lower levels of GSH in the hippocampus than non- ϵ 4 carriers (Ramassamy et al., 2000), clearly pointing to links between the *APOE* genotype and impaired antioxidant defence.

ApoE as scavenger of reactive species

Building on studies conducted in ApoE-deficient mice, researchers set to determine whether ApoE's intrinsic properties played a protective role against oxidative stress. After showing that exogenously applied ApoE protected rat neuronal cell cultures from H₂O₂-induced cell death in an isoform dependent manner (with ApoE2 being the most, and ApoE4 the least, efficient), Miyata and associates investigated the intrinsic antioxidant properties of ApoE isoforms. They first showed that ApoE also had an antioxidant activity *in vitro* with ApoE2 being the most efficient, which suggests that ApoE may act independently of the antioxidant system. They then proposed as a possible mechanism that ApoE's antioxidant activity was mediated by its metal binding capacity (Miyata & Smith, 1996).

ApoE antioxidant activity could also potentially be mediated by its ability to capture reactive species. For instance, ApoE2 is more efficient at interacting with HNE than the other two ApoE isoforms (Pedersen et al., 2000), implying a role for ApoE in processes of reactive species' detoxification.

ApoE as a response to oxidative insults and injury

Expression of ApoE in neurons following stress or injury was reviewed in section 1.3.3., including the following example: administration of kainic acid to rats induced increased *APOE* gene transcript levels in hippocampal pyramidal neurons (Boschert et al., 1999). Kainic acid is a glutamate analogue used to induce seizures in rodents to model epilepsy. Kainic acid treatment results in oxidative damage, with increased protein carbonyl content that persist 24 h post-treatment (Gluck et al., 2000). The *APOE* response in rat neurons may thus be a response to increased oxidative stress.

In a model of traumatic brain injury, the *APOE* genotype had an impact on overall levels of oxidative markers, with increased oxidation in ApoE4 mice compared to ApoE3. Despite increased expression of antioxidant related genes in ApoE3 mice following injury, Ferguson et al did not observe an interaction between *APOE* status and injury in the levels of protein damage markers. They thus hypothesised that response to injury is independent of the *APOE* genotype, but that differences at baseline would result in higher levels of oxidative markers post injury in ϵ 4-carriers (Ferguson et al., 2010).

ApoE as a cause for oxidative stress

As exposed above, ApoE can be expressed in neurons following oxidative stress or injury. However, ApoE expression could be detrimental depending on the *APOE* genotype and which isoform is expressed.

ApoE4 was shown to be more susceptible to fragmentation than ApoE3 in transfected mouse neuroblastoma cells, generating a carboxy-terminal (residues 272-299) and an amino-terminal fragment (residues 1-271) that can both also be found in AD cortex (Huang, Y. et al., 2001). In the same cell line, Nakamura and colleagues showed that the amino-terminal fragment of ApoE4 interacted with mitochondrial proteins, resulting in mitochondrial dysfunction (Nakamura et al., 2009). Thus, ApoE expression in neurons following injury could cause more damage in *APOE* ϵ 4 carriers.

1.7. ApoE in the ageing brain

1.7.1. Interaction between *APOE* polymorphism and ageing

APOE status and AD age of onset

When *APOE* ϵ 4 was identified as a major genetic risk factor for sporadic AD, it became apparent that the ϵ 4 allele was associated with a lowered age of onset. Each ϵ 4 allele resulted in a 7-year shift of onset to younger age, lowering it from ~85 years old to 76 years old with one ϵ 4 copy, and to 68 years in homozygotes (Corder et al., 1993). In a similar fashion, the ϵ 2 allele of the *APOE* gene was deemed protective against sporadic AD onset, decreasing the risk by a factor four. The frequency distribution of ϵ 2 was halved in AD cases compared to controls. The benefit of carrying ϵ 2 or the risk generated by ϵ 4 decreased with increasing age (Corder et al., 1994).

APOE polymorphism and the ageing process

There is also evidence for an association between *APOE* polymorphism and longevity, since researchers have reported increased frequency of the ϵ 2 allele after age 100 in a Finnish cohort of 179 subjects (Frisoni et al., 2001). This is in line with a bigger genetic study that reported a significant decrease of ϵ 4 frequency and a significant increase of the ϵ 2 allele frequency in centenarians compared to their younger counterparts (Schächter et al., 1994).

The involvement of ApoE in the ageing process was consolidated by studies conducted in *APOE* knock-out mice. For instance, they exhibit age-related phenotypes like premature loss of hair follicles, arrested spermatogenesis and a reduced lifespan (reviewed by Dose et al., 2016).

Interactions between *APOE* genotype, ApoE levels and age

In a study investigating associations between *APOE* status and being a centenarian, investigators also reported an influence of *APOE* polymorphism on ApoE levels, with reduction of serum ApoE levels in ϵ 4 carriers compared to ϵ 2 carriers (Panza et al., 2003). More recently, levels of ApoE in plasma were reported to be higher in non- ϵ 4 carriers, followed by ϵ 4 heterozygotes and ϵ 4 homozygotes, showing a ϵ 4 dose-dependent effect. However, this genotypic difference did not hold up in CSF, where no

differences in ApoE levels were detected. No interaction between protein levels of ApoE and age was reported here (Martínez-Morillo et al., 2014). However, others have pointed to a positive association between levels of ApoE and age in CSF. Baker-Nigh and colleagues reported increasing ApoE levels with age in both $\epsilon 4$ -carriers and non-carriers (Baker-Nigh et al., 2016).

1.7.2. Low prevalence of $\epsilon 4$ homozygotes and an animal model to overcome this

When looking at the demographics in human studies such as the ones discussed above, it is clear that $\epsilon 4$ homozygotes are harder to recruit, and data is often grouped as $\epsilon 4$ -carriers and non-carriers. For instance, only 10 subjects were $\epsilon 4/\epsilon 4$ in a total of 180 participants in the study by Baker-Nigh (Baker-Nigh et al., 2016). This is not surprising since $\epsilon 4/\epsilon 4$ subject represent less than 3% of the population according to combined studies conducted on over 2000 participants (Mahley, 1988).

A mouse model expressing human ApoE could serve as a good alternative to explore the effect of *APOE* polymorphism at different levels across lifespan. Generation of the first human ApoE targeted-replacement (ApoE-TR) mice was reported in 1997. The mouse model was developed to express human ApoE3 under the mouse ApoE promoter (Sullivan et al., 1997). ApoE2-TR and ApoE4-TR mice were later generated, as reviewed by Tai et al. One of the benefits of this model is that it is physiologically relevant to the study of the differential functions of the ApoE isoforms (reviewed by Tai et al., 2011).

Since its development, ApoE-TR mice have been crossed with transgenic mouse models of AD to incorporate the *APOE* genotype-dependent effects as well as the temporal and spatial expression of ApoE that can only be achieved under the mouse *APOE* promoter. The majority of AD/*APOE* transgenic mice used since 2010 were generated through crossing with ApoE-TR mice (reviewed by Balu et al., 2019).

ApoE-TR mice display the same isoform-dependent differences reported in humans, as reviewed by Tai et al. ApoE4 levels in plasma, CSF and brain homogenates were lower than ApoE2 and ApoE3, and levels were similar in value to what has been measured in humans. Moreover, ApoE4-TR mice displayed increased synaptic dysfunction compared to ApoE3-TR mice (reviewed by Tai et al., 2011).

1.7.3. ApoE and accelerated cognitive ageing

ApoE-deficient mice, in addition to the deficits abovementioned, also display cognitive impairment. However, improved learning capacity in the Morris water maze resulted from treatment with recombinant ApoE (Masliah et al., 1997).

In humans, *APOE* ϵ 4 is also associated with poorer cognitive outcome, even in non-demented subjects. Non-demented elderly (80 years old and above) ϵ 4 carriers had poorer scores in cognitive ability tests (Deary et al., 2002). However, the ϵ 4 allele was found to be associated with cognitive advantages in early life (Rusted et al., 2013). Analysis of pattern recruitment in mid-age adults showed that ϵ 4 was associated with a pattern usually seen later in life, in agreement with an accelerated ageing process in ϵ 4-carriers (Evans, S. et al., 2014).

APOE status-dependent cognitive outcomes were also replicated in ApoE-TR mice. ApoE4-TR mice displayed spatial memory retention deficits compared to ApoE3-TR mice (Bour et al., 2008).

1.8. Aims and objectives of this thesis

Since ApoE4 was identified as a major genetic risk factor for AD, researchers have in great part focused on differences between the three ApoE isoforms in an already established pathological setting. Poorer outcomes associated with ApoE4 in A β , Tau and synaptic pathologies are well documented and were reviewed in this introductory chapter.

This thesis is based on a slightly different approach, aiming at understanding how ApoE isoforms may differentially facilitate or hinder AD onset, and doing so independently of A β and Tau which are causative in the disease aetiology. Instead, the differences between the three ApoE isoforms were investigated in the context of three background events that shape AD pathogenesis: protein misfolding and aggregation, oxidative stress and ageing.

Below is an overview of the three objectives to be addressed in this thesis, and the resources employed to do so. Results will be tied together in a final discussion chapter that will also elude to future directions and to the potential brought by ApoE as a therapeutic approach to AD.

1.8.1. Aim 1: Self-assembly properties of ApoE

AD is in part a disease of protein misfolding and aggregation: does the principal genetic risk factor for this disorder, ApoE4, misfold and aggregate as well?

Differential self-assembly properties of ApoE isoforms were investigated using recombinant human ApoE produced in *Escherichia Coli* (*E. coli*). A thorough investigation and characterisation of any structural differences at the secondary, tertiary and quaternary levels was conducted prior to testing the differential propensity of ApoE isoform to self-assemble. A wide-range of biophysical techniques, from protein production and purification to spectroscopy and microscopy, were employed.

1.8.2. Aim 2: ApoE and oxidative stress

Oxidative stress damage has been thoroughly documented in AD. The fourth chapter of this thesis examines the different ways in which ApoE may be involved in combatting oxidative stress.

Differential effects of ApoE3 and ApoE4 on antioxidant balance and responses associated to oxidative insults were investigated *ex vivo* using brain tissue and primary neuronal cultures derived from ApoE-TR mice.

Intrinsic antioxidant properties of ApoE isoforms were also investigated *in vitro* using the previously characterised recombinant human ApoE protein as a model.

1.8.3. Aim 3: ApoE throughout lifespan

Ageing is the principal risk factor for AD, and it is accompanied by a general decline in function and accumulation of damage.

The fifth chapter aims at understanding how ApoE3 and ApoE4 may be differentially affected by passing years by looking at how its protein levels in the brain of ApoE-TR mice changes across lifespan. It also tries to address the idea of ApoE4 being associated with accelerated ageing by comparing ageing markers throughout lifespan in age-matched ApoE3-TR and ApoE4-TR mice.

Chapter 2 – Materials and methods

All materials and buffers used in experiments for this thesis are detailed in section 2.1. Protocols, grouped by broad disciplines, are detailed from section 2.2 onwards.

2.1. Materials

2.1.1. Plastics

The following plastics were used throughout to prepare samples or for cell culture purposes. Non-sterile plastics and tips are not detailed.

Tubes

Eppendorf® protein LoBind microcentrifuge tubes		(Fisher scientific)
Microcentrifuge tubes, 1.5 mL		(Fisher Scientific)
Fisherbrand™ 0.2mL PCR Tube Strips		(Fisher scientific)

96-well plates

Invitrogen™ Molecular Probes™ Nunc™ 96-Well Microplates for Fluorescence-based Assays	#15329413	(Fisher Scientific)
Greiner UV-Star® 96 well plates	M3812	(Sigma Aldrich)
96-well Roche PCR plate White	I1402-9909-BC	(Starlab)

Plastic seals

StarSeal Advanced Polyolefin Film	E2796-9795	(Starlab)
-----------------------------------	------------	-----------

Tissue culture flasks, plates and filters

Corning® Cell culture flasks		(Sigma Aldrich)
Corning® Costar® TC-Treated Multiple Well Plates		(Sigma Aldrich)
Fisherbrand™ Sterile Cell strainer, 70 µm	#11597522	(Fisher scientific)

2.1.2. Buffers, chemicals and materials for protein sample preparation

Stock solutions were prepared in ultrapure water and were used in the preparation of required buffers. All buffers were adjusted to the desired pH and filtered. Table 2.1 summarises the compounds used, with their corresponding supplier and reference number, as well as their concentration or the concentration of the stock solutions made.

Chemicals

Prepared stock solutions were stored in the fridge at 2-8°C unless stated otherwise.

Compound	Supplier	Reference #	Concentration of stock
2xYT medium	VWR	J902	-
Ampicillin	Fisher Scientific	11444582	100 mg/mL
cOmplete tablets, EASYpack, protease inhibitor cocktail	Sigma Aldrich	4693132001	-
DNase I from bovine pancreas	Sigma Aldrich	D4527	5 mg/mL
Dithiothreitol (DTT), - 20°C	Sigma Aldrich	D0632	1 M
4-(2-hydroxyethyl)-1-piperazineethanesulfonic acid (HEPES), pH 8.0	Fisher Scientific	10081113	1 M solution
H ₂ O ₂ , 30% (w/w) in H ₂ O with stabilizers	Sigma Aldrich	H1009	9.8 M solution
Imidazole	Acros Organics	10696502	1 M
Isopropyl β-D-1-thiogalactopyranoside (IPTG)	Anatrace	I1003	1 M
GuHCl	Sigma Aldrich	G7294	8 M solution
Glycerol	Fisher Scientific	10795711	-
Lennox LB broth with agar	Formedium	LBX0102	-
MgCl ₂	Sigma Aldrich	M8266	1 M
NaCl	Fisher Scientific	10428420	3 M
Na ₂ HPO ₄	Sigma Aldrich	71649	-
NaH ₂ PO ₄	Sigma Aldrich	71505	-
Phosphate buffered saline tablet	Gibco	18912-014	1X
S.O.C medium	Thermo Fisher	15544034	-
tris(2-carboxyethyl)phosphine (TCEP), -20°C	Sigma Aldrich	646547	0.5 M
ThT, filtered through a 0.2 μm filter - 20°C	Sigma Aldrich	T3516	1 mg/mL in methanol
Trifluoroacetic Acid (TFA)	Sigma Aldrich	28901	-
Tween-20	Sigma Aldrich	P1379	-

Table 2.1 Chemicals used in protein sample preparation

Media and buffers**LB-agar**

35 g Lennox LB broth with
agar
1 L water

LB-agar ampicillin

1 L autoclaved LB-agar
0.1 mg/mL ampicillin

2xYT-ampicillin

31 g 2xYT powder
1 L water
0.1 mg/mL ampicillin

Lysis Buffer (pH 8.0)

50 mM HEPES, pH 8.0
240 mM NaCl
5 mM MgCl₂
10 mM Imidazole
0.05% (v/v) Tween-20
10% (v/v) Glycerol
1 mM DTT*
1 Complete protease
inhibitor tablet per 50 mL*
50 µL DNase I per 100 mL
(7 U/m final)*

Binding buffer (pH 8.0)

50 mM HEPES, pH 8.0
240 mM NaCl
5 mM Imidazole
0.05% (v/v) Tween-20
10% (v/v) Glycerol

**TALON Elution buffer
(pH 8.0)**

50 mM HEPES, pH 8.0
240 mM NaCl
300 mM Imidazole
0.05% (v/v) Tween-20
10% (v/v) Glycerol

Heparin Elution Buffer (pH 8.0)

20 mM HEPES, pH 8.0
1000 mM NaCl
10% (v/v) Glycerol

**Size-exclusion chromatography (SEC) buffer
(pH 8.0)**

50 mM HEPES, pH 8.0
300 mM NaCl
10% (v/v) Glycerol
0.5 mM TCEP*

20 mM phosphate buffer, pH 7.4 (PB)

16 mM Na₂HPO₄
4 mM NaH₂PO₄

Phosphate buffer saline, pH 7.4 (PBS)

(10 mM PB, 2.68 mM KCl, 140 mM NaCl)
1 tablet in 500 mL H₂O

* Added on the day before use

Materials

• **Site-directed mutagenesis**

QuikChange XL mutagenesis kit	(Agilent)
QIAprep [®] Spin Miniprep kit	(Qiagen)
Template plasmid: pET17b_ApoE3	<i>(Provided by Dr Lucas Kraft)</i>
Sequencing service	(Eurofins, Germany)

• **Protein production**

<i>E. coli</i> Rosetta2(DE3) cells, #71400-3	(Merck Millipore)
PreScission protease (human rhino virus 3C protease)	<i>(Expressed and purified by Dr Kraft at the Sussex Drug Discovery Centre)</i>
TALON [®] resin, #635503	(Takara)
HiTrap [™] Heparin HP, 5 mL	(GE Healthcare Life Sciences)
HiLoad 26/600 Superdex 200 pg preparative size exclusion chromatography column	(GE Healthcare Life Sciences)

• **Dialysis and buffer exchange**

Slide-A-Lyzer [™] Dialysis Cassettes, 3.5 kDa molecular weight cut-off (MWCO)	(Thermo Fisher)
Vivaspin [®] 500 centrifugal concentrators, 3 kDa MWCO	(Sartorius)
Vivaspin [®] 20 centrifugal concentrators, 3 kDa or 10 kDa MWCO	(Sartorius)

• **Mass Spectrometry**

In-Gel digestion kit, #89871	(Thermo Fisher)
------------------------------	-----------------

2.1.3. Buffers, chemicals and materials for cell and molecular biology

All chemicals for cell culture and cell culture treatment were handled under sterile conditions, with media and compounds prepared in a cell culture hood. PBS used in this section was autoclaved. Autoclaved double distilled water (ddH₂O) was used for preparation of cell culture stock solutions; DEPC-treated water (Fisher Scientific) and Nuclease-free water (NEB) were used for molecular biology experiments.

Table 2.2 summarises the compounds used, with their corresponding supplier and reference, as well as their concentration or the concentration of the stock solutions made.

Chemicals

Compound	Supplier	Reference #	Concentration of stock
Azamethiphos	Sigma Aldrich	45331	50 mM in EtOH
B-27 supplement	Gibco	17504044	50 X
Cytosine arabinoside (AraC)	Sigma Aldrich	C1768	100 mM in ddH ₂ O
Dimethyl sulfoxide (DMSO), 99.7%, Extra dry	Acros Organics	326881000	-
Dulbecco's Modified Eagle Medium/Nutrient Mixture F-12 (DMEM/F-12)	Sigma Aldrich	D8437	-
Ethanol (EtOH)	Sigma Aldrich	32221	≥99.8%
Foetal Calf Serum (FCS)	Sigma Aldrich	F0804	-
D-(+)-Glucose solution	Sigma Aldrich	RNBG7315	45 % in H ₂ O
GlutaMAX supplement	Gibco	35050061	-
L-glutamine	Fisher Scientific	25030032	-
H ₂ O ₂ , 30% (w/w) in H ₂ O	Sigma Aldrich	H1009	9.8 M solution
Haloperidol	Sigma Aldrich	PHR1724	12.5 mM in DMSO
Hank's Balanced Salt Solution (HBSS)	Gibco	14065-056	10 X
HEPES buffer solution	Gibco	1563080	1 M
Modified Eagle Medium (MEM)	Gibco	31095-029	1 X
NaOH	Fisher Scientific	S/4920/53	-
Neurobasal Medium (NB)	Gibco	12348-017	1 X
Poly-D-Lysine (PDL)	Sigma Aldrich	P7280	4 mg/mL in ddH ₂ O
Penicillin/Streptomycin (pen/strep)	Gibco	15140-122	-
0.25% Trypsin- 2.21 mM EDTA (trypsin-EDTA)	Corning	25-053-CI	-

Table 2.2 Chemicals used in buffers and media for tissue culture and cell treatment

Dissection buffers**Dissection HBSS**

1X HBSS

0.01 M HEPES

Trituration buffer

Buffered HBSS

0.25% trypsin-EDTA

Media**Supplemented Maintenance medium**

DMEM/F-12

10% (v/v) FCS

1% (v/v) L-glutamine

1% (v/v) pen/strep

Neuronal culture plating medium

MEM

10% (v/v) FCS

1% (v/v) pen/strep

0.5% D-(+)-Glucose

Neuronal Culture Maintenance medium

NB

2% (v/v) B-27

1% (v/v) GlutaMAX

1% (v/v) pen/strep

Azamethiphos breakdown solution

A 0.1 N NaOH solution in 50% EtOH was prepared to enable the hydrolytic breakdown of azamethiphos. The breakdown solution, labelled corrosive, was kept in the fume hood and all pesticide-containing solutions were emptied into it. A minimum of 24 h was allowed for hydrolysis. Breakdown solution was neutralised before disposing to drains.

Materials

- **Cell viability assays**

ReadyProbes Cell Viability Imaging Kit, Blue/Red, R37610 (Thermo Fisher)

Live Cell Imaging Solution, A14291DJ (Thermo Fisher)

- **Protein and RNA isolation**

TRIzol Plus RNA purification kit and phasemaker tubes (Invitrogen)

DNA-free™ removal kit (Invitrogen)

- **Complementary DNA synthesis**

High-Capacity cDNA Reverse transcription kit with RNase Inhibitor (Applied Biosciences)

- **Quantitative Polymerase Chain Reaction**

Luna® Universal qPCR Master Mix (NEB)

Primers

Gene	Primer sequence
Human (h) <i>APOE</i> *	Fwd: 5'-GTCGCTTTTGGGATTACCTGC -3' Rev: 5'-CCGGGGTCAGTTGTTCCCTC -3'
h <i>GAPDH</i> §	Fwd: 5'- CTTTTGCGTCGCCAG -3' Rev: 5'- TTGATGGCAACAATATCCAC -3'
h <i>ACTB</i> ‡	Fwd: 5'- AAGTCCCTTGCCATCCTAAAA -3' Rev: 5'-ATGCTATCACCTCCCCTGTG -3'
Mouse (m) <i>ACTB</i> ¥	Fwd: 5'- ATATCGTCATCCATGGCGAAC -3' Rev: 5'- ATATCGTCATCCATGGCGAAC -3'

Table 2.3 Primers sequences

Fwd = forward; Rev = reverse; References for each set of primers: * Elliott et al., 2007; §Bordoni et al., 2019; ‡ Valdighesias et al., 2012; ¥ Debernardi et al., 2003. Primers were purchased from Sigma-Aldrich.

2.1.4. Buffers and chemicals for brain tissue protein extraction

Stock solutions were prepared in ultrapure water, adjusted to the required pH with HCl or NaOH solutions and filtered. Solutions were stored at 4°C unless stated otherwise.

Chemicals

Compound	Supplier	Reference #	Concentration of stock
DTT, -20°C	Sigma Aldrich	D0632	1 M
Ethylenediaminetetraacetic acid (EDTA)	Sigma Aldrich	E9884	50 mM, pH 8.0
HCl	Fisher Scientific	UN1789	<i>Concentrated</i>
cOmplete tablets, EASYpack, protease inhibitor cocktail	Sigma Aldrich	4693132001	25x in H ₂ O, -20°C
Pierce® RIPA buffer	Thermo Fisher	89900	-
Tris base	Fisher Scientific	BP152-1	0.5 M, pH 7.4

Table 2.4 Chemicals used in protein extraction buffers

Buffers**Fractionation buffer**

20 mM Tris-HCl

1 mM EDTA

1 mM DTT *

1x Protease inhibitor cocktail *

* Added before use, on ice

Total protein lysis buffer

RIPA buffer

1x Protease inhibitor cocktail *

2.1.5. Gel electrophoresis, western blot and agarose gel

All solutions were prepared in distilled water (dH₂O) and stored at room temperature (rt).

Chemicals

Compound	Supplier	Reference #	Concentration of stock
Agarose	Thermo Fisher	17852	-
Blotting-Grade Blocker	Bio-Rad	170-6404	-
Boric acid	Sigma Aldrich	B0394	-
DTT, -20°C	Sigma Aldrich	D0632	0.5 M
Imperial protein stain	Thermo Fisher	24615	-
Laemmli sample buffer	Bio-Rad	161-0747	4x
β-mercaptoethanol (β-ME)	Sigma Aldrich	M6250	-
Methanol (MeOH)	VWR	20847.307	-
NaCl	Sigma Aldrich	S5886	-
NaOH	Fisher Scientific	S/4920/53	-
Native sample buffer	Bio-Rad	161-0738	2x
Ponceau stain	Thermo Fisher	89900	-
Sodium dodecyl sulphate (SDS)	Sigma Aldrich	L3771	-
Tris base	Fisher Scientific	BP152-1	-
Tris-Glycine (TG) running buffer	Bio-Rad	1610734	10x
Tris-Glycine-SDS (TGS) running buffer	Bio-Rad	1610732	10x
Tween-20	Fisher Scientific	BPE337-500	-

Table 2.5 Chemicals used in gel electrophoresis and western blot

Gel electrophoresis buffers

Denaturing running buffer, pH 8.3
(25 mM Tris, 192 mM glycine, 0.1% SDS)
100 mL 10x TGS
900 mL dH₂O

Native running buffer, pH 8.3
(25 mM Tris, 192 mM glycine)
100 mL 10x TG
900 mL dH₂O

Western blot buffers and solutions**Tris Buffer Saline (TBS)**

50 mM Tris-HCl, pH 7.4
150 mM NaCl

TBS-T

0.05% (v/v) Tween-20
TBS

Blocking Buffer

5% (w/v) dried milk powder
TBS-T

Transfer buffer

(25 mM Tris, 192 mM glycine, 10% MeOH)

100 mL 10x TG
200 mL MeOH
700 mL dH₂O

Ponceau destaining solution

0.1 M NaOH in dH₂O

Stripping buffer

31.25 mM Tris-HCl, pH 6.8
2% SDS
50 mM β-ME

RNA gel electrophoresis buffer**Northern running buffer**

(36 mM H₃BO₃, 10 mM NaOH)

2.25 g H₃BO₃

0.4 g NaOH

To 1 L with dH₂O

Materials• **Gels**

4-20% Mini-PROTEAN® TGX™ precast protein gel (Bio-Rad)

12% Mini-PROTEAN® TGX™ precast protein gel

• **Blotting membranes**

Amersham™ Protran™ 0.45 μm nitrocellulose membrane (GE Healthcare Life science)

Mini Trans-Blot® filter paper (Bio-Rad)

2.1.6. Antibodies

A range of antibodies was used in immunoblotting experiments. A list of the primary and secondary antibodies and their corresponding dilutions in blocking buffer can be found in table 2.6.

Antibodies

	Antibody	Epitope	Specificity	Dilution	Source
Primary antibodies	Rabbit anti-ApoE (16H22L18), Abfinity™	240–251 amino acid region of human ApoE	Human, mouse, rat	WF - 1:2,000	ThermoFisher # 701241
	Goat anti-Apolipoprotein E	Polyclonal antibody	Human, mouse, rat	NF - 1:1,000 WF - 1:5,000	Merck Millipore # 178479
	Rabbit anti- α -Tubulin [EP1332Y]	Within N-terminal domain (1-100)	Mouse, Rat, Human, Pig, Drosophila melanogaster	CF - 1:20,000	Abcam ab52866
	Rabbit anti-GAPDH (D16H11) XP®	Residues near the carboxy terminus of human GAPDH	Human, mouse, rat, monkey	NF - 1:10,000 CF - 1:20,000	Cell Signaling Technology # 5174
Secondary antibodies	Rabbit anti- trimethyl-Histone (H3K9me3)	Polyclonal antibody	Human, mouse, rat, chicken	NF - 1:10,000	Merck Millipore # 07-442
	Goat anti-Rabbit IgG H&L – Horseradish Peroxidase (HRP)	Polyclonal antibody	Rabbit	WF - 1:2,000 CF - 1:20,000	Abcam ab205718
	Donkey anti-goat IgG (H+L) – HRP	Polyclonal antibody	Goat	NF - 1:2,000 WF - 1:5,000	Invitrogen # PA1- 28664

Table 2.6 Antibodies for immunoblotting

Antibodies were diluted accordingly depending on the samples being analysed: WF = whole fractions; NF= nuclear fractions; CF= cytosolic fractions

2.1.7. Protein assay kits

Antioxidant enzyme activity

Amplex Red Catalase assay kit	(Thermo Fisher)
Superoxide Dismutase assay	(Sigma Aldrich)
SOD from bovine erythrocytes, 15,000 units	(Sigma Aldrich)

Detection of protein carbonyl content

Protein carbonyl content assay kit	(Sigma Aldrich)
Oxidized Protein Western Blot Kit	(Abcam)

Protein concentration

Pierce™ Bicinchoninic acid (BCA) protein assay kit	(Thermo Fisher)
Bovine serum albumin (BSA) protein standards	(Bio-Rad)

2.1.8. Equipment and microscopes

Biophysics

- **Protein production and purification**

Äkta Fast Protein Liquid Chromatography (GE Healthcare Life Sciences) system

- **Mass spectrometry**

Nano-LCMS: Thermo Fisher U3000 nanoLC and Orbitrap XL mass spectrometer

PepMap100 C18 trapping cartridge (Thermo Fisher)
0.3 x 5 mm i.d.; 5 µm particle size

PepMap100 Analytical column (Thermo Fisher)
25 cm x 75 µm; 5 µm particle size

Nanospray emitter with 10 µm tip (New Objective)
#FS360-20-10-N-20

- **Analytical and preparative ultracentrifugation**

Beckman model XL-A analytical ultracentrifuge (Beckman Coulter, Fullerton, CA)
with an AnTi60 rotor

Optima™ MAX preparative ultracentrifuge (Beckman Coulter, Fullerton, CA)

- **Circular dichroism spectroscopy**

Jasco-715 CD-spectrometer	(Jasco, Goh-Umstadt, Germany)
0.01 cm transparent quartz cuvettes	(Starna Scientific, Essex, UK)
PTC-348W1 peltier thermostat	(Jasco, Goh-Umstadt, Germany)

- **Fluorescence spectroscopy**

Varian Cary Eclipse spectrophotometer	(Varian Ltd., Oxford, UK)
Varian Cary temperature controller	(Varian Ltd., Oxford, UK)
1 cm quartz cuvette	(Starna Scientific, Essex, UK)

- **Nanodrop**

NanoDrop ND2000c spectrophotomer	(Thermo Fisher)
----------------------------------	-----------------

- **Plate reader for absorbance and fluorescence measurements**

SpectraMax i3 reader	(Molecular Devices)
----------------------	---------------------

Dissections

Fisherbrand™ Dumont #5 Fine Tip Tweezers	(Fisher Scientific)
Dumont #55 Biology Tweezers	(Fisher Scientific)

Biochemistry

- **Brain tissue homogenisation, cell homogenisation**

Dounce hand-held homogeniser for tissue

Table top centrifuge

- **Gel electrophoresis and western blotting**

Mini-PROTEAN Cell	(Bio-Rad)
Mini Trans-Blot module	(Bio-Rad)
PowerPac™ HC Power supply	(Bio-Rad)

Molecular biology

Thermocycler	(Various brands)
LightCycler® 480 Instrument II	(Roche)
Mini-Sub® Cell GT Cell	(Bio-Rad)

Microscopy

- **Fluorescence microscopy**

Cell Observer Axiovert 200 M widefield (Zeiss)
microscope

ORCA camera (Hamamatsu)

Plan Fluor 10X and 20 X NA 0.3 air objective (Nikon)

- **Transmission electron microscopy**

Jeol Jem1400- plus transmission electron (Jeol, U.S.A.)
microscope

Gatan Orius SC1000 camera (Gatan Inc., UK)

400-mesh copper, carbon-coated grid (Agar Scientific, Essex, UK)

2.1.9. Animals

ApoE3- and ApoE4-TR mice (Sullivan et al., 1997; Knouff et al., 1999) were housed in a specialised facility under Home office guidelines. Mice were sacrificed at specific ages, using Schedule 1 procedures in accordance with the Animals (Scientific Procedures) Act 1986, Amendment Regulations 2012. Culling was performed either by Luca Biasseti or Dr. Kate Fennell from the Serpell lab, Devin Clarke from the Hall lab, or by an Ancillary Unit staff member. A table summarising all animals used can be found in Appendix 1, with their respective age at the time of culling, their *APOE* genotype and their sex.

Pups used for cortical dissections were sacrificed at postnatal day 0 (P0) or day 1 (P1). Colonies were looked after by the Ancillary Unit staff and managed by Alex Stuart from the King lab. Genotyping was also performed by Alex Stuart.

2.2. Routine techniques and sample preparation relative to protein-based experiments

2.2.1. Recombinant protein production and purification of human ApoE in *E. coli*

Recombinant human ApoE isoforms (rApoE) were expressed in *E. coli*. The expression and purification protocol described here is that of rApoE2, which I performed. I developed the *APOE* ϵ 2 plasmid by performing site-directed mutagenesis. The expression and purification protocol were developed by Dr Lucas Kraft at the Sussex Drug Discovery centre (Raulin, Kraft et al., 2019). An overview of the process can be found in Fig. 2.1A.

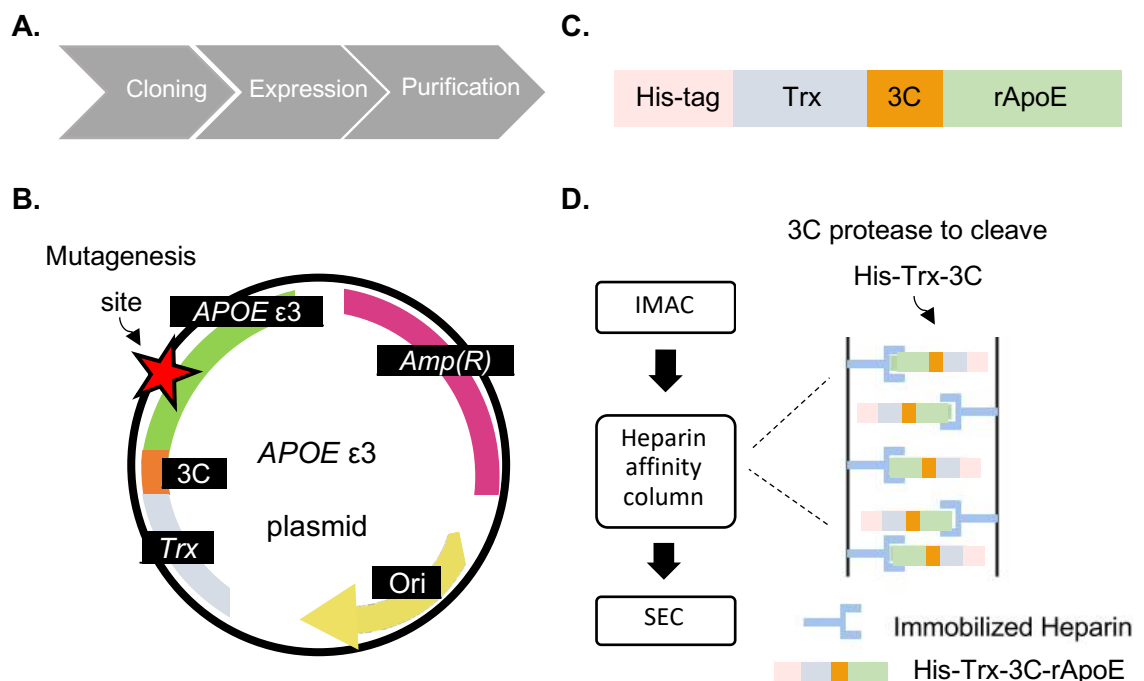


Figure 2.1 Production of rApoE isoforms.

A. The production of rApoE followed a three-step method.

B. Schematic of *APOE* ϵ 3 plasmid, depicting the ligation of *APOE* ϵ 3 to 3C-Trx. *Amp(R)* is an ampicillin resistance gene; *Ori* corresponds to the origin of replication.

C. rApoE was expressed fused to a domain comprising His-tag, Trx and a 3C site in order to facilitate its isolation.

D. Purification of rApoE was achieved using the construct His-tag interaction with the IMAC column. rApoE was then immobilised onto a heparin affinity column through binding to heparin. It was released from the fusion protein following the action of 3C protease, and further purified through a SEC column.

Site-directed mutagenesis

APOE ϵ 2 plasmid was obtained by site-directed mutagenesis of an *APOE* ϵ 3 plasmid that was provided by Dr Kraft (Raulin, Kraft et al., 2019). In the template plasmid, the *APOE* ϵ 3 gene was ligated into a Histidine-tag (His-Tag)-Thioredoxin (Trx)-3C protease cleavage site (3C) (Fig. 2.1B), resulting in an rApoE-fusion protein after bacterial expression (Fig. 2.1C). Site-directed mutagenesis on the *APOE* ϵ 3 vector using the QuikChange XL mutagenesis kit resulted in the *APOE* ϵ 2 plasmid by substituting a C for a T in the nucleic acid sequence at base pair position 3774. In brief, this was achieved in three steps. The first corresponds to the creation and amplification of the site-mutated plasmid by polymerase chain reaction (PCR), by incubating the template plasmid with mutated primers.

The primers used were the following:

- 5'-CTGATAAACTGCCAGACATT**T**CTGCAGATCATCGG-3';
- 5'-GCCGATGATCTGCAG**A**AATGTCTGGCAGTTTATCA-3'.

The cycling parameters used were optimised and resulted to be different from that of the kit's protocol, and these can be found in table 2.7.

Segment	Cycles	Temperature	Time
1	1	95°C	2 min
2	15	95°C	20 s
		59°C	30 s
		72°C	140 s
3	15	95°C	20 s
		64°C	30 s
		72°C	140 s
4	1	72°C	5 min
5	1	8°C	Infinite hold

Table 2.7 Cycling parameters for site-directed mutagenesis

The PCR reaction was divided into 5 segments. The first one corresponds to the initial denaturation of the template DNA. The second and third cycles correspond to the subsequent denaturation of the plasmid, annealing and extension of the primers. The kit provides an enzyme mixture containing the *Pfu* Fusion-based DNA polymerase as well as other enzymes ensuring ligation of any nicks present. Segment 4 corresponds to a final extension phase, followed by an optional “infinite hold” at 8°C (segment 5).

The second step of the kit consists of getting rid of the methylated, template plasmid DNA using the restriction endonuclease DPN-1. The final step corresponds to the transformation of the newly obtained mutated plasmid on provided XL10-Gold Ultracompetent Cells in S.O.C medium. Colonies were harvested from the transformation plates and grown in 2xYT-ampicillin medium overnight. The newly mutated plasmid was isolated from the bacterial culture using the QIAprep® Spin Miniprep kit and its sequence was confirmed by DNA sequencing (Eurofins, Germany).

Expression of the fusion protein

The *APOE* ϵ 2 expression vector was transformed into *E. coli* strain Rosetta 2, and the transformed competent cells were cultured in LB-agar ampicillin at 37°C. Addition of IPTG to a final concentration of 1 mM induced the expression of the fusion protein His-tag-Trx-3C-ApoE2. After 2 h, cells were harvested following centrifugation and pellets were kept at -80°C until purification.

Purification of ApoE2

The bacterial pellet was sonicated in Lysis buffer and the lysate centrifuged to get rid of cellular debris. The supernatant was incubated with a cobalt-based immobilised metal affinity chromatography (IMAC) medium (TALON resin) in Binding buffer to isolate His-tagged proteins. Following washes with the binding buffer, His-tagged proteins were eluted using the TALON elution buffer. The eluate in TALON elution buffer was then loaded on a heparin column thus immobilising rApoE2, which binds to heparin (Cardin et al., 1986) and the fusion protein was cleaved at the 3C site with PreScission protease to remove the tagged Trx from rApoE2. Following washes with binding buffer, rApoE2 was eluted from the heparin column with Heparin elution buffer and further purified through a SEC column. rApoE2 was washed out of the SEC column with SEC buffer and concentrated. The protein eluted in two peaks and only the fractions corresponding to lower mass rApoE2 were pooled (Hatters et al., 2006). Concentrated rApoE2 was either snap-frozen in liquid nitrogen for storage at -80°C or dialysed immediately after purification.

Dialysis and buffer exchange

Before use in experiments, rApoE was either extensively dialysed overnight in PB using dialysis cassettes with a 3.5 kDa MWCO or the SEC buffer was exchanged for PB using disposable centrifugal concentrators.

2.2.2. Recombinant protein sample preparation for structural characterisation

All buffers used were defined and described in 2.1.2.

Recombinant protein concentration

The exact concentrations were measured in triplicate (at least) using a NanoDrop ND2000c spectrophotometer. Concentrations were calculated using the averaged absorbance A_{280} in the Beer-Lambert law equation (1):

$$C = \frac{A_{280}}{\varepsilon \times l} \quad (1)$$

with l the 1 cm path length and ε the extinction coefficient. ε was calculated using formula (2):

$$\varepsilon = (nW \times 5500) + (nY \times 1490) + (nC \times 125) \quad (2)$$

with nW , nY and nC the number of Trp, Tyr and Cys residues respectively. Because of the small contribution of Cys in the formula, the following approximation (3) was used to calculate ε , as previously described in the literature, such as Clement-Collin et al (2006):

$$\varepsilon \approx (nW \times 5500) + (nY \times 1490) \quad (3)$$

which results in an ε value of 44,460 L.mol⁻¹.cm⁻¹.

Concentrations were recorded and used in calculations when needed.

Secondary structure and thermal denaturation

rApoE isoforms were diluted to a final concentration of ~25 μ M in PB. Samples were either used for secondary structure measurements or for thermal denaturation straight after dilution (see 2.3.3).

Intrinsic tryptophan fluorescence in native protein

rApoE isoforms were diluted to 10 μ M in PB and incubated overnight at 4°C in a 96-well microplate for fluorescence assays before Trp fluorescence measurement using a plate-reader (see 2.3.4).

Chemical denaturation study

rApoE isoforms at ~1 μM in PB, 1 mM DTT were incubated overnight at 4°C with increasing concentrations of GuHCl (0 to 6 M) (Morrow et al., 2000). To prepare the samples, two stock concentrations of the proteins were made in 0 M GuHCl, pH 7.4 and in 6 M GuHCl, pH 7.4, and the two stocks were mixed together in different ratios to prepare 40 different samples with concentrations of GuHCl ranging between 0 and 6 M (see 2.3.4).

2.2.3. Recombinant protein sample preparation for self-assembly assays

rApoE isoforms were diluted to a final concentration of ~25 μM PB. Samples were incubated without agitation at 37°C for up to 3 d. For kinetic studies, rApoE was incubated in the presence of ThT in a 1:2.2 ratio for up to 3 d.

rApoE4 was also incubated with either rApoE2 or rApoE3 at a 1:1 ratio (12.5 μM each for a total rApoE concentration of 25 μM , PB), or alone at 12.5 μM in PB, and incubated at 37°C for 24 h.

2.2.4. Recombinant protein sample preparation under oxidative and reducing conditions

Secondary structure

rApoE was diluted to ~25 μM in PB in the presence of either H_2O_2 or DTT. Samples were incubated at 4°C overnight before CD acquisition (see 2.3.3) to allow for equilibration of the protein in the oxidative or reducing environment. H_2O_2 was used at various final concentrations: 0.5 mM, 1 mM, 5 mM, 25 mM, 50 mM and 88.3 mM (1:3533; Miyata & Smith, 1996). DTT was used at various final concentrations concentration: 1 mM, 2.5 mM, 5 mM, 7.5 mM and 10 mM (1:400).

Tertiary structure

rApoE isoforms were diluted to 10 μM in PB and incubated overnight at 4°C in a 96-well microplate for fluorescence assays in the presence of 35.3 mM H_2O_2 (1:3533) or 4 mM DTT (1:400). Intrinsic Trp fluorescence was then measured using a plate-reader (see 2.3.4).

2.3. Routine techniques and sample preparation relative to cell-based experiments

2.3.1. Cell culture and dissections

SH-SY5Y human neuroblastoma culture

SH-SY5Y human neuroblastoma cell lines (ATCC, CRL-2266) were maintained in 75 cm² culture flasks in Supplemented Maintenance Medium. Cells were fed every 3 d and passaged once a week when cells reached 70-90% confluency, using 0.25% trypsin-EDTA to detach adherent cells. Maintenance cultures did not exceed 9 passages.

Cells were either plated into 24-well plates ($\sim 3 \times 10^4$ cells/mL) or passaged at a 1:5 ratio in T75 flasks, with four flasks prepared per experiment and one for maintenance.

Mouse cortical cultures

- Plate and flasks coating

Plates and flasks used to culture cortical neurons were coated prior use with PDL (20 μ g/mL, coated for 4 h up to 16 h at 37°C).

- Dissection and plating

Primary cortical neuronal cultures were prepared from either P0 or P1 ApoE-TR mice. Brains were removed following cervical dislocation under Schedule 1 of the Home office guidelines.

Cortices were isolated in Dissection HBSS and cut into small pieces using fine forceps. Cut cortices were transferred in a sterile 15 mL tube containing 1 mL of Dissection HBSS per pair of cortices and kept on ice. Dissection HBSS was carefully removed under a flow hood and replaced by Trituration HBSS. 1 mL of medium/solutions per pair of cortices was used throughout. Cortices in Trituration HBSS were incubated for 10 min at 37°C, with gentle shaking in between. Trituration HBSS was removed and cortices were washed 3 times with Neuronal culture plating medium. Cortices were resuspended in Neuronal culture plating medium and mechanically dissociated by pipetting 50 times using a 1 mL pipette and 50 times using a 200 μ L pipette. Triturated mixture was pelleted at 1,000 rpm for 5 min, and the supernatant replaced by fresh Neuronal culture plating medium. Cells were resuspended and run through a 70 μ m filter prior to counting. Cells were then diluted to 0.27×10^6 cells/mL; cells were plated at a density of 0.043 cells/cm².

Neuronal culture plating medium was replaced by Neuronal Culture Maintenance medium 2.5 h after plating.

- Maintenance

Cells were treated with 3.25 μM AraC in Neuronal Culture Maintenance medium 3 d after plating to reduce astrocyte proliferation. Neuronal Culture Maintenance medium was replaced every 3 d. Cells were used for experiments 10 d after plating.

2.3.2. Cell treatment

Treatments were applied by half media changes, resulting in the following for SH-SY5Y cells:

- No treatment: Supplemented Maintenance medium
- Positive control: 50 μM final haloperidol in Supplemented Maintenance medium
- H_2O_2 : 75 μM final in Supplemented Maintenance medium
- Azamethiphos: 50 μM final in Supplemented Maintenance medium

Treatments were applied on cortical neurons at DIV10 by half media changes, resulting in the following:

- No treatment: Neuronal Culture Maintenance medium
- H_2O_2 : 650 μM final in Neuronal Culture Maintenance medium
- Azamethiphos: 300 μM final in Neuronal Culture Maintenance medium

Cells were either used for live/dead assay (see 2.6.1) or they were used for RNA and protein extraction after 24 h treatment (see 2.3.3).

2.3.3. RNA and protein extraction from cells

For each treatment, proteins from dead cells, and RNA and protein from live cells were isolated. A diagram of the experiment can be found in Fig. 2.2.

Media was removed from treated cells, and dead cells were pelleted at 1,500xg for 5 min prior to lysis in 20 μL RIPA buffer containing protease inhibitor, on ice for 15 min. Lysates were spun at 10,000xg for 5 min; supernatants were collected and kept at -20°C . These were not used here.

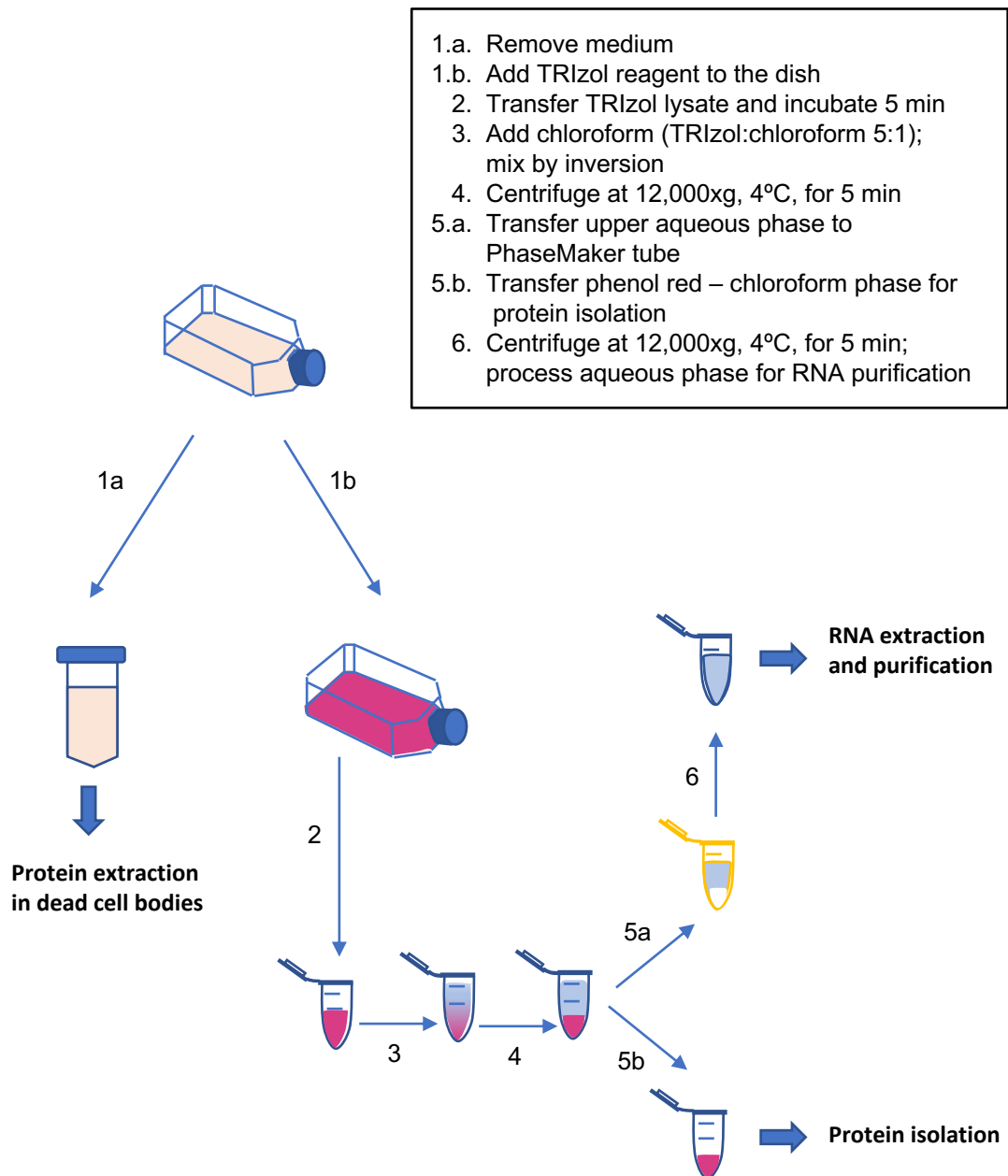


Figure 2.2 Isolation of RNA and protein from treated cells

Proteins were extracted from both the supernatant medium containing dead cell bodies, and from live cells in the cell monolayer. Only the extracts from cells in the monolayer ended up being used. RNA was extracted from the cells in the cell monolayer.

In the meantime, TRIzol reagent was directly added onto cells (1.5-2 mL in T75 flasks). RNA and proteins from cells were isolated according to the manufacturers protocol (Invitrogen). In brief, the mixture was pipetted up and down to ensure total lysis and incubated for at least 5 min to ensure the dissociation of nucleosomes. 200 μ L of chloroform were added per 1 mL of TRIzol, and vigorously mixed by inversion for 15 s.

Samples were centrifuged at 12,000xg for 5 min at 4°C. The upper, aqueous phase was processed for RNA isolation. The phenol-chloroform phase was processed for protein isolation.

RNA isolation

The upper, aqueous phase was transferred onto a Phasemaker tube containing 50 µL of TRIzol and 10 µL of chloroform, to maximize the quality and yield of RNA. Tubes were mixed by inversion, and spun with 12,000xg for 5 min at 4°C. The upper phase was mixed with 70% v/v EtOH in a 1:1 ratio and loaded onto a PureLink silica-based spin cartridge. RNA was washed according to the manufacturer protocol, before being eluted in RNase free water. RNA concentration was measured on a Nanodrop, and samples were diluted to 300 ng/µL. RNA was further purified by DNase treatment, which was conducted according to the manufacturer protocol: 0.1 volume (i.e. 5 µL for a 50 µL sample) of 10x DNase buffer was added to samples, followed by 1.5 µL of rDNase I. After gentle mixing, samples were incubated at 37°C for 20 min. Reactions were stopped by the addition of 0.15 volume (i.e. 7.5 µL for a 50 µL sample) of DNase inactivation reagent. Samples were spun at 10,000xg for 1.5 min after a 2 min incubation period. Purified RNA in the supernatant was recovered; concentration and quality were measured on a nanodrop (samples that have a A260/A280 above 1.8 are considered intact). RNA integrity was also assessed by running 1 µg of RNA mixed with loading dye in a 1% agarose gel prepared in Northern running buffer (30 min at 110V). Purified RNA was used for complementary DNA (cDNA) synthesis and subsequent quantitative PCR (qPCR) experiments (see 2.6.2).

Records of RNA purity and integrity can be found in appendix 1.

Protein isolation

DNA was precipitated from the phenol-chloroform phase by adding 100% EtOH (TRIzol EtOH 1:0.3) and pelleted at 2,000 x g, 4°C for 5 min. The supernatant was added onto a Pur-a-Lyzer dialysis tube, and extensively dialysed against 0.1% SDS for 16 h. Dialysis solution was replaced after 4h and replaced a second time after 2 h. Dialysate was spun at 10,000 x g, 4°C for 10 mins; the bulk of the protein is found as a globular mass between a clear supernatant and a viscous phase (Hummon et al., 2007). The globular mass was solubilised in 0.5% SDS, 4 M urea. Unfortunately, traces of solvents made using BCA for protein concentration determinant impossible despite diluting the extracts.

2.4. Routine techniques and sample preparation relative to brain tissue-based experiments

2.4.1. Brain tissue collection and homogenisation

Mice were sacrificed at specific ages by cervical dislocation, and brains were swiftly removed for consecutive processing. Brains were cut across the midline, with one half being fractionated and the other either extracted using RIPA buffer or used for different applications by other members of the lab (Fig. 2.3).

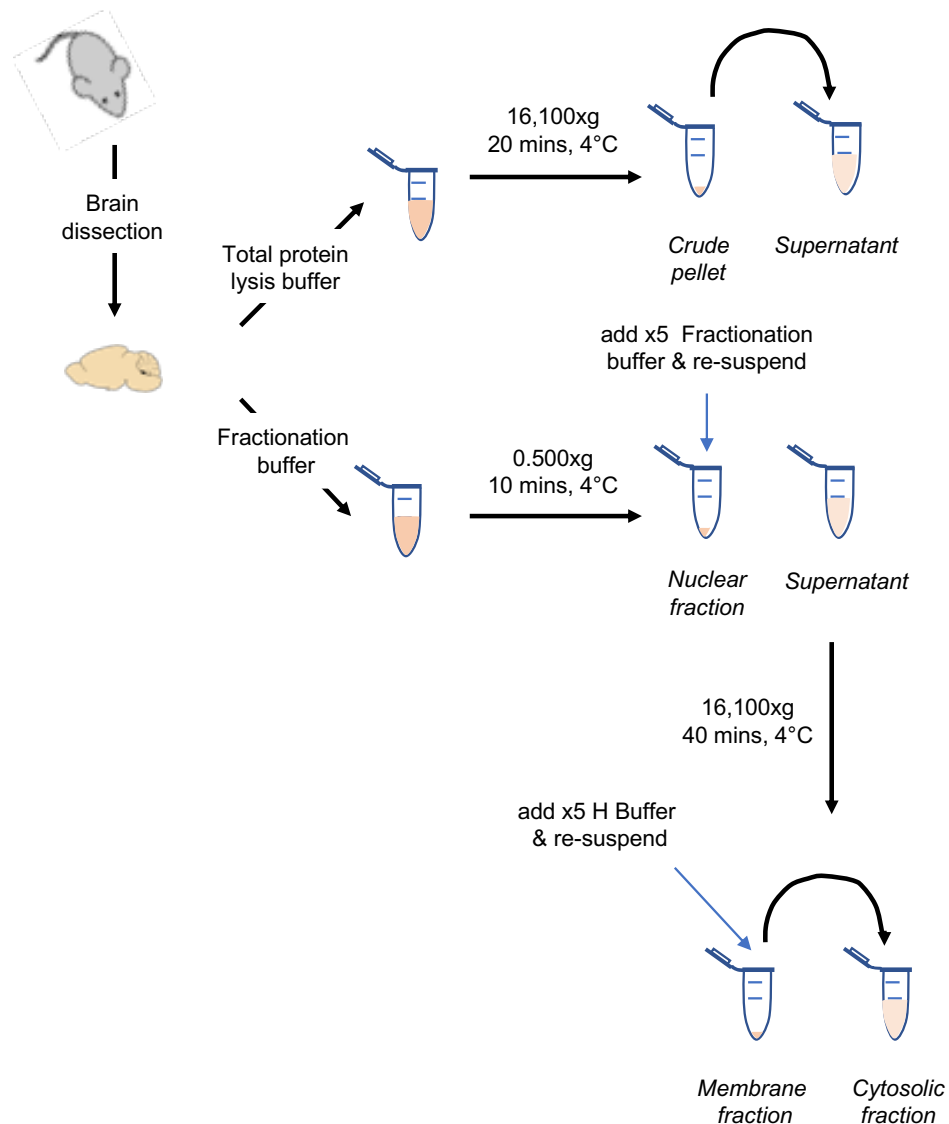


Figure 2.3 Mouse brain tissue collection and processing

Brains were isolated from mice at different ages and processed to either isolated total protein content (total protein lysis using RIPA buffer) or to fraction protein content into nuclear, membrane and cytosolic fractions.

Collected brain tissues were homogenised on ice in 5 volumes of buffer using a Dounce hand-held homogeniser. Initial tissue disruption was achieved by applying 15 strokes with a large pestle, followed by 15 strokes with a small pestle to get a homogeneous lysate. Proteins were extracted from the brain lysates following the protocols detailed below in 2.4.2.

2.4.2. Protein extraction and fractionation

Brain tissue and cell lysates were processed for protein extraction to isolate total protein content (RIPA extraction for brain tissue) or separate the proteins between nuclear, membrane and cytosolic fractions (fractionation).

RIPA buffer protein extraction

Homogenates were centrifuged at 16,100xg for 20 min. Supernatants were isolated and kept at -80°C until use. These fractions were referred to as “whole protein extracts” or “whole fractions” in this thesis.

Protein fractionation

Homogenates were centrifuged at 500xg for 2x10 min, with the pellet formed corresponding to the nuclear fraction. Supernatants were collected and centrifuged at 16,100xg for 40 min. Supernatants from this spin corresponded to the cytosolic fraction. Nuclear pellets were washed once with fractionation buffer, re-pelleted and resuspended in 600 µL fractionation buffer. Fractions show little cross-contamination (appendix 1). Both nuclear and cytosolic fractions were kept at -80°C until use.

2.5. Biophysical techniques

2.5.1. Mass spectrometry

- Principle

Mass spectrometry was used to confirm the correct amino-acid substitution in rApoE2, E3 and E4 following trypsin digestion. Mass spectrometry is an analytical technique based on the measurement of mass-to-charge ratio of ions. Peptides arising from enzymatic digestion are ionized, and their mass-to-charge ratio determined. Ionized peptides are identified by matching their mass-to-charge ratios to a database, resulting in the identification of the protein being analysed (Domon & Aebersold, 2006).

- Method

rApoE was run on an SDS-PAGE gel and stained with Imperial protein stain (see 2.4.3). Bands corresponding to rApoE2, E3 and E4 were excised from the gel and proteins were recovered using an In-Gel Trypsin Digestion kit. All three samples were run through a nano-LCMS, loaded onto a C18 trapping cartridge for 5 min at a flow-rate of 5 $\mu\text{L}/\text{min}$ in 0.1% TFA loading buffer and separated on an analytical column by a gradient from 1 to 35% acetonitrile over 28 min, in the presence of 0.1% TFA, at a flow rate of 0.3 $\mu\text{L}/\text{min}$. An emitter with 10 μm tip was used as nanospray source. Raw files were converted to .mgf format using MSConvert (Chambers et al., 2012) and identified peptides were searched against the SwissProt database on Mascot. Search parameters: 5ppm peptide mass tolerance; 0.8 Da fragment tolerance; trypsin with up to 1 missed cleavage. Variable modifications: deamidation (NQ); oxidation (M). Fixed modification: carbamidomethyl (C).

2.5.2. Analytical ultracentrifugation

- Principle

rApoE behaviour in solution was investigated using AUC, more specifically sedimentation velocity. It is a technique based on principles of hydrodynamics, which is useful to gain information on the size and shape of molecular entities present in a sample. When a strong centrifugal force is applied (40,000 rpm here), molecules move away from the air-buffer interface towards the bottom of the cell, creating boundary lines as followed by absorbance at 280 nm (Cole, 2000).

- Method

rApoE isoforms were used at a concentration of 0.8, 0.8, and 0.7 mg/mL in PB for rApoE2, E3 and E4 respectively. Samples (400 μ L) and PB (440 μ L) were loaded onto a double sector velocity cells placed in an AnTi60 rotor. Rotor speed was set to 40,000 rpm. Absorbance at 280 nm was recorded at a step size of 0.003 cm, every 25 min. The temperature was fixed to 20°C throughout the experiment. A continuous size distribution $c(s)$ Lamm equation model in the range of 0.1S-15S was fit to the scans using the programme SEDFIT version 15.01b (Schuck, 2000), solved at a confidence interval (F-ratio) of 0.95. Buffer viscosity and density were calculated using Sednterp version 20120828 BETA (Laue et al., 1992).

2.5.3. Circular dichroism spectroscopy

- Principle

Far-UV CD spectroscopy was used to study the secondary structure of rApoE. CD spectroscopy is a technique based on polarization of UV light that takes advantage of proteins' chiral chromophores, which unequally absorb left-handed and right-handed circular polarised light. Proteins' secondary structures such as random-coil, α -helix, and β -sheet, are characterised by a defined CD spectrum (Fig. 2.4).

CD spectroscopy was also used for thermal denaturation studies by following changes in secondary structure with increasing temperature at 222 nm, since rApoE is mainly α -helical in conformation.

The measured ellipticity Θ in mdeg at wavelength λ was transformed to mean residue ellipticity ($[\Theta]$ in $\text{deg}\cdot\text{cm}^2\cdot\text{dmole}^{-1}$) using equation (4):

$$[\Theta] = \frac{\Theta}{10 \cdot n \cdot C \cdot l} \quad (4)$$

with n the number of amino acid bonds in the protein, C the concentration of the sample in $\text{mol}\cdot\text{L}^{-1}$ (measured in triplicated using a Nanodrop; see 2.2.2) and l the path length in cm (Chou et al., 2005).

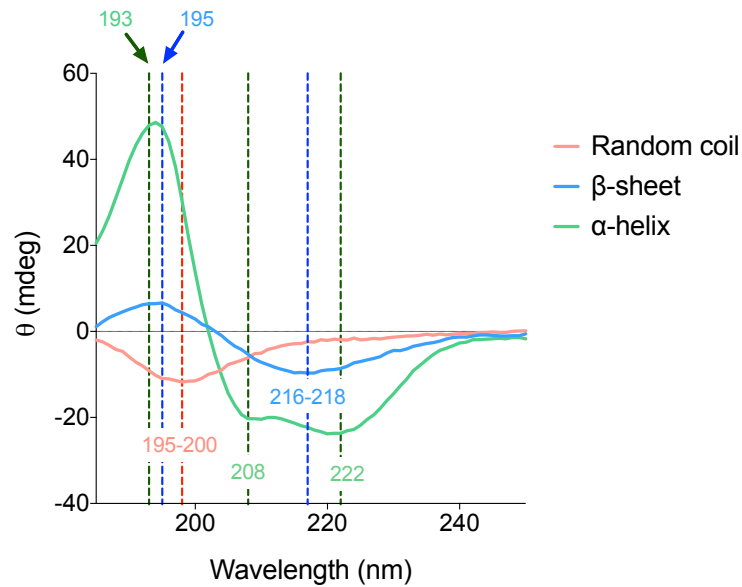


Figure 2.4 Reference CD spectra of α -helical, α -sheet and intrinsically disordered proteins

α -helical proteins present three bands, two negatives at 222 nm and 208 nm and a positive one at 193 nm. Proteins containing β -pleated sheets show negative bands at 216-218 nm and positive bands at 195 nm. Finally, disordered, random coil-containing proteins, are characterised by a single negative band at \sim 198 nm (Greenfield, N., 2007).

Spectrum measurement and treatment of data

Temperature was maintained at 21°C using a Peltier controlled, thermostated cell holder. All spectra were collected in 0.01 cm transparent quartz cuvettes in the range of 280-180 nm with a resolution of 0.1 nm. Bandwidth was set to 1 nm, the scanning-speed to 50 nm/min, response time to 4 s and sensitivity to standard. Each spectrum is the resulting average of three acquisitions, which were subsequently buffer-corrected. For each isoform, spectra were collected on protein from four different production batches and an average trace of $[\Theta]$ against wavelength was obtained using GraphPad Prism. Secondary structure of rApoE isoforms was analysed online at DICHROWEB by deconvolution of CD spectra performed with the CONTIN programme using the reference spectra set 6 (Lobley et al., 2002; Whitmore & Wallace, 2004; 2008). Results represent a mean of values from four spectra per isoform.

Thermal scans and treatment of data

Temperature was increased at a rate of 1°C/min with for thermal denaturation of rApoE. Ellipticity Θ in mdeg at a wavelength λ of 222 nm was recorded every 1.0°C from 20°C

to 80°C, with a sensitivity of 100 mdeg, a response time of 1 s and a bandwidth of 1 nm. Recordings were acquired for proteins from four different production batches and an average trace of $[\Theta]$ against temperature was obtained using GraphPad Prism. A phenomenological Boltzmann sigmoidal curve was fitted to averaged traces with the following equation (5):

$$Y = \frac{\text{Top} - \text{Bottom}}{1 + e^{\frac{T_m - X}{\text{Slope}}}} \quad (5)$$

with Top = maximum $[\Theta]$ value, Bottom = minimum $[\Theta]$ value, T_m the temperature corresponding to 50% change in α -helical content and Slope is the steepness of the curve. Calculated thermal denaturation curves were then transformed into the fraction of the protein unfolded for comparison of protein transformation with the following equation (6):

$$\text{Fraction unfolded} = \frac{[\Theta]_N - [\Theta]}{[\Theta]_N - [\Theta]_D} \quad (6)$$

with $[\Theta]_N$ the ellipticity of the protein at 20°C corresponding to the folded state and $[\Theta]_D$ the ellipticity of the denatured protein at 80°C. These newly obtained fraction unfolded curves were also fitted to a Boltzmann sigmoidal curve (equation 6), with Top and Bottom fixed to 1 and 0 respectively.

2.5.4. Tryptophan fluorescence spectroscopy

Intrinsic tryptophan fluorescence

Fluorescence scans were collected using SpectraMax i3 plate-reader. Samples were mixed for 5 s by medium orbital shake prior to acquisition. Six measurements per well were acquired from the top (1 mm height). Photomultiplier tube sensitivity was set to high; excitation bandwidths was set to 9 nm and emission bandwidths to 15 nm.

Trp residues were excited at 295 nm to reduce the contribution of tyrosine, and scans were collected with 1 nm increments between 320 nm and 465 nm. Fluorescence scans were buffer corrected. Four different production batches per isoform were used, and blank-subtracted averaged traces of fluorescence intensity against wavelength were obtained using GraphPad Prism.

Chemical denaturation

Trp fluorescence scans were acquired at 20°C in a Varian Cary Eclipse spectrophotometer paired with a Varian Cary temperature controller, in a 1 cm quartz cuvette. Five acquisitions per concentration point were collected at a scan speed of 90 nm/min and a response time of 0.05 s.

Trp residues were selectively excited at 292 nm (Kishore et al., 2012). Emission was monitored with 0.15 nm increments between 310 nm and 400 nm; excitation and emission bandwidths were both set to 10 nm. Data was acquired in triplicate using three different production batches per isoform.

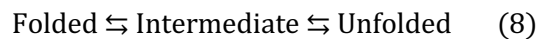
Wavelength of maximum emission (λ_{\max}) per GuHCl concentration point was determined by peak fitting of the blank-corrected, averaged emission spectra (Clément-Collin et al., 2006) to a polynomial of degree 6 (7) using Excel:

$$y = a_0x^6 + a_1x^5 + a_2x^4 + a_3x^3 + a_4x^2 + a_5x + a_6 \quad (7)$$

with $a_i = \text{INDEX}(\text{LINEST}(\text{range } Y; \text{range } X^{\{1\2\3\4\5\6\}}); 1; i + 1)$ for $i \{1 \dots 6\}$

and $a_0 = \text{INDEX}(\text{LINEST}(\text{range } Y; \text{range } X^{\{1\2\3\4\5\6\}}); 1)$.

The wavelength corresponding to the maximum fluorescence intensity was plotted against GuHCl concentration resulting in denaturation profiles for each isoform. A three-state unfolding model fitted the denaturation curves (Crisanti & Matthews, 1981; Pace, 1986), as described in equation (8):



Equation (9) depicting a three-state unfolding was fitted to the data (Tendian et al., 1995)

$$Y = \frac{Y_F ([GuHCl]) + Y_U ([GuHCl]) \times K_{app}}{1 + K_{app}} \quad (9)$$

with Y corresponding to λ_{\max} , and Y_F and Y_U the signal corresponding to the folded (F) and unfolded (U) protein respectively. Y_F and Y_U are linearly dependent on the concentration of denaturant, as displayed in equation (10):

$$Y_x = Y_x^0 + m_x [GuHCl] \quad (10)$$

with x corresponding to either the F or U state and Y_x^0 the λ_{\max} at either 0 M or 6 M GuHCl.

K_{app} is the guanidine-dependent equilibrium constant of the denaturation process, defined by equation (11):

$$K_{app} = \frac{K_1 K_2 + A K_1}{1 + (1 - A) K_1} \quad (11)$$

with K_1 , K_2 and A defined by equation (12-14)

$$K_1 = e^{\frac{-(\Delta G_{1H2O} - m_1 [GuHCl])}{RT}} \quad (12)$$

$$K_2 = e^{\frac{-(\Delta G_{2H2O} - m_2 [GuHCl])}{RT}} \quad (13)$$

$$A = \frac{(Y_i - Y_F^0)}{(Y_U^0 - Y_F^0)} \quad (14)$$

A , ΔG_{1H2O} , ΔG_{2H2O} , m_1 and m_2 are parameters determined from the curve fitting and correspond to the fractional change in λ_{max} , the free energy difference between states (F to I for ΔG_{1H2O} and I to U for ΔG_{2H2O}) and the slope of the linear extrapolation to 0 M GuHCl (Tendian et al., 1995).

The concentrations corresponding to 50% unfolding of the protein to an intermediate state ($[GuHCl]_{50,I}$) and to an unfolded state ($[GuHCl]_{50,U}$) are determined from the above-mentioned parameters, by (15) and (16) respectively:

$$[GuHCl]_{50,I} = \frac{\Delta G_{1H2O}}{m_1} \quad (15)$$

$$[GuHCl]_{50,U} = \frac{\Delta G_{2H2O}}{m_2} \quad (16)$$

The shape of ApoE unfolding curves was directly compared between the three isoforms by plotting A as a function of $[GuHCl]$ and equation (9) was fitted to the resulting unfolding curves.

2.5.5. Thioflavin-T fluorescence assay for detection of protein self-assembly

Scan acquisition with fluorometer

This method was used for acquisition of scans after 0 h and 24 h incubation times. Fluorescence measurements were obtained with a Varian Cary Eclipse spectrophotometer (using a 1 cm path length quartz cuvette). Aliquots taken from the assembling samples were diluted to 10 μ M in PB and ThT was added to a final concentration of \sim 20 μ M.

ThT fluorescence was monitored at 21°C with an excitation filter of 450 nm and its emission was monitored between 460-600 nm. Excitation and emission slits were set to 5 nm and 10 nm respectively, and the scan rate was set to 600 nm/min with 1 nm data intervals and an averaging time of 0.1 s. The photomultiplier tube detector voltage was set to 800 V (Al-hilaly et al., 2013). Scans were acquired in triplicate; three production batches were used per isoform.

Scan acquisition with plate reader

This method was used for acquisition of scans after 0 h and 3 days incubation times. Fluorescence scans of 25 µM samples in a 96-well fluorescence plate were obtained with a SpectraMax i3 plate reader. ThT was added to each well at a 2.2:1 ratio.

ThT fluorescence was monitored at rt with an excitation filter of 440 nm and its emission was monitored between 465-600 nm with 1 nm increments. Excitation and emission bandwidths were set to 9 nm and 15 nm respectively. The photomultiplier tube detector voltage was set to high. Three different production batches per isoform was used, and buffer-corrected averaged traces of ThT fluorescence intensity against wavelength were obtained using GraphPad Prism.

Kinetic acquisition

Samples in the presence of ThT were incubated at 37°C in the SpectraMax i3 plate reader to allow for kinetic recordings. 96-well plates were sealed with an optically clear polyolefin film to avoid evaporation. Readings were acquired using the same bandwidths and PMT and optics settings as for Trp fluorescence scans (see previously). ThT was excited at 440 nm and its emission at 483 nm was monitored every 15 min, with 3 s low orbital shakes before data collection. Scans were first buffer corrected. Minimum fluorescence intensity value (F_{min}) was then subtracted to fluorescence intensity at any given time point (F) for each isoform to generate adjusted scans, using equation (17):

$$Y = F - F_{min} \quad (17)$$

Scans could not be adjusted to the initial fluorescence due to the behaviour of ThT with increasing temperature (from rt to 37°C).

Adjusted fluorescence was plotted against time, and averaged traces for each isoform was obtained on GraphPad Prism. A minimum of three different production batches per isoform was used.

2.5.6. Transmission Electron microscopy

Grid preparation and imaging

Fibrillation was assessed by negative stain transmission electron microscopy (TEM). A small droplet of sample (4 μL) was placed on a 400-mesh carbon-coated grid and incubated for 1 min. After blotting the excess solution, the grid was washed with 4 μL filtered ultrapure water and blotted dry. It was then negatively stained with 4 μL filtered 0.5% uranyl acetate for 20 s and dried with filter paper. Grids were left to air-dry for at least 5 min before storage. Grids were examined on a Jeol Jem1400- plus transmission electron microscope fitted with a Gatan Orius SC100 camera at an opening voltage of 80 kV (Al-hilaly et al., 2013).

Processing of micrographs

Micrographs were selected according to the quality of the image (in terms of focus) and processed using ImageJ to insert a scale bar. When relevant, lengths and widths of species obtained were measured using ImageJ to assess changes over time.

Stereological estimators were used to measure the length of the fibrils, based on the Buffon needle's problem. This supposes the random distribution of the fibrils in the image, which was overlaid with vertical lines. 20 random regions of interest were selected per image. The averaged boundary length L of fibrils was calculated using equation (18), which is based on the probability that the fibril has to intersect a line depending on its length. and vertical lines overlaid on the image.

$$L = \frac{\sum \left(\frac{\pi}{2} \times \sum l \times d \right)}{N} \quad (18)$$

with $\sum l$ the number of intersections per fibril, d the distance between the vertical lines and N the number of objects measured per image.

The number of intersections between a fibril and a line was counted using the integrated Cell Counter macro on ImageJ, and this was done for the 20 randomly selected objects

per image (on average). Three to four images per time point were analysed in this manner.

Widths of fibrils were also measure using Image J. Three to four images were analysed per time point, and ten species were randomly selected per image. Widths were measure along species one to three times depending on their respective length.

2.5.7. X-Ray Fibre diffraction

rApoE4 at 100 μ M were incubated at 37°C for 24 h. Samples were centrifuged for 45 min at 60,000 rpm and 4°C in an Optima™ MAX Ultracentrifuge. Supernatants were put aside, and pellets were resuspended in 200 μ L filtered water to remove all the salts that can interfere with the diffraction pattern. Samples were centrifuged a second time; supernatants were discarded, and pellets washed again in 200 μ L filtered water. Final pellets were resuspended in 10 μ L filtered ultrapure water. Fibrils were aligned into bundles in a Petri dish. Bundles were obtained by suspending a 5-10 μ L droplet between two wax-tipped glass capillary tubes, separated by a 2 mm gap. Samples were allowed to dry at 4°C, resulting in partially aligned fibre samples (Morris & Serpell, 2012).

X-ray diffraction images were collected by Dr. Al-hilaly from the Serpell lab, using a Rigaku rotating anode source λ (CuK α) and a Saturn CCD detector (Morris & Serpell, 2012). Fibre samples were placed in the X-ray beam 30 s at a specimen to detector distance of 50 mm and for 60 s at 100 mm. Diffraction signals were measured using an in-house programme called CLEARER (Makin et al., 2007).

2.5.8. Waltz algorithm

The amyloidogenicity of ApoE isoforms was investigated using the WALTZ algorithm (Maurer-Stroh et al., 2010), which generates graphs indicating predicted amyloidogenic regions in the protein sequence. The primary sequence of each isoform was input into the WALTZ algorithm (<http://waltz.switchlab.org>). Data was output as a text file. Plots showing the % Amyloidogenicity against amino acid number were obtained using GraphPad Prism and the data from the text files.

2.6. Cell and molecular biology

2.6.1. Live/dead assay using fluorescence microscopy

Media was sequentially removed from cells by the means of three half washes with warmed Live cell imaging solution. ReadyProbes kit was used in accordance with the manufacturer protocol in order to evaluate cell viability (Thermo Fisher). In brief, after media exchange for Live cell imaging solution, one drop of each probe was added per well and cell plates were incubated at 37°C for 45 min before imaging.

Imaging was conducted on an Axiovert inverted CO microscope. Excitation and emission wavelengths for each dye, what they stain, and the microscope filter used to image are summarised in table 2.8.

Dye	Excitation wavelength	Emission wavelength	Filter	Staining
NucBlue®	360 nm	460 nm	DAPI	All nuclei
Propidium Iodide	535 nm	617 nm	TRITC	Nuclei of compromised cells

Table 2.8 ReadyProbes specifications

Four to five different regions were imaged per well; automated quantification was achieved using an in-house macro on ImageJ based on the detection of maxima when quantifying SH-SY5Y cells. Counting of neurons had to be done manually.

The percentage of live cells was determined in each region imaged and averaged per condition; % Live cells was then normalised to control cells and expressed as “% Live cells compared to control”. Graphs were plotted on GraphPad Prism.

2.6.2. Reverse transcription and quantitative polymerase chain reaction

RNA obtained in section 2.3.3 was reverse transcribed into cDNA for subsequent qPCR experiments.

cDNA synthesis

RNA extracted was used for cDNA synthesis using the High Capacity cDNA Reverse Transcription Kit, following the manufacturer’s instructions (Applied Biosystems). In brief,

a 20 μ L reaction was set up for each sample in 0.2 mL PCR tubes, on ice. Each tube contained 10 μ L extracted RNA, and 10 μ L of 2x Reverse Transcription master mix supplemented with RNase Inhibitor. No more than 2.5 μ g of extracted RNA per reaction was used throughout. Tubes were loaded to a thermal cycler programmed as follows: 25°C, 10 min; 37°C, 120 min; and 85°C, 5 min followed by an infinite hold at 4°C. Newly synthesised cDNA was collected and either used for qPCR straight away or stored at - 20°C until use.

qPCR

- Experiment

cDNA was used as a template for qPCR. Amplification was carried out using the Luna Universal qPCR kit, which contains the SYBR Green DNA-binding fluorescent dye. Samples were prepared according to the manufacturer protocol (NEB). Briefly, reactions were set up in a white 96-well semi-skirted PCR plate. Each reaction (20 μ L) contained 1X Luna Universal qPCR Master Mix, forward and reverse primers (optimised concentrations used are summarised in table 2.9), and 5 μ L diluted template cDNA. Template cDNA from SH-SY5Y cells were diluted at 1:10 to 1:15; template cDNA from neurons was diluted at 1:50 to 1:100. A cDNA serial dilution of 1:10, 1:100, 1:1,000 and 1:10,000 was prepared as standard curve in each experimental plate; cDNA obtained from HepG2 cells was used as a standard for SH-SY5Y cells experiments and cDNA obtained from ApoE-TR mouse cortex was used as a standard for experiments conducted in primary neurons. Negative control wells, containing only nuclease free water, were included in each plate; “No reverse transcription” control wells were also set up, with addition of 5 μ L extracted RNA instead of cDNA to ensure the absence of contaminating genomic DNA (which should have been removed following rDNase treatment as detailed in 2.3.3). cDNA amplification was carried out using the Roche LightCycler 480 II (SYBR/FAM scan mode) with an initial denaturation at 95 °C for 60 s followed by 45 cycles of denaturation at 95 °C for 15 s and extension at 60 °C for 30 s. Melt curves were also generated following the instrument’s recommendation for melt curve step.

Set of primers	<i>APOE</i> (SH-SY5Y)	<i>hACTB</i>	<i>hGAPDH</i>	<i>mACTB</i>	<i>APOE</i> (neurons)
Concentration	0.25 μ M	0.25 μ M	0.25 μ M	0.5 μ M	0.38 μ M

Table 2.9 Optimised primers concentrations

Primers sequences were given in table 2.3.

- Analysis

Transcript levels were automatically determined by the Roche LightCycler 480 service software using the standard curve method, and advanced relative quantification was also performed using the acquisition software. In order to perform this kind of analysis, one needs to ensure that the primers' efficiency for the amplification of the target gene (*hAPOE*) and for the amplification of the reference genes (*hACTB* and *hGAPDH* for SH-SY5Y and *mACTB* for cortical neurons) are within 5% of each other, and between 85%-110%. A summary of primers' efficiencies obtained for each repeat experiment can be found in appendix 1. Unfortunately, a second reference gene to normalise *APOE* levels in cortical neurons could not be optimised for due to time restrictions. Negative controls wells with an amplification cycle (Cq) above 35 were considered negative. Melt curves were also generated for each well; special attention was paid to negative control wells with Cq<35 to ensure there was no genomic DNA contamination. An example of integrated melt curves generated by the acquisition software was included in appendix 1.

Data generated by advanced relative quantification in the Roche LightCycler 480 service software was output as a ratio of target DNA sequence to a reference DNA normalised to that of a calibrator. Calibrators corresponded to control treatment both in SH-SY5Y cells' and in neurons' experiments.

2.7. Biochemistry

2.7.1. Total protein quantification

Protein concentrations of cell and protein extracts were measured using the BCA Protein Assay Kit according to the user guide. In brief, 25 μL of both standards and samples were pipetted in duplicate into a 96-well plate. A BSA standard curve was established from 0.125 mg/mL to 2 mg/mL; both cell and protein extracts were diluted in dH_2O at a 1:25 ratio. Reagent A (a buffered solution containing bicinchoninic acid) and Reagent B (containing 4% cupric sulphate) were mixed in a 50:1 ratio, and 200 μL were pipetted onto each well. Absorbance was read at 562 nm after a 30 min incubation period at 37°C. Absorbance values were buffer corrected; concentrations were determined from the standard curve and adjusted with the dilution factor.

2.7.2. One-dimension sodium dodecyl sulphate polyacrylamide gel electrophoresis

Both inner and outer chambers of a Mini-PROTEAN Cell for 1D vertical gel electrophoresis were filled with denaturing running buffer.

Recombinant protein samples for denaturing one-dimension SDS polyacrylamide gel electrophoresis (1D-SDS-PAGE) were prepared in Laemmli sample buffer to a final concentration of 3 μM , omitting the addition of any reducing agent unless stated otherwise.

Proteins extracted from cells were diluted to a final concentration of 2 mg/mL in Laemmli sample buffer containing 50 mM DTT as reducing agent. Proteins extracted from brain tissue were diluted to a final concentration of 2 mg/mL if RIPA buffer-extracted, or of 1 mg/mL if fractioned, in Laemmli sample buffer containing 50 mM DTT. The protein mixtures were incubated for 10 minutes at 70°C for denaturation, cooled down and loaded into gels.

10 μL of sample were loaded for recombinant protein gels; 10 μg of protein from cytosolic fractions and 25 μg of protein from whole protein extracts were loaded onto the brain extract gels. Gels were run at 120 V (constant voltage) for 70-80 min. Resolved proteins were stained using Imperial protein stain, a Coomassie dye R-250 containing solution.

2.7.3. Native gel electrophoresis

The inner and outer chambers of a Mini-PROTEAN Cell were filled with native running buffer. Protein samples were diluted down to 3 μ M in Native sample buffer and were directly loaded into a 4-20% TGX gel. Gels were run at 120 V (constant voltage) for 120 min. Resolved proteins were stained using a Coomassie dye R-250 containing solution.

2.7.4. Western (immuno) blotting and dot blot

- Experiment

Nitrocellulose membranes were blocked for 1 h at rt with Blocking Buffer. Membranes were then incubated for 1 h at rt or overnight at 4°C with a primary antibody diluted in blocking buffer (Table 2.6). Following 3 x 5 min washes in TBS-T, they were incubated for 1 h with the corresponding HRP conjugated secondary antibody, diluted in blocking buffer.

Samples examined by dot blot were directly spotted onto a nitrocellulose membrane (5 μ L). After letting the samples dry, membranes were soaked in TBS-T and then blocked and processed as western blots.

Antibody immunoreactivity was visualised using Clarity Western Enhanced Chemiluminescence Substrate reagents A (luminol/enhancer solution) and B (peroxide solution), mixed at a 1:1 ratio and poured over the membranes for 5 min. Immunoreactivity was visualized on the bio-imaging F-ChemiB 3.2M system.

- Quantification of protein levels

Levels of the target protein (ApoE or α -tubulin) detected using Western Blot (WB) were semi-quantified by densitometry when applicable. Band intensities in each sample were determined using ImageJ and normalised to the band intensity of a reference protein (GAPDH in both cases). The linearity of the antibodies was established over a range of protein amounts and included in appendix 1.

Since many blots had to be run to analyse all samples, one sample was elected as calibrator and was loaded on all the gels – this allows by-passing any variability due to gel transfer, binding of antibodies or detection reagents (calibrators for each set of experiments are indicated in appendix 1). All samples for semi-quantification were anyways diluted to the same concentration and the same amount of protein was added in each well. A graph showing that GAPDH levels did not vary with time or ApoE phenotype was also included in appendix 1.

Data was analysed on GraphPad prism. All ratios were grouped into age groups by genotype, and outliers were identified using the ROUT method with Q=10%, thus removing likely outliers. This allowed removal of anomalies in western blots, such as presence of bubbles or black spots that may happen because of the blocking solution, without bias. Ratios of samples were then averaged and means grouped by age and genotype.

2.7.5. Enzymatic assays

RIPA-extracted samples were thawed on ice. Protein concentration determination, CAT activity and SOD activity assays were conducted in parallel.

First, samples were diluted at a 1:25 or 1:35 ratio for protein content determination (see 2.7.1). Subsequent dilutions were made in the respective CAT and SOD activity assay buffers.

Amplex Red CAT activity assay

- Principle

Homogenates are incubated with H₂O₂. Following the incubation period, any remaining H₂O₂ reacts with Amplex Red in the presence of HRP with a 1 to 1 stoichiometry, producing the fluorophore resorufin.

- Protocol

Samples were diluted in a 1:500 ratio in 1X CAT assay buffer (0.1 M Tris-HCl, pH 7.5). CAT activity was measured following the manufacturer protocol (Thermo Fisher). Briefly, 25 µL of standards and samples were pipetted in quadruplicate in a 96-well plate. A CAT standard curve was generated in the range of 0 to 2 U/mL and included in each experimental plate. 25 µL of 40 µM H₂O₂ was added to each well and samples were incubated at rt for 30 min. 50 µL of CAT enzymatic solution (100 µM Amplex Red, 0.4 U/mL HRP) was added to each well and plates were incubated at 37°C for 30 min before absorbance measurement at 571 nm. Outlier replicate wells were identified using the ROUT method with Q=10% and subsequently removed. Change in absorption was reported as the observed absorbance at 571 nm subtracted from that of a no-catalase control. CAT activity samples, in U/mL, were calculated from the standard curve.

- Determination of CAT activity in U/mg of protein

CAT activity was expressed in U/mg of protein by normalising to total protein content determined by BCA assay. CAT activities were then grouped by age and phenotypes.

SOD activity assay

- Principle

Xanthine oxidase (XO) converts xanthine to H₂O₂ and uric acid, while generating O₂^{•-}. WST-1 reacts with superoxide anions to form a formazan dye that absorbs at 450 nm. SOD competes for O₂^{•-}, reducing its level in the system. SOD activity is thus measured indirectly by quantifying the subsequent reduction in formation of WST-formazan.

- Protocol

Samples were diluted in SOD dilution buffer (1:100 or 1:35). SOD activity was measured according to the manufacturer's instructions. 20 µL of standards and samples were pipetted in triplicate at least into a 96-well plate. A SOD standard curve was generated in the range of 0.5 to 10 U/mL (at least). 200 µL of WST-1 working solution were added to all the wells. 20 µL of XO working solution were added to standards and samples. Several blank wells were prepared: blank 1 contained dH₂O in place of sample; blank 2, prepared for each sample, contained samples, in duplicate, but dilution buffer was added instead of XO solution; blank 3 contained 20 µL dH₂O and 20 µL dilution buffer instead of sample and XO solution. Solutions in wells were mixed by pipetting, before incubating at 37°C for 20 min. Absorbance was read at 450 nm and SOD activity (expressed as inhibition rate %) was calculated using equation 19:

$$\text{Inhibition rate \%} = \frac{(A_{\text{blank1}} - A_{\text{blank3}}) - (A_{\text{sample}} - A_{\text{blank2}})}{(A_{\text{blank1}} - A_{\text{blank3}})} \times 100 \quad (19)$$

Outlier replicate wells were identified using the ROUT method with Q=10% and subsequently removed.

- Determination of SOD activity in U/mg of protein

SOD activity was expressed in U/mg of protein by normalising to total protein content determined by BCA assay. SOD activities were then grouped by age and phenotypes.

2.8. Statistical analyses

Statistical tests were performed using the GraphPad Prism software. One-way analysis of variance (ANOVA), followed by the recommended post-hoc multiple comparisons test when appropriate, was performed to analyse a factor between three or more groups. One-way repeated measures (RM) ANOVA, followed by the recommended post-hoc multiple comparisons test when appropriate, was conducted when experiments were run on matched subjects (treated cells on the same set of cells and on the same day for example).

Two-way ANOVA, followed by post-hoc multiple comparisons test when appropriate, was performed when investigating the effects of two factors on a measured parameter (for example the effect of age and phenotype of enzymatic activity).

Unpaired t-tests were performed when comparing a parameter in two groups if data was normally distributed; otherwise, unpaired Kolmogorov-Smirnov tests were conducted. Multiple t-tests followed by the recommended post-hoc test was performed when comparing a parameter in a set of independent data.

Chapter 3- Self-assembly properties of recombinant human Apolipoprotein E

3.1. Introduction

Background

Human ApoE was identified in 1975 as one of the components of VLDL (Utermann et al., 1975), and its full amino-acid sequence was first elucidated by Rall et al in 1982 (Rall, S. et al., 1982). Mature ApoE is a 299 amino acid, arginine-rich protein of approximately 34,200 Da that exists as three different isoforms, termed ApoE2, ApoE3 and ApoE4 (Utermann et al., 1977). ApoE polymorphism arises from the existence of three different *APOE* alleles $\epsilon 2$, $\epsilon 3$ and $\epsilon 4$ (Zannis et al., 1981), giving rise to three homozygous ($\epsilon 2/\epsilon 2$, $\epsilon 3/\epsilon 3$, $\epsilon 4/\epsilon 4$) and three heterozygous ($\epsilon 2/\epsilon 3$, $\epsilon 2/\epsilon 4$, $\epsilon 3/\epsilon 4$) genotypes. The resulting phenotypes agreed upon in the field are E2/2, E3/3 and E4/4 for homozygotes and E2/3, E2/4 and E3/4 for heterozygotes (Zannis et al., 1982). The three isoforms differ at amino-acid positions 112 and 158, with ApoE2 having two Cys residues, ApoE3, a Cys and an Arg, and ApoE4, two Arg (Rall, S. et al., 1982) (Fig. 3.1).

Because of its role in lipid and cholesterol transport and uptake, the structure of ApoE has been extensively characterised (Weisgraber & Mahley, 1996). Studies conducted on human ApoE3 isolated from plasma have shown it to be a highly α -helical protein that self-associates into a tetramer in solution (Yokoyama et al., 1985). Further investigations into the structure of human ApoE3 have highlighted the presence of two independent domains separated by a hinge region (Wetterau et al., 1988): the N-terminal domain (residues 1-167) containing the LDL receptor-binding activity (Innerarity et al., 1983) and the C-terminal end (residues 206-299) involved in lipid-binding (Weisgraber, 1990). This was later confirmed to also be the case for recombinant human ApoE2, E3 and E4 (Morrow et al., 2000) (Fig. 3.1A).

The crystal structure of full-length human ApoE has yet to be elucidated. Only that of the N-terminal fragment has been achieved so far. X-ray crystallography studies on the 22 kDa N-terminal domain of human plasma ApoE3 have shown that it is composed of five α -helices. Helices N1, N2, N3 and N4 are arranged in an anti-parallel, elongated four-helix bundle, with helices N1 and N2 being joined by a helical loop (Wilson et al. 1991; Weisgraber & Mahley 1996).

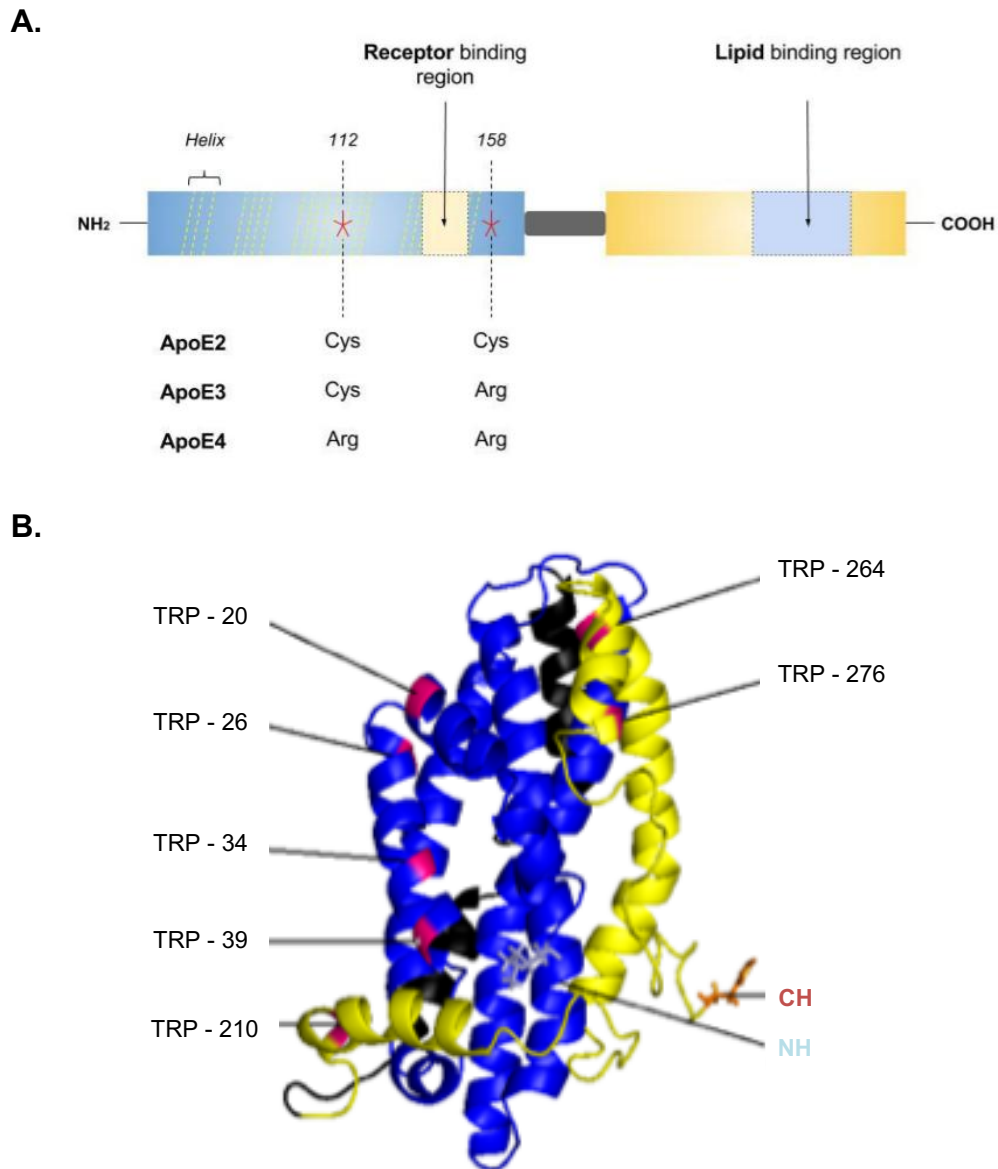


Figure 3.1 Structure of ApoE isoforms

A. ApoE4, ApoE3 and ApoE2 differ from one another at amino acid positions 112 and 158, with an Arg to Cys substitution. The three isoforms are formed of two independent domains separated by a flexible region: the amino-terminal harbouring the receptor binding region and the carboxy-terminal domain involved in lipid binding. *Adapted from* (Liu, C.-C. et al., 2013).

B. ApoE structure, generated from the NMR structure of ApoE3 (PDB 2L7B), showing the position of Trp residues

This model was later supported by NMR analysis of ApoE3. In addition, the NMR structure of ApoE3 provided structural insight into the hinge region and the C-terminal domain: the hinge region is formed of two helices that modulate interactions between the amino- and carboxy- termini; the C-terminal domain is organised into three helices C1, C2 and C3. C1 interacts with N1, and C2 and C3 with N3 and N4 (Chen, J. et al., 2011).

In the early 90s, ApoE protein was found to be associated with major pathological hallmarks of AD such as senile plaques and NFT (Namba et al., 1991). The $\epsilon 4$ allele of the *APOE* gene was later found to be a risk factor for both familial and sporadic AD (Schmechel et al., 1993), acting in a dose-dependent manner (Corder et al., 1994). Since then, ApoE has been extensively studied in relation to A β and Tau pathologies (Strittmatter et al., 1994; Deane et al., 2008; Kanekiyo et al., 2014). However, studies to establish whether ApoE itself may be subject to misfolding and aggregation are lacking. One study published by Hatters et al. in 2006 showed that recombinant human ApoE4 was more prone to formation of neurotoxic amyloid-like fibrils than ApoE2 and ApoE3 due to decreased stability and molten globule formation (Hatters et al., 2006). This has not been pursued further to date. More recently, the presence of ApoE4 aggregates in the brain of human *APOE* transgenic AD mice was suggested, with the use of antibodies specific to nonlipidated and aggregated ApoE shown to reduce A β deposition (Liao et al., 2018).

With the ApoE phenotype being one of the biggest risks for AD onset, it is of great interest to advance our understanding on whether ApoE is prone to misfolding and aggregation.

Rationale

Recombinant human ApoE produced in *E. coli* (rApoE) was used as a model to explore the self-assembly properties of ApoE under physiological conditions. This study relied on an essential and thorough structural characterisation of the three isoforms at the macromolecular and molecular level, as well as their respective stability, in order to identify any structural feature that would promote fibril formation. Data presented here point to major similarities in the secondary, tertiary and quaternary structures of the rApoE isoforms. However, rApoE4 displayed a clear propensity over the other two isoforms to self-assemble into fibrils. Pathogenicity of fibrils, and more generally of proteins and small oligomers, being essentially reliant on their structure, rApoE4 fibrils were extensively characterised to determine whether they possess amyloid-like, cross- β structure.

3.2. Summary of methods

A wide-range of biophysical techniques was used to characterise the structure of rApoE isoforms before exploring their respective propensity to misfold and aggregate.

Structural characterisation was conducted as follows. In brief, proteins were produced recombinantly in *E. coli* and purified by column chromatography (see 2.2.1). The purification process was followed using denaturing gel electrophoresis (see 2.7.2) and primary amino acid sequence of each isoform was confirmed using mass spectrometry (see 2.5.1). Their respective hydrodynamic behaviour in physiological buffer was assessed by AUC, more specifically sedimentation velocity (see 2.5.2). Secondary structure and thermal stability of rApoE isoforms were determined using CD spectroscopy (see 2.5.3). Finally, Trp fluorescence spectroscopy was used to study the tertiary structure of rApoE isoforms as well as their unfolding in the presence of a denaturant (GuHCl; see 2.5.4) (Fig. 3.1B).

Self-assembly of rApoE was explored using ThT fluorescence (see 2.5.5), negative stain TEM (see 2.5.6) and gel electrophoresis (denaturing and native; see 2.7.2 and 2.7.3). ThT is a cationic dye that has historically been used to detect and quantify amyloid fibrils *ex vivo* and *in vitro* as its fluorescence increases upon interaction with fibrils (Khurana et al., 2005). However, ThT is also a rotamer that was shown to interact with cross- α fibrils (Tayeb-Fligelman et al., 2017). In addition, ThT was used to explore rApoE self-assembly properties in the study by Hatters (Hatters et al., 2006).

Characterisation of rApoE4 fibrils was achieved using TEM, CD and X-ray fibre diffraction (see 2.5.7). X-ray fibre diffraction gives a definitive answer on whether fibrils are amyloid or not since cross- β structures in amyloid have a distinct diffraction pattern (Eanes & Glenner, 1968).

3.3. Results

Part of the findings presented here have been recently published in a peer-review journal: Raulin, A. C., Kraft, L., Al-Hilaly, Y. K., Xue, W. F., McGeehan, J. E., Atack, J. R., & Serpell, L. (2019). The Molecular Basis for Apolipoprotein E4 as the Major Risk Factor for Late-Onset Alzheimer's Disease. *Journal of molecular biology*, 431(12), 2248–2265.

Structural characterisation of recombinant human ApoE produced in E. coli

ApoE produced in *E. coli* has been extensively employed to model the structure and function of ApoE isoforms and was employed here to explore their respective self-assembly properties.

rApoE isoforms were characterised in depth to provide a definitive comparison at the macromolecular, molecular and protein stability level as self-assembly propensity is reliant on protein structure.

3.3.1. Production and purification of rApoE2

Dr Lucas Kraft established the process for the production and purification of rApoE3 and rApoE4 at the Sussex Drug Discovery Centre. Protein stocks used in this chapter were either provided by Dr Kraft in purification buffer prior to dialysis or prepared by me following the established protocols (see 2.2.1). Results presented here correspond to the production and purification of rApoE2. In short, I undertook the generation of an *APOE* ϵ 2-containing vector using site-directed mutagenesis. Consequently, rApoE2 was produced following a three-step process: cloning, expression and purification (Fig. 2.1). Denaturing gel electrophoresis of the isolated protein was used to assess its purity, and the primary sequence of the purified protein was confirmed by mass spectrometry.

Validation of site directed mutagenesis

Site-directed mutagenesis on an *APOE* ϵ 3-containing expression vector previously generated by Dr Kraft was performed to obtain a vector containing the ϵ 2 variant of *APOE*. Newly generated plasmids were transformed into *E. coli* strain Rosetta 2 and their sequence was verified by DNA sequencing (Eurofins, Germany). Fig. 3.2 shows an

excerpt of the newly obtained *APOE* $\epsilon 2$ sequence compared to *APOE* $\epsilon 4$, confirming the adequate base pair substitution c to t, giving rise to the wanted Arg to Cys amino-acid change at position 112 and 158.

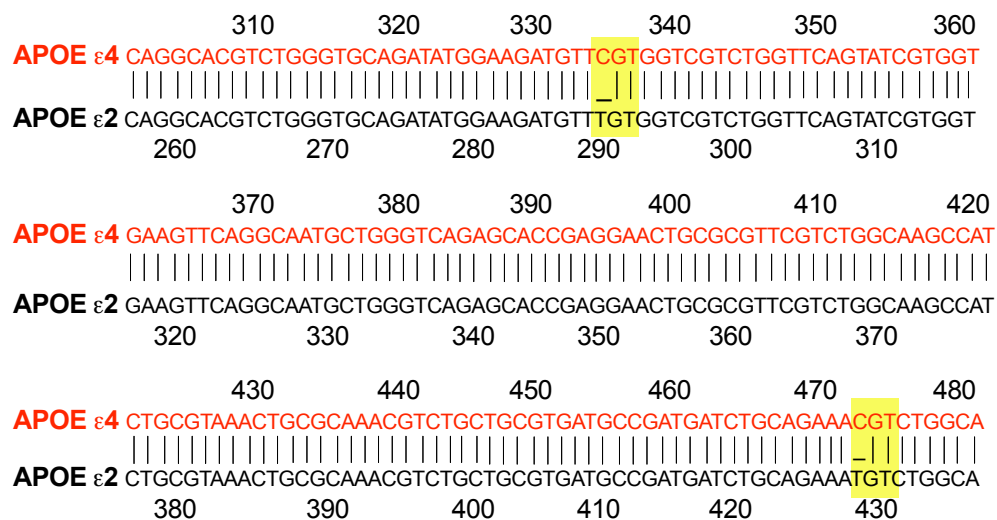


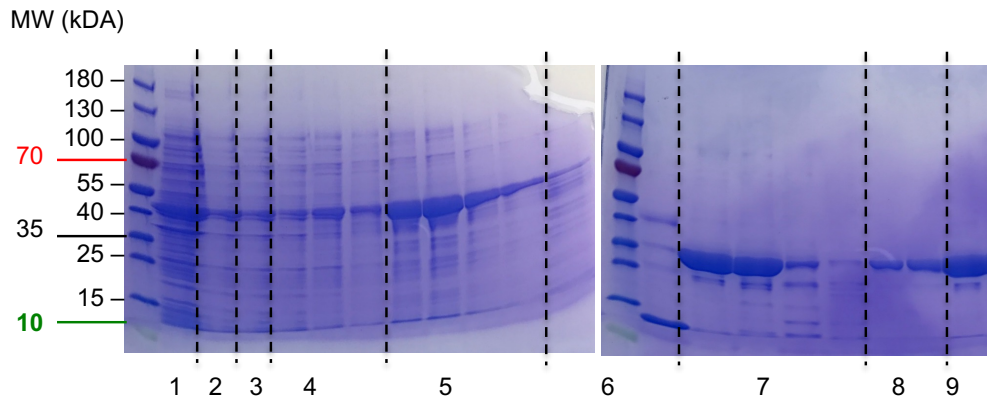
Figure 3.2 Comparison of APOE $\epsilon 2$ and APOE $\epsilon 4$ plasmid sequence

Excerpt of *APOE* $\epsilon 4$ plasmid sequence (red) and matched newly obtained *APOE* $\epsilon 2$ plasmid sequence (black). Highlighted in yellow are the sites where $\epsilon 2$ differs from $\epsilon 4$, showing the successful mutagenesis of c to t, resulting in the *APOE* $\epsilon 2$ plasmid.

Overview of the purification process by gel electrophoresis

All three isoforms were expressed as a His-tagged Trx-3C-ApoE fusion protein (Fig. 2.1B). rApoE isoforms were purified following a three-step purification protocol: IMAC, Heparin Affinity chromatography, and SEC. rApoE has four extra amino acids, coming from the 3C protease cleaving site and the retained Met. According to the online software Genome Compiler, the molecular weight (MW) of rApoE is of 34,581 Da.

Purification was followed by SDS-PAGE, from lysis of bacterial cells to elution from SEC column. An example of purification profiling for rApoE2 can be found in Fig. 3.3A. Purified proteins were dialysed, or buffer exchanged into PB for structural characterisation. As can be seen in Fig. 3.3B, all three rApoE have the expected MW of ~34 kDa.

A.

1. Lysate
2. Lysate supernatant
3. IMAC flow through
4. IMAC washes
5. IMAC elution
6. Heparin wash
7. Heparin elution
8. SEC elution
9. Concentrated protein

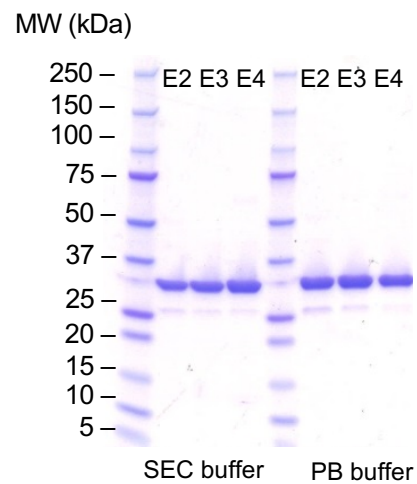
B.

Figure 3.3 Purification of rApoE2 as followed by gel electrophoresis

A. The isolation of rApoE2 from bacterial proteins was followed by SDS-PAGE. The fusion protein (~47 kDa) was enriched in the IMAC elution fraction (# 5) thanks to the his-tag. The eluate was then run through a heparin column. The fusion protein was immobilised through the strong rApoE2-heparin interaction, to allow for cleavage of Trx at the 3C protease site. Elution from the heparin column showed enrichment of a 34 kDa, presumably corresponding to rApoE2. The heparin elution fractions (# 7) were further purified through a SEC to get rid of any extra impurities. The SEC elution fraction (# 8) and the concentrated purified protein fraction (# 9) shows a highly pure protein that migrates to ~34 kDa.

B. SDS-PAGE before and after dialysis from SEC buffer to 20 mM PB buffer, pH 7.4 showed that all three purified rApoE (E2, E3 and E4) were highly pure and migrated to the same position on the gel corresponding to a ~34 kDa band.

Confirmation of primary amino-acid sequence

Before proceeding to further studies, the amino acid sequences of rApoE isoforms were analysed by mass spectrometry (Fig. 3.4). Each isoform has the appropriate amino acid substitution at position 112 and 158 (black lines under amino acid letter designation), with rApoE2 having two Cys (Fig. 3.4A), rApoE3 a Cys (Fig. 3.4B) and an Arg and rApoE4, two Arg (Fig. 3.4C). Given that the amino acid sequence of ApoE on the mass spectrometry database, SwissProt, includes the starting Met at position 1, positions 112 and 158 were shifted to 113 and 159.

A.

```

1 MKVEQAVETE PEPELRQQTE WQSGQRWELA LGRFWDYLRW VQTLSEQVQE
51 ELLSSQVTQE LRALMDETMK ELKAYKSELE EQLTPVAEET RARLSKELQA
101 AQARLGADME DVCGRLVQYR GEVQAMLGQS TEELRVRLAS HLRKLRKRL
151 RDADDLQKCL AVYQAGAREG AERGLSAIRE RLGPLVEQGR VRAATVGSIA
201 GQPLQERAQA WGERLRARME EMGSRTRDRL DEVKEQVAEV RAKLEEQAQQ
251 IRLQAEAFQA RLKSWFEPLV EDMQRQWAGL VEKVQAAVGT SAAPVPSDNH
301

```

B.

```

1 MKVEQAVETE PEPELRQQTE WQSGQRWELA LGRFWDYLRW VQTLSEQVQE
51 ELLSSQVTQE LRALMDETMK ELKAYKSELE EQLTPVAEET RARLSKELQA
101 AQARLGADME DVCGRLVQYR GEVQAMLGQS TEELRVRLAS HLRKLRKRL
151 RDADDLQKRL AVYQAGAREG AERGLSAIRE RLGPLVEQGR VRAATVGSIA
201 GQPLQERAQA WGERLRARME EMGSRTRDRL DEVKEQVAEV RAKLEEQAQQ
251 IRLQAEAFQA RLKSWFEPLV EDMQRQWAGL VEKVQAAVGT SAAPVPSDNH
301

```

C.

```

1 MKVEQAVETE PEPELRQQTE WQSGQRWELA LGRFWDYLRW VQTLSEQVQE
51 ELLSSQVTQE LRALMDETMK ELKAYKSELE EQLTPVAEET RARLSKELQA
101 AQARLGADME DVRGRVLVQYR GEVQAMLGQS TEELRVRLAS HLRKLRKRL
151 RDADDLQKRL AVYQAGAREG AERGLSAIRE RLGPLVEQGR VRAATVGSIA
201 GQPLQERAQA WGERLRARME EMGSRTRDRL DEVKEQVAEV RAKLEEQAQQ
251 IRLQAEAFQA RLKSWFEPLV EDMQRQWAGL VEKVQAAVGT SAAPVPSDNH
301

```

Figure 3.4 Primary sequence of rApoE isoforms

Amino-acid sequences of rApoE2 (A), rApoE3 (B) and rApoE4 (C). In red are the matched peptides to human ApoE2, ApoE3 and ApoE4 respectively from the Swissprot database. The sequence coverage was of 87% for rApoE2 and rApoE4 and of 88% for rApoE3. The amino acids setting the three isoforms apart are underlined in black: rApoE2 has two Cys, rApoE3 has a Cys and an Arg and rApoE4 possesses two Arg at the correct positions.

3.3.2. Structure of rApoE in phosphate buffer

The impact of the amino-acid substitutions at positions 112 and 158 on the structure of rApoE isoforms was explored by comparing their secondary, tertiary and quaternary structures in PB. The thorough characterisation conducted here was essential as subsequent behaviour such as self-assembly is dependent on native protein structure and stability.

Hydrodynamic behaviour in solution studied by sedimentation velocity

Hydrodynamic properties of rApoE in 20 mM PB were determined by sedimentation velocity, which is one of two applications of AUC.

Top graphs in Fig. 3.5A, 5B and 5C depict boundary movements in the rApoE2, rApoE3 and rApoE4-containing samples respectively. The differences in maximum absorbance values between the three samples were due to the slightly different final concentrations of diluted proteins added to velocity cells. Circles represent the experimental data recorded. Data analysis was conducted by fitting experimental points to a continuous size distribution using the Lamm equations on the programme SEDFIT. Solid lines represent best-fit profiles. The absence of sharp lines in the greyscale bitmaps in middle panels and the randomly distributed residuals (bottom panels) attest to the quality of the fit (Chou et al., 2005) (Fig. 3.5A, 5B and 5C).

Sedimentation coefficient distributions $c(S)$ were generated in the range of 0.1 S-15 S for rApoE using SEDFIT, with the confidence interval F set to 0.95 (Fig. 3.5D). $c(S)$ showed a main peak at an identical sedimentation coefficient of ~ 5 S for all three isoforms. Overall root-mean-square deviation (RMSD) values, found in table 3.1, attest to the goodness of the fit (RMSD value < 0.01) (Chou et al., 2005). The apparent MW each species and their abundance were also calculated by SEDFIT and obtained parameters can be found in table 3.1. The main peak at ~ 5 S was the most abundant, representing 85% of the species present in the sample, and the estimated MW of the corresponding species was 127 kDa, 128 kDa and 130 kDa for rApoE2, E3 and E4 respectively. These apparent MW come very close to what would be the size of a tetramer, which would have a MW of 138 kDa (given that the MW of monomeric rApoE is ~ 34.5 kDa). rApoE isoforms have a frictional ratio of 1.77, 1.81 and 1.74 for E2, E3 and E4, indicating an elongated shape.

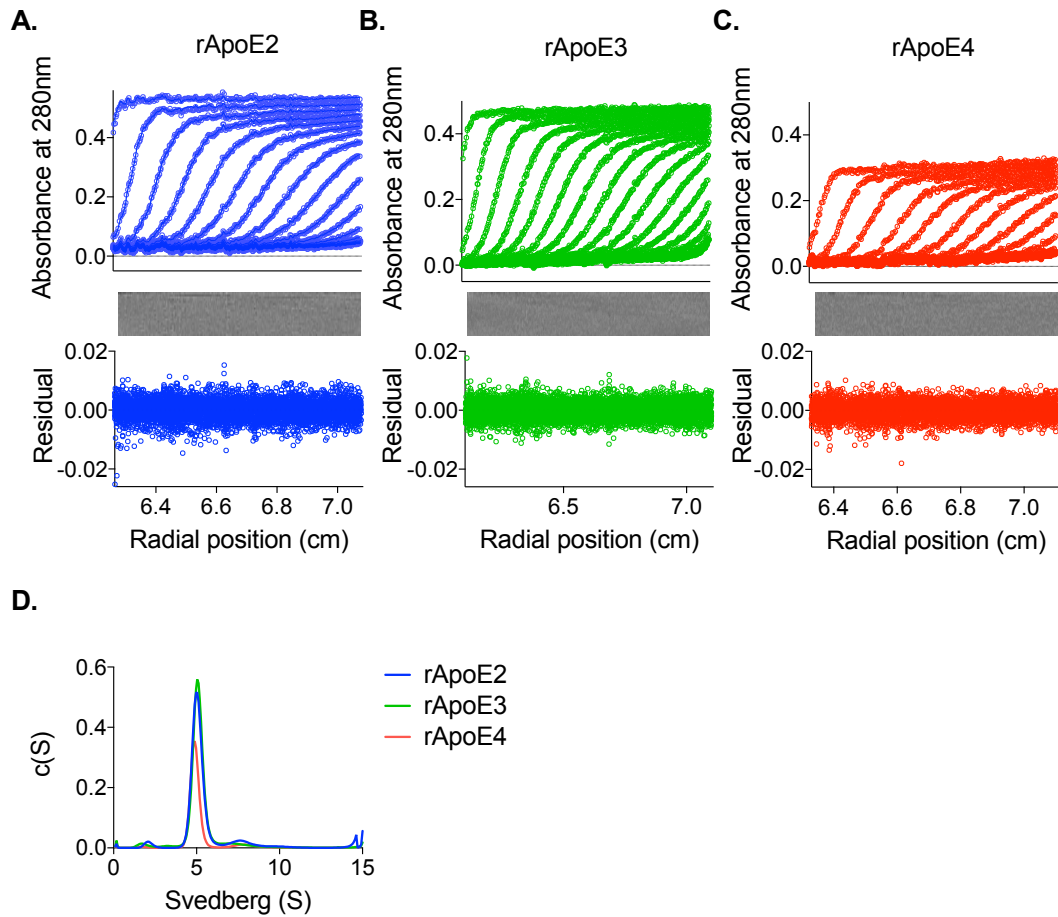


Figure 3.5 Size-distribution of rApoE in PB

Boundary movements of 9.5 μM rApoE2 (**A**), 8.5 μM rApoE3 (**B**) and 8 μM rApoE4 (**C**) in 20 mM PB, pH 7.4. Radial scans were acquired every 25 minutes, at intervals of 0.003 cm at 20°C. The rotor speed was set to 40,000 rpm. Experimental data points (circles) were fitted using the Lamm equations (solid lines). The grey scale representation of the residuals (middle panels) showed no misfits, which would have appeared as sharp lines. The randomly distributed residuals (bottom panels) also attest to the quality of the fit. (**D**) Continuous $c(S)$ size distributions of rApoE2 (blue), rApoE3 (green) and rApoE4 (red) showed the presence of a major species with a sedimentation coefficient at 5 S. All three curves superimposed each other, suggesting no major differences between the three rApoE.

	Friction ratio [†]	Sedimentation velocity (S)*	Estimated MW*	Peak integration*	Overall RMSD value ±
rApoE2	1.77	5.07	127 kDa	~84%	0.003275
rApoE3	1.81	5.10	128 kDa	~88%	0.002749
rApoE4	1.74	5.23	130 kDa	~86.5%	0.002789

Table 3.1 Sedimentation analysis of recombinant rApoE isoforms in PB

*Corresponding to the main sedimentation peak

[†]Best fit friction ratio used to calculate continuous size distribution.

±The RMSD provides evidence for the goodness of the fit.

Sedimentation analysis of rApoE shows that all three isoforms exist in a tetrameric form in 20 mM PB, pH 7.4 according to their estimated MW in solution.

Secondary structure of rApoE

The secondary structure of rApoE isoforms was investigated using CD spectroscopy. The far-UV CD spectra of rApoE2, E3 and E4 were identical, as per their superimposition (Fig. 3.6A). A main positive peak at 192 nm and two negative peaks at 208 nm and 222 nm indicated that rApoE was α -helical, which was in agreement with both the predicted secondary structure of human ApoE (Rall, S. C. et al., 1982) and the evidence gathered by others (Yokoyama et al., 1985; Chou et al., 2005). CD spectra were further analysed using the CONTIN programme on DICHROWEB (Lobley et al., 2002; Whitmore & Wallace, 2004; 2008), an online platform that allows for a detailed analysis of the secondary structure of a protein by giving the percentage of α -helix, β -sheet and turns, and random coil present. These results were summarised in table 3.2: all three recombinant isoforms shared approximately 58% α -helical content. A one-way ANOVA analysis of α -helical content showed no significant differences between the isoforms ($F(2,9)=4.197$, $p>0.05$).

rApoE was further characterised by investigating the resistance of its secondary structure to thermal denaturation. Loss of α -helical content was monitored at 222 nm between 20°C and 80°C by 1°C/min increments (Fig. 3.6B). All three rApoE isoforms displayed a sigmoidal unfolding curve. Experimental points were fitted to a Boltzmann sigmoidal curve using equation 5 (see 2.5.3). Melting temperatures T_m in °C correspond to the temperature at which 50% of the initial α -helical content has been lost. These were determined from the Boltzmann sigmoidal curve fit parameters and are displayed in table 3.3: rApoE3 and rApoE4 displayed a similar T_m of 52.39° C and 51.32°C respectively;

but rApoE2 was significantly more resistant to thermal denaturation than the other two isoforms, with a T_m of 60.28°C (table 3.3). Transition curves were also expressed as the fraction of the protein that had unfolded as a function of temperature to allow for direct comparison of the shape of unfolding between the three isoforms. Unfolding was biphasic for all three isoforms (Fig. 3.6C, rApoE2 in blue, rApoE3 in green and rApoE4 in red). The fraction-unfolded curves were also fitted to a Boltzmann sigmoidal (Fig. 3.6D), highlighting the later unfolding of rApoE2 and the similarities between rApoE3 and rApoE4. Thermal denaturation of rApoE thus followed the order of stability: rApoE4 ~ rApoE3 < rApoE2. However, it is important to note that the differences between the three isoforms at 37°C were not significant (Table 3.3; $F(2,9) = 0.9426$, $p = 0.4249$).

	α -Helix	β -Strand	β -Turn	Random Coil	NRMSD
rApoE2	57.3%	3.5%	14.1%	25.3%	0.0178
rApoE3	59.5%	3.3%	13.0%	24.2%	0.0190
rApoE4	58.4%	3.4%	13.5%	24.7%	0.0184

Table 3.2 Secondary structure analysis of rApoE isoforms

CD spectroscopy data was uploaded onto DICHROWEB and the secondary structure calculated by CONTIN programme (Lobley et al., 2002; Whitmore & Wallace, 2004; 2008). The normalised root mean square deviation (NRMSD) is an estimate of the goodness-of-fit; $NRMSD < 0.1$ is a necessary but not sufficient condition. α -helical content was comparable between the three isoforms.

	T_m (°C)	$[\Theta]_{222\text{ nm}}$ at 37°C (deg.cm ² .dmol ⁻¹)
rApoE2	60.28 ± 1.18	-19181 ± 649
rApoE3	52.39 ± 1.92	-19809 ± 961
rApoE4	51.32 ± 4.32	-19092 ± 773

Table 3.3 Thermal denaturation parameters

Parameters were extracted from the Boltzmann sigmoidal fit. T_m (°C) represents the temperature corresponding to 50% change in α -helical content. Non-linear best-fit parameters were determined on GraphPad Prism. One-way ANOVA showed that T_m was significantly different the isoforms: $F(2,9) = 12.11$, $p = 0.0028$; post-hoc Tukey multiple comparison tests: rApoE2 vs rApoE3, **, $p = 0.0083$; rApoE2 vs. rApoE4, **, $p = 0.0038$; rApoE3 vs. rApoE4, ns, $p = 0.8543$.

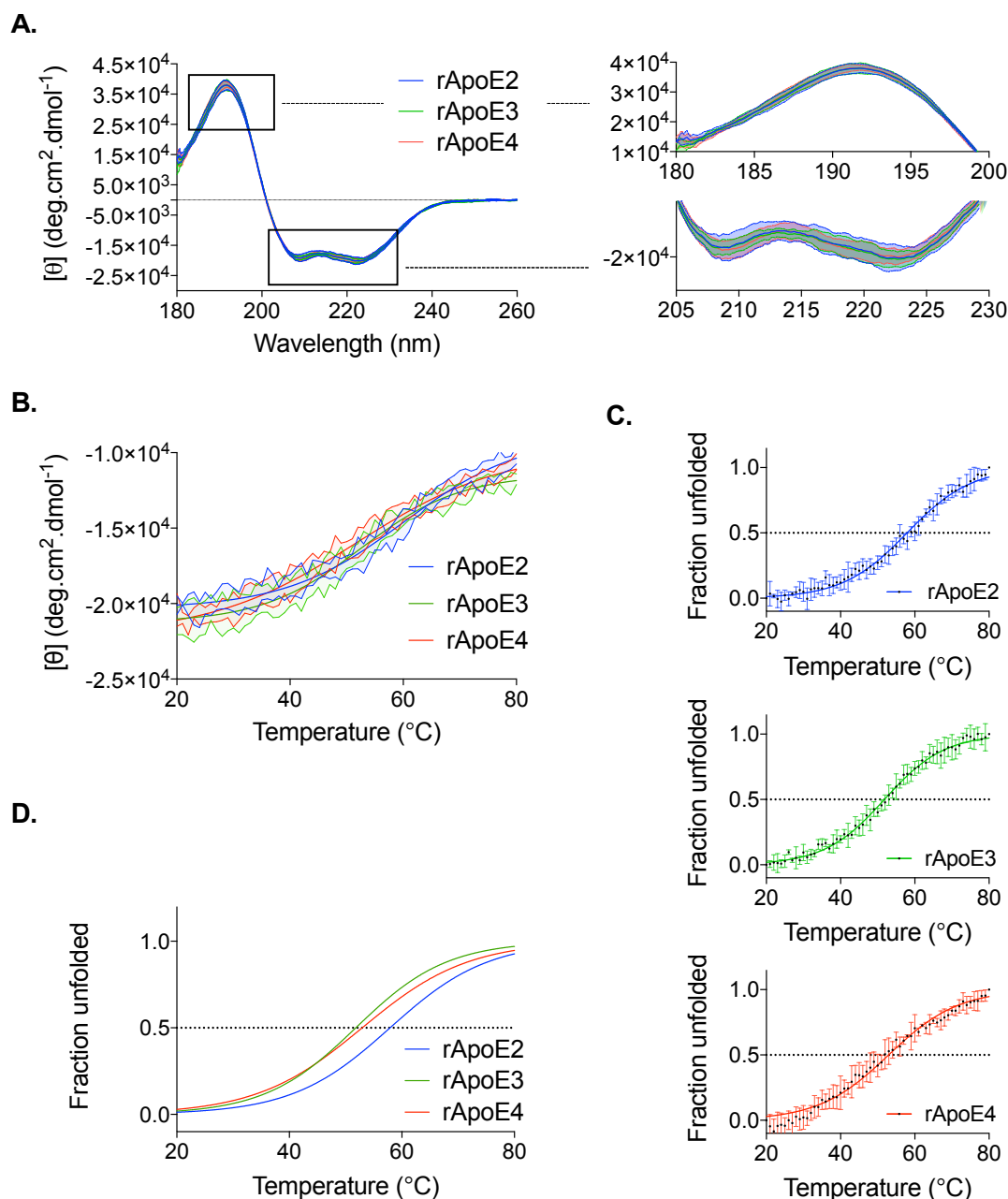


Figure 3.6 Secondary structure of rApoE isoforms characterised by CD

A. (Left panel) Far UV CD spectra of rApoE isoforms (25 μM in 20 mM PB, pH 7.4, 21 $^{\circ}\text{C}$) were superimposable (right zoom-in panels), showing comparable α -helical content. Secondary structure analysis was conducted with the CONTIN/LL programme (Provencher & Gloeckner, 1981; Stokkum, van et al., 1990) at DichroWeb (Lobley et al., 2002; Whitmore & Wallace, 2004; 2008) using the reference data set 6 (Sreerama & Woody, 2000), and results can be found in table 3.2.

B. Thermal stability of rApoE2 (blue), rApoE3 (green) and rApoE4 (red) was followed by recording changes in helical content at 222 nm with increasing temperature (1 $^{\circ}\text{C}/\text{min}$ increments). Melting temperatures T_m ($^{\circ}\text{C}$) for each isoform, corresponding to the temperature at which there was 50% change in α -helical content, were isolated from the fit parameters reported in table 3.3; α -helical content at 37 $^{\circ}\text{C}$ was also reported in table 3.3. (legend continued below)

C. The fraction unfolded of each protein was also plotted against temperature. Thermal denaturation curves were fitted to a Boltzmann sigmoidal equation. rApoE2 (top panel), rApoE3 (middle panel) and rApoE4 (bottom panel) displayed a biphasic transition.

D. Direct comparison between the thermal unfolding of rApoE isoforms indicated the following order of stability: rApoE2 >> rApoE3 ~ E4.

Data points in **A**, **B** and **C** correspond to the average of 4 different experiments using 4 different protein stocks. The envelopes correspond to the SD.

Tertiary structure of rApoE

Intrinsic Trp fluorescence was used to compare the tertiary structure of rApoE isoforms in PB: Trp emission spectra recorded between 320 nm and 460 nm showed no difference between the three proteins, with a maximum wavelength of emission of ~ 350 nm (Fig. 3.7A, rApoE2 in blue, rApoE3 in green and rApoE4 in red).

rApoE's differential resistance to chemical denaturation with GuHCl was also followed by Trp fluorescence. Upon denaturation, exposure of Trp residues to the solvent results in a red shift in the emission maximum (Kishore et al., 2012), with greater chemical instability resulting in a shift at lower concentration of denaturant.

Trp residues in rApoE were selectively excited at 292 nm (Kishore et al., 2012) and changes in maximum emission wavelengths were displayed as a function of the concentration of denaturant (Fig. 3.7B, rApoE2 in blue, rApoE3 in green and rApoE4 in red). Data points were fitted to a three-state unfolding model according to equation 9 (see 2.5.4). Two transitions could be interpreted from the shape of the curves: one from a folded to an intermediate state and a second one between the intermediate to unfolded state. ApoE has previously been observed to be formed of two independently folding domains (Wetterau et al., 1988; Morrow et al., 2000; Clément-Collin et al., 2006).

Chemical denaturation profiles of rApoE isoforms were compared by generating fraction unfolded curves using equation 6 (see 2.5.3), as it was done for the thermal denaturation data (Fig. 3.7C: rApoE2, top panel; rApoE3, middle panel; rApoE4, bottom panel). Chemical unfolding was also fitted to a three-state model and fitted curve were superimposed in Fig. 3.7D for direct comparison.

Midpoints of each transitions were calculated from the fitting parameters using equations 15 and 16 (see 2.5.4) and are summarised in table 3.4. The first transition occurred at a lower GuHCl concentration for rApoE4 than for rApoE2 and E3 (0.58 M vs ~0.7 M). However, rApoE3 and rApoE4 showed similar unfolding of the second domain, while rApoE2 was more stable (~2.65 M vs 2.84 M).

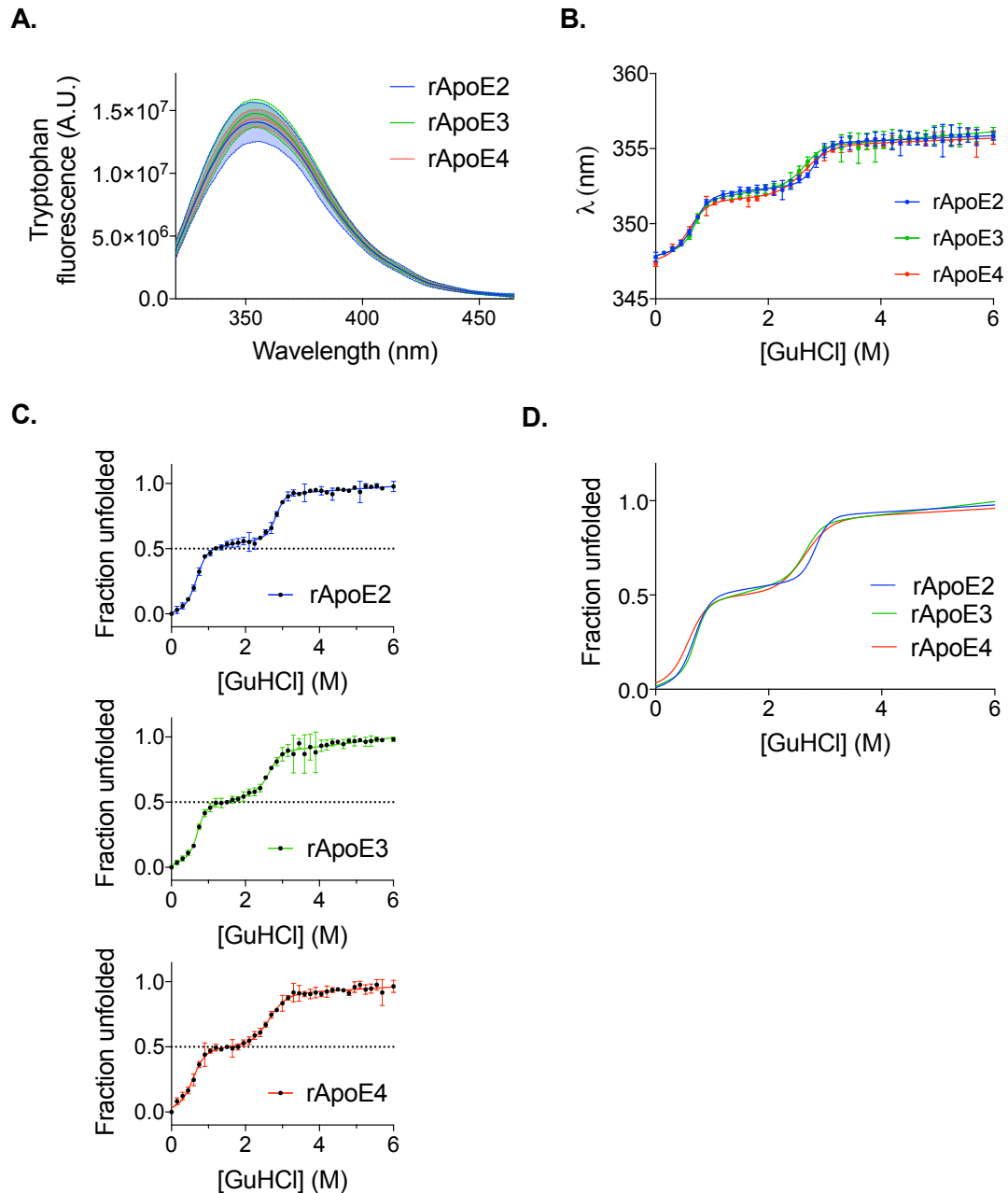


Figure 3.7 Tertiary structure of rApoE by Trp fluorescence spectroscopy

A. Intrinsic Trp fluorescence (excitation at 295 nm) indicates that all three isoforms at 25 μ M have a similar tertiary structure in 20 mM PB, pH7.4.

B. The wavelength of maximum fluorescence λ_{\max} at an excitation of 292 nm was plotted against the concentration of GuHCl for each isoform (\sim 0.05 mg/mL in 20 mM PB, 1 mM DTT, pH 7.4) resulting in chemical denaturation curves.

C. Data from rApoE2 (top panel), rApoE3 (middle panel) and rApoE4 (bottom panel) was expressed as fraction unfolded and fitted to a three-state unfolding model.

(legend continues below)

D. Fitted denaturation curves for rApoE2 (blue connective line), rApoE3 (green connective line), and rApoE4 (red connective line) were plotted onto the same graph for direct comparison of the shape of denaturation. rApoE2 transition curve was shifted very slightly to higher concentrations of denaturant.

Data points in **A** correspond to the average of four different experiments using four different protein stocks. Data points in **B** and **C** correspond to the average of three different experiments using three different protein stocks. The envelopes and error bars correspond to the SD.

	[GuHCl] _{50,I} (M)	[GuHCl] _{50,U} (M)
rApoE2	0.69 ± 0.03	2.84 ± 0.04
rApoE3	0.71 ± 0.03	2.66 ± 0.07
rApoE4	0.58 ± 0.04	2.65 ± 0.08

Table 3.4 Chemical denaturation parameters

[GuHCl]_{50, I} and [GuHCl]_{50, U} correspond to the midpoint concentrations of each transition. Non-linear best-fit parameters were determined on GraphPad Prism

To summarise, there were no differences between the three isoforms in their native state, and rApoE2 displayed a very marginally increased resistance to chemical denaturation compared to rApoE3 and rApoE4.

Differential self-assembly properties of rApoE isoforms

AD is primarily a disease of protein misfolding and aggregation. Therefore, the question of whether its main genetic risk factor is susceptible to self-assembly is of great interest.

Recombinant human ApoE4 in PBS was shown to be more prone to form toxic, soluble fibrillar oligomers than ApoE3 and ApoE2 by a group at the Gladstone Institute (Hatters et al., 2006). At first, I wanted to test whether this observation was buffer-dependent by exploring rApoE self-assembly in PB. After showing that only rApoE4 self-assembled following incubation in PB at 37°C for 24 h, I was interested to explore whether rApoE2 and E3 could also form these species over a prolonged timeframe by studying the kinetics of rApoE self-assembly at 37°C for up to 3 d. Furthermore, since ApoE phenotypes can also be heterozygous E2/4 and E3/4, I wanted to explore the effect of co-incubation of rApoE2 or rApoE3 with rApoE4 on their respective self-assembly properties.

3.3.3. rApoE4, but not E2 and E3, self-assembles under physiological conditions

ThT fluorescence was used to detect rApoE fibril formation in PB after incubation at 37°C for 24 h. ThT was also employed by Hatters to follow self-assembly of recombinant human ApoE for up to 16 h (Hatters et al., 2006). Assembly was also monitored using TEM to compare changes in morphology in rApoE alongside increases in ThT fluorescence.

Detection of fibril formation using Thioflavin-T

Fluorescence scans in the presence of ThT were acquired in a fluorimeter immediately after preparation of the samples (0 h) and after 24 h incubation at 37°C (24 h) and adjusted by removing the signal from the blank, i.e. the buffer alone (Fig. 3.8; rApoE2, left panel; rApoE3, middle panel; rApoE4, right panel).

ThT fluorescence at 0 h reached similar intensity levels for all three recombinant isoforms (~20 AU), with a maximum at 483 nm. There were no changes between the 0 h and 24 h scans for rApoE2 and rApoE3; however, ThT fluorescence intensity tripled between the 0 h and 24 h scan for rApoE4 (from 20 AU to 60 AU). This suggested changes in the

species present in the rApoE4 sample, but not in rApoE2 and rApoE3, which was further investigated by TEM.

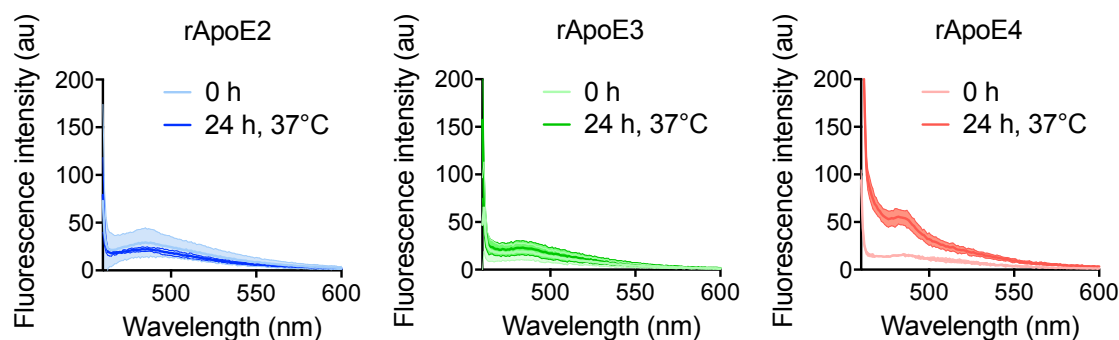


Figure 3.8 Detection of fibril formation by ThT fluorescence spectroscopy

Samples for the self-assembly assay were prepared at 25 μM in 20 mM PB, pH 7.4 Aliquots were taken at 0 h and 24 h and further diluted to 10 μM prior to acquisition. ThT was used at a final concentration of 20 μM . Comparison between ThT fluorescence scans taken before and after a 24 h incubation period at 37°C shows significant differences in signal only in the presence of rApoE4, indicative of fibril formation (right panel), but no differences in the presence of rApoE2 (left panel) or rApoE3 (middle panel). Data points correspond to the average of three different experiments using three different protein stocks. The envelopes correspond to the SD.

Evidence of rApoE4 self-assembly by transmission electron microscopy

To examine the morphology of rApoE2, rApoE3 and rApoE4, TEM grids were prepared before and after 24 h incubation at 37°C and looked at under an electron microscope.

TEM of rApoE2 (Fig. 3.9, top panels in blue) and rApoE3 (Fig. 3.9, middle panels in green) showed the presence of small amorphous and some round species at both 0 h (Fig. 3.9, top left and middle left micrographs) and after the 24 h incubation at 37°C period (Fig. 3.9, top right and middle right micrographs). This correlated with the absence of change in ThT fluorescence observed for both rApoE2 and rApoE3 (Fig. 3.8). In contrast, TEM micrographs highlighted a change in rApoE4 morphology after self-assembly induction (Fig. 3.9 bottom panels in red). At 0 h, amorphous and round species were found in rApoE4, similar to those found in rApoE2 and rApoE3, which is in accordance with the ThT fluorescence data (Fig. 3.9, left panels). At 24 h however, rApoE4 distinctly showed the presence of curvy fibrillar structures (Fig. 3.9 bottom right panel).

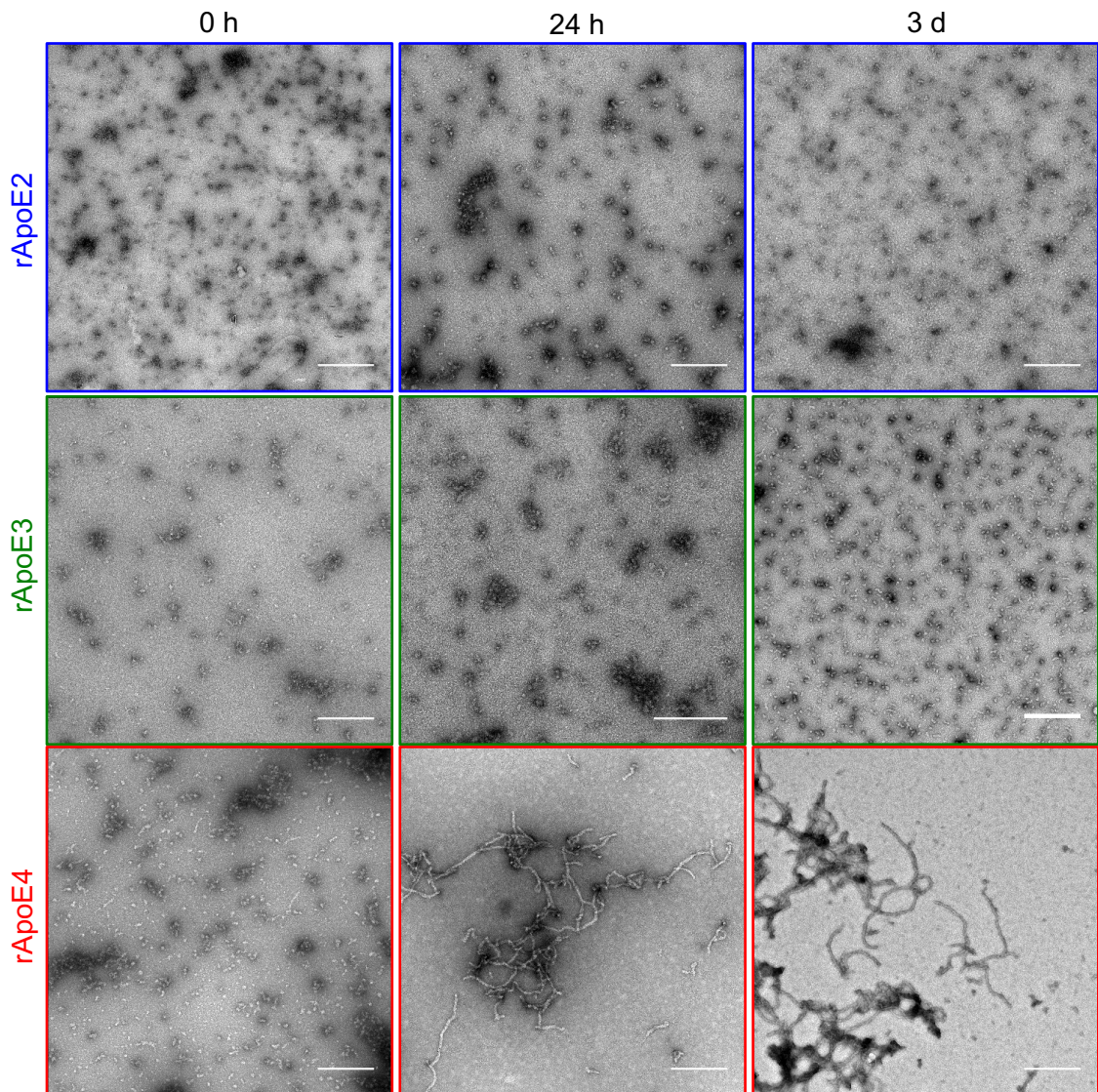


Figure 3.9 Micrographs of rApoE before and after a 24 h and a 3 d incubation period

Representative TEM of negatively stained rApoE isoforms before (0 h, left panels) at after 24 h (middle panels) and 3 d (right panels) incubation at 37°C show no fibril formation of rApoE2 (blue) and only oligomerisation of rApoE3 (green) contrary to rApoE4 (red), which self-assembled to form long, curved fibrils. Scale bars, 500 nm.

3.3.4. Kinetics of rApoE self-assembly

In the previous section, both ThT fluorescence data and TEM micrographs were presented as evidence of rApoE4 self-assembly after a 24 h incubation at 37°C. According to the data collected, rApoE2 and rApoE3 did not share the same properties as rApoE4 since they did not result in the formation of long and curved fibres. ThT measurements of rApoE and TEM micrographs were thus acquired after a 3-day incubation period to answer whether rApoE2 and rApoE3 could form fibrils after

prolonged incubation and to investigate the stability of rApoE4 fibrils. This was followed by the development of a ThT-kinetic assay to get a better understanding of the dynamics of rApoE fibril formation. Self-assembly over time was also tracked using gel electrophoresis.

Self-assembly of rApoE after 3 day-incubation

Initially, end-point ThT fluorescence scans were acquired at 0 h and 3 d to detect fibril formation in rApoE. After 3 d, there was still no detectable increase in ThT fluorescence in the rApoE2 sample (Fig. 3.10A, left graph, blue). However, a slight increase in ThT fluorescence occurred in the presence of rApoE3 at the end of the 3 d incubation period (Fig. 3.10A, middle graph, green). Still, that increase did not reach the levels of that of rApoE4, which showed an approximately four-fold increase in ThT signal (Fig. 3.10A, right graph, red). ThT fluorescence in the presence of rApoE4 was indicative of fibrillar species being present after 3 d incubation, but this measurement gave no indication on the morphology of species present.

TEM was thus used to assess morphological changes in rApoE incubated at 37°C for 3 d. No changes were evidenced in rApoE2, the presence of small amorphous species persisted by day 3 (Fig. 3.9B, right blue panel). Small round and small slightly elongated species were detected in incubated rApoE3 after 3 d (Fig. 3.9B, right green panel). Fibrils formed in rApoE4 remained after the 3 d incubation period (Fig. 3.9B, right red panels; Fig. 3.9 for rApoE4, 24 h micrograph).

Tracking self-assembly by ThT-fluorescence and gel electrophoresis

A ThT-kinetic assay was developed to follow changes in ThT fluorescence at 483 nm in the presence of rApoE continuously over the course of 3 d. Unlike end-point measurements as those obtained in 3.3.3 and in the previous section, ThT was added to the samples from 0 h. ThT had no effect on self-assembly and on the morphology of the fibrils as shown by micrographs of rApoE4 assembled for 24 h in the presence of ThT (appendix 2).

Changes in ThT fluorescence were expressed as the difference between the fluorescence F at any time point and the minimum fluorescence signal F_{\min} . $F - F_{\min}$ displayed a rapid increase in intensity for rApoE4 (Fig. 3.10B, red kinetics curve). Changes for rApoE3 only started occurring after an elongated lag phase (Fig. 3.10B, green kinetics curve) and there was very little change in fluorescence for rApoE2 up to 24 h and only minor increase within the last 20 h (Fig. 3.10B, blue kinetics curve).

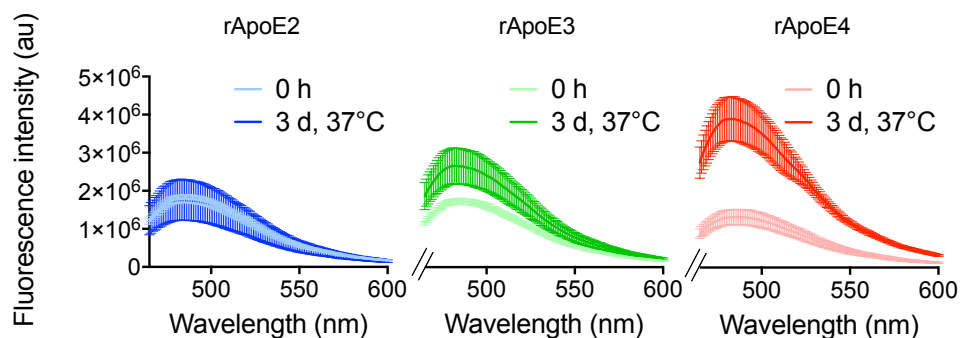
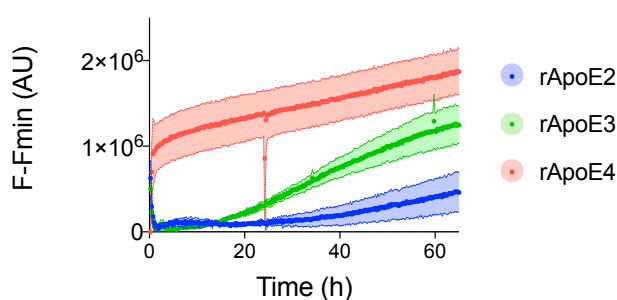
A.**B.**

Figure 3.10 Kinetics of rApoE fibril formation as followed by ThT fluorescence spectroscopy

A. rApoE samples were prepared at 25 μM in 20 mM PB, pH 7.4 and incubated over the course of 3 d in the presence of ThT at a 1:2 ratio. Scans were acquired before and after incubation with excitation at 460 nm and emission recorded between 465 nm and 600 nm. Significant difference between the 0 h and the 3 d scan only occurred in the presence of rApoE4 and was indicative of fibril formation (right graph, red). No significant changes were observed for rApoE2 (left graph, blue), and only a small increase was observed for rApoE3 (middle graph, green). Graphs represent an average of three acquisitions of three different protein stocks for each isoform; error bars represent the SD.

B. Changes in ThT fluorescence intensity at 483 nm were recorded over the course of 3 d to monitor the kinetics of rApoE self-assembly (rApoE2, blue; rApoE3, green; rApoE4, red). ThT fluorescence was adjusted to baseline by subtracting the minimum fluorescence signal F_{min} in order to allow for a direct comparison of the shape of the kinetic curves between the three recombinant isoforms. Changes in ThT fluorescence happened within the first hour in the presence of rApoE4 at 37°C, followed by a steady increase in signal over time. At the end of the incubation period, rApoE3 and rApoE4, but not rApoE2, induced changes in ThT fluorescence. The length of the lag phase was different for each isoform, with $\text{rApoE2} > \text{rApoE3} > \text{rApoE4}$. Data points correspond to an average of three experiments conducted on three different protein production stocks for each isoform; envelopes correspond to the SEM.

Self-assembly on rApoE was also monitored using non-reducing gel electrophoresis. Aliquots of assembling rApoE were taken at 0 h, 24 h and 3 d; samples were prepared both for denaturing and native gel electrophoresis. Representative gels were shown in Fig. 3.11.

Over the course of the assembly protocol, a major band migrating at ~34 kDa for all isoforms was identified by SDS-PAGE (Fig. 3.11, left) corresponding to the monomeric form of rApoE. There were no differences in rApoE4 between the 0 h (lane 1), the 24 h (lane 2) and the 3 d (lane 3) band, suggesting that rApoE4 fibrils were SDS-soluble. After 3 d incubation at 37°C (lanes 3), both rApoE2 and rApoE3, but not rApoE4, displayed the presence of higher oligomeric species. A band corresponding to a dimer of rApoE was present in the rApoE2 and rApoE3 samples, suggesting disulphide bridge formation (Fig. 3.11, left). Of note, Cys-Cys bonds are SDS-stable. In rApoE2, several additional oligomeric bands were displayed, suggesting the formation of higher species through disulphide bridge formation at 37°C over time, consistent with rApoE2 having an extra Cys residue.

Native PAGE was also used to track rApoE self-assembly over time (Fig. 3.11, right). rApoE2 and rApoE3 ran consistently at a similar mobility at 0 h and after 24 h incubation (~ 400 kDa), but after 3 d some species could be found in the wells suggesting they were too big to run through the gel. This was more pronounced in the rApoE3 sample, which could be due to the presence of the small round species detected after 3 d incubation (see Fig. 3.9, green panel).

Higher MW species prior to, and following incubation at 37°C were present in rApoE4. By 24 h, the majority of the rApoE4 protein formed higher oligomers that did not run through the gel indicating oligomerisation of rApoE4; this persisted after 3 d of incubation. Native gel electrophoresis analysis was consistent with rApoE4, and to some extent rApoE3, but not rApoE2 being capable of forming higher oligomeric species such as small round species and mature fibrils.

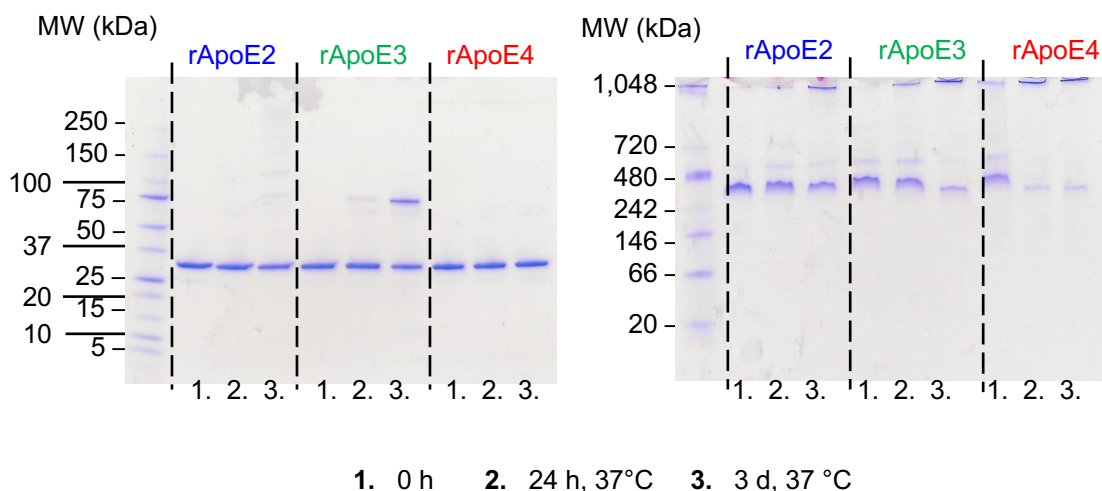


Figure 3.11 Following filament formation by gel electrophoresis

SDS-PAGE (left) and native gel (right) were used to monitor self-assembly of rApoE at 0 h (lanes 1), 24 h (lanes 2) and 3 d (lanes 3), showing the presence of oligomeric species in rApoE4 from 0 h that increase in size with time (>1,048 kDa). Higher oligomeric species in rApoE4 formed from 24 h were SDS soluble as a monomeric band was recovered in the SDS-PAGE. rApoE2 and rApoE3 had a major band at ~ 400 kDa, corresponding to the tetramers migrating at higher MW because of their elongated shape. By 3 d of incubation at 37°C, higher oligomeric species also appeared in rApoE2 and especially in rApoE3. SDS-PAGE showed the formation of disulphide bridges in rApoE2 and rApoE3, which could correspond to the species not migrating through the native gel.

3.3.5. Inhibition of rApoE4 fibril formation by rApoE3 and rApoE3

Since rApoE2 and rApoE3 did not form fibrils at 37°C after incubation of up to 3 d under the conditions used, rApoE4 was mixed in a 1:1 ratio with each of the other two isoforms to investigate whether the presence of rApoE4 would be sufficient to induce fibril formation in rApoE2 and rApoE3 over the course of 24 h and monitored using ThT fluorescence assay and TEM.

rApoE2 and rApoE3 alter the ThT kinetics of rApoE4 over 24 hours

rApoE2 and rApoE3 were mixed respectively with rApoE4 in a 1 to 1 ratio achieving a final total rApoE concentration of 25 μ M (12.5 μ M for each respective isoform). Samples were incubated at 37°C with ThT at a 1:2.2 ratio, and changes in ThT fluorescence were monitored over time. The shape of “rApoE2-rApoE4” kinetics curve (purple) did not resemble that of individual rApoE2 or rApoE4 at either 12.5 μ M or 25 μ M (Fig 3.12A). This was also the case for “rApoE3-rApoE4” (Fig 3.12B). “rApoE2-rApoE4” (purple) did

not induce changes in ThT signal to the level of rApoE4 (red); however, mixed rApoE3 (yellow) was very close by 24 h (Fig. 3.12C).

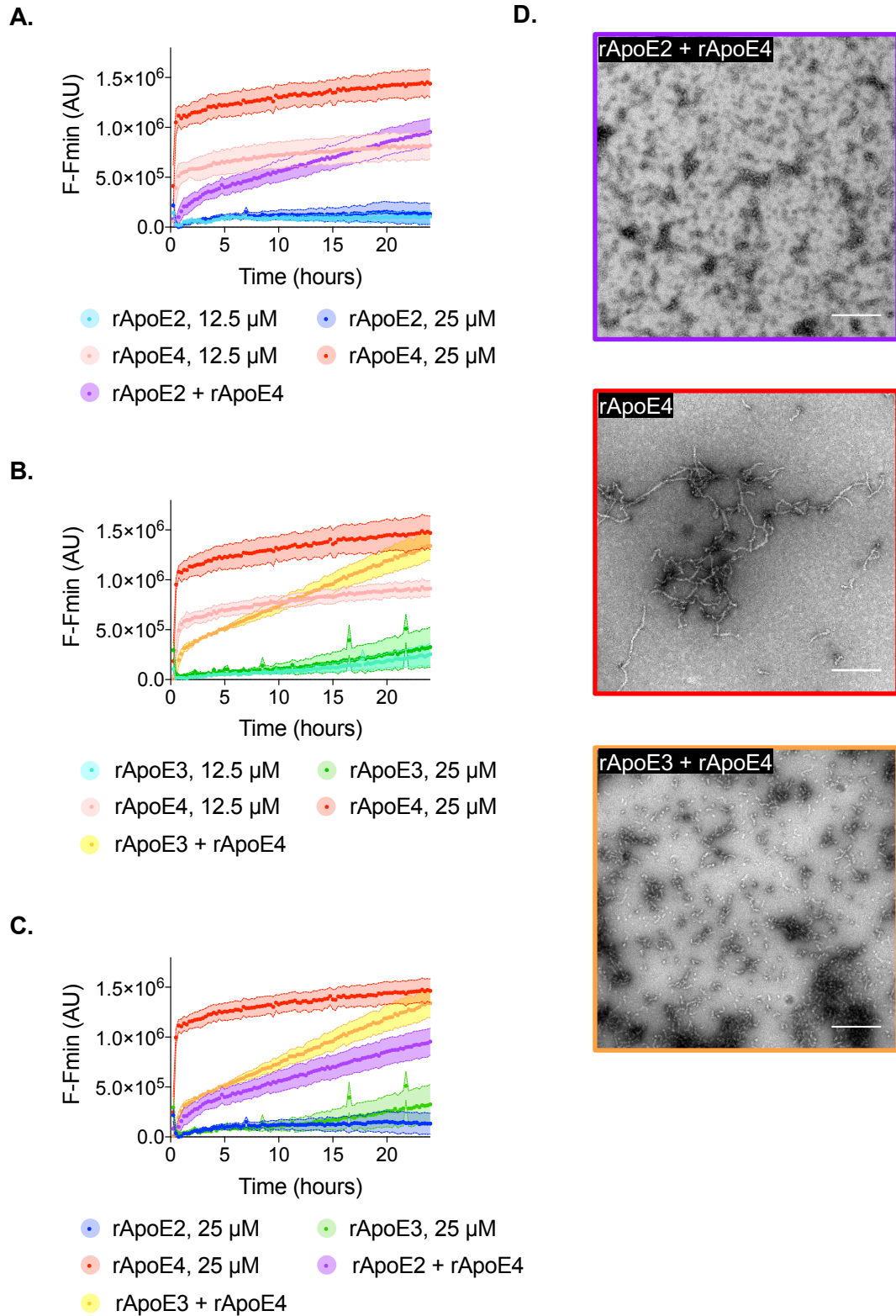


Figure 3.12 Effect of co-incubation of rApoE4 with either E2 or E3 on self-assembly

(legend continued below)

A. Changes in ThT fluorescence at 483 nm were monitored over the course of 24 h at 37°C for rApoE2 and rApoE4 alone at both 12.5 μ M and 25 μ M and rApoE2 mixed with rApoE4 (both 12.5 μ M for a total ApoE concentration of 25 μ M) in 20 mM PB pH 7.4. The presence of rApoE2 altered the rate of assembly of rApoE4. Fluorescence signal of the mixed rApoE2 never reached the level of that of rApoE4 alone. Curves represent an average of three different experiments conducted on three different protein production stocks; envelopes represent the SEM.

B. Changes in ThT fluorescence at 483 nm were monitored over the course of 24 h at 37°C for rApoE3 and rApoE4 alone at both 12.5 μ M and 25 μ M and rApoE3 mixed with rApoE4 (both 12.5 μ M for a total rApoE concentration of 25 μ M) in 20 mM PB pH 7.4. The presence of rApoE3 altered the rate of assembly of rApoE4. Fluorescence signal of the mixed rApoE3 reached similar level of that of rApoE4 alone. Curves represent an average of three different experiments conducted on three different protein production stocks; envelopes represent the SEM.

C. For clarity, changes in ThT fluorescence for mixed rApoE2 (purple), mixed rApoE3 (yellow) and individual rApoE at 25 μ M (rApoE2 in blue, rApoE3 in green and rApoE4 in red) were plotted on the same graph, showing how the presence of rApoE2 and rApoE3 altered the kinetics of rApoE4 self-assembly. Curves represent an average of three different experiments conducted on three different protein production stocks; envelopes represent the SEM.

D. Representative TEM micrographs showed a heterogeneous population, with the presence of small round and small amorphous species, but no mature fibrils when rApoE4 was incubated with rApoE2 or rApoE3 in a 1:1 ratio. Scale bar, 500 nm.

Absence of mature rApoE4 fibrils in the presence of rApoE2 and rApoE3 in the course of 24 hours

Positive fluorescence for ThT assay suggests that mixed rApoE2 and mixed rApoE3 formed species dissimilar to rApoE4 fibrils. To explore this, grids of rApoE2 and rApoE3 mixed with rApoE4 in a 1:1 ratio were prepared. The presence of rApoE2 (Fig. 3.12D, top micrograph) and of rApoE3 (Fig. 3.12D, bottom micrograph) inhibited the formation of mature rApoE4 fibrils over the course of 24 h (Fig. 3.12D, middle micrograph). Instead, both mixed samples exhibited both small round and small amorphous species.

Characterisation of rApoE4 fibrils

The formation of rApoE4 fibrils at 37°C was followed over 24 h to characterise changes in morphology. rApoE4 fibrils have been previously suggested to share some of the structural features of amyloid (Hatters et al., 2006). The structure of rApoE4 fibrils was thus also investigated using CD spectroscopy as well as X-ray fibre diffraction to determine whether rApoE4 underwent a conformational change to increased β -sheet structure, characteristic of amyloid formation (Uversky & Fink, 2004).

3.3.6. Morphology of rApoE4 fibrils

TEM was used to monitor the morphology of the assemblies over time for 25 μ M rApoE4 incubated at 37°C for up to 24 h. Aliquots of rApoE4 were taken at 0 h, 1 h, 3 h, 6 h, 12 h and 24 h. Small rounded species started to appear after as little as 1 h incubation. By 3 h incubation, short, curved filaments could be detected. These developed into curvy-linear filaments after 6 h. These filaments continued elongating into clearly identifiable fibrils by 12 h, yielding extended, curvy filaments by 24 h (Fig. 3.13). Fibrils displayed a granular appearance, unlike the twisted and smooth appearance generally exhibited by amyloid fibrils (Goldsbury et al., 2011).

To note, the small round species formed after 1 h resembled those observed for rApoE3 after 3 d incubation (Fig. 3.9, rApoE3, 3 d micrograph in green). The small spherical species appeared to correspond to the smallest building block of the structure, fusing end-to-end to form fibrils (Fig. 3.13, yellow arrowheads).

The fibrillar morphology of rApoE4 was further characterised by measuring both length and width of the fibrils using ImageJ. The length of the filaments significantly increased over time reaching an average of 363 nm after 24 h incubation (One-way ANOVA: ****, $p < 0.0001$, $F = 180.9$), while the diameter of the structures did not vary and remained between 26-30 nm (Fig. 3.14).

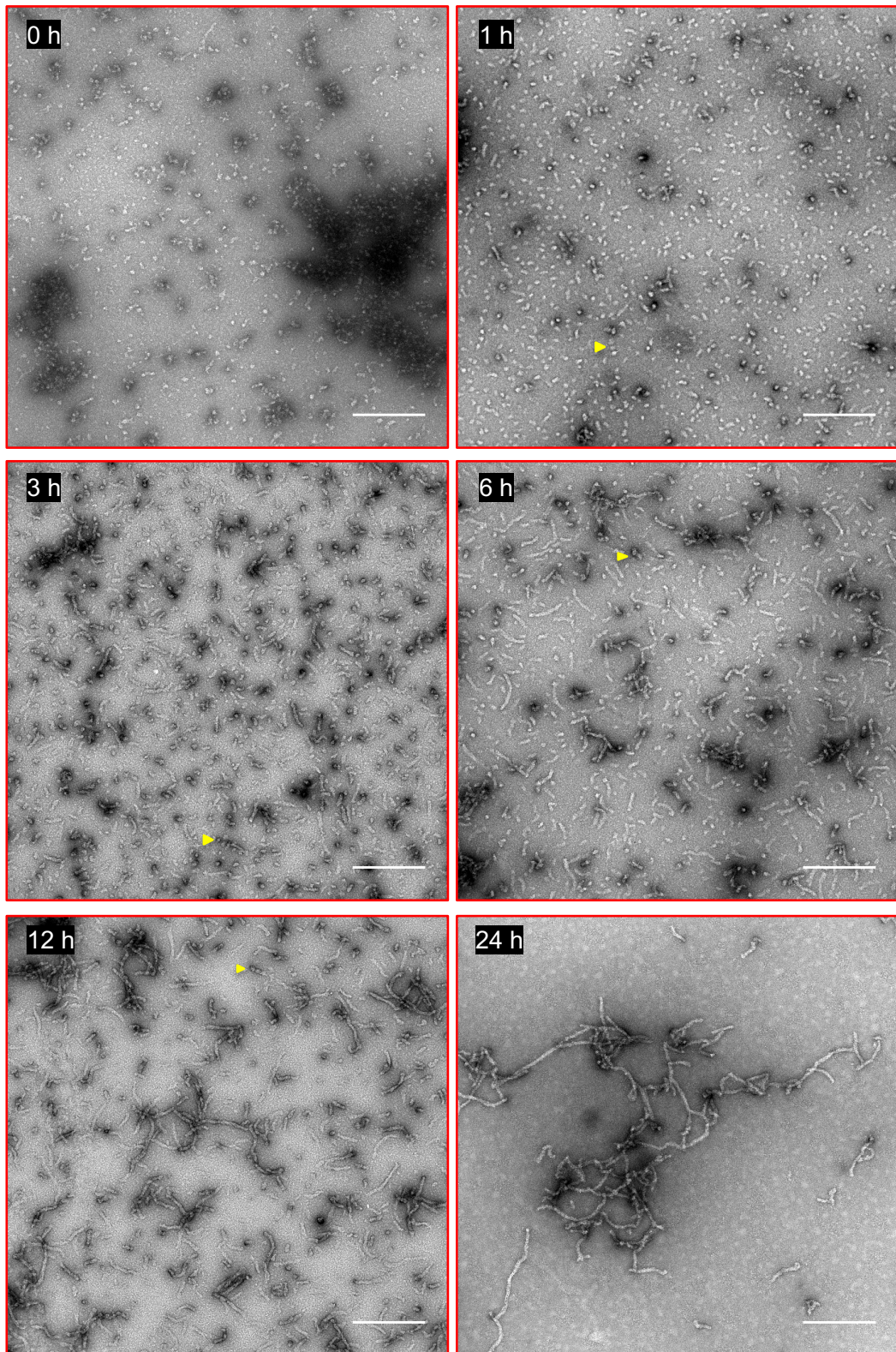


Figure 3.13 rApoE4 fibril formation followed by TEM over 24 h

Representative electron micrographs of negatively stained rApoE4 (25 μ M in 20 mM PB, pH 7.4) over the course of assembly at 37°C, taken at 0 h, 1 h, 3 h, 6 h, 12 h and 24 h. Scale bar, 500 nm. Yellow arrowheads show end-to-end fusion a small round species into longer filaments.

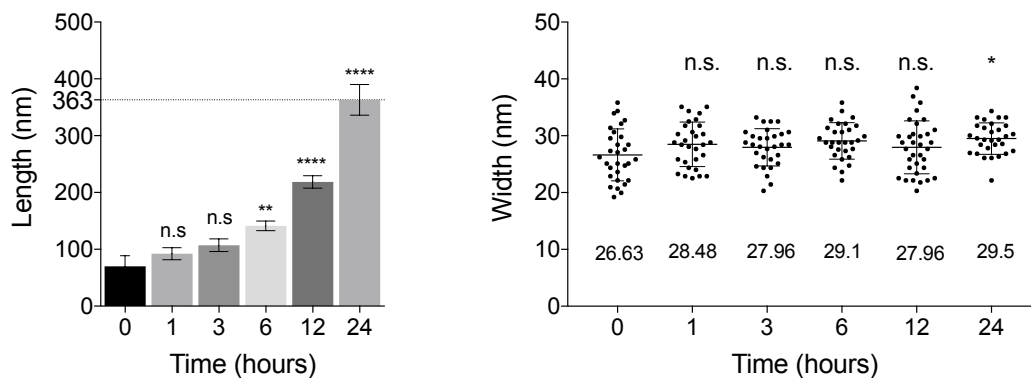


Figure 3.14 Growth of rApoE4 filaments over time

rApoE4 self-assembly was characterised by measuring changes in length (left panel) and width (right panel) of the fibrils. Changes in width were non-significant; however, with increasing incubation times, rApoE4 fibrils become significantly longer (One-way ANOVA: ****, $p < 0.0001$, $F = 180.9$).

3.3.7. Nature of rApoE4 fibrils

Hatters previously suggested that ApoE4 forms fibrils that resemble amyloid. Amyloid is defined by the cross- β structure, which is measured using X-ray fibre diffraction (Morris & Serpell, 2012). However, TEM (above) may suggest that rApoE retains its native structure given the granular appearance of the fibrils. In order to investigate the structural composition of rApoE4 fibres, its amyloidogenicity was predicted using the Waltz algorithm (Maurer-Stroh et al., 2010) and the structural changes were measured using CD and X-ray fibre diffraction.

Amyloidogenicity of rApoE4

The Waltz algorithm was designed to predict local amyloid propensity in proteins (Maurer-Stroh et al., 2010). This algorithm was run on each sequence of the ApoE isoforms to see if any differences appeared in the predictions of amyloidogenicity. The three isoforms were predicted to have amyloidogenic regions and their amyloidogenic profiles are almost identical (Fig. 3.15), which would suggest they would behave similarly under identical experimental conditions. However, as was shown previously, only rApoE4 assembled into fibrils. Based on the Waltz algorithm, rApoE4 fibrils might be amyloid.

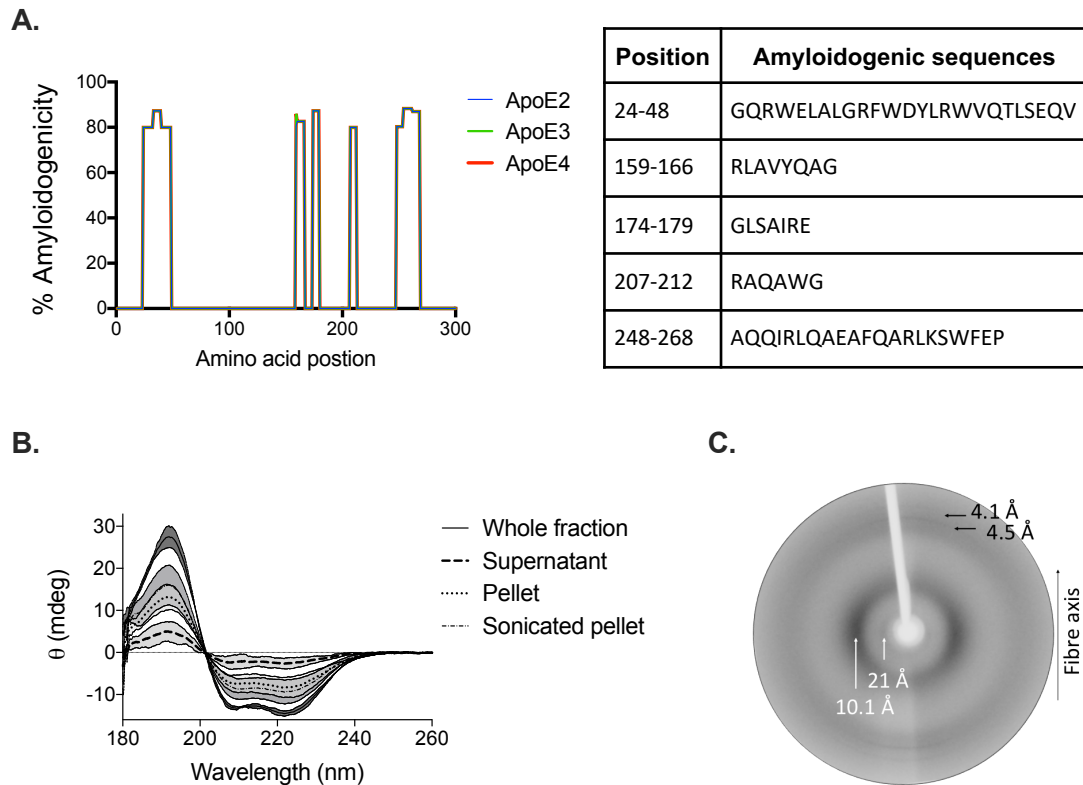


Figure 3.15 Nature of rApoE4 filaments

A. The Waltz algorithm was used to predict the amyloidogenicity of ApoE isoforms. All three isoforms had the same number of predicted amyloidogenic regions each with similar scores of amyloidogenicity.

B. α -helical secondary structure was retained after assembly (whole fraction), as shown by CD spectroscopy. Fibrils in the pellet were isolated from the supernatant (supernatant) in case soluble proteins in the supernatant were masking any secondary structure change. Fibrils in the pellet were α -helical (Pellet). Sonication was applied to ensure maximum solubilisation of fibrils, and the α -helix signal persisted (sonicated pellet).

C. X-ray fibre diffraction pattern obtained from partially aligned rApoE4 fibrils after 24 h incubation at 37°C showing positions of diffraction signals on the meridian (vertical) at 4.5 Å and 4.1 Å, and equatorial (horizontal) axes at 10.1 Å and 21 Å.

Absence of shift in secondary structure of rApoE4

Amyloid proteins are characterised by a shift in secondary structure from their starting structure to β -sheet formation under self-assembly condition (Uversky & Fink, 2004).

rApoE4 secondary structure after self-assembly was characterised by CD spectroscopy in order to identify the presence of a shift from α -helix to β -sheet. CD spectra showed

that rApoE4 remained highly α -helical following 24 h incubation (Fig. 3.15B, whole fraction), and was very similar to the spectrum at 0 h (Fig. 3.6A). Comparison of secondary structure content showed similar levels of α -helix and β -sheet (Table 3.5). To ensure that the spectrum is not being dominated by soluble, non-fibrillar rApoE4, the fibrils were pelleted by ultracentrifugation and the supernatant removed. The supernatant fraction showed very low protein content (Fig. 3.15B, supernatant). Fibrils were re-solubilised in PB in an equal volume as the supernatant. CD spectra of the pellet showed that rApoE4 retained its α -helical structure after incubation at 37°C for 24 h (Fig. 3.15B, pellet). Because not all the signal was recovered when compared to the whole fraction before ultracentrifugation, the fibre pellet was sonicated to ensure maximum protein resuspension. The CD spectrum continued to display α -helical conformation (Fig. 3.15B, sonicated pellet). Overall, no shift from α -helix to β -sheet could be detected.

rApoE4	α -Helix	β -Strand	β -Turn	Random Coil	NRMSD [‡]
0 h	60%	3.05%	12.05%	24.95%	0.0178
24 h, 37°C	56.7%	5.7%	14.05%	23.5%	0.0190

[‡] NRMSD: normalised root mean square deviation

Table 3.5 Secondary structure analysis of rApoE4 before and after self-assembly

CD spectroscopy data was uploaded onto DICHROWEB and the secondary structure calculated by CONTIN programme (Lobley et al., 2002; Whitmore & Wallace, 2004; 2008). α -helical content was comparable between the two conditions (N=2).

Diffraction pattern of rApoE4 fibrils

Mature rApoE4 fibrils were obtained from a 100 μ M preparation incubated at 37°C for 24 h. Observation of TEM micrographs confirmed that the morphology of rApoE4 fibrils were unaffected by the increased concentration (appendix 2). Fibrils were air-dried to form a partially aligned fibre bundle. The X-ray diffraction pattern (acquired by Dr. Y Al-Hilaly) showed two meridional reflections: a sharp diffraction signal at 4.5 Å and a weaker diffraction signal at 4.1 Å, while a strong but diffuse signal at 10.1 Å and a weaker reflection at approximately 21 Å were observed on the equator. This pattern is inconsistent with cross- β pattern characteristic of amyloid fibres (cross- β patterns display signals at 4.7 Å and 10 Å on perpendicular axes; Morris & Serpell, 2012).

3.4. Discussion

When ApoE4 was identified as a risk factor for AD, a wide-range of studies looking into the interactions between ApoE and pathological hallmarks of AD, such as A β and Tau, were generated. Nevertheless, very few studies have been dedicated to the understanding of how ApoE fits within AD independently of its pathological hallmarks. Protein misfolding and aggregation is a big theme within the AD field and investigating whether ApoE4 as one of the main risk factors for AD is susceptible to such conformational changes and subsequent assembly is of great interest. To tackle this question, rApoE was used to model human ApoE. Bacterial-produced ApoE was shown to have similar biophysical and functional characteristics to ApoE produced in mammalian cells (Argyri et al., 2011).

A substantial amount of information about human ApoE had already been gathered since its identification as a component of lipoproteins and as protein involved in cholesterol transport and metabolism (Mahley, 1988). The structure of rApoE generated here was extensively characterised, before exploring its self-assembly properties. A summary of the structural data can be found in table 3.6.

Sedimentation equilibrium (SE) is a technique in which a protein sample is spun to create a concentration gradient, counteracted by diffusion. Reaching the concentration gradient equilibrium solely depends on the size of the protein, hence why SE measurements obtained by AUC are useful to determine subunit stoichiometry of a protein (Cole, 2000). Such studies conducted on delipidated ApoE isolated from human plasma suggested that ApoE formed tetramers in solution over a 0.4-1 g/L concentration range (Yokoyama et al., 1985). Sedimentation velocity experiments later conducted on plasma human ApoE3 provided evidence for a tetramer-octamer association (Dergunov et al., 1992). These results were also confirmed in recombinant ApoE isoforms (Hatters et al., 2006; Barbier et al., 2006). AUC showed that all three in house rApoE isoforms formed an elongated tetramer in solution. The elongated shape of human ApoE3 was previously reported by Aggerbeck et al, with the frictional ratio of ApoE3 being 1.79 (Aggerbeck et al., 1988). This value was very similar to those obtained for rApoE (1.77, 1.81 and 1.74 for rApoE2, rApoE3 and rApoE4 respectively). The elongated shape of rApoE isoforms was also supported by small-angle X-ray scattering data (Raulin et al., 2019).

The publication of human ApoE's complete amino acid sequence by Rall and colleagues in 1982 was accompanied by a prediction of its secondary structure by application of the

Chou-Fasman algorithm (Rall, S. et al., 1982). Based on its primary sequence, ApoE was anticipated to be rich in α -helices. Far-UV CD spectrum of delipidated ApoE in PBS, pH 7.4 at 1.8 μ M and 36 μ M showed a strong negative peak at 222 nm characteristic of the presence of α -helix, with a small increase in helical content with increased concentrations (respective molar residual ellipticity of 11,000 deg.cm²/dmol and 14,000 deg.cm²/dmol) (Yokoyama et al., 1985). Examination of CD spectra of human ApoE isolated from VLDL indicated that the protein was composed of 49% α -helix, 38% random coil, 10% β -sheet and 3% β -turn (Chen, G. C. et al., 1984). The predominantly helical secondary structure was later confirmed in recombinant ApoE isoforms. Recombinant ApoE4 at 3 μ M in 20 mM PB, pH 7.4 displayed 51% α -helical content, against 64% for recombinant ApoE2 and ApoE3 when measured at 15° C (Clément-Collin et al., 2006). Another study showed that recombinant ApoE4 at ~4.5 μ M in PBS, pH 7.4 displayed close to 60% α -helical content at 20° C.

In the present study, rApoE at 25 μ M in 20 mM PB, pH 7.4 displayed close-to 60% α -helical content at physiological pH when measured at 21°C (57%, 60% and 58% for rApoE2, rApoE3 and rApoE4 respectively), with no significant difference between the three isoforms unlike the difference suggested by Clément-Collin et al (Clément-Collin et al., 2006). The absence of observable difference could be due to the higher concentration used here and/or the temperature of CD acquisition.

The stability of the secondary structure of rApoE was further characterised by subjecting the proteins to thermal denaturation. rApoE at 25 μ M in 20 mM PB, pH 7.4 was heated from 20 to 80° C over the course of an hour and changes in secondary structure were followed at 222 nm by CD producing melting curves. Denaturation of rApoE observed a two-state unfolding with $T_m(\text{ApoE2}) \gg T_m(\text{ApoE3}) \approx T_m(\text{ApoE4})$. $T_m(\text{rApoE2})$ was significantly different from that of the other two isoforms. Both results were in agreement with previously published results, albeit showing different T_m values (Morrow et al., 2000; Acharya et al., 2002; Clément-Collin et al., 2006). rApoE2 was shown to be more stable to thermal changes than rApoE3 and rApoE4, but it is worth noting that all three isoforms have the same secondary structure and level of unfolding at 37°C (table 3.3).

The tertiary structure of rApoE was studied by taking advantage of ApoE's Trp content (7 Trp at position 20, 26, 34, 39, 210, 264, 276). The maximum emission of Trp was approximately 350 nm, with no difference between the three isoforms consistent with Trp being in identical environments.

Chemical denaturation of rApoE in the presence of GuHCl was followed by plotting the red shift of Trp fluorescence emission against concentration of denaturant. rApoE isoforms followed a biphasic unfolding from folded to intermediate to unfolded state, with

slight differences between the three denaturation curves. Since the three-state model of unfolding is empirical, not much can be deduced from ΔG_{H_2O} and the slope m , but the midpoint of each transitions give an idea of the stability of each isoform: rApoE4 starts unfolding at lower denaturant concentration than rApoE2 and rApoE3 (0.58 M vs ~0.7 M); however, transitioning from intermediate to unfolded state occurred at higher guanidine concentration for rApoE2 than rApoE3 and rApoE4 (2.84 M vs ~2.65 M). Overall, it would seem that rApoE2 was marginally more resistant to chemical denaturation than the other two isoforms. This was in agreement with data published by Clement-Collin et al on recombinant ApoE (Clément-Collin et al., 2006). Human ApoE3 isolated from plasma also followed a three-state chemically-induced unfolding process as shown by following the loss of α -helical content using CD spectroscopy, with the first transition occurring at ~0.7 M as was the case here for rApoE3, and the second transition at 2.5 M (Wetterau et al., 1988).

The biphasic nature of human plasma ApoE3 and of rApoE, as shown here and by others, is consistent with the existence of two independently folded domains. This was first put forward by Wetterau et al: through limited proteolysis, the two domains were identified in human plasma ApoE3 as a 22 kDa N-terminal and a 10 kDa C-terminal domain. These two fragments have since then been used to model the two domains of ApoE3. Guanidine denaturation of both domains allowed for the attribution of the first transition to the unfolding of the C-terminal domain and the second to that of the N-terminal domain (Wetterau et al., 1988). The two independently folded domain identified by Wetterau et al were further characterised in a companion paper by studying their hydrodynamic behaviour and their respective secondary structure. The N-terminal domain was largely monomeric, compact and globular whereas the C-terminal domain readily formed tetramers in solution, possibly mediating the tetramerization of ApoE3. Both domains were highly α -helical (Aggerbeck et al., 1988). X-ray crystallography studies conducted a few years later on the amino-terminal domain of human plasma ApoE3 showed it to be formed of an elongated four-helix bundle arranged in an anti-parallel fashion (Wilson et al., 1991) (Fig. 3.1). To date, there is no crystal structure of full-length ApoE. However, the NMR structure of recombinant ApoE3 was later acquired, supporting the X-ray characterisation of the N-terminal and supplying additional structural information on the hinge region and the C-terminal domain. These domains are formed of two and three helices respectively (Chen, J. et al., 2011).

Structure		rApoE2	rApoE3	rApoE4
Primary	Plasmid sequencing	<i>Plasmid sequence confirmed through Eurofins</i>		
	SDS-PAGE	<i>Purified ApoE migrated to ~34 kDa</i>		
	Mass spectrometry	Cys-112; Cys-158	Cys-112; Arg-158	Arg-112; Arg-158
Secondary	CD spectroscopy	α -helical content, F(2,9)= 4.197, p>0.05		
		57.3%	59.5%	58.4%
	Thermal denaturation	E2 vs E3, ** p= 0.0083; E2 vs E4, ** p= 0.0038; E3 vs E4, ns p= 0.8543		
		T _m = 60.28°C	T _m = 52.39°C	T _m = 51.32°C
		α -helical content at 37°C, n.s., F(2,9)= 0.1415, p>0.05		
Tertiary	Intrinsic Trp fluorescence	<i>No significant difference</i>		
	Chemical denaturation	Three-state transition: Folded ↔ Intermediate ↔ Unfolded		
		[GuHCl] ₁ = 0.69 M; [GuHCl] ₂ = 2.84 M;	[GuHCl] ₁ = 0.71 M; [GuHCl] ₂ = 2.66 M;	[GuHCl] ₁ = 0.58 M; [GuHCl] ₂ = 2.65 M;
Quaternary	AUC	<i>Formation of tetramer in solution</i>		
		c(S)= 5.07 S	c(S)= 5.1 S	c(S)= 5.23 S
	Native gel electrophoresis	One main band		Presence of oligomers

Table 3.6 Summary of the structural characterisation of rApoE isoform

The amino-terminal domain was shown to have full LDL-receptor-binding activity, whereas the carboxy-terminal domain did not (Innerarity et al., 1983) but had the major lipid-binding function (Weisgraber, 1990). The Cys to Arg substitution at position 112 in ApoE4 was speculated to promote the formation of a salt bridge between residues Arg 61 and Glu-255, which would not occur in ApoE2 or ApoE3 (Dong & Weisgraber, 1996). The existence of such a domain interaction in ApoE4 was hypothesized to contribute to AD onset, on top of its defined role in lipoprotein preferences (Weisgraber & Mahley, 1996).

The existence of both independent amino- and carboxy-terminal domains was also observed in recombinant ApoE isoforms by Morrow et al. However, they reported a marked difference in the shape of the denaturation curve of recombinant ApoE4 compared to that of recombinant ApoE2 and ApoE3 when chemical denaturation was tracked using CD. The denaturation curve Morrow et al reported for ApoE4 presented a shoulder at ~2.5 M GuHCl, This shoulder observed in ApoE4's denaturation curve was not indicative of domain interaction, as shown by the superimposition of independently acquired denaturation curve of the N-terminal and C-terminal domain to that of full-length ApoE4 (Morrow et al., 2000). Interestingly, when followed by fluorescence as was done here, no shoulder could be observed in ApoE4 denaturation curve and no differences were found between the isoforms. Morrow et al explained that difference by pointing to the position of Trp residues, which mainly occur in helix one (helix one spans from amino acid 24 to 42 and contains three of the seven Trp residues; Wilson et al. 1991) (Fig. 3.1B), whereas the amino acid differences between ApoE4 and ApoE2/3 occur in helix three (Arg-112 to Cys-112 for ApoE2/3) and four (Arg-158 to Cys-158 for ApoE2) (Morrow et al., 2000).

Morrow et al characterised ApoE's denaturation by GuHCl in two ways: by recording loss of secondary structure, and by following changes in tertiary structure. For ApoE4, and to a lesser extent ApoE3, these two profiles did not superimpose. This was indicative of the presence of unfolding intermediates. Unlike the other two isoforms, ApoE2 displayed a cooperative unfolding (Morrow et al., 2000). This discovery led to putting forward the hypothesis that, in addition to its domain interaction, ApoE4 could be involved in AD through forming a molten globule, which is a stable folding intermediate characterised by retention of the native secondary structure, a compact structure and internal mobility exposing the hydrophobic core.

In a follow-up study, Morrow et al further investigated the amino-terminal domain of ApoE. The denaturation in urea of the 22 kDa N-terminal fragment of ApoE3 and ApoE4, but not ApoE2, fitted a three-state model, indicative of the presence of stable

intermediate species. Fourier-transform infrared spectroscopy analysis of ApoE3 and ApoE4 intermediates showed that both fragments retained their α -helical structure, with a more pronounced increase in β -sheet content in the ApoE4 N-terminal domain intermediate. Pepsin digestion of the 22 kDa fragments highlighted that ApoE4 was subjected to conformational changes by the opening of the four helix bundle, exposing its hydrophobic core; and dynamic light scattering showed that ApoE4 intermediate was slightly elongated (Morrow et al., 2002). The propensity of ApoE3, but especially ApoE4, to form molten globules could be involved in formation of aggregates (Hatters et al., 2006).

The current study presented evidence that rApoE4, but not rApoE2 or rApoE3, self-assembled after 24 h incubation at 37°C in 20 mM PB, pH 7.4. Filaments formed by rApoE4 were ThT fluorescence positive, and their morphology was observed using TEM. Micrographs of incubated rApoE clearly showed the presence of filaments in rApoE4 that arose from an end-to-end fusion of smaller round species, elongating over time while maintaining their width (26-30 nm). After 24 h incubation, filaments in rApoE4 reached close to 400 nm in length. rApoE2 and rApoE3, on the other hand, remained soluble and globular after the incubation period.

Hatters et al stated that recombinant ApoE2 and ApoE3 formed the same aggregates as ApoE4, albeit after longer incubation periods (Hatters et al., 2006). This was also investigated here, where I showed that increased incubation time did not promote fibril formation in rApoE2. However, some small round species started appearing in rApoE3 by day 3 that resemble species found in rApoE4 after 1 h-incubation. For clarity, micrographs of these species in rApoE4 and rApoE3 are presented adjacently in Fig. 3.16.

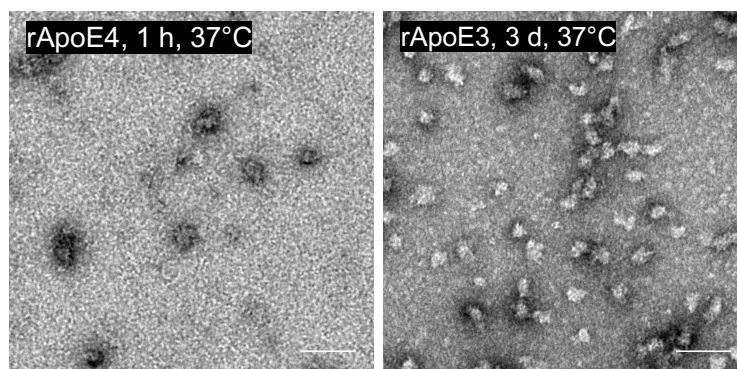


Figure 3.16 Small round species in rApoE3 and rApoE4

Incubation of rApoE3 for 3 d at 37°C prompted the formation of small round species, similar to those detected in rApoE4 after 1 h incubation under the same conditions. Scale bar: 100 nm.

These results correlated nicely with ThT fluorescence increasing in the rApoE3 sample following a ~24 h lag phase; no major change in ThT fluorescence in the rApoE2 sample occurred over three days under the conditions used.

The morphology of rApoE4 fibrils formed in 20 mM PB, pH 7.4 was dissimilar to those reported by Hatters et al, which showed the formation of thin and irregular fibres in PBS of similar width to amyloid fibrils (Hatters et al., 2006). However, similar aggregates of rApoE4 could be obtained when rApoE4 was incubated in PBS (appendix 2).

The similarity of ApoE4 aggregates with amyloid fibres as well as their capability to interact with ThT, a dye historically known for its amyloid-detection properties, prompted Hatters et al to investigate the nature of ApoE4 fibrils. They reported a marginal loss of α -helical content and a relatively small increase in β -structures in ApoE4 with incubation, which did not match the expected shift of secondary structure to β -sheet, typical amyloid formation. The X-ray fibre diffraction pattern of their ApoE4 aggregates also did not correspond to that of amyloid fibrils, which are characterised by diffusion ring at 4.8 Å and 9.6 Å, and by meridional and equatorial arcs (Serpell, 2000). Building on their results, Hatters et al put forward the hypothesis that ApoE formed unique α -helical fibres (Hatters et al., 2006).

The nature of rApoE4 fibrils was also characterised here. Initially, an analysis of the propensity of ApoE isoforms to form amyloid was generated using the Waltz algorithm. With broadly similar profiles, ApoE isoforms displayed five amyloidogenic regions (over 70% amyloidogenicity). Two main regions of 25 and 21 amino acids are located at the N-terminal and C-terminal ends of the protein respectively. The other three, shorter regions (ranging from six to eight amino acids) are comprised within the hinge region of ApoE. This result pointed to ApoE being capable of forming amyloid fibres. A number of techniques were employed to explore whether rApoE underwent the characteristic switch from native secondary structure to cross- β sheet.

rApoE4 retained its highly α -helical structure, as was shown by the overlapping of CD spectra from before and after incubation. Fibrils were pelleted to confirm that the significant α -helical content did not come from any soluble, unassembled protein. The pellet displayed levels of secondary structure similar to that of the sample before sedimentation, and the supernatant showed a very low signal intensity, which indicated that the majority of rApoE4 had assembled into fibrils. The small shift from α -helix to β -sheet reported by Hatters et al was not detected here (Hatters et al., 2006). The absence of distinctive conversion of the secondary structure to cross β -sheet was indicative of ApoE4 forming a unique kind of fibrils that are not amyloid in nature. While CD is a useful

tool to track the formation of β -sheet such as those found in amyloid fibres, X-ray fibre diffraction gives a definitive answer to whether fibrils are amyloid in nature or not. The diffraction pattern of aligned ApoE4 filaments presented two meridional reflections at 4.1 Å and 4.5 Å, as well as a diffuse but strong signal at 10.1 Å and a weak reflection at 21 Å on the equator. This pattern did not correspond to a cross- β pattern.

Taken together, the TEM, CD and X-ray diffraction data indicate that rApoE4 does not self-assemble into amyloid fibrils. A number of other results supported the view that ApoE4 does not form amyloid. Amyloid fibres are characteristically SDS-insoluble (Marshall et al., 2016), whereas self-assembled ApoE4 was SDS-soluble as it appeared as a monomeric band when ran through a denaturing gel. However, ApoE4 fibrils were not capable of migrating through native gels, highlighting the presence of high oligomeric species compared to those found in ApoE2 and ApoE3. Despite being used to detect amyloid formation, ThT is a rotamer that is not specific to β -sheet structures. For instance, ThT can fluoresce in the presence of cross- α fibrils (Tayeb-Fligelman et al., 2017).

The potential for rApoE4 to influence assembly of rApoE2 and rApoE3 was also investigated here. This is relevant since individuals can be ϵ 4 heterozygotes, and to figure out how an ApoE isoform affects the other might improve our understanding of the association between ApoE4 and risk of AD onset. The presence of rApoE4 did not lead to assembly of rApoE2 and rApoE3; rather, the presence of the other isoforms inhibited the formation of mature rApoE4 fibrils. This was both highlighted by lowered ThT emission and the absence of long fibrils on the EM micrographs. Interestingly, rApoE2 inhibited rApoE4 self-assembly even more than rApoE3. Some species that were found after 1 h incubation in rApoE4 were also found in the rApoE3-rApoE4 mixed sample, whereas only amorphous and small species were found in the rApoE2-rApoE4 mixed sample, similar to those from rApoE4 at 0 h. It would appear that the extra Cys residue in rApoE2 enhanced the inhibition of rApoE4 self-assembly, suggesting that the presence of Cys residues is responsible for the differential self-assembly of rApoE, although the mechanism behind this is still unclear.

While bacterial-produced ApoE was shown to have similar biophysical and functional characteristics to mammalian ApoE and thus has proved to be an excellent model of human ApoE (Argyri et al., 2011), limitations remain. Bacterial-produced ApoE does not harbour the same post-translational modifications as ApoE synthesised in human, which is a glycoprotein. Self-assembly of glycosylated ApoE4 produced in astrocytoma, gifted by Dr. Chroni from the Institute of Biosciences and Applications, National Center for

Scientific Research "Demokritos" in Athens, Greece, was also attempted but was not successful. Analysis of the stock received showed that the sample had deteriorated and there was not enough sample to try and optimize for assembly (appendix 2). It would be interesting to carry this study out further with production of glycosylated ApoE on site. This was not possible during this project as methods of protein production and purification on site were developed for bacterial productions.

3.5. Conclusion

In this study, recombinant human ApoE isoforms produced in bacteria was used to model human ApoE in order to highlight any differences that may confer ApoE its isoform-specific effect on AD onset. rApoE formed tetramers in solution and was highly α -helical, as expected from its primary sequence (Rall et al. 1982). Small differences appeared under thermal and chemical denaturation, with the order of stability rApoE2>>rApoE3>rApoE4 in agreement with what has been reported so far in the literature (Morrow et al., 2000; Clément-Collin et al., 2006). The major difference between the three isoforms came from their differential aggregation propensity. One of the main hypotheses behind the onset of AD revolves around protein misfolding and aggregation, hence the observation that recombinant ApoE4 was prone to fibril formation *in vitro* was of great interest (Hatters et al., 2006) and was investigated here more in depth. rApoE4 formed mature, SDS-soluble fibrils after 24 h incubation at 37°C in physiological buffer that were stable over time. They were of a unique structure as rApoE4 fibrils remained α -helical, and the X-ray diffraction pattern did not resemble that of cross- β sheet characteristic of amyloid filaments nor that of α -helical patterns.

The presence of rApoE2 and rApoE3 inhibited the formation of rApoE4 filaments, with a stronger inhibition exerted by rApoE2. Aggregation in the presence of the reducing agent DTT should provide further information on whether rApoE4 aggregates because of the absence of disulphide-bond formation.

Chapter 4 - Apolipoprotein E and oxidative stress

4.1. Introduction

Background

Oxidative stress in AD has been extensively documented. For instance, increased lipid peroxidation in AD brains compared to age-matched controls was reported by Marcus et al (Marcus et al., 1998). Lipid peroxidation occurs as a result of ROS attack on lipids and can result in alterations of cell membranes (Marcus et al., 1998).

While there is no clear consensus on the exact degree at which various antioxidant enzymes are responsible, it is clear that the antioxidant defence system is altered in AD. Marcus et al. also communicated decreased SOD activity in the frontal and temporal lobe of AD cases, and reduced CAT activity, particularly in the temporal lobe (Marcus et al., 1998). This was supported by a later study showing decreased GPx, SOD and CAT activity in synaptosome, and in mitochondrial and post-mitochondrial supernatant isolated from the frontal cortex of AD brain tissue (Ansari & Scheff, 2010).

Carrying the $\epsilon 4$ allele of *APOE* does not necessarily mean AD onset, which is why research has turned to exploring possible associations between ApoE4 and susceptibility factors for AD, such as oxidative damage and antioxidant status. Links between *APOE* genotype and oxidative stress in AD have been investigated in human brain tissue. Ramassamy et al reported increased CAT and GPx activity in AD frontal cortex tissue, especially in $\epsilon 4$ homozygotes, compared to controls ($\epsilon 3/\epsilon 3$) (Ramassamy et al., 1999). Interestingly, a year later Ramassamy et al reported decreased CAT and GPx activity in the hippocampus of AD $\epsilon 4$ carriers compared to AD $\epsilon 3/\epsilon 3$ (Ramassamy et al., 2000).

In line with this last finding, Kharrazi et al reported decreased CAT and GPx, but not Cu-Zn SOD, activity in erythrocytes of AD patients compared to control, and this was more pronounced in $\epsilon 4$ carriers. It was also the case in control $\epsilon 4$ carriers (Kharrazi et al., 2008). This observation suggests that the presence of ApoE4 is associated with an environment favourable to damage.

Data gathered on $\epsilon 4/\epsilon 4$ control subject is very limited since the allele frequency of $\epsilon 4$ in the general population is close to 15% (Liu, C.-C. et al., 2013), and $\epsilon 4$ homozygotes only represent 2% of the population (Ramassamy et al., 1999).

There is also evidence that ApoE itself may be part of protection and/or repair mechanisms as a response to injury. While ApoE in the brain is mainly produced by astrocytes, it can also be synthesised in neurons. Using *in-situ* hybridization for *APOE* mRNA, Xu et al showed that ApoE could also be produced in the frontal cortex and hippocampus of human brains, demented and non-demented alike (Xu, P.-T. et al., 1999). The same year, Boschert et al reported endogenous ApoE expression in neurons that had survived excitotoxic stress induced by kainic acid injection in the hippocampus of rats (Boschert et al., 1999). Neuronal ApoE expression following injury was also reported in human tissue, with up-regulation of neuronal ApoE after cerebral infarction (Aoki et al., 2003). Neuronal ApoE was also detected in tissue from epilepsy patients, with a genotype-dependent level of expression: neuronal ApoE expression was greater in $\epsilon 3/\epsilon 3$ than in $\epsilon 4/\epsilon 4$ patients (Aboud et al., 2012). It would thus appear that mechanisms of ApoE expression in neurons are also isoform-dependent.

The involvement of ApoE with oxidative stress may not just be related to increased vulnerability carried by ApoE4, but also to intrinsic antioxidant potential of ApoE. The investigation of the antioxidant properties of ApoE stemmed from observing an increased susceptibility of plasma lipoproteins from ApoE-deficient mice to *in vitro* oxidation. This finding was the starting point for a series of experiments performed by Miyata et al that started by looking at protective properties of ApoE against several oxidative insults in a rat neuronal cell line (Miyata & Smith, 1996). After showing that ApoE indeed protected against oxidative cytotoxicity, they moved on to *in vitro* testing of ApoE antioxidant activity. Their experiments revealed isoform-dependent protective abilities, with ApoE2 being more efficient than ApoE3, being more efficient than ApoE4, at favouring cell survival. Metal binding by ApoE was proposed as one of the mechanisms by which ApoE exerted its protective effects, as shown in an additional *in vitro* experiment based on metal ion dependent lipoprotein oxidation. However, ApoE antioxidant activity in the quenching of luminol oxidation by H_2O_2 and horseradish peroxidase was less clear cut. While ApoE metal binding may play a role here as well, the exact mechanism was not elucidated (Miyata & Smith, 1996).

It is important to note that ApoE itself can become oxidized. Jolivalt et al reported that recombinant ApoE4 was more susceptible than ApoE3 and ApoE2 to oxidation by the

myeloperoxidase enzymatic (MPO) system, which requires H_2O_2 and Cl^- . Oxidation of ApoE could result in altered physiological function, such as impaired lipid-binding capacity (Jolivalt et al., 2000).

A number of amino-acid residues are susceptible to oxidative modifications, such as Cys residues. Cys oxidation can result in inter- or intramolecular disulphide bridges, or to formation of sulfinic ($-SO_2H$) or sulfonic ($-SO_3H$) acid (Cremers & Jakob, 2013). Since ApoE4 does not contain any Cys residues, differences in antioxidant properties may arise from the absence of that particular residue (Jolivalt et al., 2000). ApoE also contains 7 Met residues (Fig. 4.1), which can be oxidized to Met sulfoxide ($-S=O$) by H_2O_2 , as has been shown to occur *in vitro* in Apolipoprotein A-I (3 Met) and Apolipoprotein A-II (1 Met) (Anantharamaiah et al., 1988). Met oxidation of ApoE *in vitro* was first hinted at by Strittmatter and colleagues when they showed that formation of $A\beta$ /ApoE complexes required oxidation of ApoE. Since ApoE4 has no Cys residues, they proposed that ApoE oxidation was possibly in part due to oxidation of Met residues (Strittmatter, Weisgraber, et al., 1993). Oxidation of Met residues in ApoE was later alluded to by Jolivalt and associates: following oxidation by the MPO system, ApoE4 was no longer susceptible to cleavage by cyanogen bromide (CNBr). CNBr fragments peptides after Met residues but does not digest oxidised Met (Jolivalt et al., 2000). Met oxidation in ApoE has not been investigated further to date.

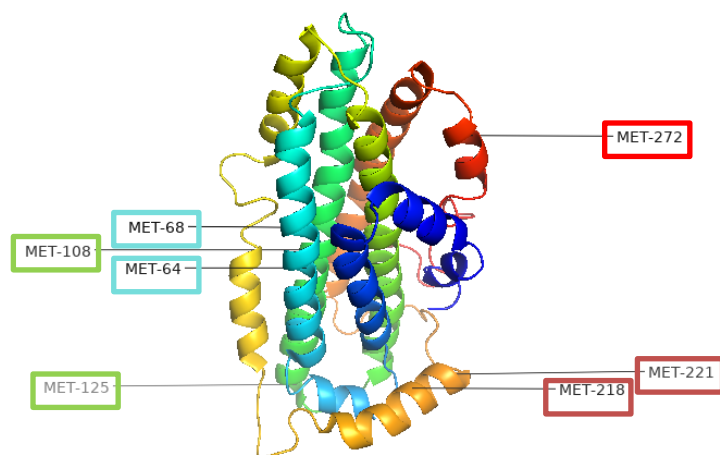


Figure 4.1 Met residues in ApoE

ApoE structure was generated from the NMR structure of ApoE3 (PDB 2L7B).

Rationale

The association between *APOE* genotype and oxidative stress was explored at two independent levels to achieve a comprehensive analysis of the links tying the two susceptibility factors together.

ApoE-TR mice express human ApoE under the control of the mouse ApoE promoter, making them an ideal model for physiological human ApoE (Sullivan et al., 1997; Tai et al., 2011). This model allows for exploration of the role of ApoE4 in a non-disease fashion, at baseline (see 1.7.2).

Increased vulnerability associated with the $\epsilon 4$ allele of *APOE* was first explored by assessing potential genotype-dependent differences in antioxidant enzyme defence in ApoE-TR mice. There are many enzymes and non-enzymatic proteins involved in protecting against oxidative stress. Evaluation of CAT and SOD activities were chosen here as a starting point, keeping in mind that they only represent a diminutive part of the whole antioxidant defence system. SOD is responsible for reduction of superoxide levels by catalysing the partition of O_2^\bullet radicals into O_2 or H_2O_2 ; in turn, CAT catalyses the breakdown of H_2O_2 into H_2O and O_2 (Romano et al., 2010).

Both CAT and SOD activities were quantified across lifespan in the brains of E3/E3 and E4/E4 mice to see whether this model replicates the lowered antioxidant defence observed in human $\epsilon 4$ carriers. Hemibrains, and not specific AD-associated brain regions, were used here to assess whether global effects of ApoE phenotype on total brain antioxidant status could be detected.

An establishment of any difference at this level is important before moving onto exploring ApoE's response to neuronal injury *in vitro*. After characterising the ApoE-related response to oxidative damage in a neuroblastoma cell line, ApoE-associated resilience and potential response to injury was investigated in neuronal cultures from E3/E3 and E4/E4 mice.

The differential ability of ApoE to respond to oxidative conditions was examined at the structural level. The effect of H_2O_2 on the secondary and tertiary structure of the protein was investigated in order to try and identify any isoform-specific behaviour and oxidative environmental response in the presence of a known ROS. Furthermore, given that the main observable difference between the three ApoE isoforms came from their distinct self-assembly properties as reported in the previous chapter, the effect of H_2O_2 on fibril formation was also investigated. As a control, secondary and tertiary structure of ApoE as well as their self-assembly properties were also investigated under reducing conditions in the presence of DTT.

4.2. Summary of methods

ApoE-TR mice were used as a model for physiological human ApoE. These mice were designed to express human ApoE under the control of the mouse ApoE promoter (see 1.7.2).

Antioxidant defence system was partially characterised by quantifying CAT and SOD activities in the brains of E3/E3 and E4/E4 mice collected at 3 m, 6 m, 12 m, 18 m and 24 m. Homogenates of hemibrains were prepared using RIPA buffer. A summary of all samples used can be found in appendix 1, including n numbers. Tissue was collected at 3, 6, 12, 18 and 24 months, reaching a minimum of three individual samples per age group. As well as assessing changes at each time point individually, samples were also grouped into age categories for analytical purposes: “adult” (3 and 6 m), “middle age” (12 m) and “old” (18 and 24 m), according to the Jackson Laboratory age report (Flurkey et al., 2007).

CAT activity was determined using a technique based on the stoichiometric reaction of a dye (Amplex Red) with unreacted H_2O_2 in the presence of HRP, leading to the production of resorufin. Detection of resorufin at 571 nm is inversely correlated to CAT activity. SOD activity was also indirectly quantified by an experiment based on the dismutation of superoxides generated by XO. Unreacted O_2^\bullet can subsequently convert WST-1 into a formazan dye that absorbs at 440 nm, quantification of which is inversely correlated to SOD activity.

Human neuroblastoma cells, SH-SY5Y, were used as an initial model to explore the ApoE-associated response to injury. Cells were exposed to H_2O_2 or to a pesticide (azamethiphos) for 24 h, after which ApoE expression was investigated by looking at both *APOE* mRNA levels by qPCR and ApoE levels by immunoblotting. Viability assays were also performed to show that ApoE expression experiments were conducted on cells that had survived injury. Azamethiphos is an organophosphate that inhibits acetyl choline esterase, but organophosphates also elicit oxidative stress (Chin-Chan et al., 2015) which is why it was employed here as a toxin. Haloperidol, a psychotropic drug, was used as a positive control since it was previously shown to up-regulate ApoE expression in SH-SY5Y cells (Vik-Mo et al., 2009).

Primary cortical cultures of neurons from ApoE-TR mice were also established to explore genotype-dependent differences in neuronal response and viability following exposure

to H₂O₂ and azamethiphos for 24 h. Neuronal cultures were treated at DIV10; cell viability was quantified and ApoE expression was assessed at the mRNA level only.

The effects of oxidative and reducing conditions on the structure of ApoE itself were identified with rApoE as a model, using a number of biophysical techniques. As previously detailed in chapter 3, secondary structure in the presence of H₂O₂ and DTT was characterised using CD (see 2.5.3); the tertiary structure using intrinsic Trp fluorescence (see 2.5.4). Fibrillisation under oxidative and reducing conditions were also investigated here since the main difference between the three recombinant isoforms came from their differential self-assembly properties. ThT and TEM experiments (see 2.5.5 and 2.5.6) were conducted to this effect in a bid to close the gap in our understanding of the distinctive susceptibility of rApoE isoforms to form fibrils.

4.3. Results

Increased susceptibility associated with APOE $\epsilon 4/\epsilon 4$

The impact of carrying two $\epsilon 4$ alleles of *APOE* on both the overall antioxidant status and the ApoE-associated response to oxidative attacks was explored using ApoE-TR mice as model.

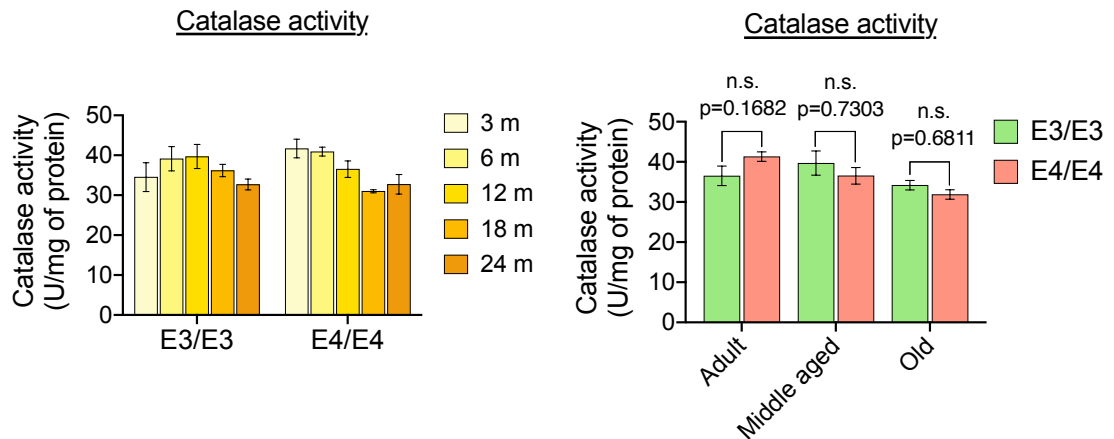
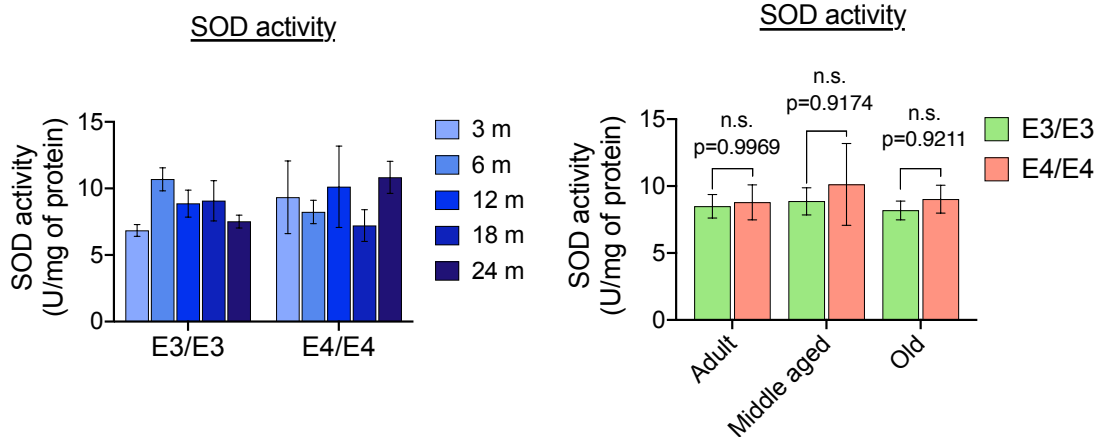
4.3.1. Impact of the APOE genotype on antioxidant balance in ApoE-TR mice

CAT and SOD activities in ApoE-TR mice across lifespan were determined in order to evaluate any *APOE*-genotype dependent differences in antioxidant balance. Results are summarised in Fig. 4.2.

Profiles of CAT activities in ApoE-TR mice were slightly different depending on the phenotype. CAT activity in E3/E3 increased after 3 m, peaking at 12 m of age before decreasing at 18 m and 24 m. In E4/E4 mice, CAT activity decreased with age from 3 m to 24 m (Fig. 4.2A, left). Values were grouped into age categories for comparison between phenotypes (Fig. 4.2A, right). CAT activity was higher in E4/E4 adult mice than in E3/E3 adult mice; however, CAT activities were slightly lower in E4/E4 middle aged and old mice.

Age had the greatest impact on CAT activity, irrespective of the genotype (two-way ANOVA analysis: $F(2, 29) = 7.000$; $p = 0.0033$). Differences in CAT activities were averaged out when looking at all ages combined ($F(1, 29) = 0.02090$; $p = 0.8861$). The interaction between age and phenotype was shy of reaching significance ($F(2, 29) = 2.879$; $p = 0.0723$). Post-hoc Sidak's multiple comparison test showed a potential trend towards higher CAT activity in adult E4/E4 mice only ($p = 0.1682$).

Profiles of SOD activities in ApoE-TR mice were harder to interpret since no clear pattern of change appeared (Fig. 4.2B, left). Comparing SOD activities between phenotypes across age groups showed no difference in adult mice, but slightly higher SOD activities in middle aged and old E4/E4 mice (Fig. 4.2B, right). Two-way ANOVA analysis showed that these marginal differences were not significant, with no impact of age, phenotype or interaction between both factors ($F(2, 29) = 0.26$, $p = 0.7701$; $F(1, 29) = 0.62$, $p = 0.4392$; and $F(2, 29) = 0.07$, $p = 0.9313$ respectively).

A.**B.****Figure 4.2 CAT and SOD activity in ApoE-TR mice across lifespan**

A. CAT activity was measured in ApoE-TR mice at 3 m, 6 m, 12 m, 18 m and 24 m in hemibrain homogenates. Profiles of CAT activity across lifespan are depicted on the left. CAT activity grouped by age category are summarised on the right. Two-way ANOVA post-hoc Sidak's comparison test between E3/E3 and E4/E4: adult, n.s., $p=0.1682$; middle aged, n.s., $p=0.7303$; old, n.s., $p=0.6811$. n numbers can be found in appendix 1. Error bars correspond to the SEM.

B. Changes in SOD activity in ApoE-TR hemibrain homogenates across lifespan showed no distinctive pattern (left). There were no differences in SOD activity between ApoE3-TR and ApoE4-TR mice in adult, middle aged and old mice (right). Two-way ANOVA post-hoc Sidak's comparison test between E3/E3 and E4/E4: adult, n.s., $p=0.9969$; middle aged, n.s., $p=0.9174$; old, n.s., $p=0.9211$. n numbers can be found in appendix 1. Error bars correspond to the SEM.

4.3.2. ApoE expression as a response to cytotoxic insults in SH-SY5Y and in primary neuronal culture

Many studies have pointed to a neuronal expression of ApoE following injury (Boschert et al., 1999; Aoki et al., 2003; Aboud et al., 2012), with some suggesting a genotype-dependent response.

In the current study, neuronal ApoE expression following injury was explored using two different models. ApoE response to toxic insults was first established using SH-SY5Y neuroblastoma cells, which are a human neuronal cell model. Since SH-SY5Y cells are $\epsilon 3/\epsilon 3$, the effect of *APOE* genotype on ApoE expression was compared later using primary cultures from ApoE-TR mice allowing analysis of E3/E3 and E4/E4.

ApoE response to toxic insults in SH-SY5Y

The literature suggests that ApoE is expressed in neurons that have survived excitotoxic stress (Boschert et al., 1999; Aoki et al., 2003; Aboud et al., 2012). Viability of SH-SY5Y cells in response to toxins was thus evaluated to ensure some, but not all, cells die. ReadyProbes reagents were used (see 2.1.3). All nuclei were stained with a blue dye detectable using a DAPI filter, and dead cells with propidium iodide in red (Fig. 4.3A). SH-SY5Y cells survived 24 h-treatment with 50 μ M Haloperidol, whereas only 60% cells survived exposure to 75 μ M H₂O₂ and 75% of cells subsisted following treatment with 25 μ M Azamethiphos (Fig. 4.3B). Mixed-effect analysis with the Geisser-Greenhouse correction attest to the significant cell death following treatment (**, $p=0.0023$). Significance for each treatment were computed by performing a Dunnett's multiple comparison test (see legend for Fig. 4.3B).

Of note, SH-SY5Y cells lift off the plating surface when they die, some get washed away in the media exchange performed prior to the addition of ReadyProbes. The percentage of cell survival given here is likely to be an overestimation.

Following treatment, RNA and proteins were extracted from cells to assess any change in transcription and translation of ApoE. RNA was isolated and cDNA subsequently synthesized for qPCR. A summary of RNA quality and qPCR primer efficiency for each reaction can be found in Appendix 1.

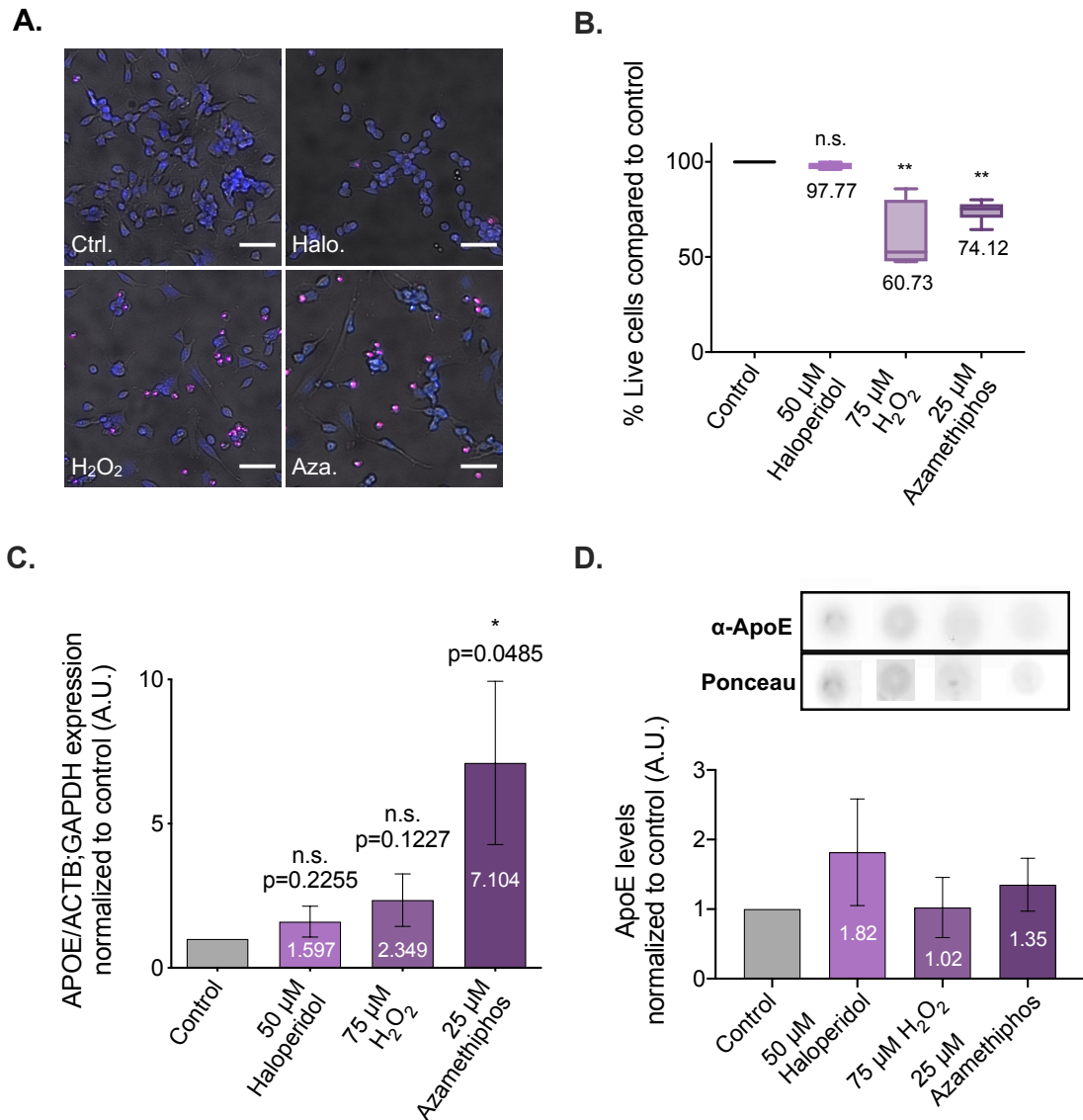


Figure 4.3 ApoE expression in SH-SY5Y following excitotoxicity

A. Example of treated SH-SY5Y cells (ctrl: control; halo.: haloperidol; Aza.: azamethiphos). All nuclei were stained in blue and dead cells in red using ReadyProbes dyes. Scale bar 50 μm .

B. Cell viability following treatment with either haloperidol (N=3), H_2O_2 (N=5) or azamethiphos (N=5) was measured as a percentage of live cells, normalised to viability in non-treated cells (N=6) (control, 100% live cells). Mean % Live cells are indicated below each box. Dunnett's multiple comparison test to control: haloperidol, n.s., $p=0.3606$; H_2O_2 , **, $p=0.0033$; azamethiphos, **, $p=0.0012$. Error bars correspond to the min to max. N refers to the number of experiments per condition. Each experiment constitutes an average of 2 to 3 experimental wells per condition, and 5 different fields of view were acquired per well.

C. qPCR analysis of *APOE* gene expression showed increased expression following all three treatments, Fold increases are indicated within each bar. p values for significance between treatment and control can be found above each bar (one-way RM ANOVA, post-hoc Dunnett's multiple comparisons test); $n=4$. Error bars correspond to the SEM. (legend continues below)

D. ApoE expression was detected using a polyclonal antibody by dot blot, normalised to total protein content (Ponceau stain) and presented as a fraction of control cells. N (dot blot) = 3, n (experiments)= 3. ApoE levels were the highest in haloperidol-treated cells. Error bars correspond to the SEM.

APOE gene expression standardized to reference genes (*ACTB* and *GAPDH*) following treatment was normalised to that of control cells. All three treatments induced an increase in *APOE* mRNA levels (Fig. 4.3C; one-way repeated measure [RM] ANOVA: *, $p= 0.0191$), the greatest effect being caused by azamethiphos, with a 7-fold increase in *APOE* mRNA (post-hoc Dunnett's multiple comparison test: *, $p=0.0485$).

Evaluation of protein expression was first attempted by WB. However, low protein concentrations made it very difficult to detect ApoE at 34 kDa, and various species were present (see Appendix 3). As an alternative, protein expression was evaluated by dot-blot (Fig. 4.3D). Treatment induced slight increases in levels of ApoE, especially after exposure to haloperidol. Given the variability of the technique and the low n number of 3, no statistical comparison was conducted.

ApoE response to toxic insults in primary cortical neurons from ApoE-TR mice

Primary cortical neurons from E3/E3 and E4/E4 mice were cultured to compare how the ApoE response to toxic insults may differ with the *APOE* genotype.

A direct comparison between the ApoE response in human and mouse cells following treatment with H₂O₂ or azamethiphos could not be performed since SH-SY5Y cells were substantially more susceptible to toxins than the primary cultures. Nonetheless, viability of primary neurons at DIV10 in response to toxins was evaluated using ReadyProbes to ensure partial cell survival (Fig. 4.4). Considerably higher concentration of both toxins had to be used on neurons to induce cell death (650 μM H₂O₂ and 300 μM azamethiphos versus 75 μM H₂O₂ and 25 μM azamethiphos in SH-SY5Y).

Cell viability pattern following toxic treatment varied with the ApoE phenotype. Compared to control, treatment induced a greater level of cell loss in E3/E3 than in E4/E4 neurons. No statistical test was performed due to great variability and low n numbers (n=2 for E3/E3 and n=3 for E4/E4). Treatment with H₂O₂ and azamethiphos in E3/E3 neurons led to similar relative levels of cell death as for SH-SY5Y (i.e. greater toxicity in H₂O₂ treated neurons than following azamethiphos treatment). Treatment with 650 μM H₂O₂ and 300 μM azamethiphos led to comparable levels of cell death in E4/E4 neurons (~15%) (Fig. 4.4B). Comparison of percentage of live cells at baseline in E3/E3 and E4/E4 neurons

(Fig. 4.4C) pointed to lowered viability in E4/E4 neurons (by 15%). This result needs to be taken with caution given the low n numbers but would suggest greater survival of E3/E3 neurons.

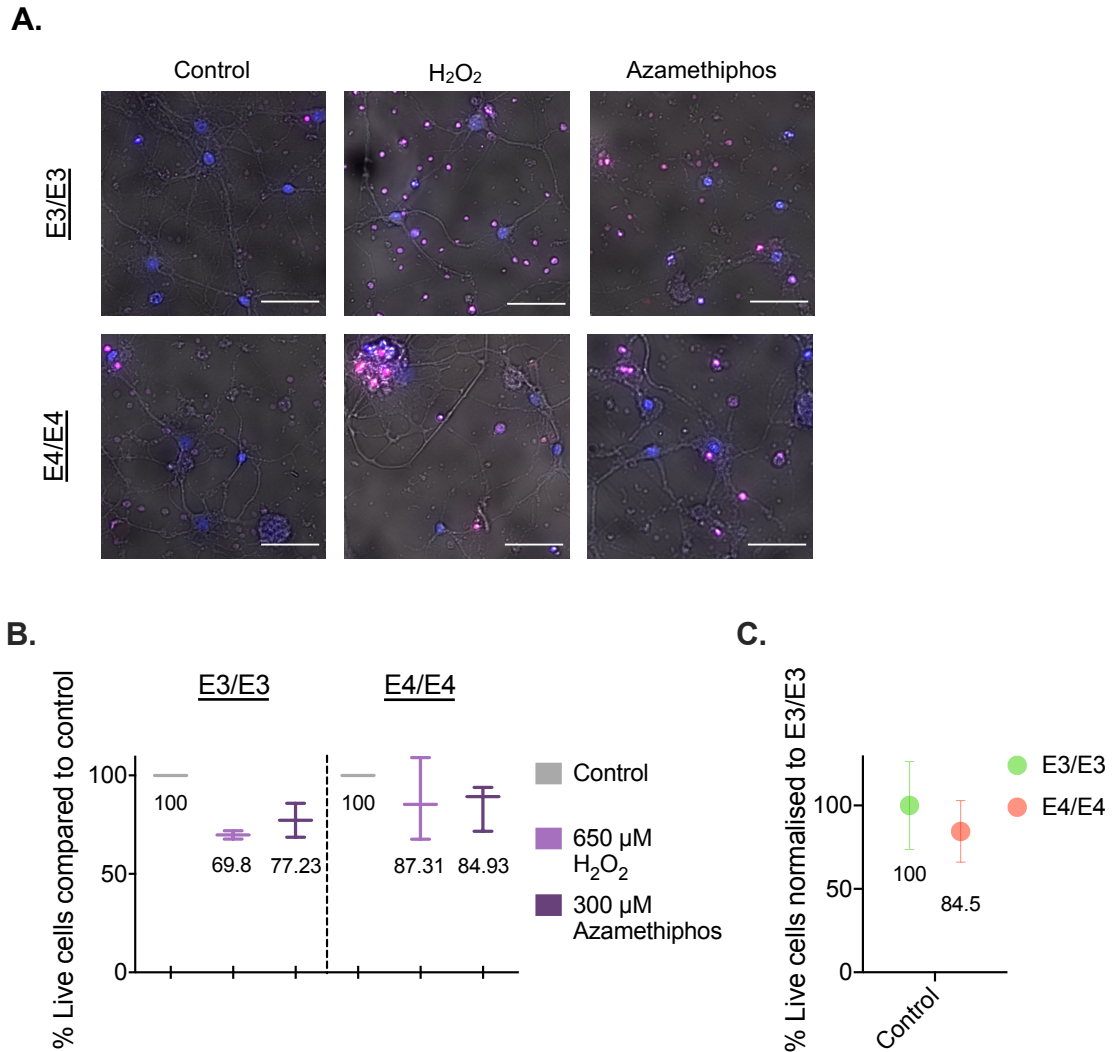


Figure 4.4 Primary cortical neurons' viability following exposure to toxins

A. Example of treated DIV10 primary neurons. All nuclei were stained in blue and dead cells in red using ReadyProbes dyes. Scale bar 50 μ m.

B. Cell viability following treatment with either H_2O_2 or azamethiphos was measured as a percentage of live cells, normalised to viability in non-treated cells (control, 100% live cells) in E3/E3 (n=2) and E4/E4 (n=3) cultures separately. Mean % Live cells are indicated below each box. Error bars correspond to the min to max. Each experiment constitutes an average of 3 experimental wells per condition, and 4 different fields of view were acquired per well.

C. Comparison of cell viability in E3/E3 and E4/E4 non-treated neurons. When normalised to E3/E3 (n=2), it appeared that E4/E4 (n=3) had a greater number of dead cells at baseline. No statistics were performed due to low n number. Error bars correspond to the SEM.

Following treatment, RNA was extracted from cells to assess any change in *APOE* gene expression.

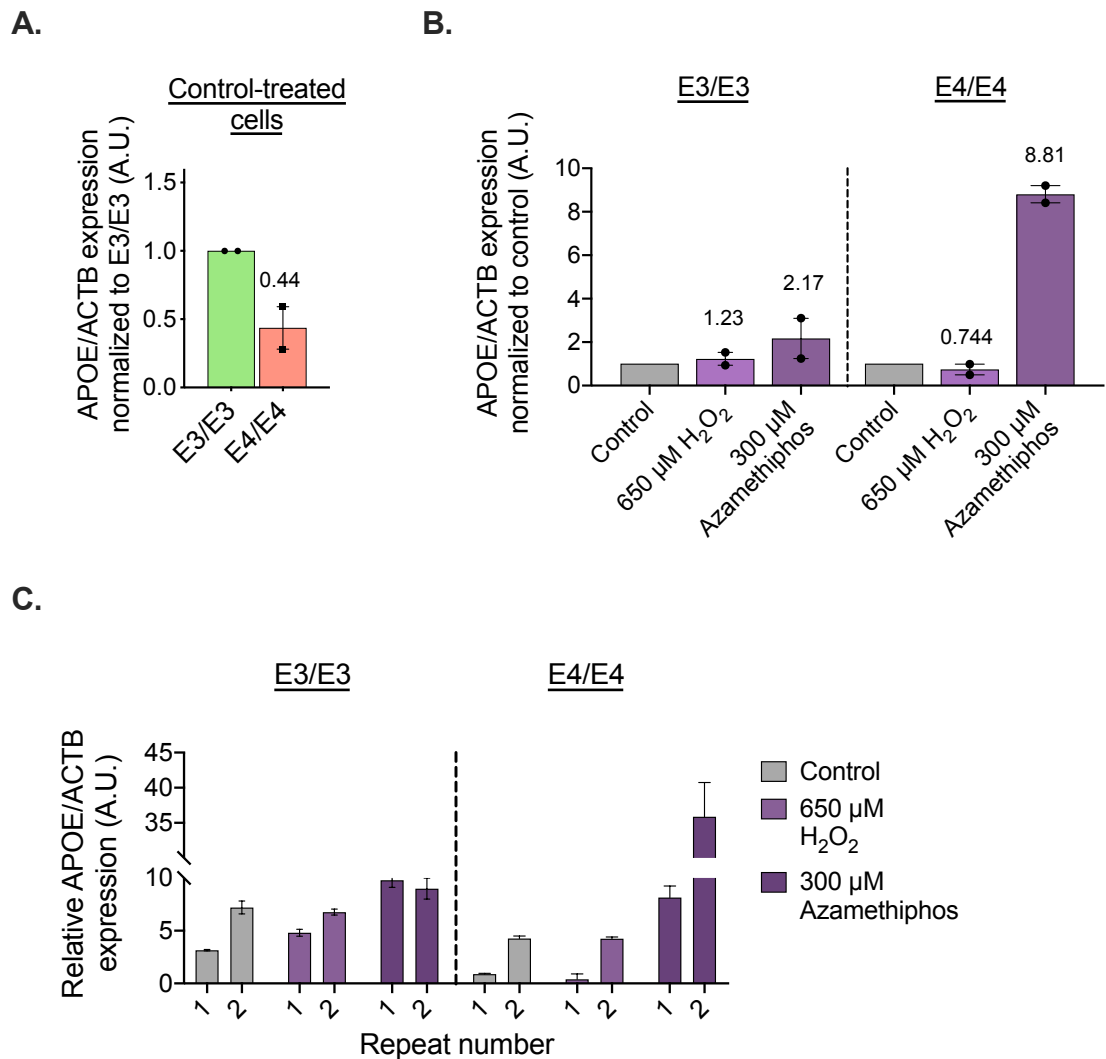


Figure 4.5 ApoE expression in primary cortical neurons following toxic exposure

A. Comparison of baseline *APOE* transcription levels in control neurons showed twice as much *APOE* gene expression in E3/E3 than in E4/E4; $n=2$. Fold change in E4/E4 is reported above the bar. Error bars correspond to the SEM.

B. qPCR analysis of *APOE/ACTB* gene expression showed genotype-dependent changes in transcription following treatment (left: E3/E3; right: E4/E4). Fold increases are reported above each bar; $n=2$. *APOE* transcription was increased following both treatment in E3/E3 neurons, whereas it was decreased following treatment with H_2O_2 , and greatly increased upon exposure to azamethiphos, in E4/E4 neurons. Error bars correspond to the SEM.

C. *APOE* gene expression in primary neurons was only assessed twice in two separate experiments. This bar chart attests to the variability between each repeat, which is why greater n numbers are required before drawing any definitive conclusions. Error bars correspond to the standard error (qPCR ran in duplicate wells).

First, differences between the two phenotypes in *APOE* transcription at baseline were evaluated by expressing *APOE* gene expression in E4/E4 control neurons as a ratio of *APOE* mRNA levels in E3/E3 control neurons. *APOE* basal transcription was halved in E4/E4 compared to E3/E3 neurons. (Fig. 4.5A).

Then, qPCR analysis of *APOE* transcription following treatment was conducted. Treatment with azamethiphos led to a doubling of *APOE* mRNA levels compared to control in E3/E3 neurons, while they were close to 9 times higher in E4/E4 neurons compared to E4/E4 controls. Treatment with H₂O₂ induced a slight increase in *APOE* mRNA in E3/E3, and a small decrease in E4/E4 (Fig. 4.5B).

Analysis of *APOE* gene expression in E3/E3 and E4/E4 neurons was only conducted twice in separate experiments (n=2 for each phenotype), which is why no statistical comparison was performed. The bar chart in Fig. 4.5C attests to the variability between experiments, which is why it needs to be repeated before drawing any definitive conclusions.

Because of the difficulties encountered when looking at protein ApoE levels in SH-SY5Y cells, immunoblotting was not attempted here (concentration of protein extracted from neurons was considerably lower due to lower cell density compared to SH-SY5Y cells). As an alternative, immunofluorescence detection of ApoE was tried once in E3/E3 and E4/E4 DIV14 neurons to see whether it could be used as a substitute technique. This needs further optimisation (appendix 3).

Effect of oxidative and reducing conditions on rApoE

The effect of redox environments on the structure of rApoE was explored using H₂O₂ as an oxidative agent and DTT as a reducing agent. ROS, such as H₂O₂, are able to induce changes to protein structure through protein oxidation (Davies, M. J., 2005). DTT can alter protein structure by blocking the formation of disulphide bridge (Loison et al., 2016). It was used to promote the reduced state of rApoE2 and rApoE3, which both contain Cys residues, unlike rApoE4.

4.3.3. Secondary and tertiary structure of rApoE under redox conditions

Both H₂O₂ and DTT were used at elevated concentrations relative to rApoE (1:3533, which is the molar ratio used by Miyata *et al.*, 1996 in their study for H₂O₂, and 1:400 molar ratio respectively) to guarantee detection of potential structural differences between the isoforms following redox treatment. Proteins were incubated with either of the agents at 4°C for 24 h prior to structural analysis to ensure an equilibrium being reached.

Secondary structure of rApoE, and rApoE2 in particular, was altered by exposure to H₂O₂, but not DTT

The secondary structure of rApoE isoforms in the presence of oxidative and reducing agents was investigated using CD spectroscopy. Far-UV CD showed no difference in spectra between rApoE under physiological and under reducing conditions, for all three isoforms. However, oxidative conditions led to changes in the spectra, suggesting conformational differences induced by H₂O₂, especially in rApoE2 (Fig. 4.6A). CD spectra were analysed using the CONTIN programme on DICHROWEB (Lobley et al., 2002; Whitmore & Wallace, 2004; 2008). Results were summarised as stacked bars charts in Fig. 4.6B and correspond to the DICHROWEB results compiled in table 4.1. DICHROWEB analysis suggested a conformational change induced by oxidative conditions, with loss of α -helical content and corresponding increased random coil as depicted in the stacked bars charts (Fig. 4.6B).

The detailed analysis of rApoE isoforms' structure under physiological, oxidative and reducing conditions were summarised in table 4.1. In PB, all three recombinant isoforms shared approximately 59% α -helical content.

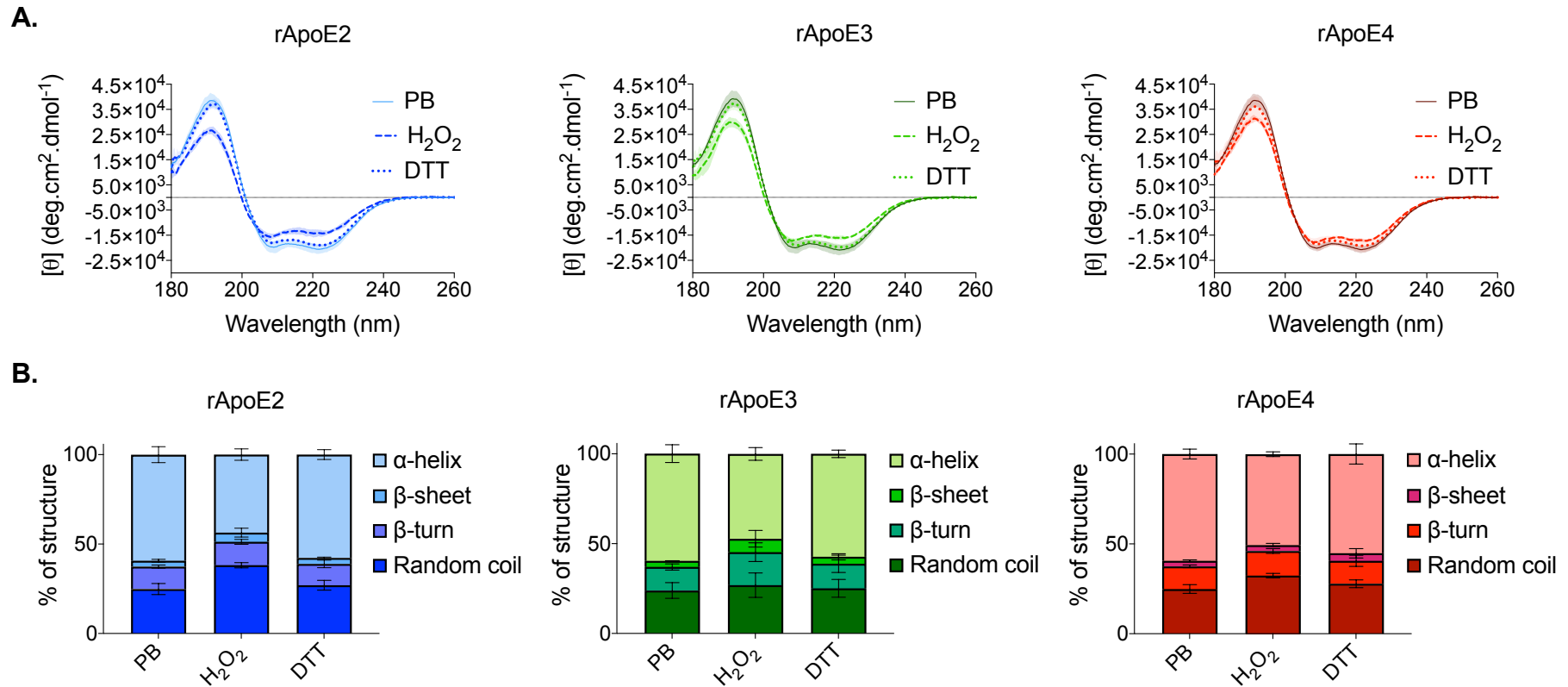


Figure 4.6 Secondary structure of rApoE isoforms in the presence of H_2O_2 and DTT

A. Far UV CD spectra at 21°C of 25 μM rApoE isoforms in PB (20 mM PB, pH 7.4), H_2O_2 (rApoE: H_2O_2 1:3533 i.e. 88.3 mM H_2O_2) or DTT (1:400 i.e. 10 mM DTT). Spectra in PB and DTT were similar. H_2O_2 induced conformational changes, which seemed more pronounced in rApoE2; $n=3$, different protein stocks.

B. Stacked bars representation of secondary structure in rApoE isoforms under physiological, oxidative and reducing conditions, corresponding to DICHROWEB analysis (Lobley et al., 2002; Whitmore & Wallace, 2004; 2008). See table 4.1 for values.

		PB	H ₂ O ₂	DTT
rApoE2	α-helix	59.3	* 43.6	57.8
	β-sheet	3.27	5.17	3.3
	β-turn	12.6	13.1	11.9
	Random coil	24.9	** 38.2	27
rApoE3	α-helix	59.7	47.2	57.3
	β-sheet	3.37	7.43	3.87
	β-turn	13.1	18.4	13.7
	Random coil	23.9	26.9	25.1
rApoE4	α-helix	59.4	* 50.6	55.3
	β-sheet	3.07	3.27	4.2
	β-turn	12.6	13.7	12.8
	Random coil	24.9	32.4	27.8

Table 4.1 Detailed secondary structure of rApoE isoform under physiological, oxidative and reducing conditions

CD spectroscopy data was uploaded onto DICHROWEB and the secondary structure calculated by CONTIN programme (Lobley et al., 2002; Whitmore & Wallace, 2004; 2008). Secondary structure in PB was comparable between the isoforms, and treatment with DTT had no major effect. Oxidative conditions, however, led to decreased α-helix and increased random coil in all three isoforms. Multiple t-test analysis (GraphPad Prism) of treatments compared to control, following correction using the Hold-Sidak method, attested to this. Loss of α-helical content following H₂O₂ treatment, compared to PB, was only significant for rApoE2 (*, p=0.023) and rApoE4 (p=0.030); gain of random coil was significant in rApoE2 (**, p=0.010).

Reducing conditions had no major effect on the secondary structure of rApoE isoforms. This was supported by multiple t-test analysis of the effect of DTT compared to PB for each isoform separately, which showed no significant differences in α-helix, β-sheet, β-turn or unordered structures following correction using the Hold-Sidak method.

However, H₂O₂ had a marked effect on the secondary structure of rApoE, with decreased α-helical content and increased random coil for all three isoforms, especially in rApoE2. Multiple t-test analysis of the effect of H₂O₂ compared to PB for each isoform separately, corrected using the Hold-Sidak method, showed a significant decrease in α-helix in rApoE2 (*, p= 0.023) and rApoE4 (*, p= 0.030), and a significant increase in random coil in rApoE2 (**, p=0.010). Greater SD for rApoE3 values most likely accounted for the non-significance of α-helix loss (Fig. 4.6B).

Levels of α -helix under oxidative conditions were also expressed as a ratio of α -helical content in PB to try and determine which isoform was most affected in its secondary structure by H_2O_2 treatment (table 4.2)

Isoform	α -helix(PB)	α -helix(H_2O_2)	α -helix(H_2O_2)/ α -helix(PB)
rApoE2	59.3	43.6	0.7379
rApoE3	59.7	47.2	0.7915
rApoE4	59.4	50.6	0.852

*, p= 0.025

Table 4.2 Effect of oxidative conditions on α -helical content

α -helical content in H_2O_2 was expressed as a ratio of α -helical content in PB. Values suggested a stronger effect of oxidative conditions on rApoE2. Ordinary one-way ANOVA ($F(2, 6) = 5,890$; $p=0.0384$) followed by Dunnett's multiple comparison test supported this observation: loss of α -helix was significantly weaker in rApoE4 compared to rApoE2 (*, $p=0.025$). Differences between rApoE2 and rApoE3 were not significant (ns, $p=0.26$). Statistical analyses were conducted using GraphPad Prism.

Overall, rApoE2 was more sensitive to oxidative conditions than the other two isoforms, while reducing conditions had little effect on rApoE secondary structure.

The shape of the α -helix spectrum also seemed to be altered by the presence of H_2O_2 . The ratio of signal at 222 nm and 208 nm, $[\theta]_{222/208 \text{ nm}}$, is related to whether a helix is part of a coiled-coil or not (ratio close to 1.1 for the former and 0.9 for the latter) (Greenfield, N. J. & Hitchcock-Degregori, 1993). This ratio was thus calculated in samples in PB and treated with H_2O_2 (Table 4.3). From looking at the values, it was apparent that oxidative conditions had an effect on the nature of α -helices in rApoE since there was a decrease in $[\theta]_{222/208 \text{ nm}}$ from ~ 1.05 to values closer to 0.9.

Isoform	$[\theta]_{222/208 \text{ nm}}$ in PB	$[\theta]_{222/208 \text{ nm}}$ in H_2O_2	Multiple comparison
rApoE2	1.052 ± 0.041	0.902 ± 0.006	***, $p=0.0005$
rApoE3	1.056 ± 0.032	0.927 ± 0.01	** , $p=0.0013$
rApoE4	1.039 ± 0.022	0.953 ± 0.022	* , $p=0.0103$

Table 4.3 Statistical comparison of $[\theta]_{222/208 \text{ nm}}$ following incubation in PB vs H_2O_2

Post-hoc Tukey multiple comparisons analysis of the effect of H_2O_2 on $[\theta]_{222/208 \text{ nm}}$ compared to PB showed particular impact of harsh oxidative conditions on the nature of α -helices in rApoE2. Two-way ANOVA analysis and post-hoc multiple comparisons were conducted using GraphPad Prism.

Two-way repeated measures ANOVA confirmed that H_2O_2 had a significant effect on $[\theta]_{222/208 \text{ nm}}$ ($F(1,6)=131.3$, $p<0.0001$). There was no interaction between treatment and isoforms ($F(2,6)=3.204$, $p=0.1131$), meaning that the effect of H_2O_2 on $[\theta]_{222/208 \text{ nm}}$ was independent of the isoform, and no significant differences between the three rApoE proteins ($F(2,6)=0.8358$, $p=0.4784$). Post-hoc multiple comparison analysis of $[\theta]_{222/208 \text{ nm}}$ in PB vs in H_2O_2 are reported in table 4.3.

To investigate this effect further, changes in $[\theta]_{222/208 \text{ nm}}$ with increasing concentrations of H_2O_2 (from 0 to rApoE: H_2O_2 at 1:3533) were monitored using CD (Fig. 4.7). The main differences between the three isoforms appeared for stronger oxidising conditions (1:2000 and 1:3533). This was substantiated by two-way repeated measures ANOVA: $[\theta]_{222/208 \text{ nm}}$ was significantly altered by H_2O_2 ($F(6,36)=37,13$, $p<0.0001$). Post-hoc Tukey multiple comparison test showed that the effect of H_2O_2 on $[\theta]_{222/208 \text{ nm}}$ began at 1:200 (all isoforms: 0 vs 1:200 onwards, $p<0.0001$). Additional multiple comparison analysis showed that the effect of higher H_2O_2 concentrations was stronger in rApoE2 samples compared to rApoE3 and rApoE4 (Table 4.42).

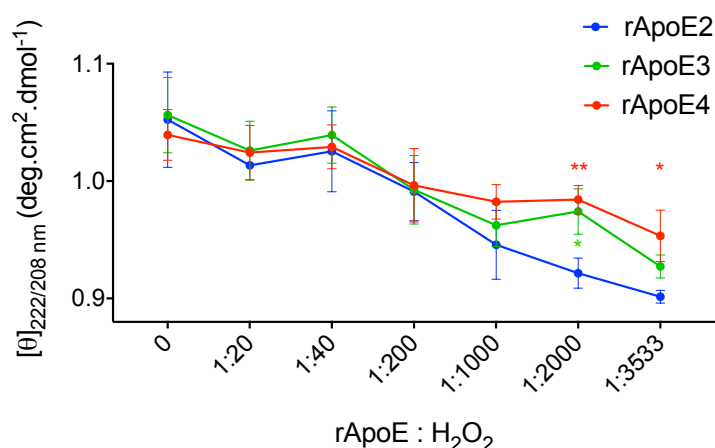


Figure 4.7 Changes in the shape of rApoE α -helices with increasing amounts of H_2O_2

The $[\theta]_{222/208 \text{ nm}}$ ratio characterises the shape of helices. A ratio closer to 1.1 indicates the presence of coiled-coil helices, whereas a ratio closer to 0.9 is indicative of single helices. H_2O_2 significantly altered that ratio (two-way ANOVA: $F(6,36)=37,13$, $p<0.0001$). Its effect on rApoE helices started when used at a concentration 200 times higher than that of rApoE ($p<0.0001$). Differences between the isoforms arose at rApoE: H_2O_2 of 1:2000 and post-hoc multiple comparison analysis was summarised in table 4.2: at 1:2000, rApoE2 vs rApoE3, *, $p=0.0238$ and rApoE2 vs rApoE4, **, $p=0.0060$; at 1:3533, rApoE2 vs rApoE4, *, $p=0.0260$. Final H_2O_2 concentrations: 1:20, 0.5 mM; 1:40, 1 mM; 1:200, 5 mM; 1:1000, 25 mM; 1:2000, 50 mM; 1:3533, 88.3 mM.

Isoform	$[\theta]_{222/208 \text{ nm}}$ at 1:2000	$[\theta]_{222/208 \text{ nm}}$ at 1:3533
rApoE2	1.052 ± 0.041	0.902 ± 0.006
rApoE3	1.056 ± 0.032	0.927 ± 0.01
rApoE4	1.039 ± 0.022	0.953 ± 0.022
Multiple comparison test	$[\theta]_{222/208 \text{ nm}}$ at 1:2000	$[\theta]_{222/208 \text{ nm}}$ at 1:3533
rApoE2 vs rApoE3	*, p=0.0238	n.s., p=0.3764
rApoE2 vs rApoE4	** , p=0.0060	*, p=0.0260
rApoE3 vs rApoE4	n.s., p=0.8584	n.s., p=0.3725

Table 4.4 Statistical comparison of $[\theta]_{222/208 \text{ nm}}$ between isoforms at higher rApoE:H₂O₂

Tukey multiple comparisons analysis following two-way repeated measure ANOVA of the effect of H₂O₂ on $[\theta]_{222/208 \text{ nm}}$ showed differences between the three isoforms when H₂O₂ was used at very high concentrations (1:2000 and 1:3533). The effect was more pronounced in rApoE2.

To sum up, H₂O₂ not only affected the level of secondary structure in rApoE, it also altered the nature of the α -helix. Oxidative conditions seemed to affect rApoE2 in particular.

Tertiary structure of rApoE was marginally altered by oxidative and reducing conditions

Potential alterations in the tertiary structure of rApoE isoforms under redox conditions were investigated by recording their respective intrinsic Trp emission between 320 nm and 460 nm (Fig.4.8A). Maximum fluorescence intensity (Fig. 4.8B) and wavelength of maximum fluorescence (Fig. 4.3C) were plotted for each isoform and in each condition in order to have a better understanding of the effect of oxidative and reducing conditions on the tertiary structure of rApoE. Both factors were determined by peak fitting.

Oxidative and reducing conditions induced a lowering of Trp maximum emission intensity in all three isoforms. In terms of wavelength of maximum fluorescence, a shift towards lower values was induced by H₂O₂ in rApoE2 and rApoE4, but not rApoE3; DTT caused a red shift in rApoE2 only. None of these changes were found to be significant by ordinary one-way ANOVA.

To conclude, both oxidative and reducing conditions resulted in a lowering of Trp maximum emission intensity, although this did not reach significance. Treatments had no significant effect on the wavelength of maximum emission, independent of the rApoE isoforms. Overall, oxidative and reducing conditions had little effect on the tertiary structure of rApoE isoforms.

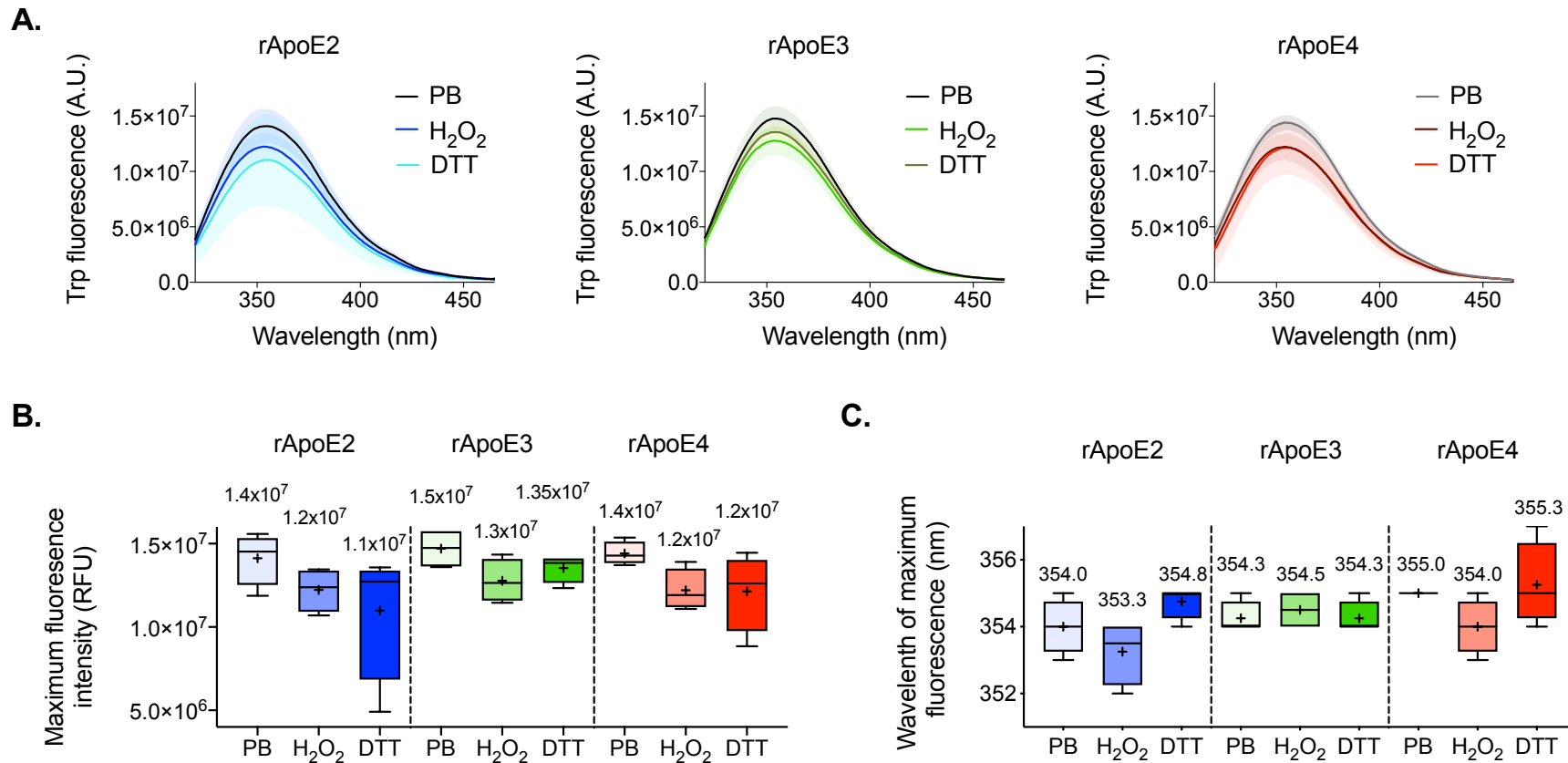


Figure 4.8 Tertiary structure of rApoE isoforms in the presence of H₂O₂ and DTT

A. Intrinsic Trp fluorescence (excitation at 295 nm) showing similar tertiary structure levels of 10 μM rApoE in the presence of H₂O₂ (1:3533 i.e. 35.3 mM H₂O₂) or DTT (1:400 i.e. 4 mM DTT) compared to PB (20 mM PB, pH7.4). n=4 (different protein stocks)

B. Maximum fluorescence intensity and **C.** Wavelength of maximum fluorescence were plotted for each isoform and each condition. Mean values (+) were given above each box.

4.3.4. Both oxidative and reducing conditions affect rApoE self-assembly

ThT fluorescence was used to detect whether H₂O₂ or DTT influenced rApoE fibril formation after incubation at 37°C for 24 h. TEM was used alongside ThT fluorescence spectroscopy to monitor self-assembly.

Strong oxidative and reducing conditions alter rApoE4 self-assembly

Incubation with H₂O₂ resulted in an increase in ThT fluorescence for all three isoforms when compared to non-treated samples. This increase was more pronounced for rApoE3 and rApoE4 compared to rApoE2 (Fig. 4.9). DTT also induced a small increase in ThT fluorescence in rApoE4 only (Fig. 4.9). Taken altogether, these results suggest that both H₂O₂ and DTT affect rApoE4 fibril formation, and that some species that interact with ThT may have formed in rApoE2 and rApoE3 under oxidative conditions. ThT kinetic scans were also acquired (n=1 per isoform) and included in appendix 3.

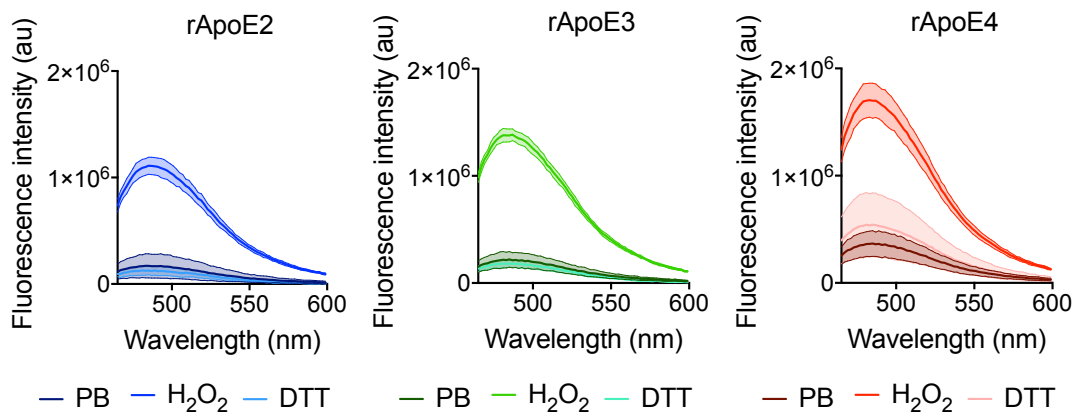


Figure 4.9 Self-assembly of rApoE under harsh oxidative and reducing conditions

Samples for self-assembly assay were prepared at 25 μM in 20 mM PB, pH 7.4, or in the presence of H₂O₂ (88.3 mM) and DTT (10 mM). ThT was added prior to the experiment, at 55 μM. ThT scans were acquired after a 24 h incubation period at 37°C. H₂O₂ induced an increased ThT signal for all three isoforms, whereas DTT marginally increased ThT fluorescence after incubation in rApoE4 only. Data points correspond to the average of 3 different experiments using 3 different protein stocks. The envelopes correspond to the SD.

Since increased in ThT fluorescence does not necessarily mean presence of fibrils, as we saw in chapter 3 since ThT interacts with oligomeric species, this was investigated further using TEM. TEM grids were prepared after 24 h incubation at 37°C under

physiological (left panels), harsh oxidative (middle panels) or harsh reducing (right panels) conditions, and representative micrographs are shown in Fig. 4.10. Fibrils have completely disappeared from rApoE4 samples under harsh reducing conditions (bottom right panel, red), suggesting that the marginally increased ThT signal when rApoE4 was incubated with DTT resulted from agglomerated small species.

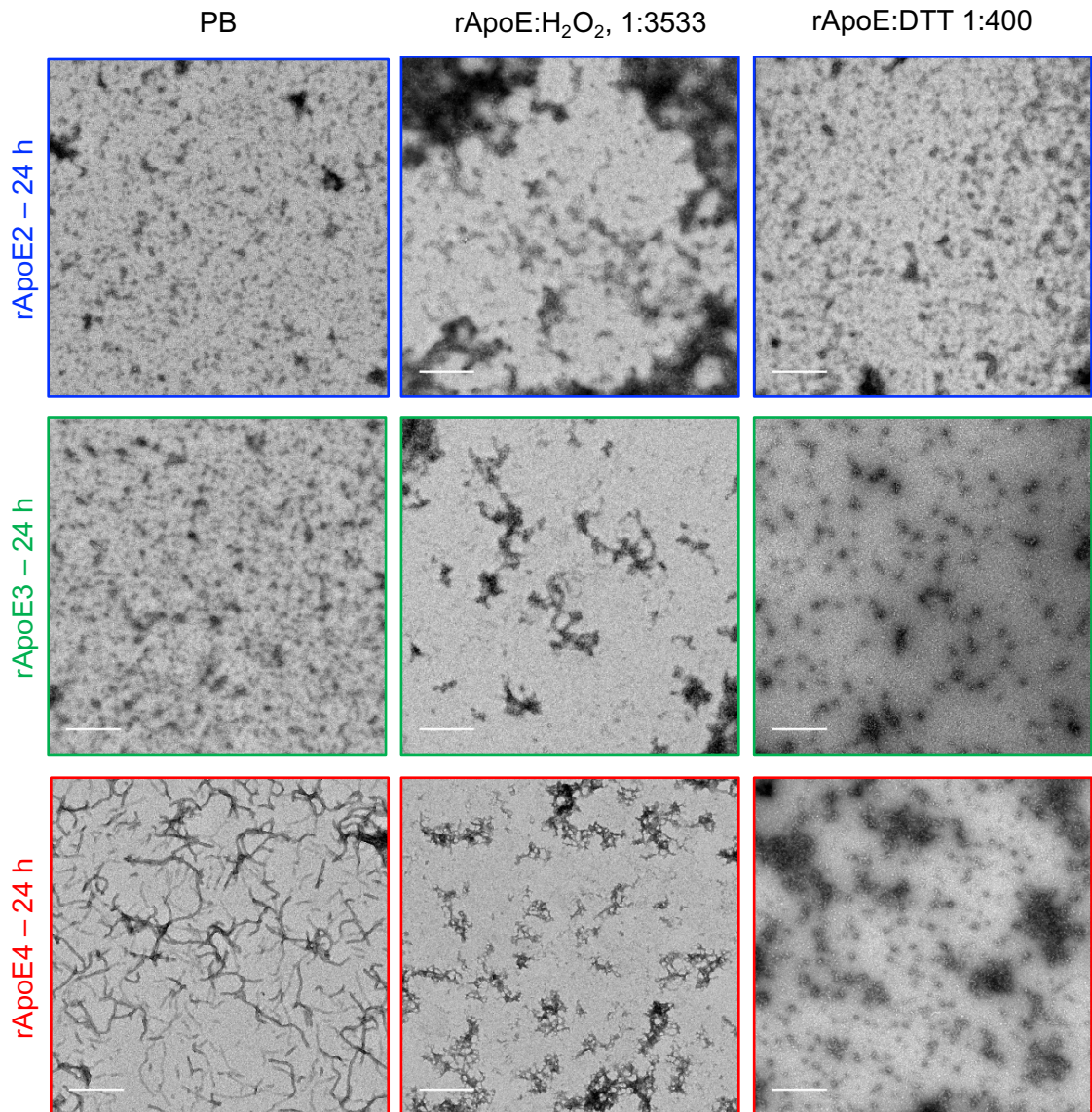


Figure 4.10 Micrographs of rApoE assembled under harsh oxidative and reducing conditions

Representative TEM micrographs of negatively stained rApoE isoforms (25 μ M) after 24 h incubation at 37°C highlighted the absence of mature fibrils in rApoE4 under reducing conditions (10 mM DTT, right panels) compared to assembly in PB (left panel). rApoE2 and rApoE3 did not self-assemble under reducing conditions. Oxidative conditions (88.3 mM H₂O₂) led to the formation of distinct polymers, different from rApoE4 fibrils formed under physiological conditions. See Fig. 4.11 for magnified images. Scale bars, 500 nm.

Fibril formation was also not induced in rApoE2 and rApoE3 under reducing conditions (right panels, blue for rApoE2 and green for rApoE3). However, all three rApoE proteins have mostly polymerized into very thin, long structures when incubated with H₂O₂. Zoomed-in micrographs for each isoform are shown in Fig. 4.11. These fibres were very distinct from rApoE4 fibrils formed under physiological conditions (Fig. 4.10, left panel, red; Fig. 3.9). Boxes were drawn around these new morphologies. Rings, thin and long fibres as well as round species and agglomerates were detected, and representative images can be found in the bottom right panel of Fig. 4.11.

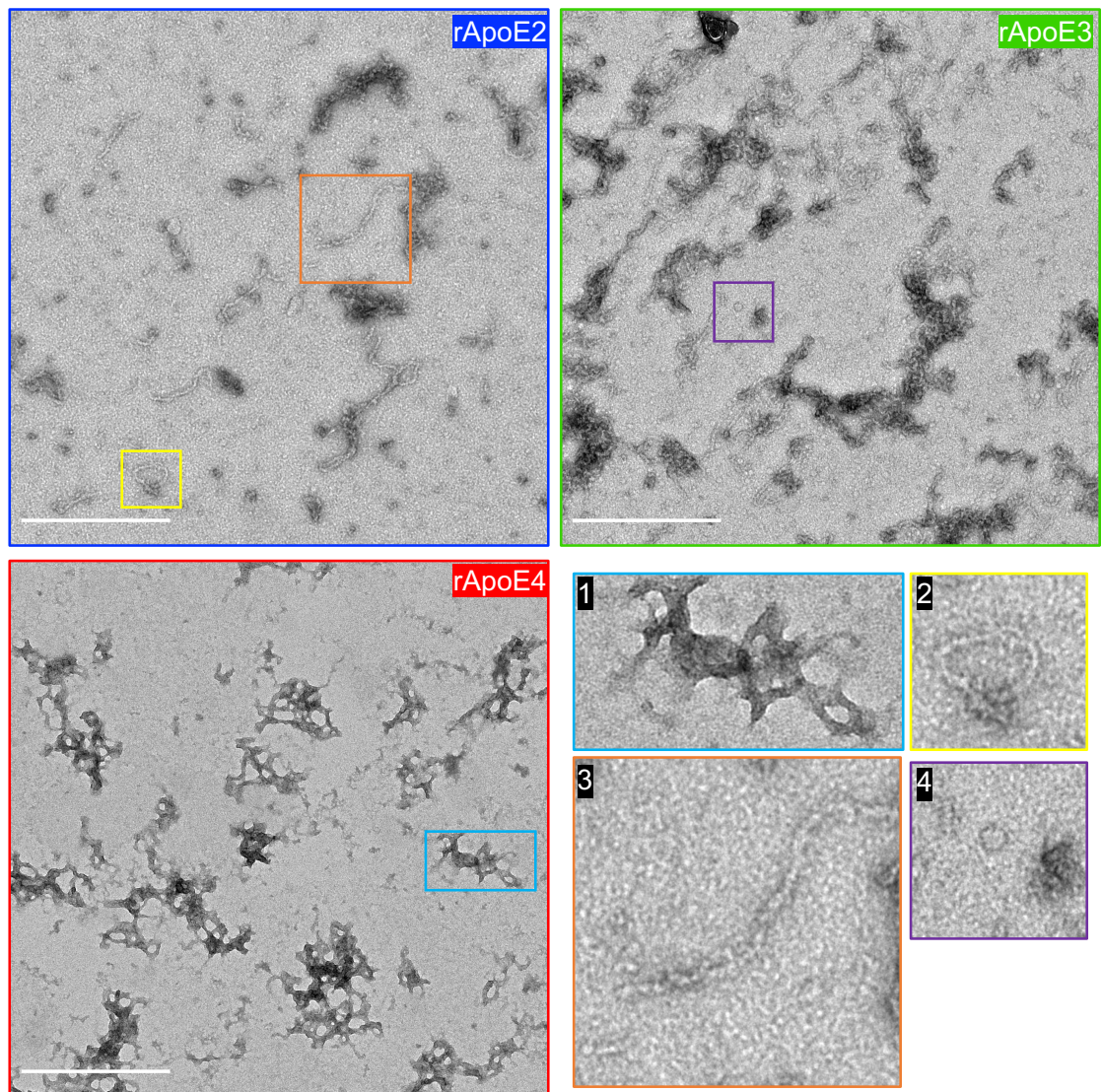


Figure 4.11 Zoomed-in micrographs of rApoE assembled under harsh oxidative conditions

Magnified images of rApoE after 24 h incubation at 37°C under harsh oxidative conditions shows that rApoE proteins have polymerised into distinct species that include agglomerates (1), rings (2), thin and long fibres (3) or round species (4). Scale bars, 500 nm. Images of the different species were magnified by 3.

Investigation of self-assembly in rApoE2 and rApoE3 under oxidative and reducing conditions that permit rApoE4 fibrillisation

Since strong oxidative and reducing environments affected rApoE4 self-assembly, incubation of rApoE4 for 24 h at 37°C in the presence of milder redox concentrations were performed. Fibril formation was assessed by TEM.

As can be seen in Fig. 4.10 and 4.11, high concentrations of H₂O₂ readily impacted rApoE4 self-assembly: under harsh oxidative conditions, rApoE4 formed thin and long polymers that co-agglomerated, and that were morphologically distinct from the fibrils obtained under physiological conditions. Self-assembly of rApoE4 under oxidative conditions was thus assessed using 6 different rApoE: H₂O₂ ratios to explore the effect of H₂O₂ further. Fibrils similar to those obtained in PB were only formed in the presence of the lowest concentration tested, 1:4 (Fig. 4.12A, rApoE: H₂O₂ 1:4, red and magnified micrograph, red box). With increasing concentrations of H₂O₂, rApoE4 fibres decreased in size and small round species started to appear, which suggested that H₂O₂ might be hindering self-assembly (Fig. 4.12A, rApoE: H₂O₂ 1:20 and 1:40). For clarity, a magnification of these round species was added to Fig. 4.12A (yellow box, left). When H₂O₂ was added to rApoE4 prior to assembly induction at a ratio higher than 1:40, thin and long fibres formed, some of them organising in ring-like structures (cyan box). These polymers were morphologically different from fibrils of rApoE4 formed in PB (Fig. 3.9).

Self-assembly of rApoE2 and rApoE3 under oxidative conditions was explored at a rApoE: H₂O₂ ratio of 1:4, corresponding to the maximum concentration of H₂O₂ that can be used without altering rApoE4 fibril formation. TEM micrographs showed that no mature fibrils were formed in rApoE2 and rApoE3 under mild oxidative conditions (Fig. 4.12B), with only small round species having formed (magnified micrographs can also be found on the right of each image).

Assembly was also assessed at end-point by non-reducing denaturing gel electrophoresis. In addition to the monomer band (34 kDa), species migrating to ~75 kDa were formed. This was particularly evident for rApoE3. In rApoE2, higher oligomeric species could also be observed (Fig. 4.12C). 75 kDa corresponds to the MW of a rApoE dimer, most likely formed through disulphide bridge since this species was not formed by rApoE4, which lacks Cys residues. Bands migrating below 25 kDa were indicative of enhanced degradation of rApoE2 and rApoE3 following incubation for 24 h at 37°C under mild oxidative conditions (Fig. 4.12C).

A.

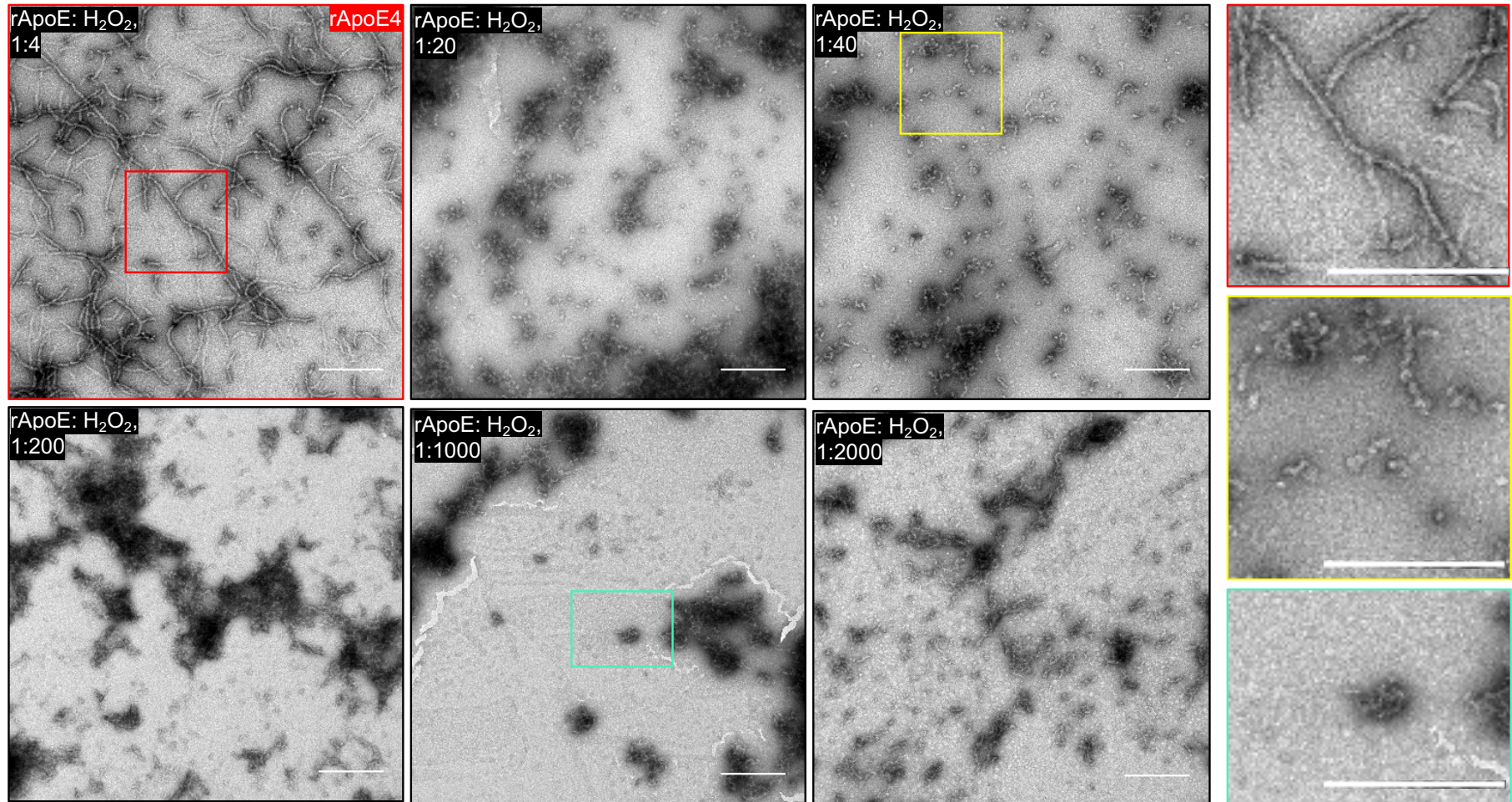


(Figure continued on next page)

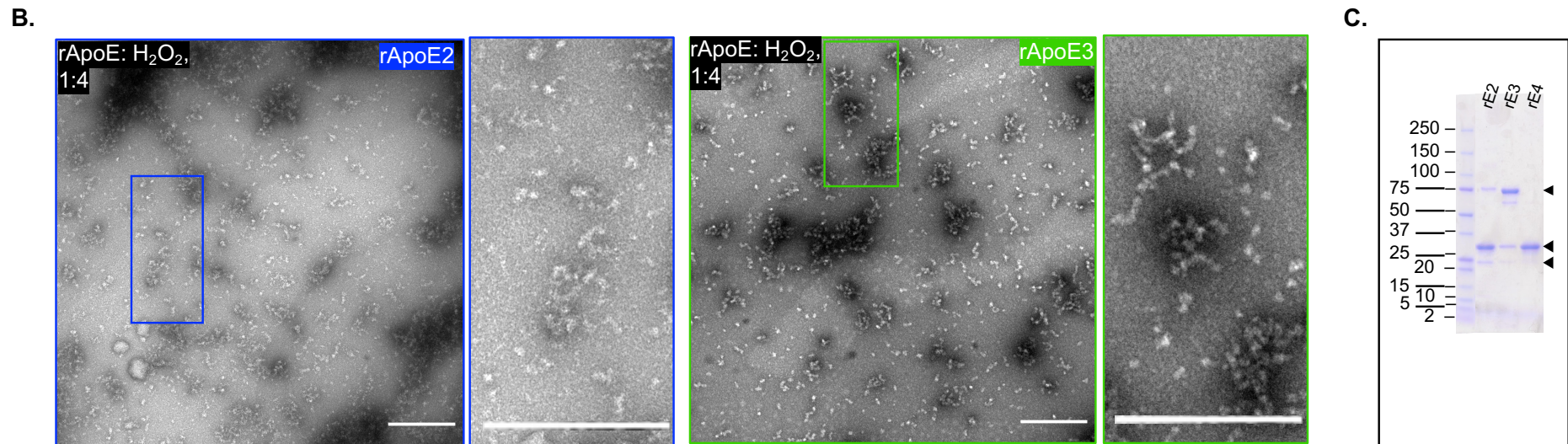


Figure 4.12 Self-assembly of rApoE under milder oxidative conditions

A. rApoE4 at 25 μ M in 20 mM PB, pH 7.4 was incubated for 24 h at 37°C in the presence of different amounts of H₂O₂, indicated in the top corner of each micrograph. Representative TEM micrographs highlighted the absence of mature fibrils in all but rApoE4:H₂O₂ at 1:4 (red box). Fibril formation in a fashion similar to that occurring in PB was hindered with increasing H₂O₂ concentrations. Small round species could still be detected at 1:20 and 1:40, but these disappeared at greater ratios to give way to thin, long polymers that also formed ring-like structures. Corresponding zoomed-in regions were added to the right, showing an example of mature fibril in rApoE4:H₂O₂ (red box), of small round species (yellow box) and of thin, ring-like fibres (cyan box). Scale bars, 500 nm.

B. rApoE2 and rApoE3 did not form mature fibrils in the presence of 1:4 H₂O₂. Instead, small round species and short fibrils could be observed. Magnified images of rApoE2 (blue box) and rApoE3 (green box) were added to the right of each micrograph. Scale bars, 500 nm.

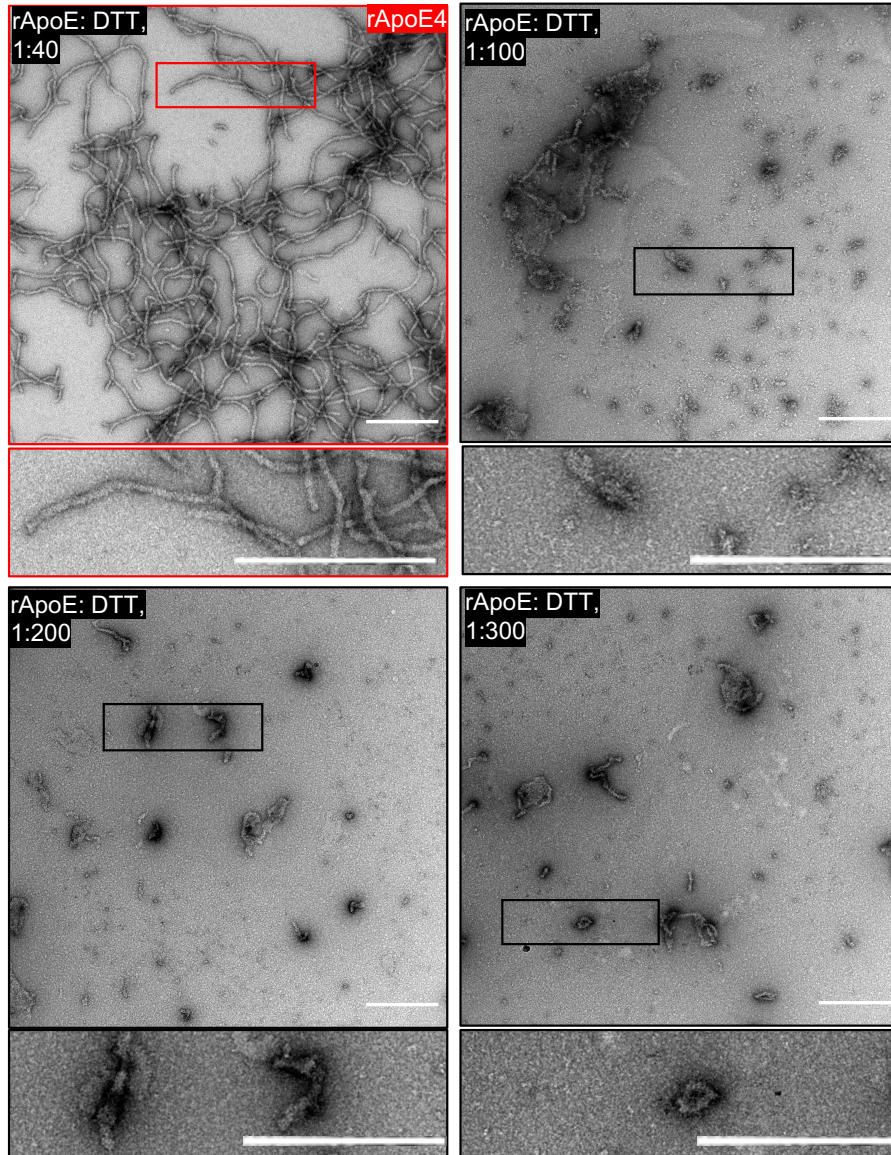
C. Non-reducing denaturing gel electrophoresis of samples after assembly with 1:4 H₂O₂ highlighted the presence of dimers (~ 75 kDa) only in rApoE2 and rApoE3, suggesting disulphide bridge formation. Higher oligomeric species in rApoE2 could also be observed. Bands lower than 25 kDa were indicative of degradation.

A similar experiment was conducted under milder reducing conditions for comparison (Fig. 4.13). rApoE4 was incubated for 24 h at 37°C with 4 different concentrations of DTT ranging from rApoE: DTT at 1:40 to 1:300. rApoE4 did not form its usual long, curvy fibrils (Fig. 3.9) under reducing conditions higher than 1:40 rApoE: DTT (Fig. 4.13A). However, short fibrils persisted up to 1:300 rApoE: DTT. Magnified images were included below each micrograph, showing the presence of short fibrils and ring-like species (Fig. 4.13A).

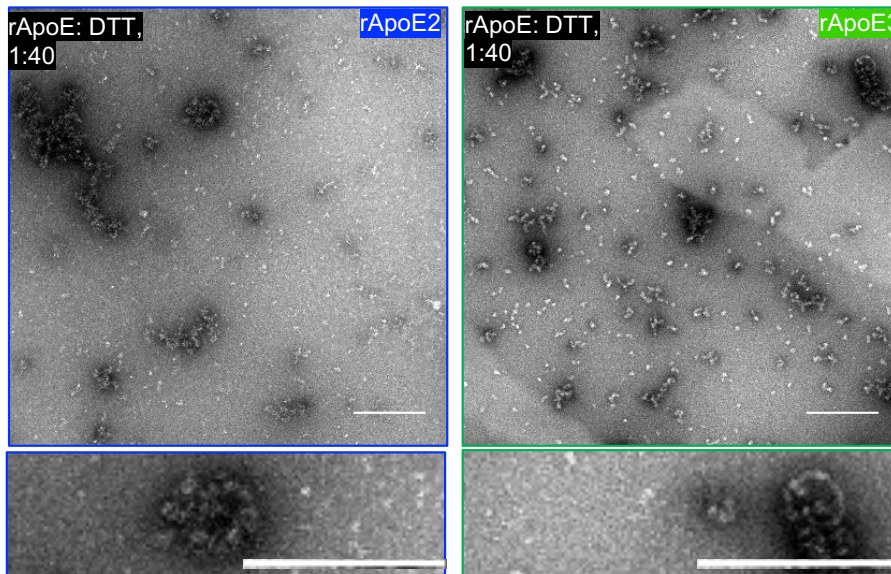
Since assembly at 1:40 DTT was most similar to assembly in PB, rApoE2 and rApoE3 self-assembly was investigated in the presence of 40 times more DTT (Fig. 4.13B). While neither formed long, mature fibrils, small round species could be observed. Magnified images of each micrograph show presence of small round species and ring-like fibres (Fig. 4.13B)

Overall, milder reducing conditions that still enabled rApoE4 self-assembly in a fashion similar to that in PB did not induce self-assembly in rApoE2 and rApoE3. H₂O₂ altered rApoE4 self-assembly for the most part and did not promote formation of fibrils similar to those obtained in PB in rApoE2 and rApoE3. Only higher oligomeric species possibly arising from polymerization through disulphide bridges (as was suggested by gel electrophoresis, Fig. 4.12C) were observed in rApoE2 and rApoE3.

A.



B.



(Legend on next page)

Figure 4.13 Self-assembly of rApoE under milder reducing conditions

A. rApoE4 for self-assembly assay were prepared at 25 μ M in 20 mM PB, pH 7.4, in the presence of different amounts of DTT. Representative TEM of negatively stained rApoE4 isoforms after 24 h incubation at 37°C highlighted the absence of mature fibrils in rApoE4 in all but rApoE:DTT of 1:40 (red box). Scale bars, 500 nm.

B. rApoE2 and rApoE3 did not form mature fibrils in the presence of 1:40 DTT Scale bars, 500 nm.

4.4. Discussion

The first evidence of ApoE having a role in protecting against oxidative stress came from experiments conducted in ApoE-deficient mice. Baseline plasma lipid peroxidation, lipoprotein oxidation status, and their respective susceptibility to oxidation were increased when compared to controls (Hayek et al., 1994). ApoE was then linked to reduction of pathological lesions and oxidative stress when expression was induced in the liver of an atherosclerosis mouse model (Tangirala et al., 2001).

There is also a large body of evidence implicating *APOE* genotype and oxidative stress in AD. Lipid damage was shown to be exacerbated in AD *post-mortem* brain, more significantly so in the temporal lobe, when opposed to age-matched control tissue (Marcus et al., 1998). When the *APOE* genotype was taken into account, it appeared that lipid peroxidation in the cortex and hippocampus of AD patients was more severe in $\epsilon 4$ carriers (Ramassamy et al., 1999; 2000).

Aggravated oxidative damage in AD could in part be due to reduced antioxidant system activity (Ramassamy et al., 1999), which is why research has focused on identifying any alteration in the antioxidant defence, particularly in endogenous antioxidant enzymes while factoring in the *APOE* genotype. Very little is known about whether or not the *APOE* genotype alters enzymatic antioxidant mechanisms in healthy age-matched brains since the availability of $\epsilon 4/\epsilon 4$ elderly brain tissue is scarce. ApoE-TR mice were thus used here as a model for physiological human ApoE to circumvent this limitation.

CAT and SOD activities were evaluated here in hemibrains of adult, middle aged and old ApoE-TR mice and no obvious or significant differences could be detected between the two phenotypes at all the ages investigated. It is necessary to point out that hemibrains were collected at different times, and that as a result of this and the time restraint, enzymatic assays were ran at different times too. Ideally, all samples should be run on the same day to avoid the impact of variables such as temperature changes, or the use of different kits. I believe that some of the variability observed in this series of experiment stems from uncontrollable variations. This observation aside, Huebbe et al similarly reported no significant differences in CAT, SOD, GPx and Trx activities in the brains of 12-week-old adult mice (activities measured in whole brain excluding the cortex and hippocampus) (Huebbe et al., 2007).

Analysis of enzymatic antioxidant activities in human AD brain tissue points to regional variations. For instance, Ramassamy et al reported opposite variations in CAT and GPx

activities in AD vs control, with increased activity in the frontal cortex and decreased activity in the hippocampus (Ramassamy et al., 1999; 2000). This regional variability was not assessed here since this study aimed at trying to identify any overall impact of ApoE4 on the antioxidant system, but regionally focused analyses would be interesting and relevant to understanding the involvement of ApoE4 in AD.

It is important to remember that CAT and SOD only represent an excerpt of the whole antioxidant system, and that data on the activities of other enzymes such as GPx or Trx as well as levels of non-enzymatic antioxidants in ApoE-TR mice are necessary to provide a full picture of the antioxidant status at baseline with the *APOE* genotype as a variable. Moreover, this study focused on overall enzymatic activity without evaluating any changes at the protein level which would also be relevant to assess in future work. For example, Persson et al recently reported reduced Trx protein levels in the hippocampus of ApoE4- compared to ApoE3-TR mice (Persson et al., 2017).

It is quite possible that the absence of differences in CAT and SOD activities between the two phenotypes could also be due to the fact that ApoE-TR mice were not exposed to any added source of oxidative stress. A similar hypothesis was first put forward by Talmud et al: risk for cardiovascular disease in ϵ 4 carriers was shown to be restricted to male smokers (Talmud et al., 2005). Vulnerability to oxidative insults was thus evaluated as a function of *APOE* genotype in primary cell culture established from ApoE-TR mice cortical tissue.

The ApoE-associated response to toxins was first evaluated in a model relevant to humans, the neuroblastoma cell-line SH-SY5Y, to establish all experimental procedures before moving to primary neurons. Cells received treatments with either haloperidol, H₂O₂ or azamethiphos for 24 h prior to RNA and protein extraction.

Haloperidol is a psychotropic drug that up-regulates ApoE at the transcript and at the protein level, notably in SH-SY5Y cells (Vik-Mo et al., 2009). It was used here as a positive control, at double the concentration used in Vik-Mo's study in an attempt to increase ApoE expression (mRNA levels of ApoE did not double as expected when using 25 μ M; data not shown here). 50 μ M haloperidol treatment for 24 h was non-toxic to cells (~98% of cells were viable compared to control), and increased *APOE* gene expression by 1.6-fold compared to control although this increase did not reach significance when statistically analysed by one-way RM ANOVA (see 4.3.2). ApoE at the protein level was also increased following haloperidol treatment.

H₂O₂ and azamethiphos were employed as toxins. H₂O₂ is an oxidizing agent and one of the ways it is produced in the body is as a result superoxide dismutation by SOD. Accumulation of H₂O₂ has been reported following exposure to A β in cells (Behl et al., 1994). Azamethiphos is an organophosphate, and organophosphate exposure could potentially be involved in AD aetiology through disruption of cholinergic function or through elevation of A β levels by increasing APP expression (Sánchez-Santed et al., 2016).

Interestingly, increased *APOE* gene expression did not correlate with cell death. Cell survival was more affected by H₂O₂ exposure than exposure to azamethiphos, but pesticide treatment resulted in 7 times more *APOE* mRNA compared to control whereas H₂O₂ led to a ~2.5-fold increase. Both H₂O₂ and azamethiphos led to marginal increases of ApoE at the protein level, although it is important to remember that the experimental technique used here was not ideal and could not be improved due to time restrictions. A more focused analysis of potential organophosphate targets, like mitochondria, could help understand why azamethiphos leads to such a significant increase in ApoE mRNA levels. In line with these overall results, others have reported increased neuronal *APOE* gene expression and ApoE levels as a consequence of apoptosis. This is particularly relevant to AD since neuronal apoptosis contributes to neurodegeneration (Elliott et al., 2007).

To factor in the *APOE* genotype, primary mouse cultures were prepared from ApoE-TR mouse cortex. Primary neurons at DIV10 were exposed to H₂O₂ and azamethiphos to evaluate the ApoE-associated response in a similar fashion to the experiments conducted in the neuroblastoma cells.

The first objective was to compare how similar the ApoE stress response was in primary E3/E3 neurons (SH-SY5Y are also E3/E3). A direct comparison could not be established since substantially greater concentrations of both toxins were required to induce partial cell death in primary cortical cultures (650 μ M H₂O₂ and 300 μ M azamethiphos in neurons vs 75 μ M and 25 μ M respectively in SH-SY5Y cells). However, E3/E3 neurons responded in a similar way to SH cells in the sense that cell viability did not correlate with *APOE* mRNA, and that *APOE* gene expression was greater following pesticide exposure.

In contrast, treatments had comparatively a reduced impact on cell survival in E4/E4 neurons compared to E3/E3. However, cell survival at baseline was lower in E4/E4 which means that treatments actually resulted in similar levels of cell survival in both phenotypes. Moreover, H₂O₂ treatment resulted in decreased *APOE* transcript levels in

E4/E4 neurons as opposed to a marginal increase in E3/E3 neurons. Additionally, azamethiphos resulted in an 8-fold increase in ApoE mRNA in E4/E4, and only to a doubling in transcript levels in E3/E3 neurons. When looking at baseline *APOE* gene expression, it appears that *APOE* mRNA levels were reduced in E4/E4 compared to E3/E3 neurons. These qPCR experiments were only conducted twice per genotype and more repeats are needed to reach a definitive conclusion.

Azamethiphos seemed to have a greater impact on *APOE* transcript levels in E4/E4 neurons than in E3/E3, compared to their respective baselines. Given that the mRNA levels in E4/E4 were lower at baseline, this response to azamethiphos may underline compensation mechanisms in E4/E4 to respond to injury and should be explored further.

How changes in *APOE* mRNA translate into changes at the protein level remains to be explored, especially because there is evidence that neuronal ApoE4 in particular undergoes cleavage into cytotoxic fragments (Harris *et al.*, 2003; Brecht *et al.*, 2004; reviewed by Mahley and Huang, 2012).

Taken together, the results presented in the first part of this chapter show that differences arise between the two phenotypes especially when a toxic challenge is presented. Further studies conducted *in vivo* would be important to complete the present one.

The second aim addressed in this chapter was the investigation of intrinsic antioxidant properties of ApoE at the protein level. While there is substantial evidence for a role of ApoE as an antioxidant, the exact mechanisms by which it carries through this effect remain unclear.

ApoE may be involved in various protective pathways. The mechanism having received the most attention is the one focusing on ApoE as a metal-binding protein. Metal homeostasis disruption in AD has been thoroughly reported, from variations in metal concentrations in the CNS and in the periphery to enrichment of metals in senile plaques and NFTs (reviewed by Xu, Finkelstein and Adlard, 2014).

Miyata *et al* provided the initial proof of ApoE's metal-binding properties using metal-chelating affinity chromatography. Recombinant ApoE showed strong affinity for copper, and some affinity for iron and zinc. They proposed that metals may be coordinated by the N-terminal four-helix bundle of ApoE as a potential mechanism of action. No difference in metal binding was reported between the three ApoE isoforms (Miyata & Smith, 1996).

Alternatively, or in conjunction with metal sequestration abilities, ApoE could be functioning as a ROS scavenger. For instance, recombinant ApoE is capable of binding HNE, which is a by-product of ROS reacting with fatty acids. Crosslinking of ApoE by HNE differed with the nature of the isoform, with E2 being more vulnerable than E3 and E4 (Pedersen et al., 2000). This was also the case in ApoE purified from plasma, with E3>E4 (Montine, T. J. et al., 1996). These results were complemented by detection of protein-HNE adduct in AD that were correlated with the presence of *APOE* ϵ 4 (Montine, K. S. et al., 1997).

The present study partly focused on investigating the potential of ApoE to capture H₂O₂ using recombinant protein as a model. rApoE isoforms were incubated at 4°C for 24 h with a very high concentration of H₂O₂ (1:3533), which was the ratio of ApoE:H₂O₂ used by Miyata et al when exploring the protective effects of ApoE against H₂O₂ insults in a rat neuronal cell model (Miyata & Smith, 1996). Changes in secondary and tertiary structure were analysed. The first observation was that H₂O₂ induced a significant decrease in α -helical content in rApoE, as shown by DICROWEB analysis (Lobley et al., 2002; Whitmore & Wallace, 2004; 2008). This effect was more pronounced in rApoE2 than rApoE3 and rApoE4 (rApoE2>rApoE3>rApoE4). The loss of α -helix in rApoE isoforms was mirrored by an increase in random coil.

Further analysis of rApoE secondary structure under harsh oxidative conditions revealed an apparent shift in the nature of α -helices present. Information on the nature of helices can be gathered from $[\theta]_{222/208\text{ nm}}$: a ratio close to 1.1 indicates the presence of coiled-coil helices, whereas a ratio close to 0.9 is indicative of single helices being present (Greenfield, N. J. & Hitchcock-Degregori, 1993). H₂O₂ induced a shift from coiled-coil to single helices in all three rApoE, and more significantly in rApoE2, followed by rApoE3 and finally rApoE4. Since H₂O₂ was used at very high concentration, shifts in secondary structure were also investigated in lower rApoE:H₂O₂ ratios. The effect of H₂O₂ started to be significant at 1:200. Isoform-specific differences started to arise at 1:2000, with rApoE2 seeing greater decrease in $[\theta]_{222/208\text{ nm}}$ than rApoE3 and rApoE4.

Harsh redox conditions only marginally affected the tertiary structure of rApoE proteins.

Overall, changes induced by H₂O₂ were greater in rApoE2 than the other two isoforms and resulted in loss of α -helical content with rearrangement of helices. This rearrangement of helices that is more pronounced in rApoE2 could arise from disulphide bridge formation. One could thus suggest that, as with HNE, rApoE2, followed by rApoE3, has a greater capacity in scavenging H₂O₂ resulting in potential detoxification. rApoE2 and rApoE3 could function in a similar fashion to GSH. GSH is an antioxidant

containing a single Cys residue. It neutralises ROS by forming a disulphide (GSSG) (equation 20) (Abedinzadeh et al., 1989).



While there has not been to the best of my knowledge any other studies looking at the specific effect of H_2O_2 on the structure of ApoE, this has been investigated in another class of apolipoprotein, ApoA-I and ApoA-II. Treatment of recombinant ApoA-I and ApoA-II with H_2O_2 , at ~1:4000 for the former and various concentrations of H_2O_2 for the latter, resulted in a decrease in helicity as shown by CD, similar to what was observed here with rApoE. Using HPLC and synthetic peptide analogs of ApoA amphiphatic helix, Anantharamaiah et al were able to identify that changes in ApoA's secondary structure were due to oxidation of Met (Anantharamaiah et al., 1988). ApoA-I and ApoA-II have 3 and 1 Met respectively; ApoE has 7 Met residues. Loss of secondary structure in rApoE could thus be a consequence of Met oxidation. Met residues have been documented to act as endogenous antioxidants in proteins (Levine et al., 1996), which could in part explain why all three ApoE isoforms act as an antioxidant.

Despite lacking Cys residues, ApoE4 is also an antioxidant and can get oxidised through its Met residues. Jolivalt et al showed that recombinant ApoE4 was more susceptible than ApoE2 and ApoE3 to Met oxidation by the MPO/ H_2O_2 oxidizing system, resulting in monomeric bands with increased apparent molecular weight by denaturing gel electrophoresis. Greater Met oxidation was correlated to greater increase in the apparent molecular weight band of the monomer ($\Delta kDa = 2.2$ for ApoE4, 2.0 for ApoE3 and 0.8 for ApoE2) (Jolivalt et al., 2000). Although they did not discuss it, it is clear from their gel electrophoresis that most recombinant ApoE2 and ApoE3 had formed disulphide bridges, which could account for lower Met oxidation of the monomer band.

Increased apparent molecular weight of the monomer was also observed in this study, with a potential increase in the apparent molecular weight of dimeric species in rApoE2 as well (Fig. 4.14) and encourages the examination of rApoE's structure under milder oxidative conditions.

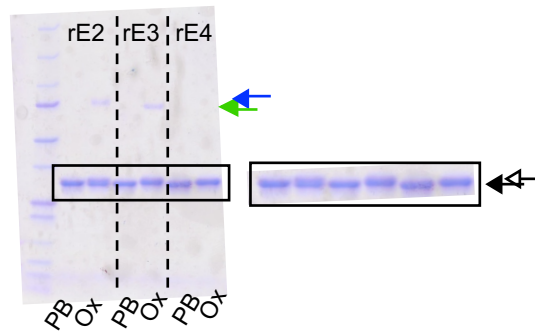


Figure 4.14 Non-reducing gel electrophoresis of rApoE before and after harsh oxidation

rApoE proteins were incubated for 24 h, at 4°C in PB or with H₂O₂ at a 1:3533 ratio. Samples were ran on a non-reducing gel electrophoresis, highlighting a slight increase in the apparent molecular weight of the monomer band (34 kDa) (black arrow to white arrow). It seems that there was also a shift in the dimer size (~ 70 kDa) between dimers in rApoE2 and rApoE3 (green arrow for rApoE3 and blue arrow for rApoE2).

What distinguishes ApoE2 and ApoE3 from ApoE4 is the presence of Cys residues, which can also get oxidized, and could be a precedent for the differential capacity for rApoE to interact with H₂O₂. Cys residues are known to form disulphide bridges under oxidative conditions. However, it is important to take into account that very high concentrations of H₂O₂ were used in this study and that it is very likely that Cys oxidation resulted in the formation of sulfonic acid. Quick analysis by gel electrophoresis suggested that most rApoE2 and rApoE3 did not undergo disulphide bridge formation (Fig. 4.14), most likely due to Cys being transformed to sulfonic acid, although this warrants a more comprehensive analysis. Investigation of the effect of H₂O₂ at lower ratio would thus be the next necessary step to complete this study, especially because disulphide bridges also function as redox switches and could account for ApoE2 and ApoE3 being more antioxidant than ApoE4. Alternatively, or in conjunction, as alluded to earlier, ApoE2 and ApoE3 could also neutralise ROS in a similar fashion to GSH (equation 21); and since ApoE2 has two Cys residues, it would be more potent at scavenging ROS and thus more protective. This correlates with the experiments performed by Miyata & Smith, where recombinant ApoE2 was more protective against Aβ which, as pointed earlier, results in accumulation of H₂O₂ accumulation in cells (Miyata & Smith, 1996; Behl et al., 1994).



Given the strong evidence of oxidative damage in AD, it was relevant to investigate whether oxidative conditions would make ApoE2 and ApoE3 behave more like ApoE4. Cys oxidation could either stabilise or destabilise ApoE2 and ApoE3. Moreover, oxidized rApoE could behave differently to non-oxidised rApoE. Since the only difference that we could observe in our *in vitro* system between the three isoforms was that only rApoE4 was able to self-assemble into fibrils, fibril formation under oxidative condition were investigated here. Experiments were conducted in parallel under reducing conditions to ensure that differential self-assembly properties were not due to disulphide bridge formation.

Since reducing conditions were also used, the secondary and tertiary structure of rApoE in the presence of DTT was characterised, and it appeared that this particular reducing agent had no significant impact on rApoE's structure.

Both strong oxidative (1:3533 rApoE:H₂O₂) and strong reducing (1:400 rApoE:DTT) conditions affected rApoE4 self-assembly. While none of the isoforms assembled under harsh reducing conditions, strong oxidative environment induced formation of long, thin polymers in all three isoforms. Self-assembly was then investigated under conditions that permitted fibrillation of rApoE4 in a fashion similar to that in PB (Fig. 3.9). Neither rApoE2 nor rApoE3 formed mature fibrils under both permissive oxidative and reducing conditions. This study was only conducted over the course of 24 h and the small species that could be observed could have potentially led to fibril formation over an extended period of time.

4.5. Conclusion

When taken together, these results attest to the complex, multifunctional role of ApoE.

The first part presented evidence of increased vulnerability carried by the E4/E4 phenotype, supported by lower viability at baseline and differential *APOE* transcription levels. The second part focused on intrinsic differential structural alterations upon exposure to oxidative agents. ApoE may thus exert its antioxidant properties through either or both detoxification mechanisms, whereby ApoE2 and ApoE3 outperform ApoE4 as ROS scavenger, and repair mechanisms, with up-regulation of *APOE* expression following injury.

These two mechanisms could potentially be tied together by linking structure to function: disulphide bridge formation was shown to participate in intracellular signalling cascades, so ApoE2 and ApoE3, but not ApoE4, could thus potentially act as a ROS sensor in addition to a detoxification agent, and participate in intracellular signalling cascade promoting cell survival.

Chapter 5 - Apolipoprotein E and ageing

5.1. Introduction

Background

The identification of *APOE*- ϵ 4 as a risk factor for AD prompted the investigation into how ApoE fits with the disease pathophysiology. Several studies have reported genotype-specific effects of ApoE on many aspects of AD, such as clearance of A β peptides, synaptic plasticity or neuronal regeneration with ApoE2 and ApoE3 outperforming ApoE4 (Rebeck et al., 1993; Koch et al., 2017; Boyles et al., 1989) As pointed by Beffert et al, many of these studies did not consider possible differences in ApoE expression, which could account for the reported disparity between the isoforms (Beffert et al., 1999). ApoE brain levels were thus investigated alongside researching its function in AD, with mixed conclusions.

Bertrand et al demonstrated significantly lower levels of soluble ApoE in the hippocampus and the cortex of AD patients when compared to non-matched controls (Bertrand et al., 1995). This was substantiated by Beffert et al in a much larger study (Beffert et al., 1999) and by Pirttilä et al, who reported lowered soluble ApoE protein levels in the frontal and temporal cortex of AD subjects when compared to age-matched control (Pirttilä et al., 1996). However, others have recorded higher ApoE protein levels in AD than in age-matched control brain tissue (Aizawa et al., 1997). Discrepancies were also reported in CSF and plasma ApoE protein amounts, with some finding no difference (Martínez-Morillo et al., 2014) and others showing increased amounts of ApoE (Aizawa et al., 1997) in AD subjects compared to control. Studies focusing on *APOE* mRNA levels also varied, with some reporting increased *APOE* mRNA levels in AD hippocampus and cortex compared to control (Diedrich et al., 1991; Yamada et al., 1995) and others communicating no changes between the two groups (Xu, P.-T. et al., 1999).

When taking the *APOE* genotype into account, results were also controversial. Pirttilä et al found no correlation between ApoE levels in the frontal and temporal cortex and the respective ApoE phenotype (Pirttilä et al., 1996), whereas Bertrand et al showed an association between presence of the ϵ 4 allele and reduced ApoE levels in the hippocampus (Bertrand et al., 1995). Beffert et al came to a similar conclusion, reporting an ϵ 4-dependent reduction of ApoE expression in AD frontal cortex and hippocampus (Beffert et al., 1999).

The absence of a clear consensus could potentially have arisen from regional variability and from differences in disease stage (Glöckner et al., 2002).

Comparison of ApoE expression in non-demented, age-matched human brain tissue of different genotypes seems to be lacking in the current literature, possibly because control elderly $\epsilon 4/\epsilon 4$ subjects are harder to come across. Although statistical analyses were not reported, results published by Beffert et al suggested lower ApoE protein levels in the hippocampus and frontal cortex of $\epsilon 3/\epsilon 4$ controls than in $\epsilon 3/\epsilon 3$ controls (Beffert et al., 1999). Similarly, Sullivan et al reported a trend difference in ApoE amounts in the brain between $\epsilon 4$ -carriers and non-carriers, with the $\epsilon 4$ -carriers having lowered ApoE protein levels (Sullivan et al., 2011). Along these lines, Martínez-Morillo and colleagues reported decreased ApoE levels in plasma in $\epsilon 4$ carriers, but not in CSF where there was no difference with non- $\epsilon 4$ carriers (Martínez-Morillo et al., 2014).

ApoE-TR mice express human ApoE under the control of the mouse *APOE* promoter, providing a physiologically relevant model to study the role of ApoE (see 1.7.2). ApoE protein levels were found to be lower in the hippocampus and cortex of ApoE4-TR mice compared to ApoE2-TR and ApoE3-TR at 20 weeks, as demonstrated using an ApoE immunoassay and western blotting (Riddell et al., 2008). This was supported by Sullivan et al, whom reported the same observation in 3-4 months mice. They also reported significantly decreased levels of ApoE in ApoE4- compared to ApoE2- and ApoE3-TR mice in both plasma and CSF (Sullivan et al., 2011).

Examination of ApoE levels at later time points in ApoE-TR mice are lacking.

Studies have pointed to differences in age of AD onset in susceptible individuals, with $\epsilon 4$ carriers developing AD at a younger age compared to $\epsilon 2$ and $\epsilon 3$ carriers (Meyer, 1998). Age is the greatest risk factor for sporadic AD, and there is evidence for an association between the $\epsilon 4$ allele of *APOE* and normal ageing itself. For instance, the presence of ApoE4 resulted in suppression of the expression of Sirtuin1, a protein linked to normal aging, in neural cells, ApoE4-TR mice and AD brain tissue as reviewed by Theendakara et al (Theendakara et al., 2018). Localisation of ApoE to the nucleus has been reported in transfected cell models, such as CHO cells (Kim, W. S. et al., 2008) or murine microglial (BV2) cells (Love et al., 2017). More specifically, Love et al reported the presence of an ApoE4 fragment in the nucleus of BV2 cells (Love et al., 2017). Nuclear localisation of ApoE is consistent with genotype-dependent direct and indirect transcriptional roles of ApoE that have been reported (Theendakara et al., 2018).

Localisation of ApoE in the nucleus in ApoE-TR mice has not been reported yet to the best of my knowledge.

Ageing is a process tightly linked to oxidative stress, and oxidation-induced formation of carbonyls is used to evaluate levels of protein damage (Stadtman, 1988). Oxidised proteins were shown to have significantly accumulated in the frontal and occipital lobes of aged controls (~70 years-old on average) compared to young controls (~39 years-old) by quantifying the levels of protein carbonyl content (Smith, C. D. et al., 1991). Comparison of AD brain tissue with age-matched controls showed elevated protein carbonyl content in AD (Smith, C. D. et al., 1991), but the *APOE* genotype, for which association to AD was yet to be demonstrated, was not factored in. Links between protein carbonyl content and *APOE* genotype were later demonstrated in vascular smooth muscle cells from human brain, whereby $\epsilon 4$ homozygotes displayed increased protein carbonyl accumulation compared to $\epsilon 3/\epsilon 4$ and $\epsilon 3/\epsilon 3$ tissue (Mazur-Kolecka et al., 2002).

Loss of α -tubulin is another marker of natural ageing, markedly so in later decades of life. Substantial decrease in tubulin protein levels at later ages are consistent with reduced brain thickness in ageing (Labisso, Raulin *et al.*, 2018). Decreased α -tubulin levels have also been reported in AD (Zhang et al., 2015). Ties to *APOE* genotype have not been established to date.

Rationale

Very few studies have focused on the examination of ApoE protein levels in control subjects. If we posit that the *APOE* genotype has an influence on AD onset and its age of onset, then it would be of great interest to evaluate variations of ApoE protein levels in control samples across lifespan, taking into account their respective ApoE phenotype. This would provide an initial assessment of interaction between age and genotype with ApoE protein levels. To this end, protein levels of ApoE were examined in human ApoE-TR mice at different age points, from 3 to 24 months, in a small pilot study.

The interaction between ApoE phenotype and ageing was further explored by assessing whether there was any difference in markers of ageing at the same age points between the two phenotypes. Protein carbonyl content, α -tubulin levels and whether or not ApoE could be found in the nucleus were investigated in both ApoE3- and ApoE4-TR mice (also referred to as E3/E3 and E4/E4 mice).

5.2. Summary of methods

The connection between ApoE phenotype and ageing was investigated both by looking at changes in ApoE protein levels with age and by evaluating differences in markers of ageing using ApoE-TR mice as a model.

Whole brain tissue was collected from ApoE3- and ApoE4-TR mice at 3, 6, 12, 18 and 24 months, achieving a minimum of three individual samples per age group (Appendix 1). In addition to looking at each time point individually, results from the extracts were also grouped by age category for analytical purposes: “adult” (3 and 6 m), “middle age” (12 m) and “old” (12 and 24 m), in agreement with the Jackson Laboratory age report (Flurkey et al., 2007). Resulting n numbers per age category are also given in Appendix 1.

RIPA-extraction yielding what is termed here “whole protein extract” as well as protein fractionation producing cytosolic and nuclear fractions were performed simultaneously, each on a hemisphere of the same brain tissue.

Protein levels of ApoE detected using WB were semi-quantified by densitometry. Band intensities in each sample were determined using ImageJ and normalised to the band intensity of a reference protein (GAPDH for whole extracts). Protein levels of α -tubulin were quantified in cytosolic fractions of “old” ApoE3-and ApoE4-mice from WB and normalised to GAPDH expression.

Protein carbonyl content was determined using a commercially available colorimetric kit (see 2.1.7) based on the generation of DNP adducts that can be detected at 375 nm following treatment with DNPH. Qualitative examination of carbonyl content was also performed using a commercial WB kit based on immunodetection of DNP residues following reaction of carbonyls with DNPH (oxyblot) (see 2.1.7).

5.3. Results

5.3.1. ApoE phenotype-dependent changes in ApoE protein levels across lifespan

Changes in ApoE protein levels across lifespan were mapped in E3/E3 and E4/E4 mice by WB using two different antibodies, a polyclonal one and a monoclonal targeting the C-terminal domain of ApoE. Whole protein extracts (lysis with RIPA buffer, see 2.4) were prepared from brain tissue collected from animals at 3 m, 6 m, 12 m, 18 m and 24 m of age. A summary table of the samples used with their respective age group and genotype can be found in appendix 1.

Detection of ApoE levels using a monoclonal and a polyclonal antibody

Fig. 5.1A shows an example of band profile in whole protein extracts for both antibodies run alongside rApoE3. The band corresponding to monomeric ApoE was the one quantified in both cases (Fig. 5.1A, red box). Example profiles for samples at each time point can be found in Fig. 5.1 corresponding to immunodetection with the monoclonal (Fig. 5.1B) and the polyclonal antibody (Fig. 5.1C). In addition to the band at ~34 kDa, an additional band at ~36 kDa was detected by the monoclonal antibody, corresponding to an isoform of ApoE according to the manufacturer (Invitrogen, #701241). This band was not quantified here (Fig. 5.1B).

Densitometry data was normalised at two different levels. First, in order to bypass any variation due to protein loading and protein transfer, ApoE band intensity was normalised to that of a protein of reference, GAPDH. Second, all samples could not be analysed on a same blot since there were 35 separate samples, so one of the samples was run in all the blots and its ApoE/GAPDH ratio was used as normaliser and attributed the arbitrary value of 1 (sample 653, see appendix 1). Normalised ApoE/GAPDH ratio were summarised in Fig. 5.1D. One can observe at first glance that profiles of ApoE levels differed with the antibody used for detection. However, both methods of detection showed common features. For instance, ApoE levels in E4/E4 mice seemed lower than in E3/E3 mice overall. Additionally, ApoE levels at 18 m and 24 m were higher than in younger age groups in E3/E3 mice; but they were unchanged with age in E4/E4 in the monoclonal antibody profile, or slightly increased at 24 m in the polyclonal antibody profile.

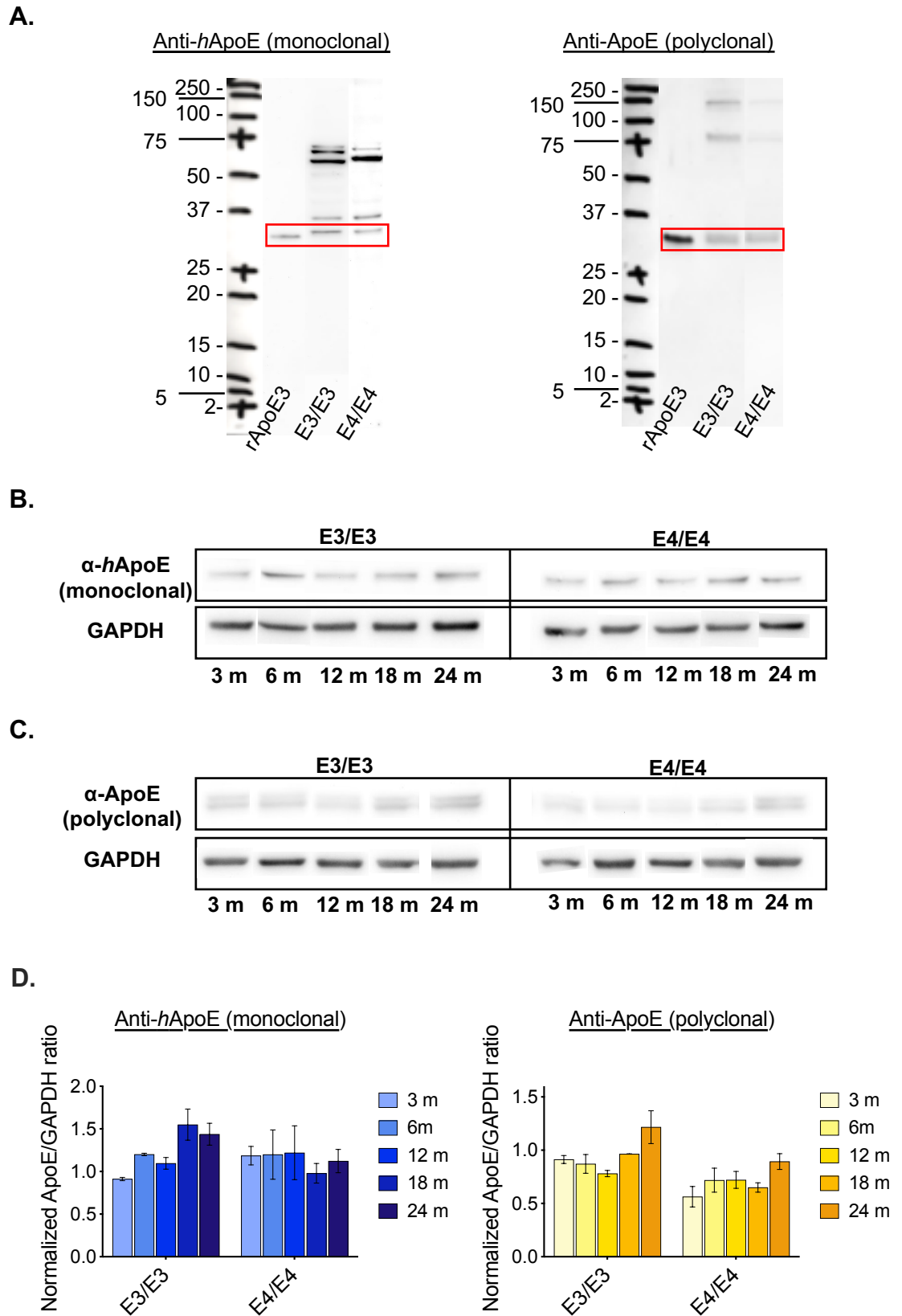


Figure 5.1 Detection of changes in ApoE levels across lifespan by WB

A. WB profiles of antibody binding for both monoclonal (left) and polyclonal (right) antibodies. (Lane 1: Ladder; 2: rApoE3; 3: E3/E3; 4: E4/E4). (legend continued below)

The monomeric band (~34 kDa; red box) was identified thanks to binding to rApoE3 and chosen to be quantified.

B. Changes of ApoE across lifespan detected using a monoclonal α -ApoE antibody (top). Left: example of E3/E3 mouse brain tissue; right: example of ApoE4-TR mouse brain tissue, extracted at 1: 3 m, 2: 6 m, 3: 12 m, 4: 18 m, 5: 24 m. ApoE levels were normalised to GAPDH (bottom).

C. Changes of ApoE across lifespan detected using a polyclonal α -ApoE antibody (top). Left: example of E3/E3 mouse brain tissue; right: example of ApoE4-TR mouse brain tissue, extracted at: 1: 3 m, 2: 6 m, 3: 12 m, 4: 18 m, 5: 24 m. ApoE levels were normalised to GAPDH (bottom).

D. Normalised ApoE/GAPDH ratio with ApoE detected using a monoclonal (left) and polyclonal (right) ApoE antibody at 3 m, 6 m, 12 m, 18 m and 24 m.

Semi-quantification of ApoE levels in ApoE3- and ApoE4-TR mice

Samples were then grouped into age categories in order to perform a statistical analysis of changes in ApoE protein levels across lifespan (Appendix 1 for n numbers) (Fig. 5.2A).

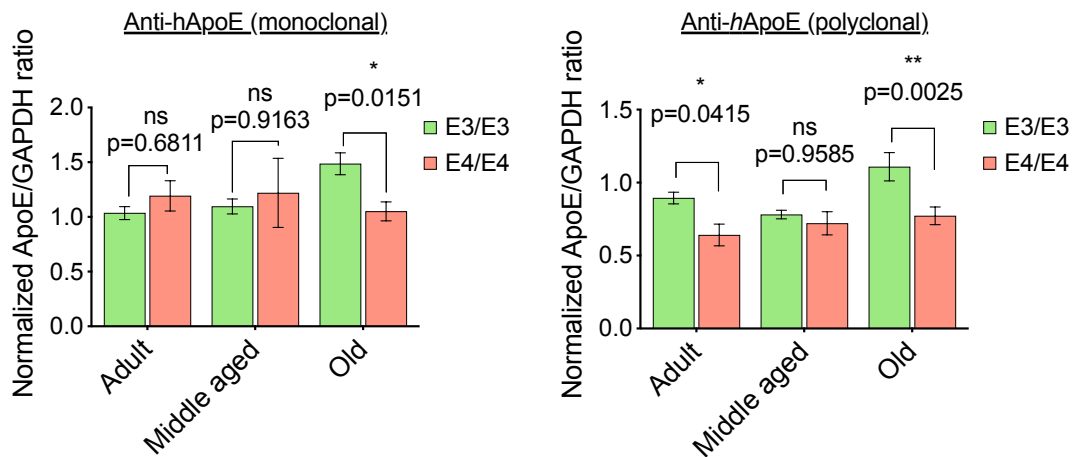
The most compelling difference was detected in old mice, with ApoE levels being 50% greater in E3/E3 than in E4/E4 (two-way ANOVA post-hoc Sidak's test - monoclonal: *, $p=0.0151$; polyclonal: **, $p=0.0025$). There was no difference in ApoE protein levels between E3/E3 and E4/E4 middle age mice.

Differences were less clear cut in the adult category since protein levels of ApoE were significantly lower in E4/E4 than in E3/E3 adult mice when detecting with the polyclonal antibody (two-way ANOVA post-hoc Sidak's test: *, $p=0.0415$), but not with the monoclonal.

ApoE levels detected by the monoclonal antibody seemed to have different trajectories with age, with ApoE levels being increased in E3/E3, but not in E4/E4, across lifespan. Ordinary two-way ANOVA analysis attested to a significant interaction between age and phenotype for ApoE levels detected by the monoclonal antibody ($F(2,29)=4.680$; $p=0.0173$). There was no obvious interaction between age and phenotype on ApoE protein levels when detected using the polyclonal antibody. However, combined ApoE levels significantly increased with age ($F(2, 29)=4.476$; $p=0.0202$).

Overall ApoE levels were also compared between phenotypes by combining all the age categories (Fig. 5.2B). ApoE content was lower in E4/E4 mice. This difference was more pronounced (0.25 times lower) and reached significance when levels were detected using the polyclonal antibody as shown by Kolmogorov-Smirnov test (**, $p=0.0038$), but not when using the monoclonal antibody (~10% lower; unpaired t-test, $p=0.3752$).

A.



B.

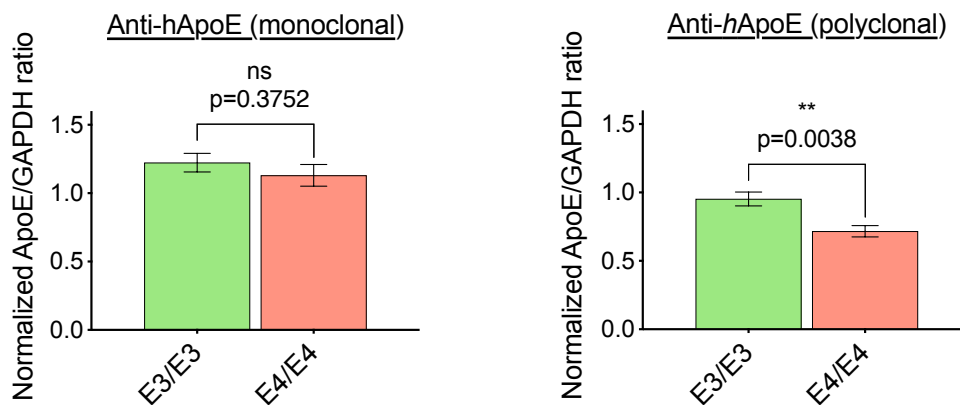


Figure 5.2 Comparison of ApoE levels in ApoE3-TR and ApoE4-TR mice

A. Levels of ApoE were compared between E3/E3 and E4/E4 mice grouped into three different categories: adult (3 m and 6 m), middle aged (12 m) and old (18 m and 24 m). ApoE levels in E4/E4 were significantly lower than in E3/E3 at old age, and this was detected using both antibodies; two-way ANOVA post-hoc Sidak's test: left, monoclonal, *, $p=0.01251$; right, polyclonal, *, $p=0.0025$. Left, monoclonal antibody, two-way ANOVA showed no significance influence of age ($F(2, 29)=1.129$; $p=0.3373$) and phenotype ($F(1,29)=0.2668$; $p=0.6094$) on ApoE levels. However, there was an interaction between age and phenotype, with increased ApoE levels in E3/E3 but not in E4/E4 across lifespan ($F(2,29)=4.680$; $p=0.0173$); right, polyclonal antibody, Age x Phenotype by two-way ANOVA was not significant ($F(2, 29)=1.476$; $p=0.2453$). However both age and phenotype had an effect of ApoE levels ($F(2,29)=4.476$; $p=0.0202$ and $F(1, 29)=12.00$; $p=0.0017$). Differences were also recorded in the adult category - post-hoc Sidak's test: *, $p=0.0415$.

B. ApoE4-TR mice had lower overall ApoE levels than ApoE3-TR mice. This difference only reached significance when using the polyclonal antibody (Kolmogorov-Smirnov test, **, $p=0.0038$).

5.3.2. Nuclear localisation of ApoE

The presence of ApoE in the nucleus in E3/E3 and E4/E4 mice was investigated here. Brain tissue collected at 3 m and 24 m was used to investigate whether ApoE could be found in the nucleus at different ages. ApoE levels were detected using a polyclonal anti-ApoE antibody. An antibody targeted to a covalent modification of histone 3 (H3K9Me3) was used as a nucleus specific marker (specific to heterochromatin). An example profile can be found in Fig. 5.3A.

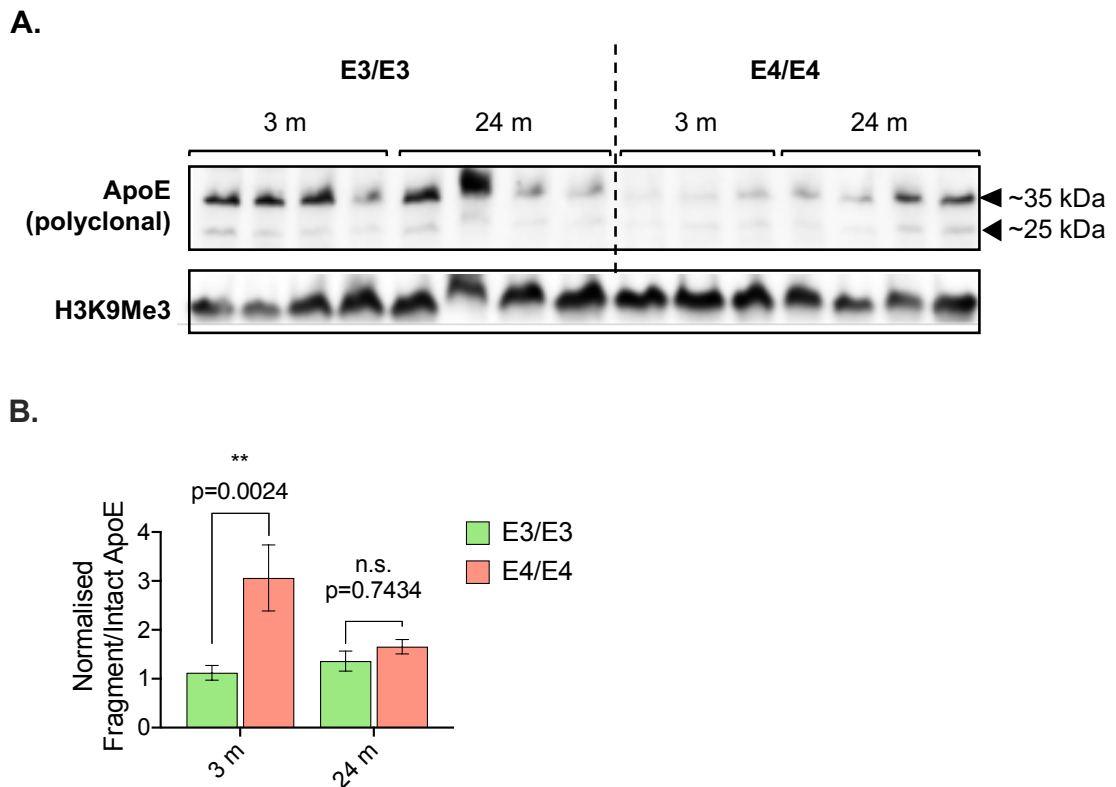


Figure 5.3 ApoE in the nucleus

A. Bands migrating to ~35 kDa and ~25 kDa were detected using a polyclonal α -ApoE antibody (top) at 3 m and 24 m. H3K9Me3 (bottom) served as a nuclear reference.

B. The relative levels of ApoE-25 to intact ApoE were significantly greater in ApoE4-TR mice at 3 m. Two-way ANOVA: effect of age x phenotype ($F(1,11) = 7.298$; $p=0.0206$) and effect of phenotype ($F(1,11)=13.43$; $p=0.0037$) were significant. Overall Fragment/Intact ApoE ratio was not significantly affected by age ($F(1,11)= 3.664$; $p=0.0820$). p values derived from post-hoc Sidak multiple comparison test: at 3 m, **, $p=0.0024$; at 24 m, n.s., $p=0.7434$. $n(E3/E3, 3 m)= 4$, $n(E3/E3, 24 m)=4$; $n(E4/E4, 3 m)= 3$, $n(E4/E4, 24 m)= 4$.

Semi-quantification of ApoE levels in the nucleus could not be performed here since the only antibody against a nuclear protein that I had at my disposal was the one against

H3K9Me3, and H3K9Me3 levels have been reported to vary with age (Maleszewska et al., 2016). Nevertheless, an interesting finding came from looking at the immunoblot in Fig. 5.3A: in addition to the band migrating at 35 kDa as I have seen previously (5.3.1), there was an additional band migrating at ~25 kDa (ApoE-25). The ratio of fragmented ApoE to intact protein was calculated here, and normalised values are reported in Fig. 5.3B (fragment/intact ApoE in sample 654 was used as a normaliser between blots; appendix 1). Immunoblot showed significantly more fragmented ApoE relative to intact ApoE in the nuclear fractions from E4/E4 than in E3/E3 at 3 m (three times as much). Levels of ApoE-25 relative to intact ApoE was similar between the two phenotypes at 24 m. Two-way ANOVA showed an overall effect of phenotype in the nucleus ($F(1, 11) = 13.43$; $p=0.0037$), and an interaction between age and phenotype ($F(1, 11) = 7.298$; $p=0.0206$). Post-hoc Sidak multiple comparison test showed a significant difference at 3 m ($p=0.00204$).

5.3.3. Levels of age markers in E3/E3 and E4/E4 mice are phenotype-dependent

Earlier age of AD onset in $\epsilon 4$ carriers prompted the question of whether the presence of ApoE4 was associated with increased markers of ageing compared to age-matched $\epsilon 3$ carriers. To answer it, protein carbonyl content and α -tubulin levels were quantified in E3/E3 and E4/E4 mice of old age (18 m and 24 m).

Protein carbonyl content in old ApoE-TR mice

Protein carbonyl content in ApoE-TR mice of 18 and 24 m of age were quantified, and mean values given here correspond to mean \pm SEM. Results are summarised in Fig. 5.4.

Protein carbonyl levels were unchanged in E3/E3 mice, remaining at a similar level at 18 and 24 m (3.501 ± 0.351 nmole/mg protein and 3.401 ± 0.230 nmole/mg protein respectively). However, protein carbonyl content increased with age in E4/E4 mice by 30% although this difference was not significant (3.252 ± 0.231 nmole/mg protein at 18 m and 4.279 ± 0.521 nmole/mg protein at 24 m; Fig. 5.4A).

Comparing protein carbonyl content between the two phenotypes showed similar levels at 18 m (3.500 ± 0.351 nmole/mg in E3/E3 and 3.252 ± 0.231 nmole/mg in E4/E4), and 25% more oxidatively modified proteins in E4/E4 than in E3/E3 at 24 m (4.279 ± 0.521

nmole/mg protein and 3.400 ± 0.230 nmole/mg protein respectively). Nevertheless, this difference did not reach significance (Fig. 5.4B).

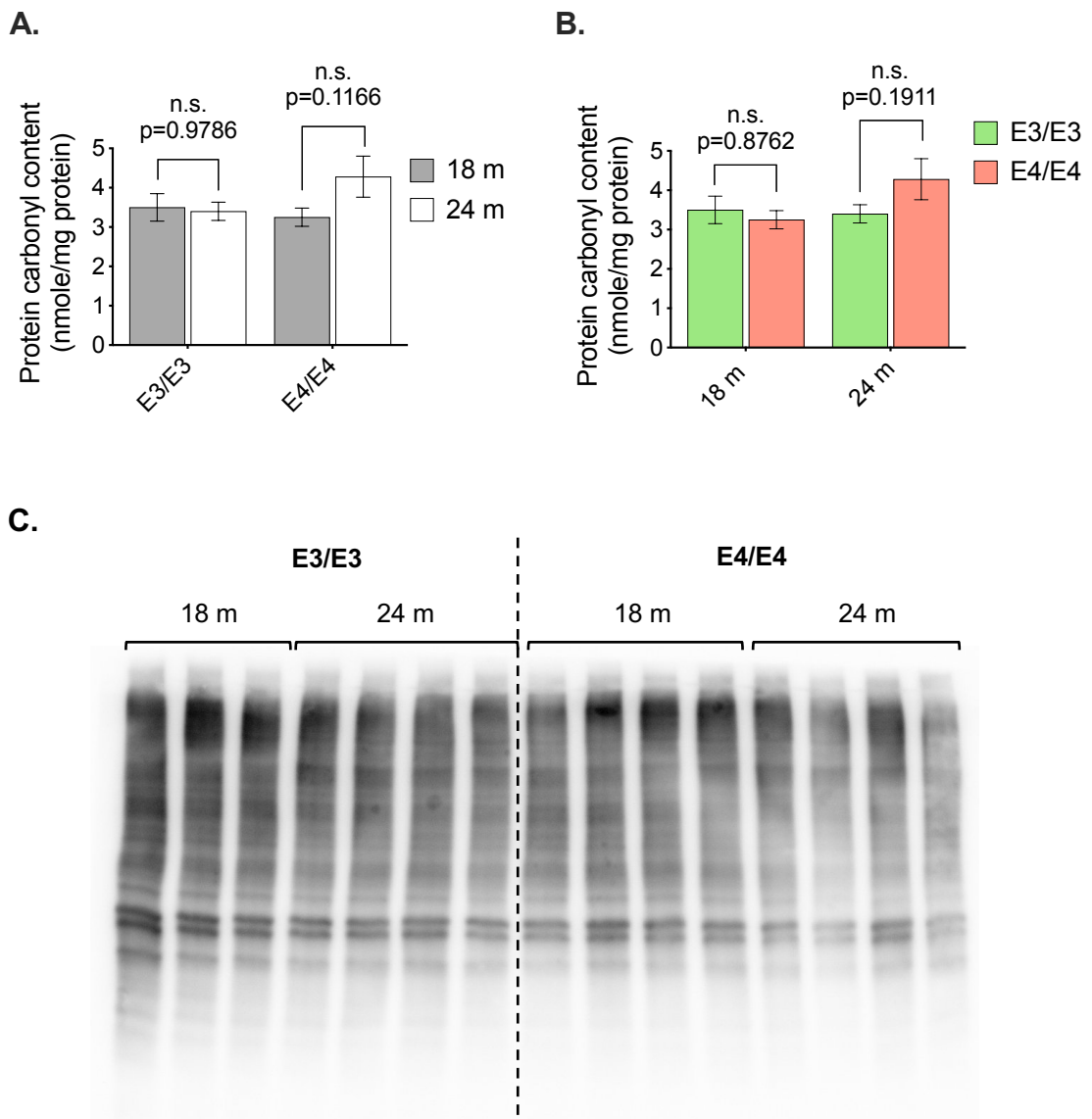


Figure 5.4 Protein carbonyl content in old ApoE3- and ApoE4- TR mice

A. Quantification of protein carbonyls showed no difference between 18 m and 24 m in E3/E3, and an increase trend in E4/E4 mice. Two-way ANOVA: effect of age x phenotype was not significant ($F(1,11) = 2.440$; $p=0.1466$). Overall protein carbonyl content was not significantly affected by age ($F(1,11) = 0.7629$; $p=0.4011$) or phenotype ($F(1,11) = 1.651$; $p=0.2252$). p values were derived from post-hoc Sidak multiple comparison test. $n(E3/E3, 18 m) = 3$, $n(E3/E3, 24 m) = 4$; $n(E4/E4, 18 m) = 4$, $n(E4/E4, 24 m) = 4$.

B. Comparison of protein carbonyl content between the two phenotypes showed no difference at 18 m and increased levels in E4/E4 at 24 m, but this difference did not reach significance. p values were derived from post-hoc Sidak multiple comparison test. n numbers above.

C. Oxyblot profiles of old (18 m and 24 m) E3/E3 (left) and E4/E4 (right) mice.

Given the variance in the data, increasing n numbers might be necessary for the effects of age and phenotype to reach significance.

A qualitative oxyblot was also run to see if there was any obvious difference in protein carbonyl profiles between the two phenotypes, but they appeared to be similar (Fig. 5.4C).

α -Tubulin levels in old ApoE-TR mice

α -Tubulin levels were semi-quantified in ApoE3- and ApoE4-TR mice by WB. Cytosolic fractions of protein extracts were prepared from brain tissue collected at 18 m and 24 m of age. An example blot can be found in Fig. 5.5A.

α -Tubulin band intensity was normalised to that of GAPDH to circumvent any discrepancy due to protein loading and transfer. One of the samples' α -Tubulin/GAPDH ratio was used as normaliser and attributed the arbitrary value of 1 (sample 443, see appendix 1).

The impact of age and phenotype on α -Tubulin levels were both investigated. There was a significant decrease in α -Tubulin levels between 18 m and 24 m in both phenotypes (Fig. 5.5B). Loss of α -Tubulin was more pronounced in E3/E3 with an approximate 20% reduction between the two ages. α -Tubulin levels were reduced by ~10% between 18 m and 24 m in E4/E4 (two-way ANOVA followed by post-hoc Sidak multiple comparison test: ***, $p=0.001$ and *, $p=0.0193$ respectively).

When comparing α -Tubulin levels within the same age group according to phenotype (Fig. 5.5C), it appeared that phenotype only had an influence at 18 m, with a trend towards decreased α -Tubulin levels in E4/E4 (~10% reduction compared to E3/E3, $p=0.0646$). Levels of α -Tubulin were similar in E3/E3 and E4/E4 at 24 m.

Two-way ANOVA analysis showed a significant effect of age on α -Tubulin levels ($F(1,11)=32.51$; $p=0.0001$) and the effect of phenotype on α -Tubulin levels almost reached significance ($F(1,11) = 4.496$; $p=0.0575$). There was no significant interaction between age and phenotype on α -Tubulin levels ($F(1,11) = 2.122$; $p=0.1724$).

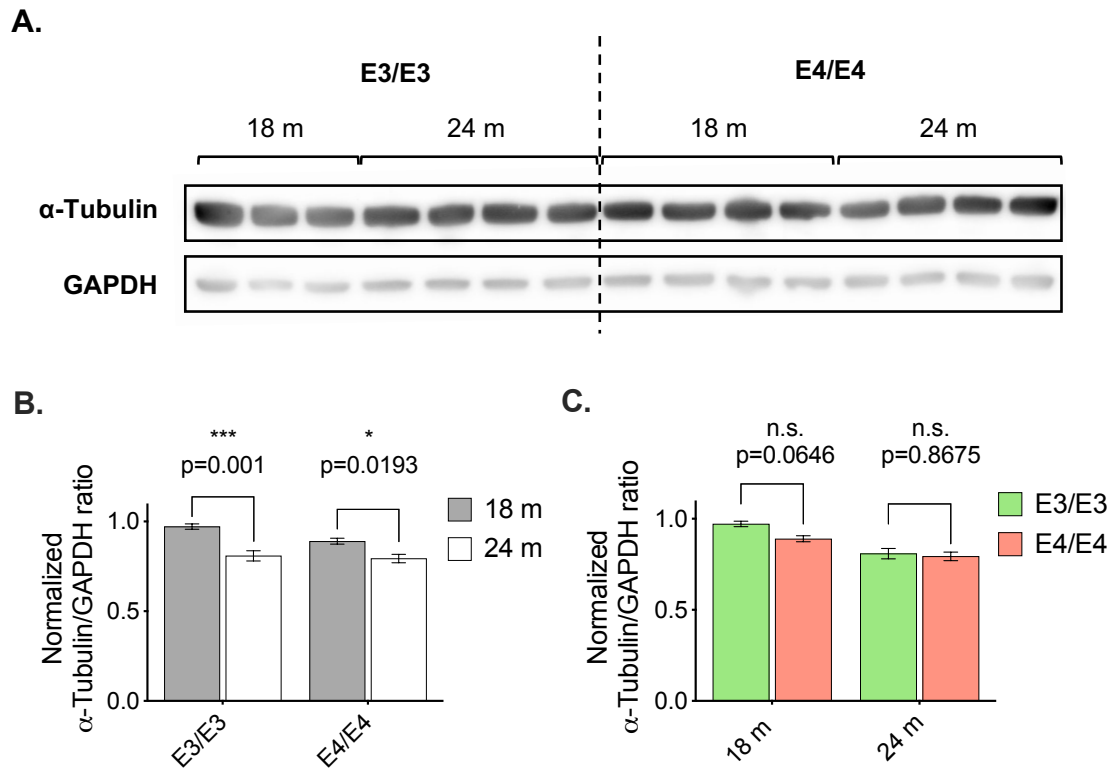


Figure 5.5 Changes in α -Tubulin levels in old ApoE-TR mice

A. α -Tubulin levels were semi-quantified in 18 m and 24 m ApoE-TR mice (left: E3/E3; right: E4/E4). GAPDH was used as a reference protein.

B. α -Tubulin levels significantly decreased from 18 m to 24 m in both E3/E3 and E4/E4 mice. Two-way ANOVA age effect: ($F(1,11)=32.51$; $p=0.0001$); post-hoc Sidak multiple comparison tests: ***, $p=0.001$ for ApoE3-TR mice, *, $p=0.0193$ for ApoE4-TR mice. $n(\text{E3/E3}, 18 \text{ m})=3$, $n(\text{E3/E3}, 24 \text{ m})=4$; $n(\text{E4/E4}, 18 \text{ m})=4$, $n(\text{E4/E4}, 24 \text{ m})=4$.

C. Differences in α -Tubulin levels between phenotype did not reach significance; however, α -Tubulin content was decreased at 18 m in E4/E4 compared to E3/E3 mice. Two-way ANOVA phenotype effect: ($F(1,11) = 4.496$; $p=0.0575$); post-hoc Sidak multiple comparison test showed a trend towards decreased α -Tubulin levels in E4/E4 at 18 m: $p=0.0646$.

5.4. Discussion

When evidence linking ApoE4 to impaired physiological function began to pile up, research turned to investigate whether levels of ApoE, and not just an isoform-dependent altered function, played a role in AD pathogenesis. Studies initially focused on the comparison of brain ApoE levels between control and AD subjects. Results looking at ApoE protein and mRNA levels were already controversial at this stage (Beffert et al., 1999; Aizawa et al., 1997; Diedrich et al., 1991; Xu, P.-T. et al., 1999) and the introduction of *APOE* genotype as a factor did not aid in reaching a consensus.

While being most relevant in terms of studying AD pathology, the use of human brain tissue comes with its own challenges. AD is a progressive disorder with several disease stages, starting with mild cognitive impairment before moving to mild, moderate, severe and ultimately very severe AD (Burns & Iliffe, 2009). As pointed out by Glockner et al, reported discrepancies in ApoE expression and levels could be a result of differences in disease stage (Glöckner et al., 2002).

Another challenge of conducting studies characterising ApoE levels in brain tissue is the reduced number of $\epsilon 4/\epsilon 4$ elderly, non-demented subjects; this is also true for studies conducted in living patients (Winnock et al., 2002). Homozygous $\epsilon 4$ represent 15% of the worldwide population only, and those individuals are 12 times more likely to develop dementia, with earlier age of onset. Transgenic animals expressing human ApoE are thus an appropriate model to be used in conjunction to human brain tissue-based studies.

Human ApoE transgenic mice were developed to deepen our understanding of the physiological function of ApoE. One of those models is the ApoE-TR mouse where ApoE expression is driven by the mouse *APOE* promoter, resulting in a physiologically relevant model. ApoE-TR mice replicate isoform-dependent characteristics, such as reduced synaptic activity or memory decline in ApoE4-TR mice (Tai et al., 2011; Bour et al., 2008). Additionally, levels of ApoE4 were reduced in the plasma, CSF and brain of adult mice compared to ApoE2 and ApoE3 (Sullivan et al., 2011), at similar levels to what is observed in humans (Tai et al., 2011). However, data at later time points is lacking.

A thorough characterisation of ApoE levels throughout lifespan is of great importance since both *APOE* genotype and age have an impact on AD onset. Isoform-specific levels of soluble ApoE were thus investigated here in a longitudinal pilot study conducted on ApoE-TR mouse hemibrain tissue. Brains were not dissected into specific brain region

such as cortex or hippocampus because the idea behind this pilot study was to investigate correlations between ApoE levels and ageing in the brain in general and not in particular regions linked to AD.

Proteins were extracted from brain tissue collected at 3, 6, 12, 18 and 24 m using RIPA buffer, and ApoE levels in each sample were semi-quantified by WB using two different antibodies. WB was chosen as a method for semi-quantification because, unlike quantification with ELISA, immunoblots allow for the visualization of antibody binding profiles and for the subsequent choice of the band to quantify. Bands intensity quantified corresponded to the monomeric species migrating at ~34 kDa for both monoclonal and polyclonal antibodies (Fig. 5.1A).

Results communicated here were in part dependent on the antibody of detection, although some observations were common to both. For example, ApoE3 levels were significantly higher than ApoE4 levels in old mice (Fig. 5.2A), suggesting that the presence of $\epsilon 4$ results in lowered ApoE expression. This is in line with one of the few studies that have reported a comparison of elderly (~75 year-olds) $\epsilon 3$ - and $\epsilon 4$ -carriers control human tissue: quantification of hippocampal and cortical ApoE levels by ELISA in age-matched healthy $\epsilon 3/\epsilon 3$ and $\epsilon 3/\epsilon 4$ subjects showed decrease ApoE in $\epsilon 4$ carriers (hippocampus: 169.9 ± 17.3 ng/mg protein in $\epsilon 3/\epsilon 3$ vs 135.7 ± 10.3 ng/mg protein in $\epsilon 3/\epsilon 4$; cortex: 155.3 ± 9.6 ng/mg protein in $\epsilon 3/\epsilon 3$ vs 116.7 ± 12.3 ng/mg protein in $\epsilon 3/\epsilon 4$) (Beffert et al., 1999).

This genotype-dependent difference in ApoE levels at old age was also reported in a mouse model of AD (PDAPP) crossed with ApoE-TR mice (PDAPP/TREx, with x: 2, 3 or 4 corresponding to the crosses with mice of different hApoE genotype). Bales et al reported lower ApoE4 in the hippocampus at 18 m compared to ApoE2 and ApoE3, but not in the cortex (Bales et al., 2009). When looking at the 18 m group specifically (Fig. 5.1D), I also found higher ApoE in E3/E3 than in E4/E4 mice.

ApoE levels in middle age mice (12 m) were similar for both genotypes, and there was no difference between the two antibodies. Bales et al also looked at 12 m old PDAPP/TREx mice and found significantly lower levels of ApoE in the hippocampus, but not the cortex, of E4/E4 mice (Bales et al., 2009).

In adult mice, differences in ApoE levels were antibody-dependent: ApoE levels were higher in E3/E3 than in E4/E4 when using the polyclonal antibody whereas levels were fairly similar when a monoclonal antibody was used. Bales et al also investigated ApoE levels at 3 m old, in ApoE-TR mice this time. They reported lowered soluble ApoE levels

in E4/E4 mice both in the cortex and hippocampus (Bales et al., 2009). Riddell et al also reported lower hippocampal and cortical ApoE levels in E4/E4 mice compared to E3/E3 at 12 weeks (Riddell et al., 2008).

Finally, overall ApoE levels obtained by combining all ages were lower in ApoE4-TR than in ApoE3-TR mice. This difference only reached significance when ApoE was detected with the polyclonal antibody.

Another observation common to both methods of ApoE detection was that ApoE levels seem to remain constant throughout in E4/E4 mice, whereas they increased at old age in ApoE3-TR mice (Fig. 5.2A). For better visualization, levels were grouped by phenotype in Fig. 5.6.

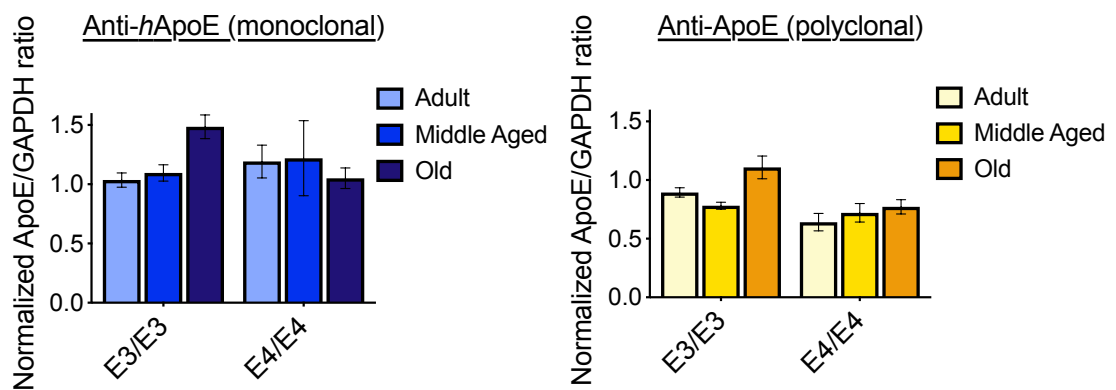


Figure 5.6 Normalised ApoE levels by age groups

Normalised ApoE/GAPDH ratio with ApoE detected using a monoclonal (left) and polyclonal (right) ApoE antibody in adult (3 m and 6 m), middle age (12 m) and old (18 m and 24 m) mice.

Unlike what was described in this pilot study, Bales et al communicated decreasing ApoE levels with age (3 m, 12 m and 18 m) for both PDAPP/TRE3 and PDAPP/TRE4. A significant difference between Bales' study and the results reported here is that Bales et al quantified ApoE levels in the hippocampus and cortex whereas in the present study, soluble ApoE was quantified from hemibrain extracts (Bales et al., 2009).

Semi-quantification of ApoE levels using WB followed by densitometry proved to be difficult. WB is a method that is quite unreliable since there are many sources of variation such as uneven transfer, variable antibody-binding, inconsistent ECL detection etc... To avoid variations due to uneven transfer and inconsistent protein loading (which can arise from pipetting errors or protein sample preparation), band intensity was normalised

to an internal reference (GAPDH), and to avoid differences between blots, a normaliser sample was loaded in all blots in duplicate.

However, in order to be able to detect GAPDH, blots had to be stripped since GAPDH migrates at 37 kDa, overlapping with the monomeric ApoE band (~34 kDa). Actin and tubulin are other alternatives to GAPDH for normalisation, but actin also overlaps with ApoE (42 kDa), and I showed here that tubulin levels varied with age (Fig. 5.5B). Stripping and re-probing with GAPDH introduces another level of variability, which is why changes in ApoE levels were also reported skipping normalization with GAPDH in appendix 4 (protein samples were prepared to the same concentration and loading variations should normally average out). Fortunately, profiles with and without normalization to GAPDH levels were alike, for both antibodies. One way to avoid overlapping bands is to use fluorescent-labelled secondary antibodies; however, this could not be done here because of incompatibilities between primary antibodies used and availability of corresponding secondary antibody.

Profiles of ApoE levels slightly differed depending on the antibody used for detection. The monoclonal antibody employed here detects an epitope in the C-terminal domain of the protein. There could possibly be differential binding of the antibody between the isoforms, depending on how exposed the epitope is, and that may account for the differences observed between the two ApoE level profiles. This antibody-dependent variation can also be problematic for ELISA-based approaches. Mass spectrometry studies are in development to circumvent these antibody-related issues (Belloy et al., 2019). Others have already succeeded in using mass spectrometry to quantify ApoE (Martínez-Morillo et al., 2014; Sullivan et al., 2011).

Finally, it is important to highlight that only soluble ApoE was quantified here. RIPA buffer extraction results in a supernatant fraction containing RIPA-soluble proteins, and a pellet containing RIPA-insoluble proteins. RIPA-insoluble proteins could be further extracted with 6 M GuHCl for example, in order to quantify complexed ApoE.

Since ApoE was also reported to have transcriptional effects, (Theendakara et al., 2016) the presence of ApoE in the nucleus in ApoE-TR mice was also investigated. Nuclear extracts from 3 m and 24 m extracts were used for to see whether ApoE localised to the nucleus across lifespan. Running nuclear fractions was particularly difficult due to the presence of DNA which adds viscosity to the sample and alters protein separation by SDS-PAGE, as can be seen in Fig. 5.3A, which is in part why semi-quantification was not attempted here. Kim et al have shown that endogenous tagged-ApoE localised to

the nucleus of CHO cells and that its levels were increased under stress conditions (Kim, W. S. et al., 2008). They did not explore any phenotype-dependent effect of ApoE nuclear localisation. It would thus be interesting in the future to investigate differences in levels of ApoE between E3/E3 and E4/E4 mice, across lifespan. There are no studies that have investigated this so far to the best of my knowledge.

A ~25 kDa band could be detected in nuclear fractions, corresponding to a fragment of ApoE. This fragment seemed to be enriched in the nuclear fraction since I could not detect it in whole protein fractions. However, detection of nuclear ApoE required the use of more concentrated primary antibody, which may account for why the 25 kDa band was not observed in whole fractions' blots.

Looking at the proportion of fragmented ApoE relative to intact ApoE highlighted that a greater fraction of ApoE had significantly fragmented in E4/E4 compared to E3/E3 at 3 m. Love et al reported the presence of a 17 kDa N-terminal fragment in the nucleus of glial cells in AD brains, and the uptake and trafficking of said fragment when applied exogenously to murine microglial cells (Love et al., 2017).

Even though these results are preliminary, they suggest that ApoE can indeed be found in nuclear fractions, and that ApoE4 is either more prone to cleavage than ApoE3, which has previously been reported in recombinant models of ApoE (Morrow et al., 2000), or that ApoE4 fragments are preferentially translocated.

Ageing is the main environmental risk factor for AD, and $\epsilon 4$ has a particular impact on AD age of onset, which is why the influence of ApoE4 on the presence of ageing markers was investigated here. Two markers were selected: protein carbonylation and α -tubulin levels.

Protein carbonyl content is a known marker of ageing, associated with irreversible oxidation of certain amino acids by ROS (Pro, Arg, Lys and His in particular) (Dalle-Donne et al., 2003). Damaged proteins tend to accumulate with age, due to an imbalance between levels of ROS and the antioxidant system, as well as decreased proteasome activity (Dalle-Donne et al., 2006). Protein carbonyl content is increased in AD subjects compared to age-matched control (Smith, C. D. et al., 1991); however, there are very few reports taking into account the *APOE* genotype. There was no significant difference in carbonyl content between ApoE3-TR and ApoE4-TR mice, but it was slightly more elevated in E4/E4 at 24 m.

The other marker of ageing selected was levels of α -tubulin. Loss of α -tubulin has been reported with ageing in human brains as well as in AD (Zhang *et al.*, 2015; Labisso, Raulin *et al.*, 2018). Quantification of α -tubulin in ApoE-TR mice of 18 m and 24 m of age showed that α -tubulin levels also significantly decreased with age in ApoE-TR mice (Fig. 5.5B). Interestingly, while comparable at 24 m, α -tubulin levels were decreased in E4/E4 mice at 18 m although this did not reach significance (Fig. 5.5C). Loss of β -tubulin and increased levels of acetylated α -tubulin are also markers of ageing that are increased in AD (Zhang *et al.*, 2015; Labisso, Raulin *et al.*, 2018). Quantification of these markers ApoE-TR would complement the current pilot study.

5.5. Conclusion

The results presented here were obtained from a relatively small cohort (3 to 4 animals per age group, per genotype). There is a great variability in brain tissue both due to individual variations and variability introduced during tissue processing and subsequent experimentation. Although preliminary, when taken together, these results support previous observations of lowered ApoE levels in $\epsilon 4$ carriers. Moreover, it appears that ApoE4-TR mice have increased markers of ageing, especially when looking at loss of tubulin levels, compared to age-matched ApoE3-TR mice. This points to either increased vulnerability or alternatively premature ageing due to the presence of ApoE4.

Since this was a pilot study, greater n numbers would help in understanding how age and phenotype interact.

Chapter 6 - Discussion and future directions

Sporadic AD is a very complex, multifaceted disorder with many hypotheses behind it, ranging from protein misfolding and aggregation of key proteins to oxidative stress or inflammation (Fig. 6.1). It is complicated by a myriad of genetic and environmental factors modulating its onset. The $\epsilon 4$ allele of the *APOE* gene is one of those factors (Querfurth & LaFerla, 2010; Reitz & Mayeux, 2014). It gives rise to ApoE4, one of the three main ApoE isoforms, which is associated with a dose-dependent risk of AD onset (Zannis et al., 1982; Corder et al., 1993).

ApoE4 was studied here in the context of protein misfolding and aggregation, oxidative stress and ageing to try and elucidate the ways in which ApoE4 increases vulnerability to AD pathogenesis. The three ApoE isoforms are differentially linked to risk of developing AD.

This discussion and future directions chapter is divided into five sections. Key findings presented in this thesis are summarised and extrapolated to what could be happening *in vivo* in the first three sections. The fourth section focuses on ApoE as a therapeutic target for AD. The final section consists of concluding remarks. Future directions have been introduced throughout this discussion chapter when appropriate.

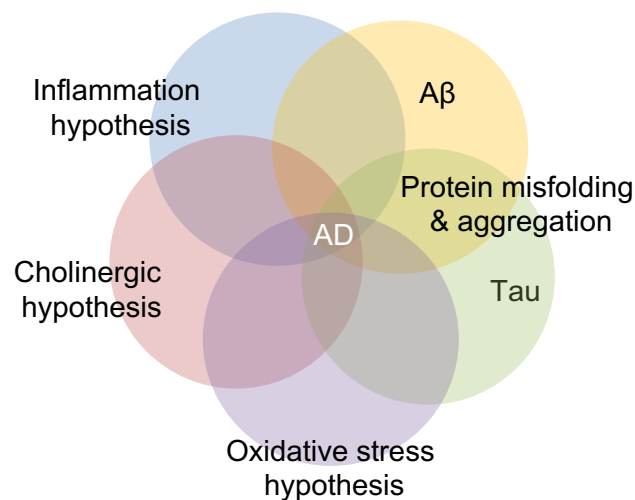


Figure 6.1 Hypotheses behind sporadic AD

6.1. Self-assembly of ApoE

6.1.1. Self-assembly of ApoE *in vitro* is restricted to rApoE4

Apart from distinct differences in their respective amino acid sequences at positions 112 and 158 (ApoE2 has two Cys residues, ApoE3 a Cys and an Arg and ApoE4 two Arg) (Rall, S. et al., 1982), the three ApoE isoforms are structurally similar. Using recombinant ApoE produced in *E. coli*, I showed that rApoE isoforms formed tetramers in solution, and that they were highly α -helical in terms of their secondary structure. Differences in their tertiary structure only appeared under harsh conditions, either under extreme temperatures or in the presence of a chemical denaturant (see 3.3.2). It is unsurprising that differences between the three isoforms are not obvious, since all three proteins are functional and are not directly pathogenic. The only clear difference between the three isoforms came from the marked ability of rApoE4 to self-assemble in PB, at pH 7.4 into non-amyloid fibres (see 3.3.3 and 3.3.7). The ability of ApoE4 to form molten globules is most likely responsible for its self-assembly propensity, since molten globules are destabilised structures that have been associated with the aggregation process. More generally, molten globules have also been associated with disease (Dobson et al., 2001; Morrow et al., 2002; Dobson, 2003; Hatters et al., 2006). Co-incubation with rApoE4 did not promote self-assembly of rApoE2 or rApoE3. On the contrary, rApoE2 and rApoE3 rather hindered rApoE4 self-assembly *in vitro*. It is not clear at this stage how rApoE2/3 associate with rApoE4 to reduce its assembly (see 3.3.5). One possibility is that heterotetramers of rApoE2/3 and rApoE4 form in solution and this could be investigated by Förster resonance energy transfer binding assay with fluorescent-tagged proteins. This technique has been employed to analyse multi-protein interactions *in vitro* (Martin et al., 2008). I was not able to uncover evidence of ApoE isoforms forming heterotetramers in *APOE* heterozygotes individuals, but it would still be interesting to see whether this can happen as an artefact *in vitro*.

Harsh oxidative and reducing conditions altered self-assembly of rApoE4. Under harsh oxidative conditions, rApoE isoforms formed very thin fibrils that were unlike those formed by rApoE4 under physiological conditions. In addition to these thin, long fibrils, small round species, rings and agglomerates could sporadically be detected (see 4.3.4). Under harsh reducing conditions, rApoE isoforms remained largely un-assembled. Incubation of rApoE2/3 in milder oxidative and reducing environments that still allowed for rApoE4 self-assembly in a fashion most similar to that observed under physiological conditions was not sufficient to induce self-assembly.

Investigation of rApoE self-assembly properties could be pursued further by trying to understand whether the positive charges provided by the two Arg residues are necessary for rApoE4 fibril formation. Cysteamine modification of Cys residues would introduce a positive charge by creating a Lys analogue (Weisgraber et al., 1982). Chemical modification of Arg residues is limited (deGruyter et al., 2017) and thus it is not viable avenue to study Arg influence on assembly. Instead, Ala-mutagenesis could be employed to replace Arg residues and see if and how assembly is affected. Ala site-directed mutagenesis studies have been employed to elucidate a specific role played by a residue. For instance, this technique was used to show that the salt bridge between Arg-61 and Glu-255 in ApoE4 was responsible for its preferential binding to VLDL (Dong et al., 1994; Dong & Weisgraber, 1996).

Differential self-assembly of rApoE isoforms was the only clear difference identified between the three proteins. Understanding how this process works *in vitro*, even if this process might not be physiologically relevant, may bring us closer to understanding what sets apart an isoform from the other, and ultimately answer why ApoE4 is associated with a risk for AD.

6.1.2. Self-assembly of ApoE *in vivo*

It is unclear whether ApoE isoforms, and more specifically ApoE4, can aggregate in the human brain. There is mainly evidence for ApoE co-localising at senile plaques and with NFT (Namba et al., 1991; Strittmatter, Saunders, et al., 1993). However, a recent study conducted in APPPS1-21/ApoE4 mice, which are a model for AD with an *APOE* ϵ 4 knock-in background, showed that targeting nonlipidated, aggregated ApoE4 with antibodies led to a decrease in A β pathology in the brain. One of the antibodies used, HAE-4, was shown to preferentially bind to nonlipidated, aggregated ApoE4, and to localise to A β plaques, suggesting that ApoE4 in A β plaques is most likely aggregated – and nonlipidated (Liao et al., 2018). It would be interesting to test whether this HAE-4 antibody recognises rApoE4 fibrils, or alternatively to find an antibody that does, that could be used in immunostaining of human brain tissue, with the aim of answering whether these aggregates also happen in the human brain.

Of note, nonlipidated ApoE only represents a very small fraction of total ApoE due to its high avidity for lipids, and phospholipids in particular (Huang, Y. & Mahley, 2014). However, this small portion of nonlipidated ApoE, and especially nonlipidated ApoE4, could be detrimental and enhance A β pathology through its own aggregation propensity.

This is supported by a study showing that the absence of ABCA1, a lipid transport protein involved in the lipidation of apolipoproteins, decreases the levels of soluble ApoE, but increases the proportion of insoluble ApoE, in murine amyloid pathology models of AD. It even increased A β load in one of the models employed (Tg-SwDI/B) (Hirsch-Reinshagen et al., 2005). A β plaques extracted from brain tissue are found in what is called the insoluble fraction, which has to be further solubilised using a denaturant such as GuHCl (Hirsch-Reinshagen et al., 2005). The increase in the proportion of insoluble ApoE is thus consistent with localisation to A β plaques, where it is most likely aggregated.

It is interesting to point out that I reported decreased levels of soluble ApoE in ApoE4-TR compared to ApoE3-TR mice (Fig. 5.2). Examination of *APOE* mRNA levels across lifespan as well as quantification of insoluble ApoE levels would allow for clarification of whether ApoE4 soluble levels are decreased due to poorer lipidation, or because of reduced transcription.

To better understand the association between ApoE and A β , it is important to remember that A β is produced in endosomes (reviewed by Selkoe, 2001) and that it can also be found in lysosomes (Selkoe, 1994; Zheng et al., 2013). Exogenous addition of synthetic A β to primary neurons showed that A β was readily internalised and trafficked via the endo-lysosomal pathway to lysosomes where it accumulates, as shown by real time tracking of tagged A β (preprint: Marshall et al., 2019). Endosomes and lysosomes are acidic compartments and low pH has been shown to promote A β fibrillisation *in vitro* (Selkoe, 1994; Wood, Maleeff, et al., 1996).

As was discussed at lengths in 1.4.1, there is evidence for ApoE and A β forming complexes, with lipidated ApoE4- A β complexes being less stable. ApoE- A β aggregates could potentially be internalised through lipoprotein receptors and endocytosed into endosomes charged with transport to lysosomes for degradation. Acidic conditions in early- and late- endosomes would dissociate ApoE from its lipids and from A β , leaving A β to aggregate in overwhelmed lysosomes (proposed by Kanekiyo et al., 2014) (Fig. 6.2). Examination of rApoE self-assembly at pH 5.0 to pH 6.0 could point to whether ApoE could self-assemble *in vivo* in those acidic compartments, where it could potentially be located with A β and participate in A β deposition or self-assemble itself. There is already evidence for enhanced aggregation of recombinant ApoE at pH 4.5 (Garai et al., 2011).

Additional *in vitro* studies that could also be conducted to explore whether ApoE assembly occurs in the brain include testing self-assembly of rApoE at lower

concentrations (1 μM or 0.1 μM) instead of 12 μM (appendix 2) or 25 μM (see 3.3.3) and using different buffers with varied salt concentrations (appendix 2). Moreover, the use of recombinant ApoE produced in a mammalian cell line would provide an answer to how post-translational modifications, such as glycosylation, might differentially (or not) modulate ApoE self-assembly *in vitro*.

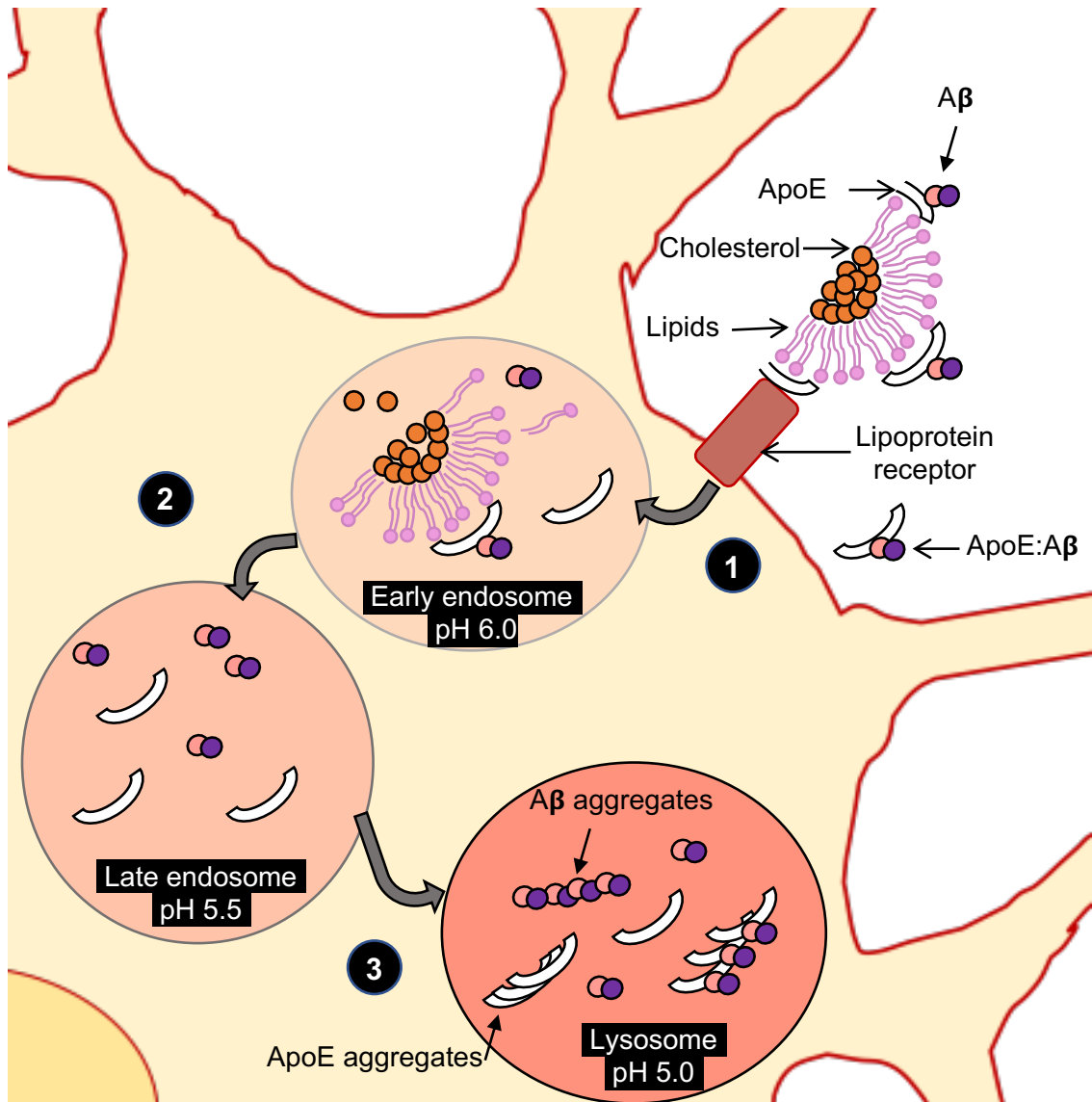


Figure 6.2 ApoE and A β in acidic compartments, inspired by Kanekiyo et al., 2014.

ApoE, A β and ApoE-A β complexes (depicted here) can be endocytosed through binding with lipoprotein receptors (1). In endosomes (pH 5.5-6.0), ApoE dissociates from lipids and cholesterol (2). A β and ApoE can then be delivered to lysosomes for degradation (3) although they can also be recycled (not depicted here). Low pH in lysosomes (pH 5.0) is a suitable environment for A β aggregation. Since ApoE self-assembly also seems favoured in acidic conditions (Garai et al., 2011), it is a possibility that it could also aggregate in lysosomes.

6.2. ApoE and the antioxidant system

6.2.1. ApoE as an antioxidant protein

The structure of rApoE isoforms was investigated in the presence of H₂O₂ to explore the ROS scavenging properties of ApoE, first proposed by Pedersen and colleagues (Pedersen et al., 2000). The structure of rApoE2 was the most affected by harsh oxidative conditions, with a marked loss in α -helical content and a shift in the conformation of α -helices (see 4.3.3). All three isoforms have antioxidant properties nonetheless (Miyata & Smith, 1996). They could either stem from their metal sequestration abilities (Miyata & Smith, 1996), or from direct interaction with ROS through residues such as Met (Jolivalt et al., 2000). Shifts in the apparent molecular weight of rApoE following incubation with H₂O₂ at a 1:3533 ratio when examined by denaturing gel electrophoresis was consistent with Met oxidation (Fig. 4.14) (Jolivalt et al., 2000). Met oxidation in rApoE could be further explored by CNBr cleavage since CNBr cleaves peptides after Met, but not oxidised Met, residues (Jolivalt et al., 2000), or using HPLC since Met oxidation results in a shift in retention time as shown in ApoA-I and ApoA-II (Anantharamaiah et al., 1988). Met residues are more than just a hydrophobic amino acid. They can be reversibly oxidised, and reduction of oxidised Met can be catalysed by Methionine sulfoxide reductase A or B (Aledo, 2019). It would thus be interesting to investigate whether ApoE is a substrate for either of those enzymes. More generally, Met residues have been proposed to act as ROS scavengers, and thus function as endogenous antioxidants (Levine et al., 1996). Unlike ApoE4, ApoE3 and ApoE2 have one and two Cys residues respectively. Cys residues can form disulphide bridges following oxidation. One explanation for the increased antioxidant capacity of ApoE2, followed by ApoE3 (ApoE2>ApoE3>ApoE4), could stem from the presence of Cys. ApoE2 and ApoE3 could function as antioxidants in a similar way to the small peptide GSH (equation 20). GSH oxidation is reversible, and GSSG can be reduced by glutathione reductase (Poljsak & Milisav, 2013). It would thus be interesting to explore whether ApoE2 and ApoE3 are a substrate for reductase enzymes.

Exposure to toxic insults, in the form of a pesticide or directly via application of H₂O₂, resulted in an ApoE-response in cells, with increased levels of *APOE* gene transcripts (see 4.3.2). It is well established that ApoE (most likely secreted by astrocytes) is involved in maintaining and repairing membranes and synapses following injury (reviewed by Bu, 2009). In addition, ApoE is also synthesised in neuroblastoma cells

undergoing apoptosis and can also be synthesised in hippocampal neurons following excitotoxic stress (Boschert et al., 1999; Elliott et al., 2007). Oxidative stress has been described as a mediator of apoptosis in cells (reviewed by Kannan & Jain, 2000); and as was alluded to in 1.6.2, exposure to kainic acid results in oxidative damage (Gluck et al., 2000). It is thus a possibility that the ApoE-response following stress or injury is not just a repair response, but it could also be part of an antioxidant defence response. This hypothesis is supported by the results presented in this thesis, with oxidative insults resulting in increased *APOE* transcription (see 4.3.2). An ApoE-response as part of the antioxidant defence system could be explored further by uncovering what happens to ApoE after transcription and where it localises in the cell, by using immunofluorescence microscopy for example.

6.2.2. ApoE and the antioxidant balance across lifespan

Association between *APOE* status and antioxidant balance was explored in 4.3.1, and results were inconclusive with no clear patterns of activity change across lifespan, and no obvious difference between E3/E3 and E4/E4 phenotypes. However, interesting patterns appeared when correlating antioxidant activity with soluble ApoE levels (Fig. 6.3A). CAT and SOD activities were normalised to that of sample 653, the normaliser used for the examination of soluble ApoE levels across lifespan (see 5.3.1). Data points were fitted to a segmental linear regression. Soluble ApoE levels in ApoE3-TR mice decreased from 3 m to 12 m and increased from 12 m to 24 m. Soluble ApoE levels in ApoE4-TR were harder to fit to a pattern: levels of ApoE4 increased from 3m to 6m, followed by a decrease from 6 m to 18 m and another increase 18 m to 24 m, which is why segmental linear regression in ApoE4 data excluded values corresponding to 3 m.

The pattern of change in CAT activity in ApoE3-TR mice was a direct inverse of the pattern of change in soluble ApoE3 levels across lifespan. This was also true for changes in SOD activity, despite the greater variability in the data points, where it increased when soluble ApoE3 levels decreased and vice-versa. This was not the case in ApoE4-TR mice: both CAT and SOD activities seemed to mirror changes in soluble ApoE4 levels (Fig. 6.3A). Table 6.1 summarises the respective slopes of each segment for normalised CAT and SOD activities and normalised protein levels. It is unclear what these temporal associations mean, but it is nonetheless interesting to note that they varied with *APOE* status.

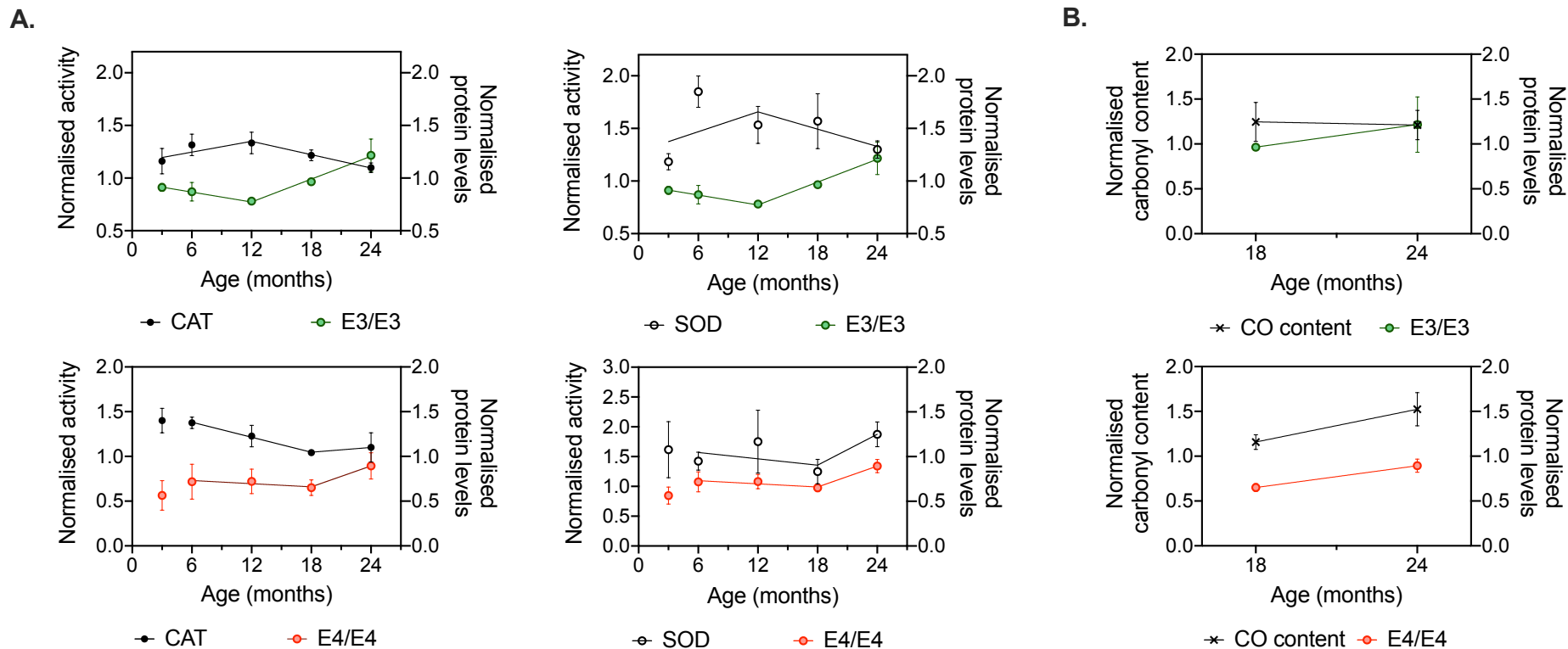


Figure 6.3 Associations between antioxidant enzyme activities and oxidative damage with soluble ApoE levels across lifespan in ApoE-TR mice

A. Normalised enzymatic (CAT and SOD) activities increased from 3 m to 12 m while ApoE3 decreased, and they decreased while ApoE3 increased between 12 m and 24 m in ApoE3-TR mice (top). Enzymatic activities followed the same pattern of change as ApoE4 with a decrease between 6 and 18 m and an increase between 18 and 24 m (bottom).

B. Normalised carbonyl (CO) content remained constant between 18 m and 24 m while soluble ApoE3 increased (top). CO content increased with ApoE4 levels between 18 m and 24 m (bottom). Quantification of CO levels across lifespan would evidence any temporal links between oxidative damage and APOE status.

	Slope	ApoE levels	CAT activity	SOD activity
E3/E3	a	- 0.0157	0.0171	0.0315
	b	0.0362	- 0.021	- 0.0274
E4/E4	a'	- 0.0059	- 0.028	- 0.0178
	b'	0.0390	0.0089	0.0863

Table 6.1 Segmental linear regression best-fit slopes

Slopes were extracted from the segmental linear regression fit obtained using GraphPad Prism. “a” corresponds to the slope between 3 m and 12 m and “b” to the slope between 12 m and 24 m in ApoE3-TR mice. “a’ ” corresponds to the slope between 6 m and 18 m and “b’ “ to the slope between 18 m and 24 m in ApoE4-TR mice

Links between ApoE levels and carbonyl content were also investigated in a similar fashion (Fig. 6.3B). No clear associations appeared here since only two time points were looked at in this study – 18 m and 24 m. It would thus be interesting to quantify carbonyl content across lifespan in ApoE-TR mice to see whether oxidative damage is directly associated with variations in soluble ApoE levels.

6.3. ApoE, a direct and indirect transcription factor?

6.3.1. Nuclear localisation of ApoE and implications

In chapter 5, I presented evidence for nuclear localisation of ApoE in ApoE-TR mice at 3 m and 24 m (see 5.3.2). This is consistent with reports of ApoE directly interacting with DNA. Using chromatin immunoprecipitation with ApoE antibodies, Theendakara and colleagues identified 3080 promoter peaks, of which close to 1700 were only associated with ApoE4 (Theendakara et al., 2016). It thus appears that ApoE plays a role as a direct transcription factor. The binding of ApoE to genes associated with AD, such as genes involved in neuronal signalling or inflammation among other broad categories, were restricted to ApoE4 (Theendakara et al., 2016). An analysis of the temporal association of ApoE with genes linked to AD might provide additional information on the mechanisms through which ApoE4 participates in establishing an environment favourable to AD onset and development.

6.3.2. Disulphide bridge formation – a signalling moiety

The ability of ApoE2 and ApoE3 to form disulphide bridges through their respective Cys residues could potentially play a role that is not restricted to a direct antioxidant defence mechanism, as was proposed in 6.2.1.

ApoE dimers formed through disulphide bridges have been detected in ApoE3 frontal cortex and hippocampus in the human brain. The direct functional consequences of disulphide bridged ApoE dimers are unclear (Elliott et al., 2010).

A role for ApoE in signalling cascades through binding to lipoprotein receptors has extensively been reviewed (Bu, 2009). However, ApoE dimers do not have the same binding properties to lipoprotein receptors as their monomeric counterparts; for example, ApoE3 homodimers had reduced binding activity to the LDL receptor (Weisgraber & Shinto, 1991). Investigation of binding propensity of disulphide-linked ApoE dimers to different lipoprotein receptors would clarify how these dimers might modulate ApoE signalling effect properties.

In chapter 4, I showed that the ApoE-response to oxidative insults was genotype dependent. It would thus be interesting to investigate whether disulphide bridge formation in ApoE2 and ApoE3 can serve as a redox sensor leading to a signalling cascade that would result in increased *APOE* transcription. Said feedback mechanism would be restricted to ApoE2 and ApoE3 since ApoE4 lacks Cys residue.

6.4. ApoE as a therapeutic target

So far, disease-modifying therapies developed to thwart AD have mainly been targeted to A β and Tau since both A β and Tau pathologies are central to AD pathogenesis (Wischnik et al., 2014; Selkoe & Hardy, 2016). The discovery of *APOE* ϵ 4 as a major genetic risk factor for AD resulted in a boom in ApoE-related research focused on the pathobiology of ApoE (Mahley, 2016). Consequently, strategies have been developed to target ApoE4 in AD (Yamazaki et al., 2016; Suidan & Ramaswamy, 2019). These strategies can broadly be classified into three categories that are summarised in table 6.2.

	Strategy	Reasoning
Regulation of ApoE levels	Up-regulation	ApoE levels decreased in AD; possible relation to cognitive deficits
	Reduction	ApoE-deficiency in mice decreases A β pathology
	Mimetic peptides	Compensate loss-of-function associated with ApoE4
	Gene therapy	Regulation of ApoE brain levels through <i>APOE</i> ϵ 2 gene delivery or <i>APOE</i> ϵ 4 gene silencing (antisense oligonucleotide)
Adaptation of ApoE properties	Structural correctors	Modify the structure of ApoE4 to make it ApoE3-like
	Increase ApoE lipidation	Favour A β clearance/reduce A β aggregation
	ApoE immunotherapy	Block nonlipidated ApoE- A β interaction that would promote aggregation
Indirect ApoE therapies	Regulation of lipoprotein receptors	Enhance A β clearance in ϵ 4 carriers
	Blood-brain barrier repair	Counter ApoE4-mediated damages

Table 6.2 ApoE-targeted therapies

Strategies devised to target ApoE in AD fall into three broad categories: regulation of ApoE levels, adaptation of ApoE properties and indirect approaches. Reasonings behind each strategies were compiled from Yamazaki et al., 2016 and Suidan & Ramaswamy, 2019.

The results presented in this thesis provide some discussion points for a number of these strategies, mainly in the “Regulation of ApoE levels” and “Adaptation of ApoE properties” categories delineated in table 6.2.

Increasing ApoE4 levels would in theory aid in countering “loss of functions” associated with this isoform, which were summarised in Fig. 1.7. While I did report reduced levels of soluble ApoE in ApoE4-TR mice (see 5.3.1), increasing ApoE4 levels may not be the best approach. On the contrary, increasing ApoE4 levels could result in exacerbation of ApoE4 gain of toxic functions, such as generation of neurotoxic fragments or aggregation (Fig. 1.7; Hatters et al., 2006). Moreover, as I mentioned in 6.1.2, soluble ApoE4 levels may be decreased due to a shift to insoluble fractions, i.e. ApoE4 may aggregate and result in decreased soluble levels. This would be consistent with ApoE4 being less lipidated than ApoE2 and ApoE3 in humans (Hanson et al., 2013). Based on the reasons exposed here, I believe an approach aimed at increasing ApoE4 lipidation would be more appropriate than increasing its levels.

Another approach aimed at altering and improving ApoE4 function is based on designing structural correctors, with the intent of making ApoE4 structurally similar to ApoE3. These small molecules have proven successful in attenuating ApoE4 gain of toxic functions related to A β and Tau pathologies as well as neuronal degeneration, in human pluripotent stem cells-derived neurons (Wang et al., 2018).

Differential self-assembly of rApoE isoforms was the only clear structural difference that I could identify. This property, specific to rApoE4, could be used to identify and test for novel structural correctors based on ThT fluorescence or on TEM experiments.

6.5. Concluding remarks

In addition to the clear genetic links identified in 1993, researchers have established explicit associations between ApoE and pathologies occurring in AD. This thesis aimed at going beyond pathological hallmarks and characterise the role of ApoE in increasing vulnerability to AD onset (Fig. 6.4). With this in mind, ApoE biology was explored in the context of self-assembly, oxidative stress and ageing. While extremely distinct, these three contexts are part of the background events interacting to enable AD pathogenesis and development. I showed that rApoE4 had a unique propensity to self-assemble, and this ability could be detrimental, provided it occurs with ApoE4 in the human brain. Moreover, I showed that ApoE was associated with response to oxidative insults using cell models, and that all three rApoE isoforms have intrinsic antioxidant abilities. Their difference in primary sequence could result in further differences at the antioxidant level, with ApoE2 and ApoE3 outperforming ApoE4. Finally, temporal changes in ApoE across lifespan could have a great impact on antioxidant status and on ageing itself. These findings go beyond AD pathology and are relevant to a number of other neurodegenerative disorders. Further understanding of how our genetic backgrounds interact with our environments will be key in tackling AD and more generally neurodegeneration. Prevention of disease onset may be, in the end, more effective than treatment.

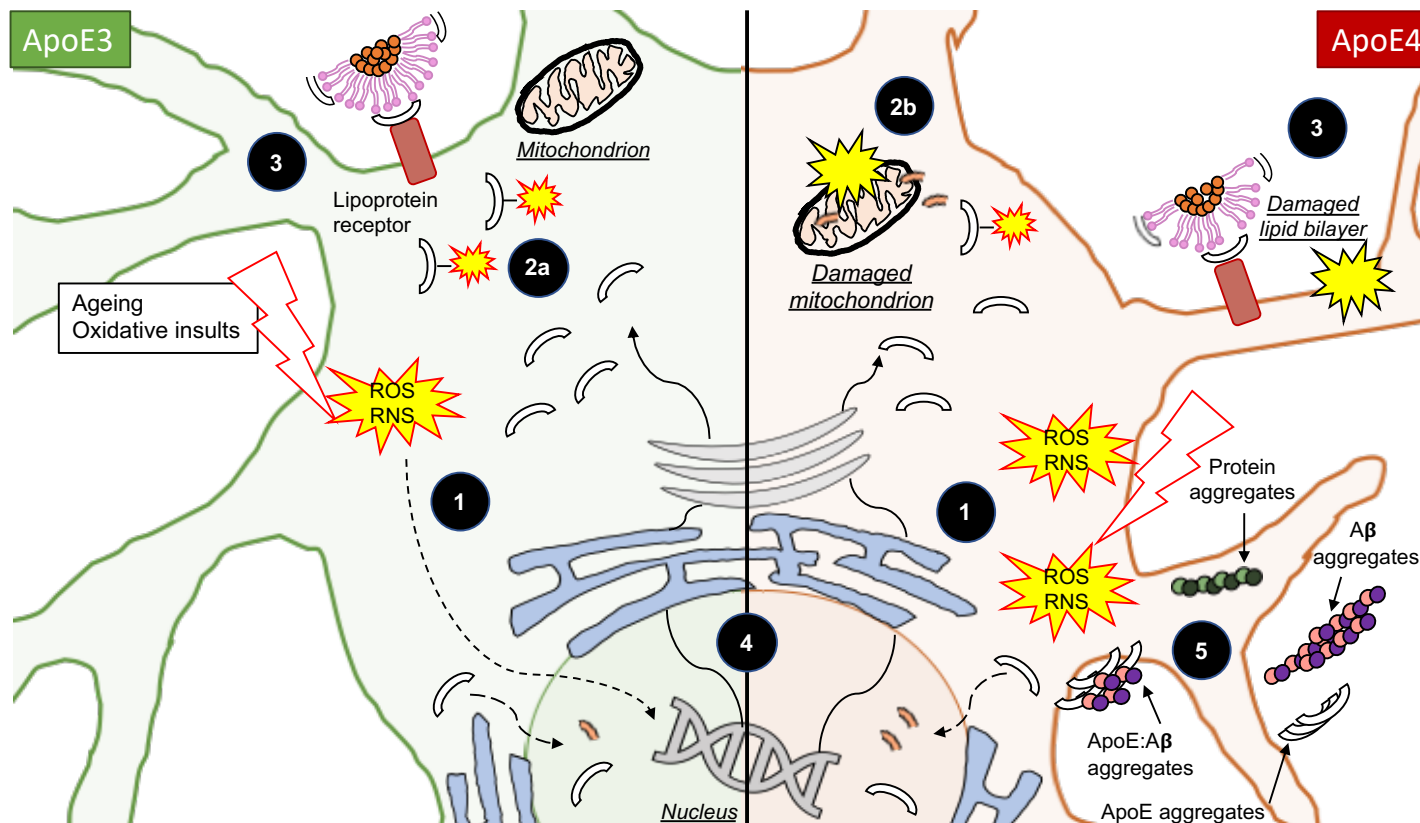


Figure 6.4 Summary

Following excitotoxic stress, neurons produce ApoE, with $APOE3 > APOE4$ at the transcript level (1). Neuronal ApoE may act as a ROS/RNS scavenger, with ApoE3 outperforming ApoE4 (2a). However, neuronal ApoE may be detrimental due to proteolytic cleavage (ApoE4>ApoE3). Fragments can damage organelles such as mitochondria (2b). Astrocyte-secreted ApoE aids in repairing membranes following injury, with ApoE3>ApoE4. ApoE4 is poorly lipidated compared to ApoE3 (3). ApoE can also be found in the nucleus, where it can fragment, with the proportion of fragmented ApoE4>ApoE3 (4). Accumulating damage can lead to intra- and extracellular protein aggregation: ApoE4>ApoE3.

Bibliography

- Abedinzadeh, Z., Gardes-Albert, M., and Ferradini, C. 1989. "Kinetic Study of the Oxidation Mechanism of Glutathione by Hydrogen Peroxide in Neutral Aqueous Medium." *Canadian Journal of Chemistry* 67 (7): 1247–55. <https://doi.org/10.1139/v89-190>.
- About, O., Mrak, R.E., Boop, F., and Griffin, S.T. 2012. "Apolipoprotein Epsilon 3 Alleles Are Associated with Indicators of Neuronal Resilience." *BMC Medicine* 10. <https://doi.org/10.1186/1741-7015-10-35>.
- Acharya, P., Segall, M.L., Zaiou, M., Morrow, J.A., Weisgraber, K.H., Phillips, M.C., Lund-Katz, S., and Snow, J. 2002. "Comparison of the Stabilities and Unfolding Pathways of Human Apolipoprotein E Isoforms by Differential Scanning Calorimetry and Circular Dichroism." *Biochimica et Biophysica Acta (BBA) - Molecular and Cell Biology of Lipids* 1584 (1): 9–19. [https://doi.org/10.1016/S1388-1981\(02\)00263-9](https://doi.org/10.1016/S1388-1981(02)00263-9).
- Aggerbeck, L.P., Wetterau, J.R., Weisgraber, K.H., Wu, C.-S.C., and Lindgren, F.T. 1988. "Human Apolipoprotein E3 in Aqueous Solution II. Properties of the Amino- and Carboxyl-Terminal Domains*." *Journal of Biological Chemistry* 263 (13): 6249–58.
- Aizawa, Y., Fukatsu, R., Takamaru, Y., Tsuzuki, K., Chiba, H., Kobayashi, K., Fujii, N., and Takahata, N. 1997. "Amino-Terminus Truncated Apolipoprotein E Is the Major Species in Amyloid Deposits in Alzheimer's Disease-Affected Brains: A Possible Role for Apolipoprotein E in Alzheimer's Disease." *Brain Research* 768 (1–2): 208–14. [https://doi.org/10.1016/S0006-8993\(97\)00640-9](https://doi.org/10.1016/S0006-8993(97)00640-9).
- Al-hilaly, Y.K., Williams, T.L., Stewart-parker, M., Ford, L., Skaria, E., Cole, M., Bucher, W.G., et al. 2013. "A Central Role for Dityrosine Crosslinking of Amyloid- β in Alzheimer's Disease," 1–17.
- Aledo, J.C. 2019. "Methionine in Proteins: The Cinderella of the Proteinogenic Amino Acids." *Protein Science* 28 (10): 1785–96. <https://doi.org/10.1002/pro.3698>.
- Aleshkov, S., Abraham, C.R., and Zannis, V.I. 1997. "Interaction of Nascent Apoe2, Apoe3, and Apoe4 Isoforms Expressed in Mammalian Cells with Amyloid Peptide ?? (1-40). Relevance to Alzheimer's Disease." *Biochemistry* 36 (34): 10571–80. <https://doi.org/10.1021/bi9626362>.
- Alzheimer's Association. 2017. "2017 Alzheimer's Disease Facts and Figures." *Alzheimers Dement* 13: 325–73.
- Alzheimer's Disease International. 2008. "The Prevalence of Dementia Worldwide." *Alzheimer's Disease International*, no. December: 1–2. <https://doi.org/10.1097/00002093-198802040-00015>.
- Anantharamaiah, G.M., Hughes, T.A., Iqbal, M., Gawish, A., Neame, P.J., Medley, M.F., and

- Segrest, J.P. 1988. "Effect of Oxidation on the Properties of Apolipoproteins A-1 and A-II." *Journal of Lipid Research* 29 (3): 309–18.
- Anfinsen, C.B. 1973. "Principles That Govern the Folding of Protein Chains." *Science* 181 (4096): 223–30.
- Ansari, M.A., and Scheff, S.W. 2010. "Oxidative Stress in the Progression of Alzheimer Disease in the Frontal Cortex" 69 (2): 155–67.
- Aoki, K., Uchihara, T., Sanjo, N., Nakamura, A., Ikeda, K., Tsuchiya, K., and Wakayama, Y. 2003. "Increased Expression of Neuronal Apolipoprotein E in Human Brain with Cerebral Infarction." *Stroke* 34 (4): 875–80. <https://doi.org/10.1161/01.STR.0000064320.73388.C6>.
- Argyri, L., Skamnaki, V., Stratikos, E., and Chroni, A. 2011. "A Simple Approach for Human Recombinant Apolipoprotein E4 Expression and Purification." *Protein Expression and Purification* 79 (2): 251–57. <https://doi.org/10.1016/j.pep.2011.06.011>.
- Baker-Nigh, A.T., Mawuenyega, K.G., Bollinger, J.G., Ovod, V., Kasten, T., Franklin, E.E., Liao, F., et al. 2016. "Human Central Nervous System (CNS) ApoE Isoforms Are Increased by Age, Differentially Altered by Amyloidosis, and Relative Amounts Reversed in the CNS Compared with Plasma." *Journal of Biological Chemistry* 291 (53): 27204–18. <https://doi.org/10.1074/jbc.M116.721779>.
- Bales, K.R., Liu, F., Wu, S., Lin, S., Koger, D., DeLong, C., Hansen, J.C., Sullivan, P.M., and Paul, S.M. 2009. "Human APOE Isoform-Dependent Effects on Brain β -Amyloid Levels in PDAPP Transgenic Mice." *Journal of Neuroscience* 29 (21): 6771–79. <https://doi.org/10.1523/JNEUROSCI.0887-09.2009>.
- Bales, K.R., Verina, T., Cummins, D.J., Du, Y., Dodel, R.C., Saura, J., Fishman, C.E., et al. 1999. "Apolipoprotein E Is Essential for Amyloid Deposition in the APPV717F Transgenic Mouse Model of Alzheimer's Disease." *Proceedings of the National Academy of Sciences* 96 (26): 15233–38. <https://doi.org/10.1073/pnas.96.26.15233>.
- Balu, D., Karstens, A.J., Loukenas, E., Maldonado Weng, J., York, J.M., Valencia-Olvera, A.C., and LaDu, M.J. 2019. "The Role of APOE in Transgenic Mouse Models of AD." *Neuroscience Letters* 707 (May): 134285. <https://doi.org/10.1016/j.neulet.2019.134285>.
- Barbier, A., Clément-Collin, V., Dergunov, A.D., Visvikis, A., Siest, G., and Aggerbeck, L.P. 2006. "The Structure of Human Apolipoprotein E2, E3 and E4 in Solution: 1. Tertiary and Quaternary Structure." *Biophysical Chemistry* 119 (2): 158–69. <https://doi.org/10.1016/j.bpc.2005.07.010>.
- Basaiawmoit, R.V., and Rattan, S.I.S. 2010. "Cellular Stress and Protein Misfolding During Aging." In *Methods in Molecular Biology*, 648:107–17. https://doi.org/10.1007/978-1-60761-756-3_7.

- Beffert, U., Cohn, J.S., Petit-Turcotte, C., Tremblay, M., Aumont, N., Ramassamy, C., Davignon, J., and Poirier, J. 1999. "Apolipoprotein E and β -Amyloid Levels in the Hippocampus and Frontal Cortex of Alzheimer's Disease Subjects Are Disease-Related and Apolipoprotein E Genotype Dependent." *Brain Research* 843 (1–2): 87–94. [https://doi.org/10.1016/S0006-8993\(99\)01894-6](https://doi.org/10.1016/S0006-8993(99)01894-6).
- Behl, C., Davis, J.B., Lesley, R., and Schubert, D. 1994. "Hydrogen Peroxide Mediates Amyloid β Protein Toxicity." *Cell* 77 (6): 817–27. [https://doi.org/10.1016/0092-8674\(94\)90131-7](https://doi.org/10.1016/0092-8674(94)90131-7).
- Beisiegel, U., Weber, W., and Ihrke, G. 1989. "The LDL-Receptor-Related Protein, LRP, Is an Apolipoprotein E-Binding Protein" 341 (September): 162–64.
- Belloy, M.E., Napolioni, V., and Greicius, M.D. 2019. "A Quarter Century of APOE and Alzheimer's Disease: Progress to Date and the Path Forward." *Neuron* 101 (5): 820–38. <https://doi.org/10.1016/j.neuron.2019.01.056>.
- Bertrand, P., Poirier, J., Oda, T., Finch, C.E., and Pasinetti, G.M. 1995. "Association of Apolipoprotein E Genotype with Brain Levels of Apolipoprotein E and Apolipoprotein J (Clusterin) in Alzheimer Disease." *Molecular Brain Research* 33 (1): 174–78. [https://doi.org/10.1016/0169-328X\(95\)00097-C](https://doi.org/10.1016/0169-328X(95)00097-C).
- Bordoni, M., Pansarasa, O., Dell'Orco, M., Crippa, V., Gagliardi, S., Sproviero, D., Bernuzzi, S., et al. 2019. "Nuclear Phospho-SOD1 Protects DNA from Oxidative Stress Damage in Amyotrophic Lateral Sclerosis." *Journal of Clinical Medicine* 8 (5): 729. <https://doi.org/10.3390/jcm8050729>.
- Boschert, U., Merlo-Pich, E., Higgins, G., Roses, A.D., and Catsicas, S. 1999. "Apolipoprotein E Expression by Neurons Surviving Excitotoxic Stress." *Neurobiol Dis* 6: 508–14. <https://doi.org/10.1006/nbdi.1999.0251>.
- Bour, A., Grootendorst, J., Vogel, E., Kelche, C., Dodart, J.C., Bales, K.R., Moreau, P.H., Sullivan, P.M., and Mathis, C. 2008. "Middle-Aged Human ApoE4 Targeted-Replacement Mice Show Retention Deficits on a Wide Range of Spatial Memory Tasks." *Behavioural Brain Research* 193 (2): 174–82. <https://doi.org/10.1016/j.bbr.2008.05.008>.
- Boyles, J.K., Pitas, R.E., Wilson, E., Mahley, R.W., and Taylor, J.M. 1985. "Apolipoprotein E Associated with Astrocytic Glia of the Central Nervous System and with Nonmyelinating Glia of the Peripheral Nervous System." *Journal of Clinical Investigation* 76 (4): 1501–13. <https://doi.org/10.1172/JCI112130>.
- Boyles, J.K., Zoellner, C.D., Anderson, L.J., Kosik, L.M., Pitas, R.E., Weisgraber, K.H., Hui, D.Y., Mahley, R.W., Gebicke-Haerter, P.J., and Ignatius, M.J. 1989. "A Role for Apolipoprotein E, Apolipoprotein A-I, and Low Density Lipoprotein Receptors in Cholesterol Transport during Regeneration and Remyelination of the Rat Sciatic Nerve." *Journal of Clinical Investigation* 83 (3): 1015–31. <https://doi.org/10.1172/JCI113943>.

- Brecht, W.J., Harris, F.M., Chang, S., Tesseur, I., Yu, G.-Q., Xu, Q., Fish, J.D., et al. 2004. "Neuron-Specific Apolipoprotein E4 Proteolysis Is Associated with Increased Tau Phosphorylation in Brains of Transgenic Mice" 24 (10): 2527–34. <https://doi.org/10.1523/JNEUROSCI.4315-03.2004>.
- Bu, G. 2009. "Apolipoprotein E and Its Receptors in Alzheimer's Disease: Pathways, Pathogenesis and Therapy." *Nature Reviews Neuroscience* 10 (5): 333–44. <https://doi.org/10.1038/nrn2620>.
- Burns, A., and Iliffe, S. 2009. "Alzheimer's Disease." *BMJ* 338 (feb05 1): b158–b158. <https://doi.org/10.1136/bmj.b158>.
- Cardin, A.D., Hirose, N., Blankenship, D.T., Jackson, R.L., Harmony, J.A.K., Sparrow, D.A., and Sparrow, J.T. 1986. "Binding of a High Reactive Heparin to Human Apolipoprotein E: Identification of Two Heparin-Binding Domains." *Biochemical and Biophysical Research Communications* 134 (2): 783–89. [https://doi.org/10.1016/S0006-291X\(86\)80489-2](https://doi.org/10.1016/S0006-291X(86)80489-2).
- Castellani, R.J., Zhu, X., Lee, H.G., Smith, M.A., and Perry, G. 2009. "Molecular Pathogenesis of Alzheimer's Disease: Reductionist versus Expansionist Approaches." *International Journal of Molecular Sciences* 10 (3): 1386–1406. <https://doi.org/10.3390/ijms10031386>.
- Chambers, M.C., Maclean, B., Burke, R., Amodei, D., Ruderman, D.L., Neumann, S., Gatto, L., et al. 2012. "A Cross-Platform Toolkit for Mass Spectrometry and Proteomics." *Nature Biotechnology* 30 (10): 918–20. <https://doi.org/10.1038/nbt.2377>.
- Chen, G.C., Hamilton, R.L., Kane, J.P., Guo, L.S.S., Gordon, V., and Richards, E.G. 1984. "Circular Dichroic Spectra of Apolipoprotein E in Model Complexes and Cholesterol-Rich Lipoproteins: Lipid Contribution." *Biochemistry* 23 (26): 6530–38. <https://doi.org/10.1021/bi00321a039>.
- Chen, J., Li, Q., and Wang, J. 2011. "Topology of Human Apolipoprotein E3 Uniquely Regulates Its Diverse Biological Functions." *Proceedings of the National Academy of Sciences* 108 (36): 14813–18. <https://doi.org/10.1073/pnas.1106420108>.
- Chen, Jen-hau, Lin, K., and Chen, Y. 2009. "Risk Factors for Dementia." *Journal of the Formosan Medical Association* 108 (10): 754–64. [https://doi.org/10.1016/S0929-6646\(09\)60402-2](https://doi.org/10.1016/S0929-6646(09)60402-2).
- Chen, Y., Chen, K., Zhang, J., Li, X., Shu, N., Wang, J., Zhang, Z., and Reiman, E.M. 2015. "Disrupted Functional and Structural Networks in Cognitively Normal Elderly Subjects with the APOE E4 Allele." *Neuropsychopharmacology* 40 (5): 1181–91. <https://doi.org/10.1038/npp.2014.302>.
- Chin-Chan, M., Navarro-Yepes, J., and Quintanilla-Vega, B. 2015. "Environmental Pollutants as Risk Factors for Neurodegenerative Disorders: Alzheimer and Parkinson Diseases." *Frontiers in Cellular Neuroscience* 9 (April): 124. <https://doi.org/10.3389/fncel.2015.00124>.

- Chou, C.-Y., Lin, Y.-L., Huang, Y.-C., Sheu, S.-Y., Lin, T.-H., Tsay, H.-J., Chang, G.-G., and Shiao, M.-S. 2005. "Structural Variation in Human Apolipoprotein E3 and E4: Secondary Structure, Tertiary Structure, and Size Distribution." *Biophysical Journal* 88 (1): 455–66. <https://doi.org/10.1529/biophysj.104.046813>.
- Clément-Collin, V., Barbier, A., Dergunov, A.D., Visvikis, A., Siest, G., Desmadril, M., Takahashi, M., and Aggerbeck, L.P. 2006. "The Structure of Human Apolipoprotein E2, E3 and E4 in Solution. 2. Multidomain Organization Correlates with the Stability of ApoE Structure." *Biophysical Chemistry* 119 (2): 170–85. <https://doi.org/10.1016/j.bpc.2005.07.009>.
- Cole, J.L. 2000. "CENTRIFUGATION | Analytical Ultracentrifugation." In *Encyclopedia of Separation Science*, 313–19. John Wiley Humana Press Springer-Verlag BioafTnity Chromatography Elsevier. <https://doi.org/10.1016/b0-12-226770-2/07311-7>.
- Corder, E.H., Saunders, A.M., Risch, N.J., Strittmatter, W.J., Schmechel, D.E., Gaskell, Jr., P.C., Rimmler, J.B., et al. 1994. "Protective Effect of Apolipoprotein E Type 2 Allele for Late Onset Alzheimer Disease." *Nature Genetics* 7: 180–84.
- Corder, E.H., Saunders, A.M., Schmechel, D.E., Gaskell, P.C., Small, G.W., and Roses, A.D. 1993. "Gene Dose of Apolipoprotein E Type 4 Allele and the Risk of Alzheimer ' s Disease in Late Onset Families." *Science*, 921–24.
- Cremers, C.M., and Jakob, U. 2013. "Oxidant Sensing by Reversible Disulfide Bond Formation." *Journal of Biological Chemistry* 288 (37): 26489–96. <https://doi.org/10.1074/jbc.R113.462929>.
- Crisanti, M.M., and Matthews, C.R. 1981. "Characterization of the Slow Steps in the Folding of the a Subunit of Tryptophan Synthase." *Biochemistry* 20 (9): 2700–2706. <https://doi.org/10.1021/bi00512a052>.
- Dalle-Donne, I., Giustarini, D., Colombo, R., Rossi, R., and Milzani, A. 2003. "Protein Carbonylation in Human Diseases." *Trends in Molecular Medicine* 9 (4): 169–76. [https://doi.org/10.1016/S1471-4914\(03\)00031-5](https://doi.org/10.1016/S1471-4914(03)00031-5).
- Dalle-Donne, I., Rossi, R., Colombo, R., Giustarini, D., and Milzani, A. 2006. "Biomarkers of Oxidative Damage in Human Disease." *Clinical Chemistry* 52 (4): 601–23. <https://doi.org/10.1373/clinchem.2005.061408>.
- Davies, C.A., Mann, D.M.A., Sumpter, P.Q., and Yates, P.O. 1987. "A Quantitative Morphometric Analysis of the Neuronal and Synaptic Content of the Frontal and Temporal Cortex in Patients with Alzheimer's Disease." *Journal of the Neurological Sciences* 78 (2): 151–64. [https://doi.org/10.1016/0022-510X\(87\)90057-8](https://doi.org/10.1016/0022-510X(87)90057-8).
- Davies, M.J. 2005. "The Oxidative Environment and Protein Damage." *Biochimica et Biophysica Acta - Proteins and Proteomics* 1703 (2): 93–109. <https://doi.org/10.1016/j.bbapap.2004.08.007>.

- Davies, P., and Maloney, A.J.F. 1976. "SELECTIVE LOSS OF CENTRAL CHOLINERGIC NEURONS IN ALZHEIMER'S DISEASE." *The Lancet* 308 (8000): 1403. [https://doi.org/10.1016/S0140-6736\(76\)91936-X](https://doi.org/10.1016/S0140-6736(76)91936-X).
- Deane, R., Sagare, A., Hamm, K., Parisi, M., Lane, S., Finn, M.B., Holtzman, D.M., and Zlokovic, B. V. 2008. "ApoE Isoform – Specific Disruption of Amyloid β Peptide Clearance from Mouse Brain." *The Journal of Clinical Investigation* 118 (12): 4002–13. <https://doi.org/10.1172/JCI36663DS1>.
- Deary, I.J., Whiteman, M.C., Pattie, A., Starr, J.M., Hayward, C., Wright, A.F., Carothers, A., and Whalley, L.J. 2002. "Ageing: Cognitive Change and the APOE E4 Allele." *Nature* 418 (6901): 932. <https://doi.org/10.1038/418932a>.
- Debernardi, R., Pierre, K., Lengacher, S., Magistretti, P.J., and Pellerin, L. 2003. "Cell-Specific Expression Pattern of Monocarboxylate Transporters in Astrocytes and Neurons Observed in Different Mouse Brain Cortical Cell Cultures." *Journal of Neuroscience Research* 73 (2): 141–55. <https://doi.org/10.1002/jnr.10660>.
- deGruyter, J.N., Malins, L.R., and Baran, P.S. 2017. "Residue-Specific Peptide Modification: A Chemist's Guide." *Biochemistry* 56 (30): 3863–73. <https://doi.org/10.1021/acs.biochem.7b00536>.
- Dergunov, A.D., Shuvaev, V. V., and Yanushevskaja, E. V. 1992. "Quaternary Structure of Apolipoprotein E in Solution: Fluorimetric, Chromatographie and Immunochemical Studies." *Biological Chemistry Hoppe-Seyler*. West Germany. <https://doi.org/10.1515/bchm3.1992.373.1.323>.
- Diedrich, J.F., Minnigan, H., Carp, R.I., Whitaker, J.N., Race, R., Frey, W., and Haase, A.T. 1991. "Neuropathological Changes in Scrapie and Alzheimer's Disease Are Associated with Increased Expression of Apolipoprotein E and Cathepsin D in Astrocytes." *Journal of Virology* 65 (9): 4759–68.
- Dobson, C.M. 2003. "Protein Folding and Misfolding." *Nature* 426 (6968): 884–90. <https://doi.org/10.1038/nature02261>.
- Dobson, C.M., Swoboda, B.E.P., Joniau, M., and Weissman, C. 2001. "The Structural Basis of Protein Folding and Its Links with Human Disease." *Philosophical Transactions of the Royal Society B: Biological Sciences* 356 (1406): 133–45. <https://doi.org/10.1098/rstb.2000.0758>.
- Domon, B., and Aebersold, R. 2006. "Mass Spectrometry and Protein Analysis." *Science* 312 (5771): 212–17. <https://doi.org/10.1126/science.1124619>.
- Dong, L., and Weisgraber, K.H. 1996. "Human Apolipoprotein E4 Domain Interaction: Arginine 61 and Glutamic Acid 255 Interact to Direct the Preference for Very Low Density Lipoproteins." *Journal of Biological Chemistry* 271 (32): 19053–57. <https://doi.org/10.1074/jbc.271.32.19053>.

- Dong, L., Wilson, C., Wardells, M.R., Simmons, T., Mahley, R.W., Weisgraber, K.H., and Agard, D.A. 1994. "Human Apolipoprotein E: Role of Arginine 61 in Mediating the Lipoprotein Preferences of the E3 and E4 Isoforms." *The Journal of Biological Chemistry* 269 (September 2): 22358–65.
- Dose, J., Huebbe, P., Nebel, A., and Rimbach, G. 2016. "APOE Genotype and Stress Response - a Mini Review." *Lipids in Health and Disease* 15 (1): 121. <https://doi.org/10.1186/s12944-016-0288-2>.
- Eanes, E.D., and Glenner, G.G. 1968. "X-Ray Diffraction Studies on Amyloid Filaments." *Journal of Histochemistry & Cytochemistry* 16 (11): 673–77. <https://doi.org/10.1177/16.11.673>.
- Elliott, D.A., Halliday, G.M., and Garner, B. 2010. "Apolipoprotein-E Forms Dimers in Human Frontal Cortex and Hippocampus." *BMC Neuroscience* 11 (23). <https://doi.org/10.1186/1471-2202-11-23>.
- Elliott, D.A., Kim, W.S., Jans, D.A., and Garner, B. 2007. "Apoptosis Induces Neuronal Apolipoprotein-E Synthesis and Localization in Apoptotic Bodies" 416: 206–10. <https://doi.org/10.1016/j.neulet.2007.02.014>.
- Evans, K.C., Berger, E.P., Choon, C.G., Weisgraber, K.H., and Lansbury, P.T. 1995. "Apolipoprotein E Is a Kinetic but Not a Thermodynamic Inhibitor of Amyloid Formation: Implications for the Pathogenesis and Treatment of Alzheimer Disease." *Proceedings of the National Academy of Sciences of the United States of America* 92 (3): 763–67. <https://doi.org/10.1073/pnas.92.3.763>.
- Evans, S., Dowell, N.G., Tabet, N., Tofts, P.S., King, S.L., and Rusted, J.M. 2014. "Cognitive and Neural Signatures of the APOE E4 Allele in Mid-Aged Adults." *Neurobiology of Aging* 35 (7): 1615–23. <https://doi.org/10.1016/j.neurobiolaging.2014.01.145>.
- Fakhoury, M. 2018. "Microglia and Astrocytes in Alzheimer's Disease: Implications for Therapy." *Current Neuropharmacology* 16 (5): 508–18. <https://doi.org/10.2174/1570159X15666170720095240>.
- Farrer, L.A., Cupples, L.A., Haines, J.L., Hyman, B.T., Kukull, W.A., Mayeux, R., Myers, R.H., Pericak-Vance, M.A., Risch, N.J., and Duijn, C. van. 1997. "Effects of Age, Sex, and Ethnicity on the Association Between Apolipoprotein E Genotype and Alzheimer Disease." *JAMA* 278 (16): 1349. <https://doi.org/10.1001/jama.1997.03550160069041>.
- Fenoglio, C., Scarpini, E., Serpente, M., and Galimberti, D. 2018. "Role of Genetics and Epigenetics in the Pathogenesis of Alzheimer's Disease and Frontotemporal Dementia." Edited by G. Perry, J. Avila, M. Tabaton, and X. Zhu. *Journal of Alzheimer's Disease* 62 (3): 913–32. <https://doi.org/10.3233/JAD-170702>.
- Ferguson, S., Mouzon, B., Kayihan, G., Wood, M., Poon, F., Doore, S., Mathura, V., et al. 2010. "Apolipoprotein E Genotype and Oxidative Stress Response to Traumatic Brain Injury."

- Neuroscience* 168 (3): 811–19. <https://doi.org/10.1016/j.neuroscience.2010.01.031>.
- Flurkey, K., Curren, J.M., and Harrison, D.E. 2007. "Mouse Models in Aging Research." In *The Mouse in Biomedical Research*, 637–72. Elsevier. <https://doi.org/10.1016/B978-012369454-6/50074-1>.
- Frisoni, G.B., Louhija, J., Geroldi, C., and Trabucchi, M. 2001. "Longevity and the E2 Allele of Apolipoprotein E: The Finnish Centenarians Study." *Journals of Gerontology - Series A Biological Sciences and Medical Sciences* 56 (2): 100–101. <https://doi.org/10.1093/gerona/56.2.M75>.
- Fu, Y., Zhao, J., Atagi, Y., Nielsen, H.M., Liu, C.C., Zheng, H., Shinohara, M., Kanekiyo, T., and Bu, G. 2016. "Apolipoprotein e Lipoprotein Particles Inhibit Amyloid- β Uptake through Cell Surface Heparan Sulphate Proteoglycan." *Molecular Neurodegeneration* 11 (1): 1–11. <https://doi.org/10.1186/s13024-016-0099-y>.
- Garai, K., Baban, B., and Frieden, C. 2011. "Self-Association and Stability of the ApoE Isoforms at Low PH: Implications for ApoE-Lipid Interactions." *Biochemistry* 50 (29): 6356–64. <https://doi.org/10.1021/bi2006702>.
- Ghosh, S., Sil, T.B., Dolai, S., and Garai, K. 2019. "High-affinity Multivalent Interactions between Apolipoprotein E and the Oligomers of Amyloid- β ." *The FEBS Journal*, febs.14988. <https://doi.org/10.1111/febs.14988>.
- Giri, M., Zhang, M., and Lü, Y. 2016. "Genes Associated with Alzheimer's Disease: An Overview and Current Status." *Clinical Interventions in Aging* 11: 665–81. <https://doi.org/10.2147/CIA.S105769>.
- Glenner, G.G., and Wong, C.W. 1984. "Alzheimer's Disease: Initial Report of the Purification and Characterization of a Novel Cerebrovascular Amyloid Protein." *Biochemical and Biophysical Research Communications* 120 (3): 885–90. [https://doi.org/10.1016/S0006-291X\(84\)80190-4](https://doi.org/10.1016/S0006-291X(84)80190-4).
- Glöckner, F., Meske, V., and Ohm, T.G. 2002. "Genotype-Related Differences of Hippocampal Apolipoprotein E Levels Only in Early Stages of Neuropathological Changes in Alzheimer's Disease." *Neuroscience* 114 (4): 1103–14. [https://doi.org/10.1016/S0306-4522\(02\)00178-1](https://doi.org/10.1016/S0306-4522(02)00178-1).
- Gluck, M.R., Jayatileke, E., Shaw, S., Rowan, A.J., and Haroutunian, V. 2000. "CNS Oxidative Stress Associated with the Kainic Acid Rodent Model of Experimental Epilepsy." *Epilepsy Research* 39 (1): 63–71. [https://doi.org/10.1016/S0920-1211\(99\)00111-4](https://doi.org/10.1016/S0920-1211(99)00111-4).
- Goldsbury, C., Baxa, U., Simon, M.N., Steven, A.C., Engel, A., Wall, J.S., Aebi, U., and Müller, S.A. 2011. "Amyloid Structure and Assembly: Insights from Scanning Transmission Electron Microscopy." *Journal of Structural Biology* 173 (1): 1–13. <https://doi.org/10.1016/j.jsb.2010.09.018>.

- Gómez-Ramos, A., Díaz-Nido, J., Smith, M.A., Perry, G., and Avila, J. 2003. "Effect of the Lipid Peroxidation Product Acrolein on Tau Phosphorylation in Neural Cells." *Journal of Neuroscience Research* 71 (6): 863–70. <https://doi.org/10.1002/jnr.10525>.
- Greenfield, N. 2007. "Using Circular Dichroism Spectra to Estimate Protein Secondary Structure." *Nat Protoc.* 1 (6): 2876–90. <https://doi.org/10.1038/nprot.2006.202>. Using.
- Greenfield, N.J., and Hitchcock-Degregori, S.E. 1993. "Conformational Intermediates in the Folding of a Coiled-Coil Model Peptide of the N-Terminus of Tropomyosin and α -Tropomyosin." *Protein Science* 2 (8): 1263–73. <https://doi.org/10.1002/pro.5560020809>.
- Hanson, A.J., Bayer-Carter, J.L., Green, P.S., Montine, T.J., Wilkinson, C.W., Baker, L.D., Watson, G.S., et al. 2013. "Effect of Apolipoprotein e Genotype and Diet on Apolipoprotein e Lipidation and Amyloid Peptides Randomized Clinical Trial." *JAMA Neurology* 70 (8): 972–80. <https://doi.org/10.1001/jamaneurol.2013.396>.
- Hardy, J.A., and Higgins, G.A. 1992. "Alzheimer ' s Disease : The Amyloid Cascade Hypothesis Published by : American Association for the Advancement of Science Alzheimer ' s Disease : The Amyloid Cascade Hypothesis." *Science* 256 (5054): 184–85.
- Harold, D., Abraham, R., Hollingworth, P., Sims, R., Hamshere, M., Pahwa, J.S., Moskvin, V., et al. 2009. "Genome-Wide Association Study Identifies Variants at CLU and PICALM Associated with Alzheimer's Disease, and Shows Evidence for Additional Susceptibility Genes." *Nature Genetics* 41 (10): 1088–93. <https://doi.org/10.1038/ng.440>. Genome-wide.
- Harris, F.M., Brecht, W.J., Xu, Q., Tesseur, I., Kekoni, L., Wyss-Coray, T., Fish, J.D., et al. 2003. "Carboxyl-Terminal-Truncated Apolipoprotein E4 Causes Alzheimer's Disease-like Neurodegeneration and Behavioral Deficits in Transgenic Mice." *Proceedings of the National Academy of Sciences of the United States of America* 100 (19): 10966–71. <https://doi.org/10.1073/pnas.1434398100>.
- Hatters, D.M., Zhong, N., Rutenber, E., and Weisgraber, K.H. 2006. "Amino-Terminal Domain Stability Mediates Apolipoprotein E Aggregation into Neurotoxic Fibrils." *Journal of Molecular Biology.* <https://doi.org/10.1016/j.jmb.2006.06.080>.
- Havel, R.J., and Kane, J.P. 1973. "Primary Dysbetalipoproteinemia: Predominance of a Specific Apoprotein Species in Triglyceride-Rich Lipoproteins." *Proceedings of the National Academy of Sciences of the United States of America* 70 (7): 2015–19. <https://doi.org/10.1073/pnas.70.7.2015>.
- Hayek, T., Oiknine, J., Brook, J.G., and Aviram, M. 1994. "Increased Plasma and Lipoprotein Lipid Peroxidation in Apo E-Deficient Mice." *Biochemical and Biophysical Research Communications.* <https://doi.org/10.1006/bbrc.1994.1883>.
- Hirsch-Reinshagen, V., Maia, L.F., Burgess, B.L., Blain, J.F., Naus, K.E., Mclsaac, S.A., Parkinson, P.F., et al. 2005. "The Absence of ABCA1 Decreases Soluble ApoE Levels but

- Does Not Diminish Amyloid Deposition in Two Murine Models of Alzheimer Disease.” *Journal of Biological Chemistry* 280 (52): 43243–56. <https://doi.org/10.1074/jbc.M508781200>.
- Hollingworth, P., Harold, D., Sims, R., Gerrish, A., Lambert, J.C., Carrasquillo, M.M., Abraham, R., et al. 2011. “Common Variants at ABCA7, MS4A6A/MS4A4E, EPHA1, CD33 and CD2AP Are Associated with Alzheimer’s Disease.” *Nature Genetics* 43 (5): 429–36. <https://doi.org/10.1038/ng.803>.
- Huang, W.-J., Zhang, X., and Chen, W.-W. 2016. “Role of Oxidative Stress in Alzheimer’s Disease.” *Biomedical Reports* 4 (5): 519–22. <https://doi.org/10.3892/br.2016.630>.
- Huang, Y.-W.A., Zhou, B., Wernig, M., and Südhof, T.C. 2017. “ApoE2, ApoE3, and ApoE4 Differentially Stimulate APP Transcription and A β Secretion.” *Cell* 168 (3): 427–441.e21. <https://doi.org/10.1016/j.cell.2016.12.044>.
- Huang, Y., Liu, X.Q., Wyss-Coray, T., Brecht, W.J., Sanan, D.A., and Mahley, R.W. 2001. “Apolipoprotein E Fragments Present in Alzheimer’s Disease Brains Induce Neurofibrillary Tangle-like Intracellular Inclusions in Neurons.” *Proceedings of the National Academy of Sciences of the United States of America* 98: 8838–43. <https://doi.org/10.1073/pnas.151254698>.
- Huang, Y., and Mahley, R.W. 2014. “Apolipoprotein E: Structure and Function in Lipid Metabolism, Neurobiology, and Alzheimer’s Diseases.” *Neurobiology of Disease* 72 (Part A): 3–12. <https://doi.org/10.1016/j.nbd.2014.08.025>.
- Huebbe, P., Jofre-Monseny, L., Boesch-Saadatmandi, C., Minihane, A.M., and Rimbach, G. 2007. “Effect of ApoE Genotype and Vitamin E on Biomarkers of Oxidative Stress in Cultured Neuronal Cells and the Brain of Targeted Replacement Mice.” *Journal of Physiology and Pharmacology* 58 (4): 683–98.
- Hummon, A.B., Lim, S.R., Difilippantonio, M.J., and Ried, T. 2007. “Isolation and Solubilization of Proteins after TRIzol® Extraction of RNA and DNA from Patient Material Following Prolonged Storage.” *BioTechniques* 42 (4): 467–72. <https://doi.org/10.2144/000112401>.
- Ignatius, M.J., Gebicke-Harter, P.J., Skene, J.H., Schilling, J.W., Weisgraber, K.H., Mahley, R.W., and Shooter, E.M. 1986. “Expression of Apolipoprotein E during Nerve Degeneration and Regeneration.” *Proceedings of the National Academy of Sciences* 83 (4): 1125–29. <https://doi.org/10.1073/pnas.83.4.1125>.
- Innerarity, T.L., Friedlander, E.J., Rall, S.C., Weisgraber, K.H., and Mahley, R.W. 1983. “The Receptor-Binding Domain of Human Apolipoprotein E: Binding of Apolipoprotein E Fragments.” *Journal of Biological Chemistry* 258 (20): 12341–47.
- Jain, R.S., and Quarfordt, S.H. 1979. “The Carbohydrate Content of Apolipoprotein E from Human Very Low Density Lipoproteins.” *Life Sciences* 25: 1315–24.

- Ji, Z., Sanan, D.A., and Mahley, R.W. 1995. "Intravenous Heparinase Inhibits Remnant Lipoprotein Clearance from the Plasma and Uptake by the Liver : In Vivo Role of Heparan Sulfate Proteoglycans" 36: 583–92.
- Jolivalt, C., Leininger-Muller, B., Bertrand, P., Herber, R., Christen, Y., and Siest, G. 2000. "Differential Oxidation of Apolipoprotein E Isoforms and Interaction with Phospholipids." *Free Radical Biology and Medicine* 28 (1): 129–40. [https://doi.org/10.1016/S0891-5849\(99\)00232-4](https://doi.org/10.1016/S0891-5849(99)00232-4).
- Joshi, A., Ringman, J.M., Lee, A.S., Juarez, K.O., and Mendez, M.F. 2012. "Comparison of Clinical Characteristics between Familial and Non-Familial Early Onset Alzheimer's Disease." *Journal of Neurology* 259 (10): 2182–88. <https://doi.org/10.1007/s00415-012-6481-y>.
- Kanekiyo, T., Xu, H., and Bu, G. 2014a. "ApoE and Abeta in Alzheimer's Disease: Accidental Encounters or Partners?" *Neuron*. <https://doi.org/10.1016/j.neuron.2014.01.045>.
- . 2014b. "ApoE and A β in Alzheimer's Disease: Accidental Encounters or Partners?" *Neuron* 81 (4): 740–54. <https://doi.org/10.1016/j.neuron.2014.01.045>.
- Kannan, K., and Jain, S.K. 2000. "Oxidative Stress and Apoptosis." *Pathophysiology* 7 (3): 153–63. [https://doi.org/10.1016/S0928-4680\(00\)00053-5](https://doi.org/10.1016/S0928-4680(00)00053-5).
- Kharrazi, H., Vaisi-Raygani, A., Rahimi, Z., Tavilani, H., Aminian, M., and Pourmotabbed, T. 2008. "Association between Enzymatic and Non-Enzymatic Antioxidant Defense Mechanism with Apolipoprotein E Genotypes in Alzheimer Disease." *Clinical Biochemistry* 41 (12): 932–36. <https://doi.org/10.1016/j.clinbiochem.2008.05.001>.
- Khurana, R., Coleman, C., Ionescu-Zanetti, C., Carter, S.A., Krishna, V., Grover, R.K., Roy, R., and Singh, S. 2005. "Mechanism of Thioflavin T Binding to Amyloid Fibrils." *Journal of Structural Biology* 151 (3): 229–38. <https://doi.org/10.1016/j.jsb.2005.06.006>.
- Kim, W.S., Elliott, D.A., Kockx, M., Kritharides, L., Rye, K.A., Jans, D.A., and Garner, B. 2008. "Analysis of Apolipoprotein E Nuclear Localization Using Green Fluorescent Protein and Biotinylation Approaches." *Biochemical Journal* 409 (3): 701–9. <https://doi.org/10.1042/BJ20071261>.
- Kim, Y.E., Hipp, M.S., Bracher, A., Hayer-Hartl, M., and Ulrich Hartl, F. 2013. *Molecular Chaperone Functions in Protein Folding and Proteostasis. Annual Review of Biochemistry*. Vol. 82. <https://doi.org/10.1146/annurev-biochem-060208-092442>.
- Kishore, D., Kundu, S., and Kayastha, A.M. 2012. "Thermal, Chemical and PH Induced Denaturation of a Multimeric β -Galactosidase Reveals Multiple Unfolding Pathways." *PLoS ONE* 7 (11). <https://doi.org/10.1371/journal.pone.0050380>.
- Kita, T., Goldstein, J.L., Brown, M.S., Watanabet, Y., Hornickt, C.A., and Havelf, R.J. 1982.

- "Hepatic Uptake of Chylomicron Remnants in WHHL Rabbits: A Mechanism Genetically Distinct from the Low Density Lipoprotein Receptor" 79 (June): 3623–27.
- Knouff, C., Hinsdale, M.E., Mezdour, H., Altenburg, M.K., Watanabe, M., Quarfordt, S.H., Sullivan, P.M., and Maeda, N. 1999. "Apo E Structure Determines VLDL Clearance and Atherosclerosis Risk in Mice." *Journal of Clinical Investigation* 103 (11): 1579–86. <https://doi.org/10.1172/JCI6172>.
- Koch, G., Lorenzo, F. Di, Loizzo, S., Motta, C., Travaglione, S., Baiula, M., Rimondini, R., et al. 2017. "CSF Tau Is Associated with Impaired Cortical Plasticity, Cognitive Decline and Astrocyte Survival Only in APOE4-Positive Alzheimer's Disease." *Scientific Reports* 7 (1): 1–12. <https://doi.org/10.1038/s41598-017-14204-3>.
- Kornecook, T.J., McKinney, A.P., Ferguson, M.T., and Dodart, J.C. 2010. "Isoform-Specific Effects of Apolipoprotein E on Cognitive Performance in Targeted-Replacement Mice Overexpressing Human APP." *Genes, Brain and Behavior* 9 (2): 182–92. <https://doi.org/10.1111/j.1601-183X.2009.00545.x>.
- Kosik, K.S., Joachim, C.L., and Selkoe, D.J. 1986. "Microtubule-Associated Protein Tau (Tau) Is a Major Antigenic Component of Paired Helical Filaments in Alzheimer Disease." *Proceedings of the National Academy of Sciences of the United States of America* 83 (11): 4044–48. <https://doi.org/10.1097/00002093-198701030-00022>.
- Kowal, R.C., Herz, J., Goldstein, J.L., Esser, V., and Brown, M.S. 1989. "Low Density Lipoprotein Receptor-Related Protein Mediates Uptake of Cholesteryl Esters Derived from Apoprotein E-Enriched Lipoproteins" 86 (August): 5810–14.
- Krasemann, S., Madore, C., Cialic, R., Baufeld, C., Calcagno, N., Fatimy, R. El, Beckers, L., et al. 2017. "The TREM2-APOE Pathway Drives the Transcriptional Phenotype of Dysfunctional Microglia in Neurodegenerative Diseases." *Immunity* 47 (3): 566-581.e9. <https://doi.org/10.1016/j.immuni.2017.08.008>.
- Labisso, W.L., Raulin, A.C., Nwido, L.L., Kocon, A., Wayne, D., Erdozain, A.M., Morentin, B., et al. 2018. "The Loss of α - and β -Tubulin Proteins Are a Pathological Hallmark of Chronic Alcohol Consumption and Natural Brain Ageing." *Brain Sciences* 8 (9). <https://doi.org/10.3390/brainsci8090175>.
- LaDu, M.J., Falduto, M.T., Manelli, A.M., Reardon, C.A., Getz, G.S., and Frail, D.E. 1994. "Isoform-Specific Binding of Apolipoprotein E to β -Amyloid." *Journal of Biological Chemistry* 269 (38): 23403–6.
- LaFerla, F.M., Green, K.N., and Oddo, S. 2007. "Intracellular Amyloid- β in Alzheimer's Disease." *Nature Reviews Neuroscience* 8 (7): 499–509. <https://doi.org/10.1038/nrn2168>.
- Lambert, J.C., Heath, S., Even, G., Campion, D., Sleegers, K., Hiltunen, M., Combarros, O., et al. 2009. "Genome-Wide Association Study Identifies Variants at CLU and CR1 Associated

- with Alzheimer's Disease." *Nature Genetics* 41 (10): 1094–99. <https://doi.org/10.1038/ng.439>.
- Lambert, J.C., Ibrahim-Verbaas, C.A., Harold, D., Naj, A.C., Sims, R., Bellenguez, C., Jun, G., et al. 2013. "Meta-Analysis of 74,046 Individuals Identifies 11 New Susceptibility Loci for Alzheimer's Disease." *Nature Genetics* 45 (12): 1452–58. <https://doi.org/10.1038/ng.2802>.
- Lane, C.A., Hardy, J., and Schott, J.M. 2018. "Alzheimer's Disease." *European Journal of Neurology* 25 (1): 59–70. <https://doi.org/10.1111/ene.13439>.
- Lanz, T.A., Carter, D.B., and Merchant, K.M. 2003. "Dendritic Spine Loss in the Hippocampus of Young PDAPP and Tg2576 Mice and Its Prevention by the ApoE2 Genotype." *Neurobiology of Disease* 13 (3): 246–53. [https://doi.org/10.1016/S0969-9961\(03\)00079-2](https://doi.org/10.1016/S0969-9961(03)00079-2).
- Laue, T., Shah, B., Ridgeway, T., and Pelletier, S. 1992. "Computer-Aided Interpretation of Sedimentation Data for Proteins in Harding, SE, Rowe, AJ, Horton, JC (Ed.),. Analytical Ultracentrifugation in Biochemistry and Polymer Science." Royal Society of Chemistry, Cambridge.
- LeVine, H. 1999. "[18] Quantification of β -Sheet Amyloid Fibril Structures with Thioflavin T." In *Methods in Enzymology*, 309:274–84. [https://doi.org/10.1016/S0076-6879\(99\)09020-5](https://doi.org/10.1016/S0076-6879(99)09020-5).
- Levine, R.L., Mosoni, L., Berlett, B.S., and Stadtman, E.R. 1996. "Methionine Residues as Endogenous Antioxidants in Proteins." *Proceedings of the National Academy of Sciences of the United States of America* 93 (26): 15036–40. <https://doi.org/10.1073/pnas.93.26.15036>.
- Liao, F., Li, A., Xiong, M., Bien-ly, N., Jiang, H., Zhang, Y., Finn, M.B., et al. 2018. "Targeting of Nonlipidated, Aggregated ApoE with Antibodies Inhibits Amyloid Accumulation." *The Journal of Clinical Investigation* 128 (5): 2144–55.
- Lim, Y.Y., and Mormino, E.C. 2017. "APOE Genotype and Early β -Amyloid Accumulation in Older Adults without Dementia." *Neurology* 89 (10): 1028–34. <https://doi.org/10.1212/WNL.0000000000004336>.
- Liu, C.-C., Kanekiyo, T., Xu, H., and Bu, G. 2013. "Apolipoprotein E and Alzheimer Disease: Risk, Mechanisms and Therapy." *Nature Reviews Neurology* 9 (2): 106–18. <https://doi.org/10.1038/nrneurol.2012.263>.
- Liu, S., Park, S., Allington, G., Prelli, F., Sun, Y., Martá-Ariza, M., Scholtzova, H., et al. 2017. "Targeting Apolipoprotein E/Amyloid β Binding by Peptoid CPO-A β 17-21 P Ameliorates Alzheimer's Disease Related Pathology and Cognitive Decline." *Scientific Reports* 7 (1): 1–12. <https://doi.org/10.1038/s41598-017-08604-8>.
- Lobley, A., Whitmore, L., and Wallace, B.A. 2002. "DICHROWEB: An Interactive Website for the Analysis of Protein Secondary Structure from Circular Dichroism Spectra." *Bioinformatics*

18 (1): 211–12. <https://doi.org/10.1093/bioinformatics/18.1.211>.

- Loison, P., Majou, D., Gelhaye, E., Boudaud, N., and Gantzer, C. 2016. “Impact of Reducing and Oxidizing Agents on the Infectivity of Q β Phage and the Overall Structure of Its Capsid.” *FEMS Microbiology Ecology* 92 (11): 1–11. <https://doi.org/10.1093/femsec/iw153>.
- Love, J.E., Day, R.J., Gause, J.W., Brown, R.J., Pu, X., Theis, D.I., Caraway, C.A., et al. 2017. “Nuclear Uptake of an Amino-Terminal Fragment of Apolipoprotein E4 Promotes Cell Death and Localizes within Microglia of the Alzheimer’s Disease Brain.” *International Journal of Physiology, Pathophysiology and Pharmacology* 9 (2): 40–57.
- Ma, J., Yee, A., Brewer, H., Das, S., and Potter, H. 1994. “The Amyloid-Associated Proteins Alpha1-Antichymotrypsin and Apolipoprotein E Promote the Assembly of the Alzheimer β Protein into Filaments.” *Nature* 372 (November): 92–94.
- Mahley, R.W. 1988. “Apolipoprotein E: Cholesterol Transport Protein with Expanding Role in Cell Biology.” *Science* 240 (4852): 622–30. <https://doi.org/10.1126/science.3283935>.
- . 2016. “Apolipoprotein E: From Cardiovascular Disease to Neurodegenerative Disorders.” *Journal of Molecular Medicine* 94 (7): 739–46. <https://doi.org/10.1007/s00109-016-1427-y>.
- Mahley, R.W., and Huang, Y. 1999. “Apolipoprotein E: From Atherosclerosis to Alzheimer’s Disease and Beyond.” *Current Opinion in Lipidology* 10 (3): 207–17. <http://www.ncbi.nlm.nih.gov/pubmed/10431657>.
- Mahley, R.W., and Huang, Y. 2012. “Apolipoprotein E Sets the Stage: Response to Injury Triggers Neuropathology, Including Alzheimer’s Disease.” *Neuron* 76 (5): 871–85. <https://doi.org/10.1007/978-1-4614-5915-6>.
- Mahley, R.W., Innerarity, T.L., Rall, S.C., and Weisgraber, K.H. 1984. “Plasma Lipoproteins: Apolipoprotein Structure and Function.” *Journal of Lipid Research* 25: 1277–94.
- Makin, O.S., Sikorski, P., and Serpell, L.C. 2007. “CLEARER : A New Tool for the Analysis of X-Ray Fibre Diffraction Patterns and Diffraction Simulation from Atomic Structural Models Supporting Information,” 1–8.
- Maleszewska, M., Mawer, J.S.P., and Tessarz, P. 2016. “Histone Modifications in Ageing and Lifespan Regulation.” *Current Molecular Biology Reports* 2 (1): 26–35. <https://doi.org/10.1007/s40610-016-0031-9>.
- Mann, W.A., Meyer, N., Weber, W., Meyer, S., Greten, H., and Beisiegel, U. 1995. “Apolipoprotein E Isoforms and Rare Mutations: Parallel Reduction in Binding to Cells and to Heparin Reflects Severity of Associated Type III Hyperlipoproteinemia.” *Journal of Lipid Research* 36 (3): 517–25. <http://www.ncbi.nlm.nih.gov/pubmed/7775863>.
- Marcus, D.L., Thomas, C., Rodriguez, C., Simberkoff, K., Tsai, J.S., Strafaci, J.A., and Freedman, M.L. 1998. “Increased Peroxidation and Reduced Antioxidant Enzyme Activity in

- Alzheimer's Disease." *Experimental Neurology* 150 (1): 40–44. <https://doi.org/10.1006/exnr.1997.6750>.
- Marshall, K.E., and Serpell, L.C. 2009. "Insights into the Structure of Amyloid Fibrils." *The Open Biology Journal* 2 (1): 185–92. <https://doi.org/10.2174/1874196700902010185>.
- Marshall, K.E., Vadukul, D., Staras, K., and Serpell, L.C. 2019. "Misfolded Amyloid β -42 Induced Impairment of the Endosomal-Lysosomal Pathway Revealed by Real-Time Optical Monitoring." *BioRxiv*, January, 598540. <https://doi.org/10.1101/598540>.
- Marshall, K.E., Vadukul, D.M., Dahal, L., Theisen, A., Fowler, M.W., Al-Hilaly, Y., Ford, L., et al. 2016. "A Critical Role for the Self-Assembly of Amyloid-B1-42 in Neurodegeneration." *Scientific Reports* 6 (July): 1–13. <https://doi.org/10.1038/srep30182>.
- Martin, S.F., Tatham, M.H., Hay, R.T., and Samuel, I.D.W. 2008. "Quantitative Analysis of Multi-Protein Interactions Using FRET: Application to the SUMO Pathway." *Protein Science* 17 (4): 777–84. <https://doi.org/10.1110/ps.073369608>.
- Martínez-Morillo, E., Hansson, O., Atagi, Y., Bu, G., Minthon, L., Diamandis, E.P., and Nielsen, H.M. 2014. "Total Apolipoprotein E Levels and Specific Isoform Composition in Cerebrospinal Fluid and Plasma from Alzheimer's Disease Patients and Controls." *Acta Neuropathologica* 127 (5): 633–43. <https://doi.org/10.1007/s00401-014-1266-2>.
- Masliah, E., Samuel, W., Veinbergs, I., Mallory, M., Mante, M., and Saitoh, T. 1997. "Neurodegeneration and Cognitive Impairment in ApoE-Deficient Mice Is Ameliorated by Infusion of Recombinant ApoE." *Brain Research* 751 (2): 307–14. [https://doi.org/10.1016/S0006-8993\(96\)01420-5](https://doi.org/10.1016/S0006-8993(96)01420-5).
- Maurer-Stroh, S., Debulpaep, M., Kuemmerer, N., La Paz, M.L. De, Martins, I.C., Reumers, J., Morris, K.L., et al. 2010. "Exploring the Sequence Determinants of Amyloid Structure Using Position-Specific Scoring Matrices." *Nature Methods* 7 (3): 237–42. <https://doi.org/10.1038/nmeth.1432>.
- Mayeux, R., and Stern, Y. 2012. "Epidemiology of Alzheimer Disease." *Cold Spring Harbor Perspectives in Medicine* 2 (8): a006239–a006239. <https://doi.org/10.1101/cshperspect.a006239>.
- Mazur-Kolecka, B., Frackowiak, J., Kowal, D., Krzeslowska, J., and Dickson, D. 2002. "Oxidative Protein Damage in Cells Engaged in β -Amyloidosis Is Related to ApoE Genotype." *NeuroReport* 13 (4): 465–68. <https://doi.org/10.1097/00001756-200203250-00021>.
- Mecocci, P., MacGarvey, U., and Beal, M.F. 1994. "Oxidative Damage to Mitochondrial DNA Is Increased in Alzheimer's Disease." *Annals of Neurology* 36 (5): 747–51. <https://doi.org/10.1002/ana.410360510>.
- Misonou, H., Morishima-Kawashima, M., and Ihara, Y. 2000. "Oxidative Stress Induces

- Intracellular Accumulation of Amyloid β - Protein ($A\beta$) in Human Neuroblastoma Cells." *Biochemistry* 39 (23): 6951–59. <https://doi.org/10.1021/bi000169p>.
- Miyata, M., and Smith, J.D. 1996. "Apolipoprotein E Allele-Specific Antioxidant Activity and Effects on Cytotoxicity by Oxidative Insults and Beta-Amyloid Peptides." *Nature Genetics* 14 (1): 55–61. <https://doi.org/10.1038/ng0996-55>.
- Montine, K.S., Oison, S.J., Amarnath, V., Whetsell, W.O., Graham, D.G., and Montine, T.J. 1997. "Immunohistochemical Detection of 4-Hydroxy-2-Nonenal Adducts in Alzheimer's Disease Is Associated with Inheritance of APOE4." *American Journal of Pathology* 150 (2): 437–43.
- Montine, T.J., Huang, D.Y., Valentine, W.M., Amaranath, V., Saunders, A.M., Weisgraber, K.H., Graham, D.G., and Strittmatter, W.J. 1996. "Crosslinking of Apolipoprotein E by Products of Lipid Peroxidation." *Journal of Neuropathology and Experimental Neurology* 55 (2): 202–10. <https://doi.org/10.1097/00005072-199602000-00009>.
- Morris, K.L., and Serpell, L.C. 2012. "X-Ray Fibre Diffraction Studies of Amyloid Fibrils." In *Amyloid Proteins. Methods in Molecular Biology (Methods and Protocols)*, edited by E. Sigurdsson, M. Calero, and M. Gasset. Vol. 849. Humana Press. [https://doi.org/10.1016/S0140-6736\(80\)92687-2](https://doi.org/10.1016/S0140-6736(80)92687-2).
- Morrow, J.A., Hatters, D.M., Lu, B., Höchtl, P., Oberg, K.A., Rupp, B., and Weisgraber, K.H. 2002. "Apolipoprotein E4 Forms a Molten Globule: A Potential Basis for Its Association with Disease." *Journal of Biological Chemistry*. <https://doi.org/10.1074/jbc.M204898200>.
- Morrow, J.A., Segall, M.L., Lund-Katz, S., Phillips, M.C., Knapp, M., Rupp, B., and Weisgraber, K.H. 2000. "Differences in Stability among the Human Apolipoprotein E Isoforms Determined by the Amino-Terminal Domain." *Biochemistry* 39 (38): 11657–66. <https://doi.org/10.1021/bi000099m>.
- Naj, A.C., Jun, G., Beecham, G.W., Wang, L.S., Vardarajan, B.N., Buross, J., Gallins, P.J., et al. 2011. "Common Variants at MS4A4/MS4A6E, CD2AP, CD33 and EPHA1 Are Associated with Late-Onset Alzheimer's Disease." *Nature Genetics* 43 (5): 436–43. <https://doi.org/10.1038/ng.801>.
- Nakamura, T., Watanabe, A., Fujino, T., Hosono, T., and Michikawa, M. 2009. "Apolipoprotein E4 (1-272) Fragment Is Associated with Mitochondrial Proteins and Affects Mitochondrial Function in Neuronal Cells." *Molecular Neurodegeneration* 4 (1). <https://doi.org/10.1186/1750-1326-4-35>.
- Namba, Y., Tomonaga, M., Kawasaki, H., Otomo, E., and Ikeda, K. 1991. "Apolipoprotein E Immunoreactivity in Cerebral Amyloid Deposits and Neurofibrillary Tangles in Alzheimer's Disease and Kuru Plaque Amyloid in Creutzfeldt-Jakob Disease." *Brain Research* 541 (1): 163–66. [https://doi.org/10.1016/0006-8993\(91\)91092-F](https://doi.org/10.1016/0006-8993(91)91092-F).
- Nathan, B., Bellosta, S., Sanan, D., Weisgraber, K., Mahley, R.W., and Pitas, R. 1994.

- "Differential Effects of Apolipoproteins E3 and E4 on Neuronal Growth in Vitro." *Science* 264 (5160): 850–52. <https://doi.org/10.1126/science.8171342>.
- Nunomura, A., Perry, G., Pappolla, M.A., Friedland, R.P., Hirai, K., Chiba, S., and Smith, M.A. 2000. "Neuronal Oxidative Stress Precedes Amyloid- β Deposition in down Syndrome." *Journal of Neuropathology and Experimental Neurology* 59 (11): 1011–17. <https://doi.org/10.1093/jnen/59.11.1011>.
- Pace, C.N. 1986. "Determination and Analysis of Urea and Guanidine Hydrochloride Denaturation Curves." In *Methods in Enzymology*, 131:266–80. [https://doi.org/10.1016/0076-6879\(86\)31045-0](https://doi.org/10.1016/0076-6879(86)31045-0).
- Panza, F., Solfrizzi, V., Colacicco, A.M., Basile, A.M., D'Introno, A., Capurso, C., Sabba, M., Capurso, S., and Capurso, A. 2003. "Apolipoprotein E (APOE) Polymorphism Influences Serum APOE Levels in Alzheimer's Disease Patients and Centenarians." *NeuroReport* 14 (4): 605–8. <https://doi.org/10.1097/00001756-200303240-00016>.
- Patterson, C. 2018. "The State of the Art of Dementia Research: New Frontiers." *World Alzheimer Report 2018*. https://doi.org/10.1111/j.0033-0124.1950.24_14.x.
- Pedersen, W.A., Chan, S.L., and Mattson, M.P. 2000. "A Mechanism for the Neuroprotective Effect of Apolipoprotein E: Isoform- Specific Modification by the Lipid Peroxidation Product 4-Hydroxynonenal." *Journal of Neurochemistry* 74 (4): 1426–33. <https://doi.org/10.1046/j.1471-4159.2000.0741426.x>.
- Pericak-Vance, M.A., Beboutt, J.L., Gaskell, P.C.J., Yamaokat, L.H., Hung, W.-Y., Alberts, M.J., Walker, A.P., et al. 1991. "Linkage Studies in Familial Alzheimer Disease: Evidence for Chromosome 19 Linkage." *American Journal of Human Genetics* 48 (6): 1034–50. <https://www.ncbi.nlm.nih.gov/pmc/articles/PMC1683100/pdf/ajhg00090-0019.pdf>.
- Permanne, B., Perez, C., Soto, C., Frangione, B., and Wisniewski, T. 1997. "Detection of Apolipoprotein E/Dimeric Soluble Amyloid [Beta] Complexes in Alzheimer's Disease Brain Supernatants." *Biochemical and Biophysical Research Communications* 240 (3): 715–20. <https://doi.org/10.1006/bbrc.1997.7727>.
- Perry, E.K., Tomlinson, B.E., Blessed, G., Bergmann, K., Gibson, P.H., and Perry, R.H. 1978. "Correlation of Cholinergic Abnormalities with Senile Plaques and Mental Test Scores in Senile Dementia." *British Medical Journal* 2 (6150): 1457–59. <https://doi.org/10.1136/bmj.2.6150.1457>.
- Persson, T., Lattanzio, F., Calvo-Garrido, J., Rimondini, R., Rubio-Rodrigo, M., Sundström, E., Maioli, S., Sandebring-Matton, A., and Cedazo-Mínguez, Á. 2017. "Apolipoprotein E4 Elicits Lysosomal Cathepsin D Release, Decreased Thioredoxin-1 Levels, and Apoptosis." *Journal of Alzheimer's Disease* 56 (2): 601–17. <https://doi.org/10.3233/JAD-150738>.
- Pirttilä, T., Soininen, H., Heinonen, O., Lehtimäki, T., Bogdanovic, N., Paljärvi, L., Kosunen, O.,

- et al. 1996. "Apolipoprotein E (ApoE) Levels in Brains from Alzheimer Disease Patients and Controls." *Brain Research* 722 (1–2): 71–77. [https://doi.org/10.1016/0006-8993\(96\)00183-7](https://doi.org/10.1016/0006-8993(96)00183-7).
- Poljsak, B., and Milisav, I. 2013. "Aging, Oxidative Stress and Antioxidants." In *Oxidative Stress and Chronic Degenerative Diseases - A Role for Antioxidants*. InTech. <https://doi.org/10.5772/51609>.
- Provencher, S.W., and Gloeckner, J. 1981. "Estimation of Globular Protein Secondary Structure from Circular Dichroism." *Biochemistry* 20 (1): 33–37. <https://doi.org/10.1021/bi00504a006>.
- Querfurth, H.W., and LaFerla, F.M. 2010. "Alzheimer's Disease." *New England Journal of Medicine* 362 (4): 329–44. <https://doi.org/10.1056/NEJMra0909142>.
- Rall, S., Weisgraber, K.H., and Mahley, R.W. 1982. "Human Apolipoprotein E: The Complete Amino Acid Sequence." *Biological Chemistry* 257 (8): 4171–78.
- Rall, S.C., Weisgraber, K.H., Innerarity, T.L., and Mahley, R.W. 1982. "Structural Basis for Receptor Binding Heterogeneity of Apolipoprotein E from Type III Hyperlipoproteinemic Subjects." *Proceedings of the National Academy of Sciences of the United States of America* 79 (15): 4696–4700. <https://doi.org/10.1073/pnas.79.15.4696>.
- Ramassamy, C., Averill, D., Beffert, U., Bastianetto, S., Theroux, L., Lussier-Cacan, S., Cohn, J.S., et al. 1999. "Oxidative Damage and Protection by Antioxidants in the Frontal Cortex of Alzheimer's Disease Is Related to the Apolipoprotein E Genotype." *Free Radical Biology and Medicine* 27 (5–6): 544–53. [https://doi.org/10.1016/S0891-5849\(99\)00102-1](https://doi.org/10.1016/S0891-5849(99)00102-1).
- Ramassamy, C., Averill, D., Beffert, U., Theroux, L., Lussier-Cacan, S., Cohn, J.S., Christen, Y., Schoofs, A., Davignon, J., and Poirier, J. 2000. "Oxidative Insults Are Associated with Apolipoprotein E Genotype in Alzheimer's Disease Brain." *Neurobiology of Disease* 7 (1): 23–37. <https://doi.org/10.1006/nbdi.1999.0273>.
- Ramassamy, C., Krzykowski, P., Averill, D., Lussier-Cacan, S., Theroux, L., Christen, Y., Davignon, J., and Poirier, J. 2001. "Impact of ApoE Deficiency on Oxidative Insults and Antioxidant Levels in the Brain." *Molecular Brain Research* 86 (1–2): 76–83. [https://doi.org/10.1016/S0169-328X\(00\)00268-0](https://doi.org/10.1016/S0169-328X(00)00268-0).
- Rambaran, R.N., and Serpell, L.C. 2008. "Amyloid Fibrils: Abnormal Protein Assembly." *Prion* 2 (3): 112–17. <https://doi.org/10.4161/pri.2.3.7488>.
- Raulin, A.C., Kraft, L., Al-Hilaly, Y.K., Xue, W.F., McGeehan, J.E., Atack, J.R., and Serpell, L. 2019. "The Molecular Basis for Apolipoprotein E4 as the Major Risk Factor for Late-Onset Alzheimer's Disease." *Journal of Molecular Biology* 431 (12): 2248–65. <https://doi.org/10.1016/j.jmb.2019.04.019>.
- Rebeck, W.G., Reiter, J.S., Strickland, D.K., and Hyman, B.T. 1993. "Apolipoprotein E in Sporadic

- Alzheimer's Disease: Allelic Variation and Receptor Interactions." *Neuron* 11 (4): 575–80. [https://doi.org/10.1016/0896-6273\(93\)90070-8](https://doi.org/10.1016/0896-6273(93)90070-8).
- Reitz, C., and Mayeux, R. 2014. "Alzheimer Disease: Epidemiology, Diagnostic Criteria, Risk Factors and Biomarkers." *Biochemical Pharmacology* 88 (4): 640–51. <https://doi.org/10.1016/j.bcp.2013.12.024>.
- Richardson, J.R., Roy, A., Shalat, S.L., Stein, R.T. Von, Hossain, M.M., Buckley, B., Gearing, M., and Levey, A.I. 2014. "Elevated Serum Pesticide Levels and Risk for Alzheimer Disease." *JAMA Neurology* 71 (3): 284–90. <https://doi.org/10.1001/jamaneurol.2013.6030.Elevated>.
- Riddell, D.R., Zhou, H., Atchison, K., Warwick, H.K., Atkinson, P.J., Jefferson, J., Xu, L., et al. 2008. "Impact of Apolipoprotein E (ApoE) Polymorphism on Brain ApoE Levels." *Journal of Neuroscience* 28 (45): 11445–53. <https://doi.org/10.1523/JNEUROSCI.1972-08.2008>.
- Rius-Pérez, S., Tormos, A.M., Pérez, S., and Taléns-Visconti, R. 2018. "Vascular Pathology: Cause or Effect in Alzheimer Disease?" *Neurologia* 33 (2): 121–28. <https://doi.org/10.1016/j.nrl.2015.07.010>.
- Rogaeva, E., Meng, Y., Lee, J.H., Gu, Y., Kawarai, T., Zou, F., Katayama, T., et al. 2007. "The Neuronal Sortilin-Related Receptor SORL1 Is Genetically Associated with Alzheimer Disease." *Nature Genetics* 39 (2): 168–77. <https://doi.org/10.1038/ng1943>.
- Romano, A.D., Serviddio, G., Matthaeis, A. De, and Bellanti, F. 2010. "Oxidative Stress and Aging." *Journal of Nephrology* 23 (2).
- Ross, C.A., and Poirier, M.A. 2004. "Protein Aggregation and Neurodegenerative Disease." *Nature Medicine* 10 (S7): S10–17. <https://doi.org/10.1038/nm1066>.
- Rusted, J.M., Evans, S.L., King, S.L., Dowell, N., Tabet, N., and Tofts, P.S. 2013. "APOE E4 Polymorphism in Young Adults Is Associated with Improved Attention and Indexed by Distinct Neural Signatures." *NeuroImage* 65: 364–73. <https://doi.org/10.1016/j.neuroimage.2012.10.010>.
- Sánchez-Santed, F., Colomina, M.T., and Herrero Hernández, E. 2016. "Organophosphate Pesticide Exposure and Neurodegeneration." *Cortex* 74: 417–26. <https://doi.org/10.1016/j.cortex.2015.10.003>.
- Sayre, L.M., Zelasko, D.A., Harris, P.L., Perry, G., Salomon, R.G., and Smith, M.A. 1997. "4-Hydroxynonenal-Derived Advanced Lipid Peroxidation End Products Are Increased in Alzheimer's Disease." *Journal of Neurochemistry* 68 (5): 2092–97. <https://doi.org/10.1046/j.1471-4159.1997.68052092.x>.
- Schächter, F., Faure-Delanef, L., Guénot, F., Rouger, H., Froguel, P., Lesueur-Ginot, L., and Cohen, D. 1994. "Genetic Associations with Human Longevity at the APOE and ACE Loci." *Nature Genetics* 6 (1): 29–32. <https://doi.org/10.1038/ng0194-29>.

- Schmechel, D.E., Saunders, A.M., Strittmatter, W.J., Crain, B.J., Hulette, C.M., Joo, S.H., Pericak-Vance, M.A., Goldgaber, D., and Roses, A.D. 1993. "Increased Amyloid Beta-Peptide Deposition in Cerebral Cortex as a Consequence of Apolipoprotein E Genotype in Late-Onset Alzheimer Disease." *Proceedings of the National Academy of Sciences of the United States of America* 90 (20): 9649–53. <https://doi.org/10.1073/pnas.90.20.9649>.
- Schuck, P. 2000. "Size-Distribution Analysis of Macromolecules by Sedimentation Velocity Ultracentrifugation and Lamm Equation Modeling." *Biophysical Journal*. [https://doi.org/10.1016/S0006-3495\(00\)76713-0](https://doi.org/10.1016/S0006-3495(00)76713-0).
- Selkoe, D.J. 1994. "Alzheimer's Disease: A Central Role for Amyloid." *Journal of Neuropathology & Experimental Neurology* 53 (5): 438–47. <https://doi.org/10.1097/00005072-199409000-00003>.
- . 2001. "Alzheimer's Disease: Genes, Proteins, and Therapy." *Physiological Reviews* 81 (2): 741–66. <https://doi.org/10.1152/physrev.2001.81.2.741>.
- . 2002. "Alzheimer's Disease Is a Synaptic Failure." *Science* 298 (5594): 789–91. <https://doi.org/10.1126/science.1074069>.
- Selkoe, D.J., and Hardy, J. 2016. "The Amyloid Hypothesis of Alzheimer's Disease at 25 Years." *EMBO Molecular Medicine* 8 (6): 595–608. <https://doi.org/10.15252/emmm.201606210>.
- Serpell, L.C. 2000. "Alzheimer's Amyloid Fibrils: Structure and Assembly." *Biochimica et Biophysica Acta (BBA)* 1502: 16–30.
- Seshadri, S., Fitzpatrick, A.L., Ikram, M.A., DeStefano, A.L., Gudnason, V., Boada, M., Bis, J.C., et al. 2010. "Genome-Wide Analysis of Genetic Loci Associated with Alzheimer Disease." *JAMA - Journal of the American Medical Association* 303 (18): 1832–40. <https://doi.org/10.1001/jama.2010.574>.
- Shea, T.B., Rogers, E., Ashline, D., Ortiz, D., and Sheu, M.S. 2002. "Apolipoprotein E Deficiency Promotes Increased Oxidative Stress and Compensatory Increases in Antioxidants in Brain Tissue." *Free Radical Biology and Medicine* 33 (8): 1115–20. [https://doi.org/10.1016/S0891-5849\(02\)01001-8](https://doi.org/10.1016/S0891-5849(02)01001-8).
- Shi, Y., Yamada, K., Liddelow, S.A., Smith, S.T., Zhao, L., Luo, W., Tsai, R.M., et al. 2017. "ApoE4 Markedly Exacerbates Tau-Mediated Neurodegeneration in a Mouse Model of Tauopathy." *Nature* 549 (7673): 523–27. <https://doi.org/10.1038/nature24016>.
- Shore, V.G., and Shore, B. 1973. "Heterogeneity of Human Plasma Very Low Density Lipoproteins. Separation of Species Differing in Protein Components." *Biochemistry* 12 (3): 502–7. <https://doi.org/10.1021/bi00727a022>.
- Smith, C.D., Carney, J.M., Starke-Reed, P.E., Oliver, C.N., Stadtman, E.R., Floyd, R.A., and Markesbery, W.R. 1991. "Excess Brain Protein Oxidation and Enzyme Dysfunction in

- Normal Aging and in Alzheimer Disease.” *Proceedings of the National Academy of Sciences of the United States of America* 88 (23): 10540–43. <https://doi.org/10.1073/pnas.88.23.10540>.
- Smith, M. a, Harris, P.L., Sayre, L.M., and Perry, G. 1997. “Iron Accumulation in Alzheimer Disease Is a Source of Redox-Generated Free Radicals.” *Proceedings of the National Academy of Sciences of the United States of America* 94 (September): 9866–68. <https://doi.org/10.1073/pnas.94.18.9866>.
- Sreerama, N., and Woody, R.W. 2000. “Estimation of Protein Secondary Structure from Circular Dichroism Spectra: Comparison of CONTIN, SELCON, and CDSSTR Methods with an Expanded Reference Set.” *Analytical Biochemistry* 287 (2): 252–60. <https://doi.org/10.1006/abio.2000.4880>.
- Stadtman, E.R. 1988. “Protein Modification in Aging.” *Journal of Gerontology* 43 (5): B112–20. <https://doi.org/10.1093/geronj/43.5.B112>.
- Stelzmann, R.A., Schnitzlein, H.N., and Murtagh, F.R. 1995. “An English Translation of Alzheimer’s 1907 Paper.” *Clinical Anatomy* 8 (6): 429–31. <https://doi.org/10.1002/ca.980080612>.
- Stokkum, I.H.M. van, Spoelder, H.J.. W., Bloemendal, M., Grondelle, R. van, and Groen, F.C.A. 1990. “Estimation of Protein Secondary Structure from Synchrotron Radiation Circular Dichroism Spectra.” *Analytical Biochemistry* 191: 110–18.
- Stožická, Z., Žilka, N., and Novák, M. 2007. “Risk and Protective Factors for Sporadic Alzheimer’s Disease.” *Acta Virologica* 51 (4): 205–22.
- Strittmatter, W.J., Saunders, A.M., Goedert, M., Weisgraber, K.H., Dong, L., Jakes, R., Huang, D.Y., Pericak-Vance, M.A., Schmechel, D., and Roses, A.D. 1994. “Isoform-Specific Interactions of Apolipoprotein E with Microtubule-Associated Protein Tau: Implications for Alzheimer Disease.” *Proceedings of the National Academy of Sciences of the United States of America* 91 (23): 11183–86. <https://doi.org/10.1073/pnas.91.23.11183>.
- Strittmatter, W.J., Saunders, A.M., Schmechel, D., Pericak-Vance, M.A., Enghild, J., Salvesen, G.S., and Roses, A.D. 1993. “Apolipoprotein E: High-Avidity Binding to β -Amyloid and Increased Frequency of Type 4 Allele in Late-Onset Familial Alzheimer Disease.” *Proceedings of the National Academy of Sciences of the United States of America* 90 (5): 1977–81. <https://doi.org/10.1073/pnas.90.5.1977>.
- Strittmatter, W.J., Weisgraber, K.H., Huang, D.Y., Dong, L., Salvesen, G.S., Pericak-Vance, M., Schmechel, D., Saunders, A.M., Goldgaber, D., and Roses, A.D. 1993. “Binding of Human Apolipoprotein E to Synthetic Amyloid Beta Peptide: Isoform-Specific Effects and Implications for Late-Onset Alzheimer Disease.” *Proceedings of the National Academy of Sciences* 90 (17): 8098–8102. <https://doi.org/10.1073/pnas.90.17.8098>.

- Suidan, G.L., and Ramaswamy, G. 2019. "Targeting Apolipoprotein E for Alzheimer's Disease: An Industry Perspective." *International Journal of Molecular Sciences* 20 (9). <https://doi.org/10.3390/ijms20092161>.
- Sullivan, P.M., Han, B., Liu, F., Mace, B.E., Ervin, J.F., Wu, S., Koger, D., Paul, S., and Bales, K.R. 2011. "Reduced Levels of Human ApoE4 Protein in an Animal Model of Cognitive Impairment." *Neurobiology of Aging* 32 (5): 791–801. <https://doi.org/10.1016/j.neurobiolaging.2009.05.011>.
- Sullivan, P.M., Mezdour, H., Aratani, Y., Knouff, C., Najib, J., Reddick, R.L., Quarfordt, S.H., and Maeda, N. 1997. "Targeted Replacement of the Mouse Apolipoprotein E Gene with the Common Human APOE3 Allele Enhances Diet-Induced Hypercholesterolemia and Atherosclerosis." *Journal of Biological Chemistry* 272 (29): 17972–80. <https://doi.org/10.1074/jbc.272.29.17972>.
- Sun, Y., Wu, S., Bu, G., Onifade, M.K., Patel, S.N., LaDu, M.J., Fagan, a M., and Holtzman, D.M. 1998. "Glial Fibrillary Acidic Protein-Apolipoprotein E (ApoE) Transgenic Mice: Astrocyte-Specific Expression and Differing Biological Effects of Astrocyte-Secreted ApoE3 and ApoE4 Lipoproteins." *The Journal of Neuroscience : The Official Journal of the Society for Neuroscience* 18 (9): 3261–72.
- Tai, L.M., Youmans, K.L., Jungbauer, L., Yu, C., and LaDu, M.J. 2011. "Introducing Human APOE into A β Transgenic Mouse Models." *International Journal of Alzheimer's Disease* 2011 (2). <https://doi.org/10.4061/2011/810981>.
- Talmud, P.J., Stephens, J.W., Hawe, E., Demissie, S., Cupples, L.A., Hurel, S.J., Humphries, S.E., and Ordovas, J.M. 2005. "The Significant Increase in Cardiovascular Disease Risk in APOE E4 Carriers Is Evident Only in Men Who Smoke: Potential Relationship between Reduced Antioxidant Status and ApoE4." *Annals of Human Genetics* 69 (6): 613–22. <https://doi.org/10.1111/j.1529-8817.2005.00205.x>.
- Tangirala, R.K., Praticó, D., FitzGerald, G.A., Chun, S., Tsukamoto, K., Maugeais, C., Usher, D.C., Puré, E., and Rader, D.J. 2001. "Reduction of Isoprostanes and Regression of Advanced Atherosclerosis by Apolipoprotein E." *Journal of Biological Chemistry* 276 (1): 261–66. <https://doi.org/10.1074/jbc.M003324200>.
- Tayeb-Fligelman, E., Tabachnikov, O., Moshe, A., Goldshmidt-Tran, O., Sawaya, M.R., Coquelle, N., Colletier, J., and Landau, M. 2017. "The Cytotoxic Staphylococcus Aureus PSM α 3 Reveals a Cross- α Amyloid-like Fibril." *Science* 355 (6327): 831–33. <https://doi.org/10.1126/science.aaf4901>.
- Tendian, S.W., Brouillette, C.G., Myszka, D.G., Sweet, R.W., and Chaiken, I.M. 1995. "Interdomain Communication of T-Cell CD4 Studied by Absorbance and Fluorescence Difference Spectroscopy Measurements of Urea-Induced Unfolding." *Biochemistry* 34 (19): 6464–74. <https://doi.org/10.1021/bi00019a028>.

- Terry, R.D., Masliah, E., Salmon, D.P., Butters, N., DeTeresa, R., Hill, R., Hansen, L.A., and Katzman, R. 1991. "Physical Basis of Cognitive Alterations in Alzheimer's Disease: Synapse Loss Is the Major Correlate of Cognitive Impairment." *Annals of Neurology* 30 (4): 572–80. <https://doi.org/10.1002/ana.410300410>.
- Theendakara, V., Peters-Libeu, C.A., Bredesen, D.E., and Rao, R. V. 2018. "Transcriptional Effects of ApoE4: Relevance to Alzheimer's Disease." *Molecular Neurobiology* 55 (6): 5243–54. <https://doi.org/10.1007/s12035-017-0757-2>.
- Theendakara, V., Peters-Libeu, C.A., Spilman, P., Poksay, K.S., Bredesen, D.E., and Rao, R. V. 2016. "Direct Transcriptional Effects of Apolipoprotein E." *Journal of Neuroscience* 36 (3): 685–700. <https://doi.org/10.1523/JNEUROSCI.3562-15.2016>.
- Tracy, T.E., and Gan, L. 2018. "Tau-Mediated Synaptic and Neuronal Dysfunction in Neurodegenerative Disease." *Current Opinion in Neurobiology* 51: 134–38. <https://doi.org/10.1016/j.conb.2018.04.027>.
- Utermann, G., Hees, M., and Steinmetz, A. 1977. "Polymorphism of Apolipoprotein E and Occurrence of Dysbetalipoproteinaemia in Man." *Nature* 269: 604–7. <https://doi.org/10.1038/267585a0>.
- Utermann, G., Jaeschke, M., and Menzel, J. 1975. "Familial Hyperlipoproteinemia Type Iii: Deficiency of a Specific Apolipoprotein (Apo e-iii) in the Very-Low-Density Lipoproteins." *FEBS Letters* 56 (2): 352–55.
- Utermann, G., Langenbeck, U., and Beisiegel, U. 1980. "Genetics of the Apolipoprotein E System in Man." *American Journal of Human Genetics* 32: 339–47.
- Utermann, G., Steinmetz, A., and Weber, W. 1982. "Genetic Control of Human Apolipoprotein E Polymorphism: Comparison of One- and Two-Dimensional Techniques of Isoprotein Analysis." *Human Genetics* 60 (4): 344–51. <https://doi.org/10.1007/BF00569216>.
- Uversky, V.N., and Fink, A.L. 2004. "Conformational Constraints for Amyloid Fibrillation: The Importance of Being Unfolded." *Biochimica et Biophysica Acta - Proteins and Proteomics* 1698 (2): 131–53. <https://doi.org/10.1016/j.bbapap.2003.12.008>.
- Valdiglesias, V., Fernández-Tajes, J., Pásaro, E., Méndez, J., and Laffon, B. 2012. "Identification of Differentially Expressed Genes in SHSY5Y Cells Exposed to Okadaic Acid by Suppression Subtractive Hybridization." *BMC Genomics* 13 (1). <https://doi.org/10.1186/1471-2164-13-46>.
- Vik-Mo, A.O., Fernø, J., Skrede, S., and Steen, V.M. 2009. "Psychotropic Drugs Up-Regulate the Expression of Cholesterol Transport Proteins Including ApoE in Cultured Human CNS- and Liver Cells." *BMC Pharmacology* 9 (1): 10. <https://doi.org/10.1186/1471-2210-9-10>.
- Walsh, D.M., Klyubin, I., Fadeeva, J. V., Cullen, W.K., Anwyl, R., Wolfe, M.S., Rowan, M.J., and

- Selkoe, D.J. 2002. "Naturally Secreted Oligomers of Amyloid β Protein Potently Inhibit Hippocampal Long-Term Potentiation in Vivo." *Nature* 416 (6880): 535–39. <https://doi.org/10.1038/416535a>.
- Wang, C., Najm, R., Xu, Q., Jeong, D.E., Walker, D., Balestra, M.E., Yoon, S.Y., et al. 2018. "Gain of Toxic Apolipoprotein E4 Effects in Human iPSC-Derived Neurons Is Ameliorated by a Small-Molecule Structure Corrector Article." *Nature Medicine* 24 (5): 647–57. <https://doi.org/10.1038/s41591-018-0004-z>.
- Weisgraber, K.H. 1990. "Apolipoprotein E Distribution among Human Plasma Lipoproteins: Role of the Cysteine-Arginine Interchange at Residue 112." *Journal of Lipid Research* 31: 1503–11. <https://doi.org/10.1016/j.enpol.2009.04.023>.
- Weisgraber, K.H., Innerarity, T.L., and Mahley, R.W. 1982. "Abnormal Lipoprotein Receptor-Binding Activity of the Human E Apoprotein Due to Cysteine-Arginine Interchange at a Single Site." *Journal of Biological Chemistry* 257 (5): 2518–21.
- Weisgraber, K.H., and Mahley, R.W. 1996. "Human Apolipoprotein E : The Alzheimer's Disease Connection." *The FASEB Journal* 10 (13): 1485–94.
- Weisgraber, K.H., Rall, S.C., and Mahley, R.W. 1981. "Human E Apoprotein Heterogeneity." *The Journal of Biological Chemistry* 256 (17): 9077–83. <http://www.ncbi.nlm.nih.gov/pubmed/7263700><http://www.jbc.org/content/256/17/9077.full.pdf>.
- Weisgraber, K.H., and Shinto, L.H. 1991. "Identification of the Disulfide-Linked Homodimer of Apolipoprotein E3 in Plasma: Impact on Receptor Binding Activity." *Journal of Biological Chemistry* 266 (18): 12029–34.
- Wetterau, J.R., Aggerbeck, L.P., Rall, S.C., and Weisgraber, K.H. 1988. "Human Apolipoprotein E3 in Aqueous Solution. I. Evidence for Two Structural Domains." *The Journal of Biological Chemistry* 263 (13): 6240–48. <http://www.ncbi.nlm.nih.gov/pubmed/3360781>.
- Whitehouse, P., Price, D., Struble, R., Clark, A., Coyle, J., and Delon, M. 1982. "Alzheimer's Disease and Senile Dementia: Loss of Neurons in the Basal Forebrain." *Science* 215 (4537): 1237–39. <https://doi.org/10.1126/science.7058341>.
- Whitmore, L., and Wallace, B.A. 2004. "DICHROWEB, an Online Server for Protein Secondary Structure Analyses from Circular Dichroism Spectroscopic Data." *Nucleic Acids Research* 32 (WEB SERVER ISS.): 668–73. <https://doi.org/10.1093/nar/gkh371>.
- . 2008. "Protein Secondary Structure Analyses from Circular Dichroism Spectroscopy: Methods and Reference Databases." *Biopolymers* 89 (5): 392–400. <https://doi.org/10.1002/bip.20853>.
- Wilson, C., Wardell, M.R., Weisgraber, K.H., Mahley, R.W., and Agard, D.A. 1991. "Three-

- Dimensional Structure of the LDL Receptor-Binding Domain of Human Apolipoprotein E." *Science (New York, N.Y.)* 252 (5014): 1817–22. <https://doi.org/2063194>.
- Winnock, M., Letenneur, L., Jacqmin-Gadda, H., Dallongeville, J., Amouyel, P., and Dartigues, J.F. 2002. "Longitudinal Analysis of the Effect of Apolipoprotein E E4 and Education on Cognitive Performance in Elderly Subjects: The PAQUID Study." *Journal of Neurology Neurosurgery and Psychiatry* 72 (6): 794–97. <https://doi.org/10.1136/jnnp.72.6.794>.
- Wischik, C.M., Harrington, C.R., and Storey, J.M.D. 2014. "Tau-Aggregation Inhibitor Therapy for Alzheimer's Disease." *Biochemical Pharmacology* 88 (4): 529–39. <https://doi.org/10.1016/j.bcp.2013.12.008>.
- Wood, S.J., Chan, W., and Wetzel, R. 1996a. "An ApoE-A β Inhibition Complex in A β Fibril Extension." *Chemistry and Biology* 3 (11): 949–56. [https://doi.org/10.1016/S1074-5521\(96\)90183-0](https://doi.org/10.1016/S1074-5521(96)90183-0).
- . 1996b. "Seeding of A β Fibril Formation Is Inhibited by All Three Isotypes of Apolipoprotein E." *Biochemistry* 35 (38): 12623–28. <https://doi.org/10.1021/bi961074j>.
- Wood, S.J., Maleeff, B., Hart, T., and Wetzel, R. 1996. "Physical, Morphological and Functional Differences between PH 5.8 and 7.4 Aggregates of the Alzheimer's Amyloid Peptide A β ." *Journal of Molecular Biology* 256 (5): 870–77. <https://doi.org/10.1006/jmbi.1996.0133>.
- Xu, H., Finkelstein, D.I., and Adlard, P.A. 2014. "Interactions of Metals and Apolipoprotein e in Alzheimer's Disease." *Frontiers in Aging Neuroscience* 6 (JUN): 1–7. <https://doi.org/10.3389/fnagi.2014.00121>.
- Xu, P.-T., Gilbert, J.R., Qiu, H.-L., Ervin, J., Rothrock-Christian, T.R., Hulette, C., and Schmechel, D.E. 1999. "Specific Regional Transcription of Apolipoprotein E in Human Brain Neurons." *The American Journal of Pathology* 154 (2): 601–11. [https://doi.org/10.1016/S0002-9440\(10\)65305-9](https://doi.org/10.1016/S0002-9440(10)65305-9).
- Yamada, T., Kondo, A., Takamatsu, J. ich, Tateishi, J., and Goto, I. 1995. "Apolipoprotein E MRNA in the Brains of Patients with Alzheimer's Disease." *Journal of the Neurological Sciences* 129 (1): 56–61. [https://doi.org/10.1016/0022-510X\(94\)00249-N](https://doi.org/10.1016/0022-510X(94)00249-N).
- Yamazaki, Y., Painter, M.M., Bu, G., and Kanekiyo, T. 2016. "Apolipoprotein E as a Therapeutic Target in Alzheimer's Disease: A Review of Basic Research and Clinical Evidence." *CNS Drugs* 30 (9): 773–89. <https://doi.org/10.1007/s40263-016-0361-4>.
- Yang, Y., Cudaback, E., Jorstad, N.L., Hemingway, J.F., Hagan, C.E., Melief, E.J., Li, X., et al. 2013. "APOE3, but Not APOE4, Bone Marrow Transplantation Mitigates Behavioral and Pathological Changes in a Mouse Model of Alzheimer Disease." *American Journal of Pathology* 183 (3): 905–17. <https://doi.org/10.1016/j.ajpath.2013.05.009>.
- Ye, S., Huang, Y., Müllendorff, K., Dong, L., Giedt, G., Meng, E.C., Cohen, F.E., Kuntz, I.D.,

- Weisgraber, K.H., and Mahley, R.W. 2005. "Apolipoprotein (Apo) E4 Enhances Amyloid Beta Peptide Production in Cultured Neuronal Cells: ApoE Structure as a Potential Therapeutic Target." *Proceedings of the National Academy of Sciences of the United States of America* 102 (51): 18700–705. <https://doi.org/10.1073/pnas.0508693102>.
- Yegambaram, M., Manivannan, B., Beach, T.G., and Halden, R.U. 2015. "Role of Environmental Contaminants in the Etiology of Alzheimer ' s Disease : A Review." *Current Alzheimer Research* 12: 116–46.
- Yokoyama, S., Kawai, Y., Tajima, S., and Yamamoto, A. 1985. "Behavior of Human Apolipoprotein E in Aqueous Solutions and at Interfaces." *The Journal of Biological Chemistry* 260 (30): 16375–82. <http://www.ncbi.nlm.nih.gov/pubmed/4066713>.
- Zannis, V.I., and Breslow, J.L. 1980. "Characterization of a Unique Human Apolipoprotein E Variant Associated with Type III Hyperlipoproteinemia." *The Jou* 255 (March 10): 1759–63.
- Zannis, V.I., Breslow, J.L., Utermann, G., Mahley, R.W., Weisgraber, K.H., Havel, R.J., Goldstein, J.L., et al. 1982. "Proposed Nomenclature of ApoE Isoproteins, ApoE Genotypes, and Phenotypes." *Journal Of Lipid Research* 23: 911–14.
- Zannis, V.I., Just, P.W., and Breslow, J.L. 1981. "Human Apolipoprotein E Isoprotein Subclasses Are Genetically Determined." *American Journal of Human Genetics* 33 (1): 11–24. <http://www.pubmedcentral.nih.gov/articlerender.fcgi?artid=1684875&tool=pmcentrez&rendertype=abstract>.
- Zhang, F., Su, B., Wang, C., Siedlak, S.L., Mondragon-Rodriguez, S., Lee, H. gon, Wang, X., Perry, G., and Zhu, X. 2015. "Posttranslational Modifications of α -Tubulin in Alzheimer Disease." *Translational Neurodegeneration* 4 (1): 1–9. <https://doi.org/10.1186/s40035-015-0030-4>.
- Zhao, Y., and Zhao, B. 2013. "Oxidative Stress and the Pathogenesis of Alzheimer's Disease." *Oxidative Medicine and Cellular Longevity* 2013: 1–10. <https://doi.org/10.1155/2013/316523>.
- Zheng, L., Calvo-Garrido, J., Hallbeck, M., Hultenby, K., Marcusson, J., Cedazo-Minguez, A., and Terman, A. 2013. "Intracellular Localization of Amyloid- β Peptide in SH-SY5Y Neuroblastoma Cells." *Journal of Alzheimer's Disease* 37 (4): 713–33. <https://doi.org/10.3233/JAD-122455>.
- Zhong, N., and Weisgraber, K.H. 2009. "Understanding the Association of Apolipoprotein E4 with Alzheimer Disease: Clues from Its Structure." *Journal of Biological Chemistry* 284 (10): 6027–31. <https://doi.org/10.1074/jbc.R800009200>.

Appendix 1

Animals

- Table of animals used

ID.	Sex	D.O.B.	D.A.C.	APOE	Normaliser	Age group	Age category
653	M	23/05/2018	27/08/2018	ε3/ε3	A	3 m	Adult
654	M	23/05/2018	27/08/2018	ε3/ε3	B	3 m	
656	F	23/05/2018	27/08/2018	ε3/ε3		3 m	
755	M	30/11/2018	07/03/2019	ε3/ε3		3 m	
684	M	19/07/2018	22/01/2019	ε3/ε3		6 m	
687	F	19/07/2018	22/01/2019	ε3/ε3		6 m	
688	F	19/07/2018	22/01/2019	ε3/ε3		6 m	
471	M	28/11/2017	29/11/2018	ε3/ε3		12 m	Middle age
472	F	28/11/2017	29/11/2018	ε3/ε3		12 m	
477	F	28/11/2017	29/11/2018	ε3/ε3		12 m	
478	F	28/11/2017	29/11/2018	ε3/ε3		12 m	
378	F	23/09/2017	26/03/2019	ε3/ε3		18 m	Old
442	M	18/10/2017	25/04/2019	ε3/ε3		18 m	
443	M	18/10/2017	25/04/2019	ε3/ε3	C	18 m	
94	M	25/09/2016	25/09/2018	ε3/ε3		24 m	
96	M	25/09/2016	25/09/2018	ε3/ε3		24 m	
110	M	27/09/2016	09/10/2018	ε3/ε3		24 m	
186	M	03/02/2017	06/02/2019	ε3/ε3		24 m	
756	M	30/11/2018	07/03/2019	ε4/ε4		3 m	Adult
758	F	30/11/2018	07/03/2019	ε4/ε4		3 m	
796	F	08/04/2019	23/07/2019	ε4/ε4		3 m	
695	M	19/07/2018	22/01/2019	ε4/ε4		6 m	
716	F	11/08/2018	13/02/2019	ε4/ε4		6 m	
726	F	03/09/2018	07/03/2019	ε4/ε4		6 m	

(Table continued below)

ID	Sex	D.O.B.	D.A.C.	APOE	Normaliser	Age group	Age category
354	F	23/08/2017	21/08/2018	$\epsilon 4/\epsilon 4$		12 m	Middle age
356	F	23/08/2017	21/08/2018	$\epsilon 4/\epsilon 4$		12 m	
692	M	17/07/2018	23/07/2019	$\epsilon 4/\epsilon 4$		12 m	
236	M	03/02/2017	21/08/2018	$\epsilon 4/\epsilon 4$		18 m	Old
241	F	03/02/2017	21/08/2018	$\epsilon 4/\epsilon 4$		18 m	
268	F	18/05/2017	19/11/2018	$\epsilon 4/\epsilon 4$		18 m	
287a	F	06/07/2017	09/01/2019	$\epsilon 4/\epsilon 4$		18 m	
162	F	20/12/2016	10/12/2018	$\epsilon 4/\epsilon 4$		24 m	
173	M	29/12/2016	19/11/2018	$\epsilon 4/\epsilon 4$		24 m	
174	M	29/12/2016	09/01/2019	$\epsilon 4/\epsilon 4$		24 m	
207	M	23/04/2017	25/04/2019	$\epsilon 4/\epsilon 4$		24 m	

D.O.B= date of birth; D.A.C= date at culling;

A= Normaliser for ApoE protein levels across lifespan in whole fractions (5.3.1);

B= Normaliser for fragment/intact ApoE protein in nuclear fractions (5.3.2);

C= Normaliser for α -Tubulin levels in old ApoE-TR mice (5.3.3);

- **Summary of n numbers**

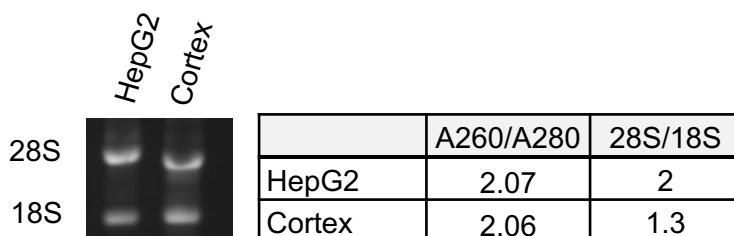
$\epsilon 3/\epsilon 3$					$\epsilon 4/\epsilon 4$				
3 m	6 m	12 m	18 m	24 m	3 m	6 m	12 m	18 m	24 m
n=4	n=3	n=4	n=3	n=4	n=3	n=3	n=3	n=4	n=4
Adult		M.A.	Old		Adult		M.A.	Old	
n=7		n=4	n=7		n=6		n=3	n=8	
N=18					N=17				

M.A.= middle age

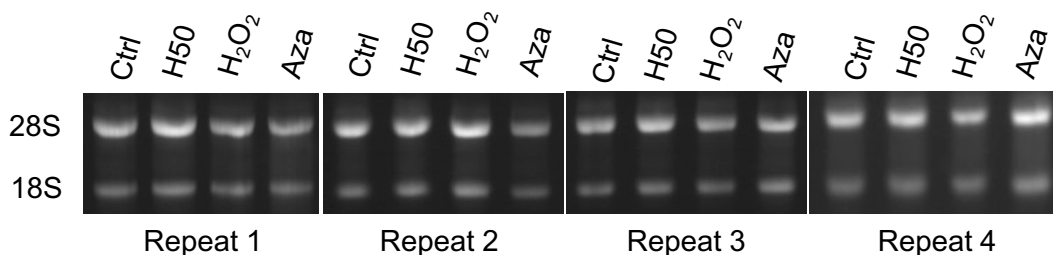
RNA integrity and quality

The ratio between the absorbance of an RNA sample at 260 nm and at 280 nm (A260/280), measured by UV spectroscopy, is used to assess RNA quality. The A260/280 ratio of highly pure RNA is comprised between 1.8 and 2.1. RNA integrity was evaluated here by agarose gel containing ethidium bromide. Intact RNA has two distinct bands corresponding to ribosomal RNA: 28S and 18S. Theoretically, the 28S:18S ratio is around 2.7:1. Anything from a 2:1 ratio is considered to correspond to intact RNA (ThermoFisher). Overall RNA quality and integrity was appreciated as a combination of the two assessments – if agarose gel showed two distinct bands and a A260/280 of 2, RNA was used for further experiments even if 28S/18S was lower than 2. RNA can degrade between extraction and running the gel.

- **RNA extracted from HepG2 cells and ApoE-TR mouse cortex**



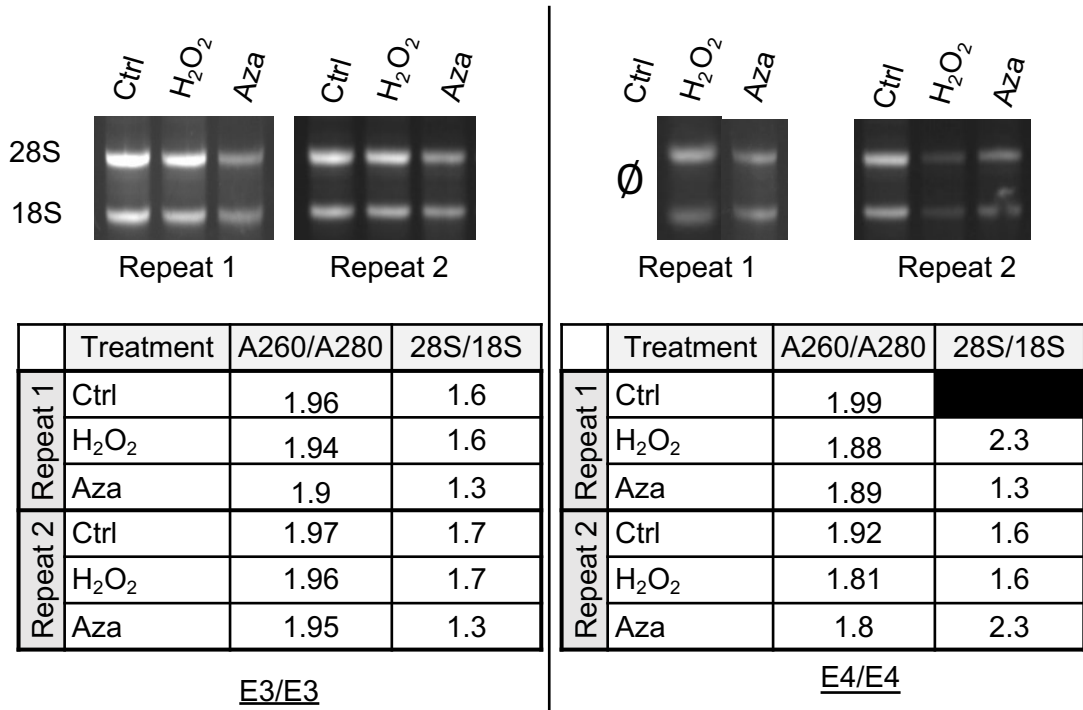
- **RNA extracted from SH-SY5Y cells**



	Treatment	A260/A280	28S/18S		Treatment	A260/A280	28S/18S
Repeat 1	Ctrl	2.01	2.5	Repeat 3	Ctrl	2.04	2.9
	H50	2.02	2.5		H50	2.01	2.6
	H ₂ O ₂	2.01	2.2		H ₂ O ₂	2.06	2.3
	Aza	2.01	2.1		Aza	2.04	1.9
Repeat 2	Ctrl	2.04	2.9	Repeat 4	Ctrl	2.04	2.7
	H50	2.04	2.6		H50	2.06	2.6
	H ₂ O ₂	1.99	2.2		H ₂ O ₂	1.96	2.2
	Aza	2.01	2.3		Aza	2.03	2.3

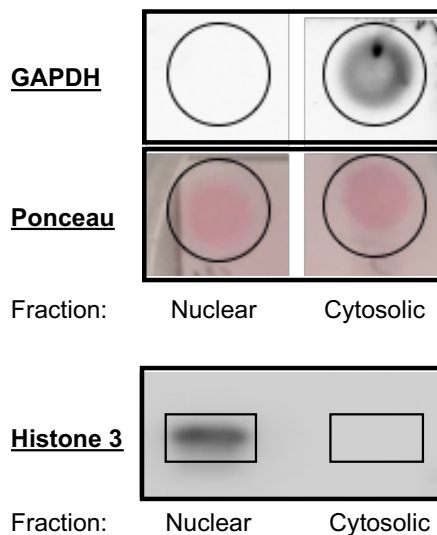
Ctrl= control; H50= 50 μ M haloperidol; H₂O₂= 75 μ M hydrogen peroxide; Aza= 25 μ M azamethiphos.

- RNA extracted from primary cortical neurons



Ctrl= control; H₂O₂= 650 μM hydrogen peroxide; Aza= 300 μM azamethiphos. ∅: no sample left to run on agarose gel.

Protein fractionation



Proteins were fractionated and cross-contamination assessed by immunoblotting. Nuclear fractions contain nuclear markers (histone 3), but no cytosolic marker (GAPDH) whereas cytosolic fractions stained for GAPDH but not histone 3.

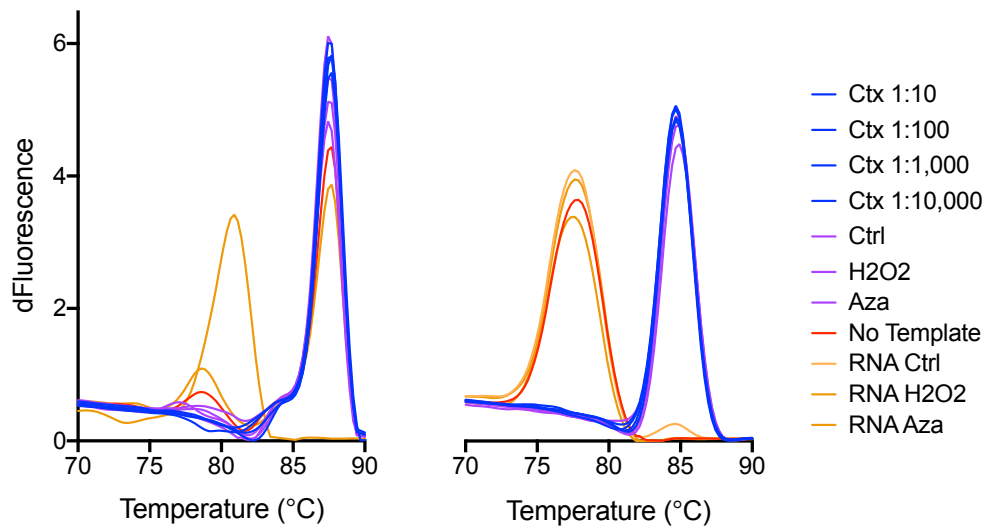
qPCR

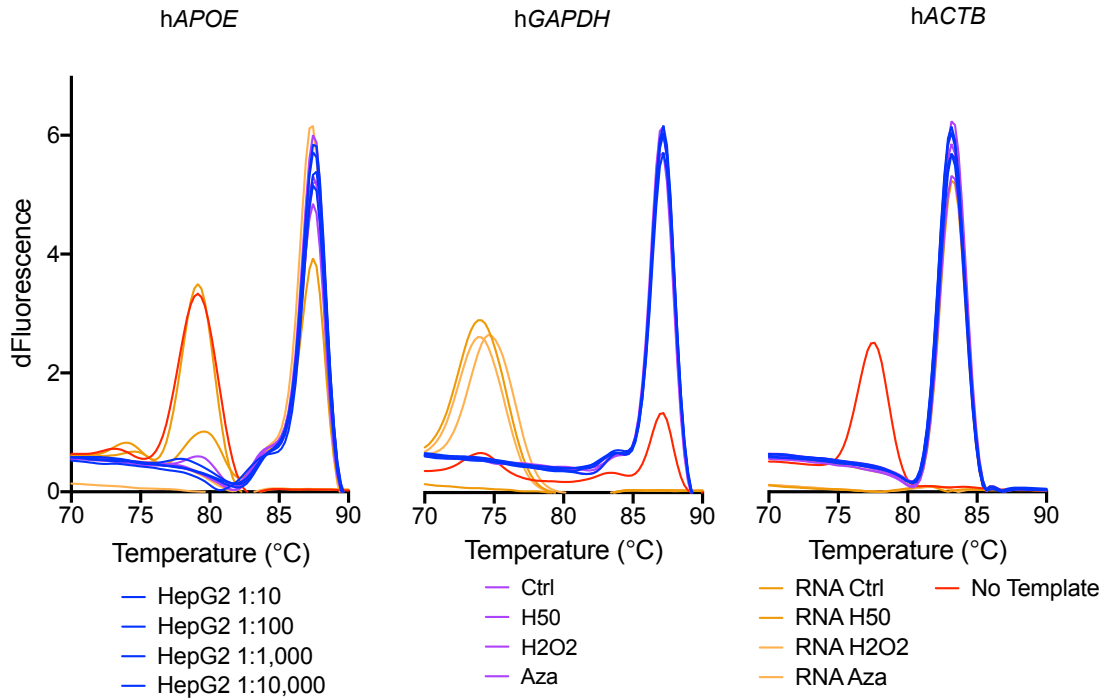
- **Primers efficiency**

		<i>APOE</i>	<i>hACTB</i>	<i>hGAPDH</i>
SH-SY5Y	Repeat 1	92%	94.3%	93.2%
	Repeat 2	89.9%	92.7%	90.5%
	Repeat 3	90.2%	91.1%	87.1%
	Repeat 4	87.3%	94.2%	92.6%

		<i>APOE</i>	<i>ACTB</i>
Neurons	Repeat 1	92.1%	93.5%
	Repeat 2	91.2%	88.5%

- **Example of integrated melt curves**

Cortical neurons

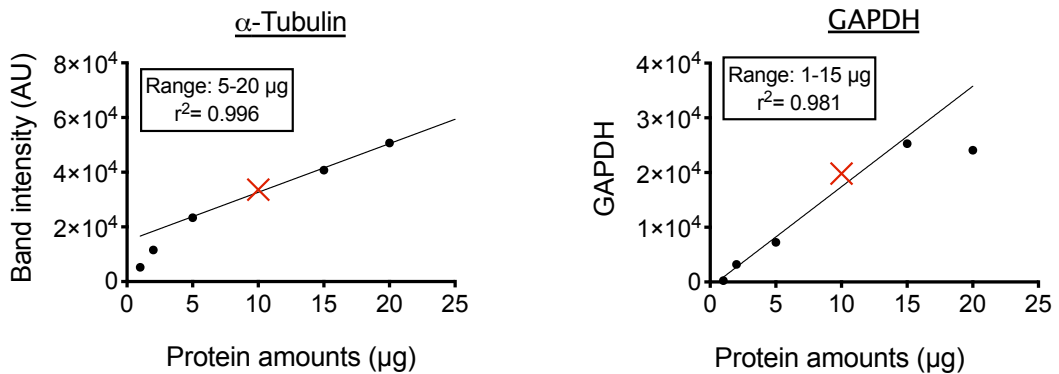
SH-SY5Y

It is very easy to get genomic DNA contamination. All Cq for negative controls were above 35. Positive peaks in melt curve can also be indicative of primer-dimers.

Antibodies linearity

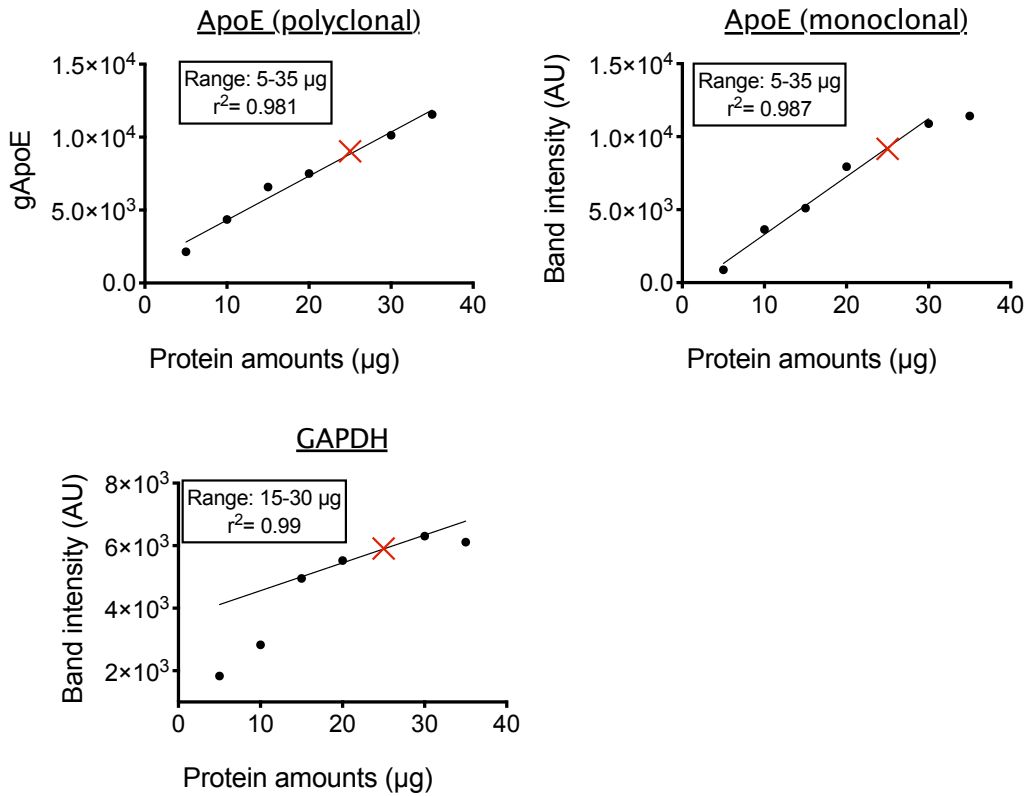
The amount of protein to load was selected to ensure it was in the linearity range of the antibodies used.

- **Antibodies used on cytosolic fractions**



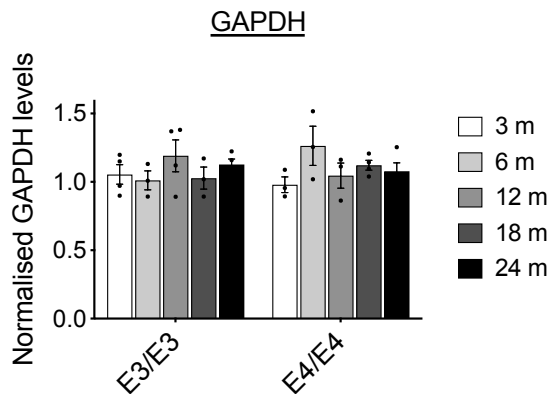
10 μ g (X) of cytosolic extracts were loaded for semi-quantification of changes in α -Tubulin levels.

• **Antibodies used on whole fractions**



25 µg (X) of cytosolic extracts were loaded for semi-quantification of changes in ApoE levels.

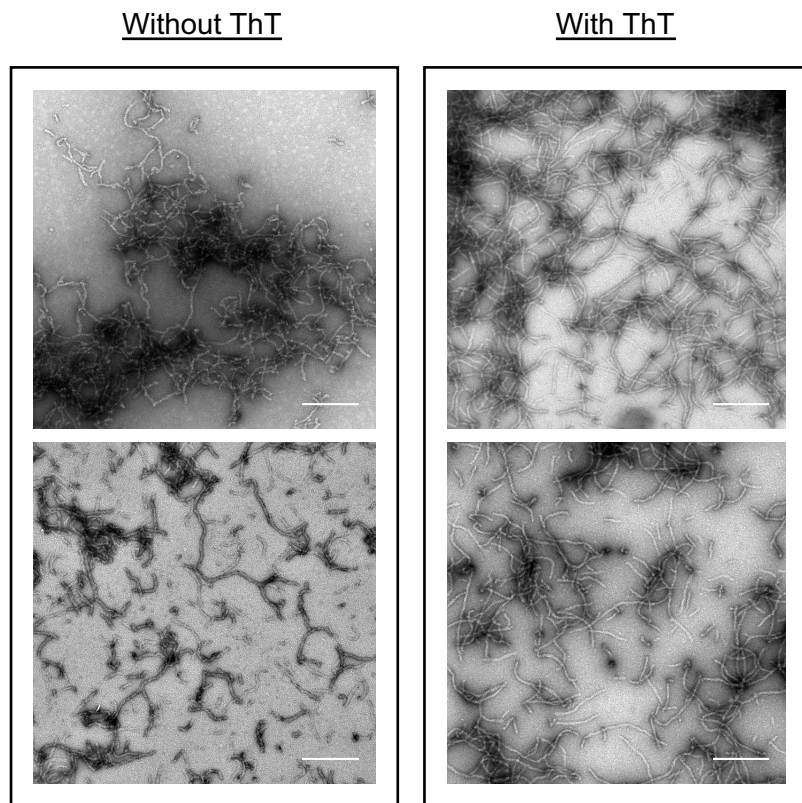
GAPDH levels over time in ApoE3-TR and ApoE4-TR mice



GAPDH levels remained fairly constant with age and phenotype here, as shown by two-way ANOVA (interaction Age x Phenotype: $F(4, 25) = 1.784, p = 0.1636$; phenotype effect $F(1, 25) = 0.09193, p = 0.7642$; age effect $F(4, 25) = 0.6510, p = 0.6315$). The variability comes from sample preparation and loading on the gel, since GAPDH levels were not normalised to an internal marker.

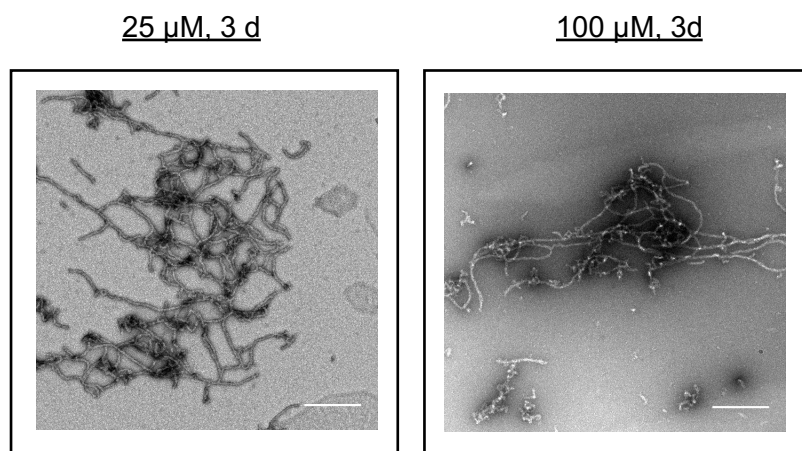
Appendix 2

ThT had no effect of rApoE4 fibril formation and morphology

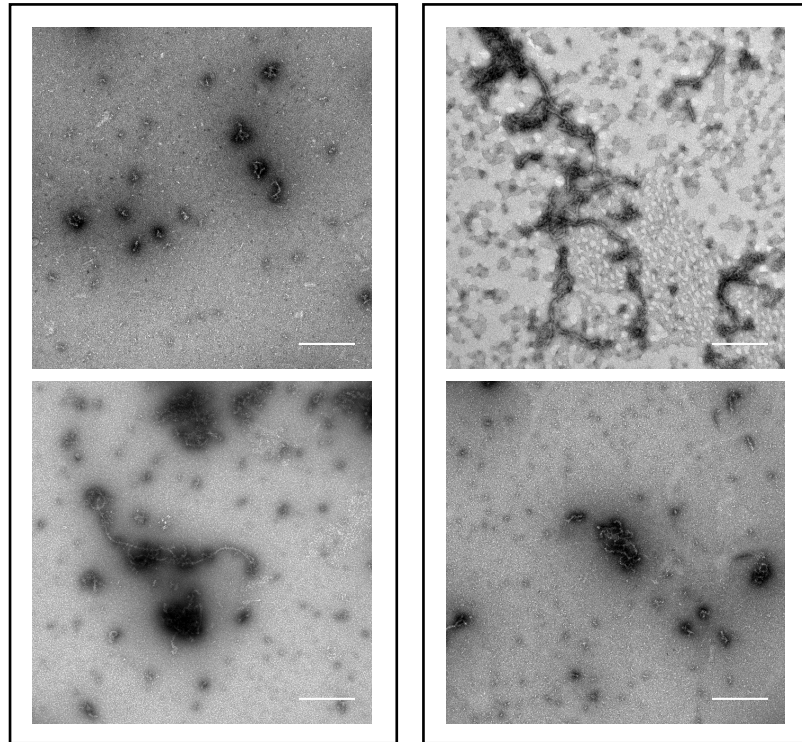


Scale bar= 500 nm

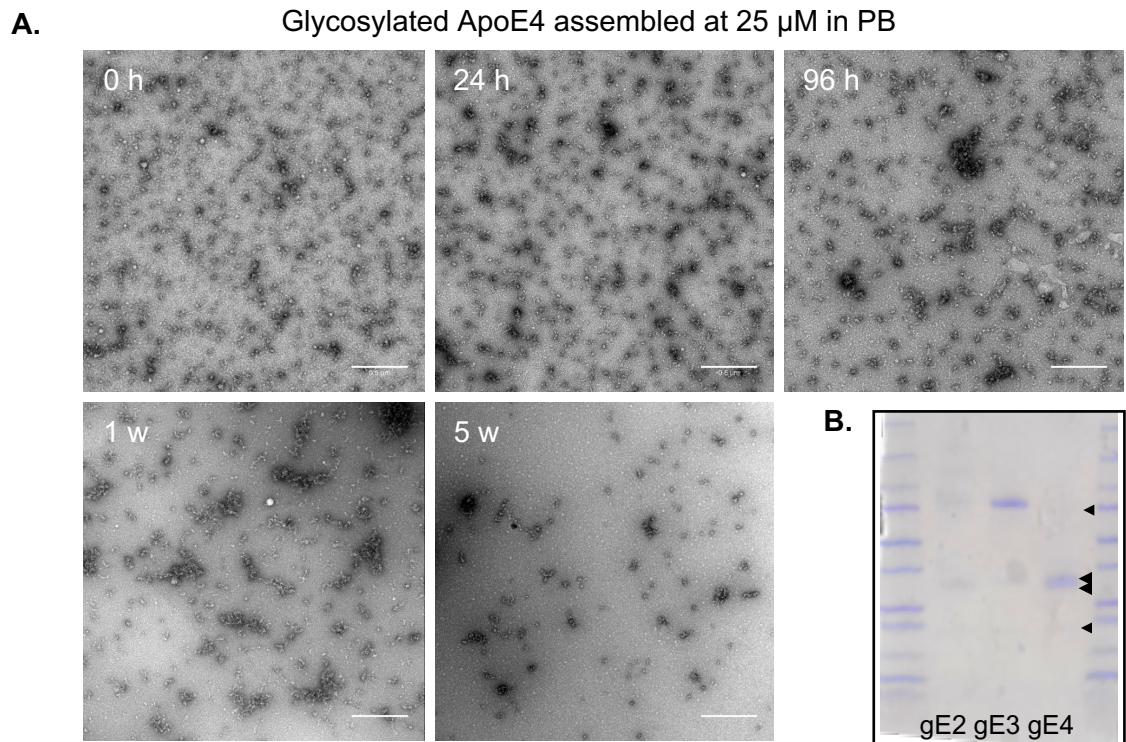
Increased protein concentration had no effect on the morphology of rApoE4 fibrils



Scale bar= 500 nm

rApoE4 fibril formation in PBSrApoE4 assembled at 25 μ M for 24 h in PBS

Scale bar= 500 nm

Incubation of glycosylated ApoE4 for an extended period of time

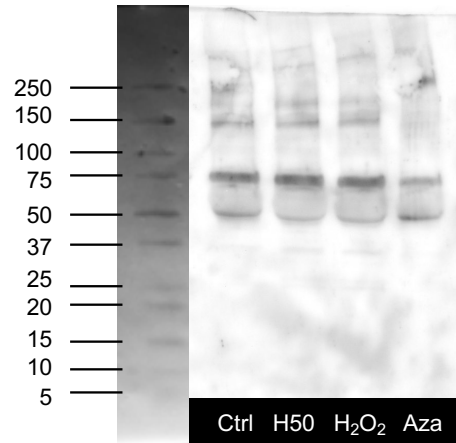
A. Fibril formation in glycosylated ApoE4 was investigated for up to 5 weeks (w).

Scale bar= 500 nm

B. Glycosylated ApoE isoforms were degraded

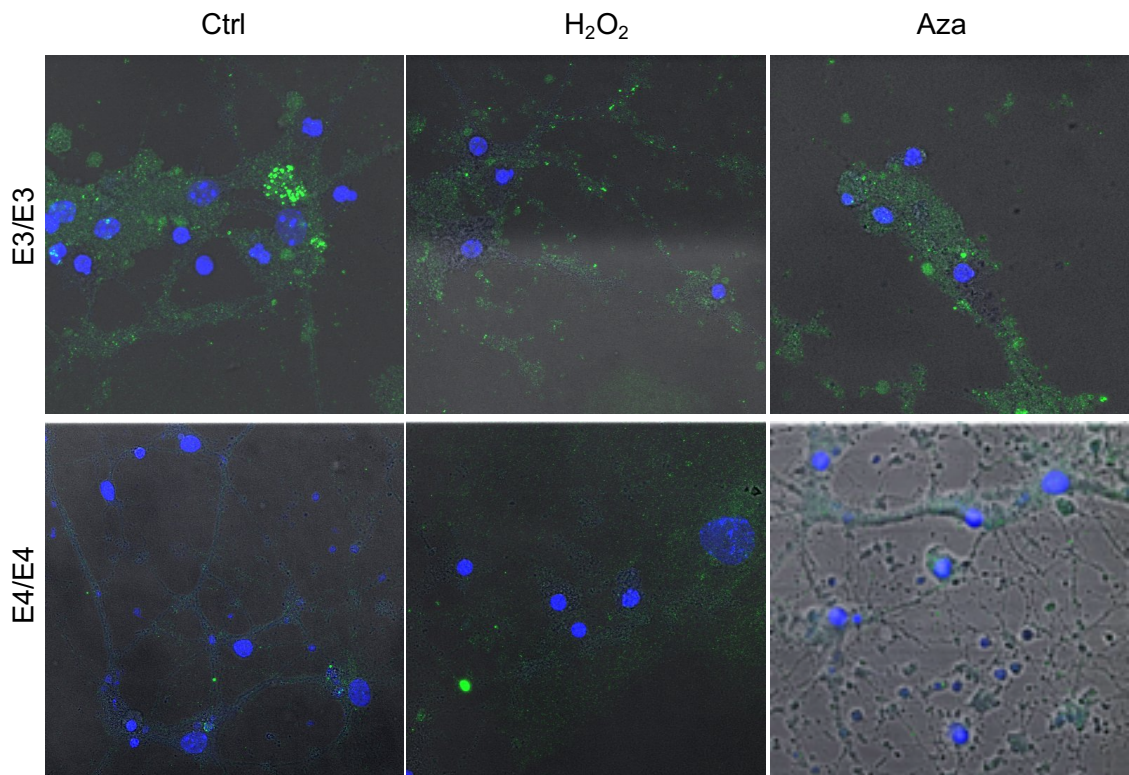
Appendix 3

Western blot to assess ApoE expression in SH-SY5Y cells

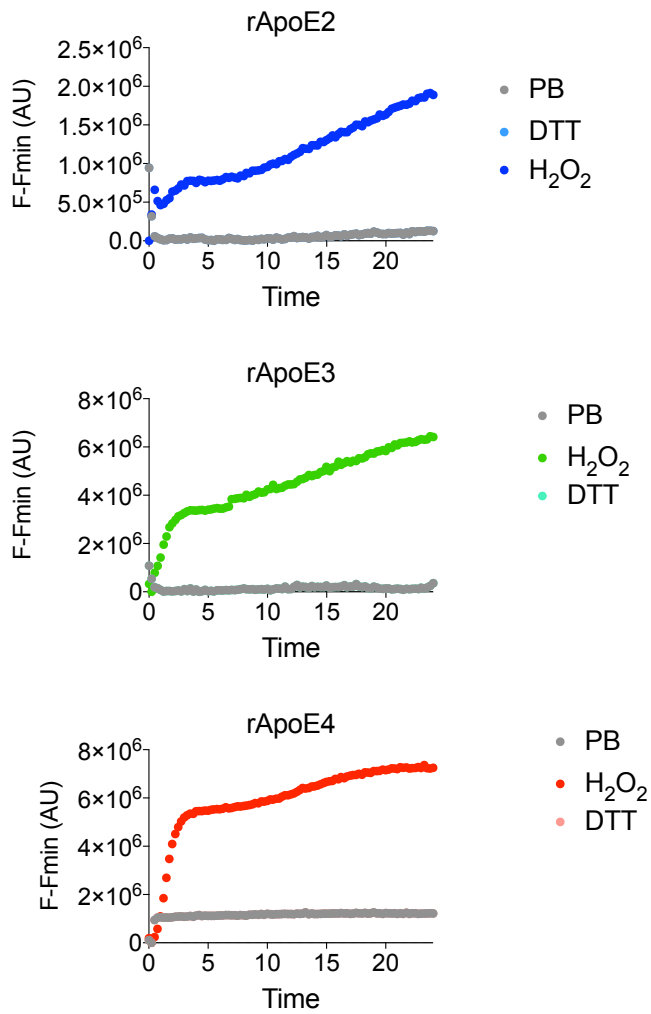


Ctrl= control; H₂O₂= 75 μ M hydrogen peroxide; Aza= 25 μ M azamethiphos.

Immunofluorescence to assess ApoE expression in cortical neurons



Ctrl= control; H₂O₂= 650 μ M hydrogen peroxide; Aza= 300 μ M azamethiphos.

Kinetics of rApoE self-assembly under redox conditions

rApoE isoforms were incubated in PB, H₂O₂ (1:3533) or DTT (1:400) with ThT. Kinetic scans were buffer-corrected, and baseline adjusted.

Appendix 4

ApoE levels in ApoE-TR mice brain tissue extracts (whole fractions) across lifespan, without normalising to GAPDH levels

